An exploration of mechanisms and effects of oncogenic KRAS on the tumour immune microenvironment

Amit Samani

Institute of Cancer Research
and
The Francis Crick Institute
PhD Supervisor: Professor Julian Downward

A thesis submitted for the degree of
Doctor of Philosophy
Institute of Cancer Research
February 2022

Declaration

I Amit Samani confirm that the work presented in this thesis is my own. Where information has been derived from other sources, I confirm that this has been indicated in the thesis.

Abstract

Oncogenic KRAS influences several cancer hallmarks including autonomy from growth promoting signals, enhanced cell survival and altered tumour metabolism. Beyond these, it is now established that oncogenic KRAS can polarise the tumour immune microenvironment, aiding tumour immune evasion.

Tristetraprolin (TTP) is an RNA-binding protein, which destabilises its targets through binding to AU-rich elements in their 3'-untranslated regions. It is important in the resolution of macrophage responses to inflammatory stimuli. Additionally, it can bind and destabilise targets in tumour cells. Oncogenic KRAS, through inhibitory phosphorylation of TTP, can prevent it from destabilising its targets, resulting in upregulation of oncogenic proteins including programmed death-ligand 1.

We interrogated the transcriptome-wide effect of TTP overexpression in an immunogenic KRAS-mutant murine colon carcinoma model. Using RNA-seq, we showed that TTP targets are involved in several tumourigenic hallmarks. We discovered that many such targets overlap with those of KRAS, and that this relationship extends across model systems. Co-perturbation of KRAS and TTP in a single model system resulted in modest effect.

Next, we used single-cell profiling to understand the effect of mutant-specific oncogenic KRAS inhibition in an orthotopic murine lung carcinoma model. We showed that such inhibition results in compositional change in the repertoire of macrophages with concomitant alteration of gene expression including downregulation of several immunosuppressive transcripts. Furthermore, we showed that tumour cell proliferation is altered, and that the expression of many oncogenic transcripts are reduced. Conversely some oncogenic transcripts, including the emerging clinical target CD47, are upregulated upon KRAS inhibition and may represent potential strategies for combination therapy.

Acknowledgements

Firstly, I would like to thank Julian for showing faith in me and accepting me into his lab. Also for his enduring patience and flexibility when things were tough, and giving for me the opportunity to work on an incredibly interesting and rewarding project. I have developed immensely during my time in his lab, and I am hugely grateful for that.

Next, I would like to thank Miriam Molina Arcas and Sophie De Carne. Both are brilliant and inspirational scientists in their own right. They have been there to teach and guide me and have given up significant portions of their own time to do so. They have helped me keep my head above water, and I would not have got close to completing this programme without them. Thank you.

Thanks also to Dave Hancock, a constant source of wisdom, great human and unfortunate Bolton Wanderers supporter. To Sophia Kontakkis for all the happy chats and always being there for help when I needed it. There are many more in Julian's lab who have patiently taught me wet-lab skills, helped me with *in vivo* work and looked at my code. Thank you especially to Chris, Debbie, Edurne, Goran, Jesse, Megan, Mona, Rachel, Romain and Sareena amongst others. Also the science technology platforms at the Crick who have used their expertise to make a lot of this happen, and have been a pleasure to work with. Special mention to Phil East for his bioinformatics expertise and time he has given to guide me.

Alan Melcher has been ever-present as my co-supervisor and mentor. Indebted for the pleasant chats and invaluable career advice that he has given on a regular basis. He is genuinely an inspiration and it has been a privilege to have learnt from him. Also to Sanjay Popat who offered sage words, including about the PhD and writing process (all of which proved to be true) and who has therefore ensured that I managed to get this completed. Thank you to Robert Huddart for offering his mentorship, we have developed a plan together and I

am excited to see where it leads. To Amanda Swain for her kindness and pastoral support.

Thank you to my thesis committee - Charlie Swanton and Francesca Ciccarelli – they have always encouraged and supported me and helped keep me on track. Thank you for showing a genuine interest in me, and encouraging me to push forward.

To two of my PhD colleagues - Sviatoslav (Slava) Sidorov and Sara Ali. They have both helped me understand single cell data but more than that, they are both brilliant, selfless, individuals and friends who I can’t praise enough. Big thank you to them.

Finally, to my Mum, Dad, Meera, Kamal, Komal and Nima Masi. Ultimately this is all because of them, and for them.

Table of Contents

Table of figures

List of tables

Abbreviations

ADT: Antibody Derived Tag

CLR: Centred log ratio (method of normalisation)

DE: Differential expression or Differentially expressed

GSEA: Gene set enrichment analysis

IEGs: Immediate early genes

NES: Normalised enrichment ratio

SCT: scTransform (method of single-cellnormalisation)

TTP: Tristetraprolin

UMAP: Uniform Manifold Approximation and Projection for dimension reduction

WNN: Weighted nearest neighbour

Chapter 1. Introduction

1.1 Biology of RAS

1.1.1 RAS and downstream signalling cascades

The RAS superfamily of GTP-binding proteins consists of over 150 small GTPases divided into several subfamilies. The members KRAS, HRAS and NRAS (hereafter, RAS proteins) are membrane-associated molecules which participate in the transduction of external signals to intracellular cascades influencing diverse processes. Canonically, activation of these proteins promotes cell proliferation and survival. More broadly, RAS-induced signals affect metabolism, motility and immune polarisation of the local microenvironment (Pylayeva-Gupta, Grabocka and Bar-Sagi, 2011a) .

The name RAS stems from the discovery that certain viruses were able to induce sarcoma in rats (**ra**t **s**arcoma virus). These viruses had incorporated host sequences into their genome. Later, probes from these viral sequences were found to hybridize with human tumour DNA capable of transforming NIH-3T3 cells, and this led to the discovery that the transforming oncogenes contained in the rat viruses (Hras and Kras) had human homologues (Malumbres and Barbacid, 2003). A third member of this gene subfamily, NRAS, was identified shortly thereafter.

As small GTPases, these proteins exist in two conformations. The GTP-bound form is ‘on’, capable of binding and activating downstream effectors while the GDP-bound form is ‘off’, unable to trigger downstream signalling. The switch between them is mediated by two main classes of proteins. GTPase activating proteins (GAPs, e.g. NF1) accelerate the otherwise low intrinsic GTPase activity of the RAS proteins while guanine nucleotide exchange factors (GEFs, e.g. Son of Sevenless 1 (SOS1)) promote exchange of GDP for GTP. Binding of GTP induces conformational change in the proteins, specifically in two ‘switch regions’ important for effector binding (Mccormick, 2018).

Effector binding following this conformational change activates intracellular signalling cascades with diverse outcomes. The most-well characterised cascade, the mitogen activated protein kinase/ extracellular signal regulated kinase (MAPK/ERK) cascade is the prototypical example of a MAPK cascade which, in this case, culminates in activation of ERK (Plotnikov *et al.*, 2011). In such cascades a series of proteins phosphorylate and activate one another in sequence. Thus, RAS activates the Rapidly Activated Fibrosarcoma (RAF) kinases (MAP3Ks) which in turn activate the MAPK/ERK kinases (MEK 1/2 or MAP2K) which culminate with ERK 1/2 activation. Activated ERK can act cytosolically or translocate to the nucleus where it may phosphorylate transcription factors. These include Ets family transcription factors (e.g. Elk-1) forming part of the serum response factor (SRF). The net result of ERK-driven transcription includes proliferative signalling networks involving cell cycle regulators such as cyclin D1 (Gimple and Wang, 2019). Beyond the ERK-MAPK cascade, RAS is able to activate several other pathways including the PI3K/AKT/mTOR pathway and effectors such as RAL guanine nucleotide dissociation stimulator (RALGDS) with effects including promotion of cell survival and reorganisation of the actin cytoskeleton respectively (Downward, 2003) (Figure 1).

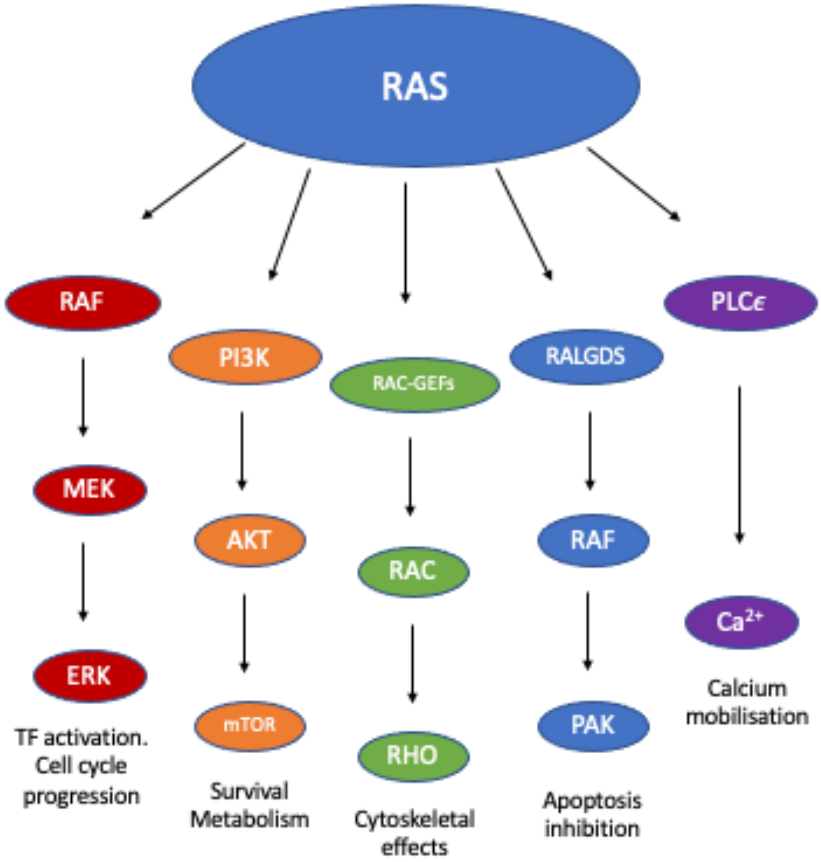

Figure 1. Simplified schema of RAS signalling Adapted from (Downward, 2003; Malumbres and Barbacid, 2003)

1.1.2 RAS proteins and cancer

RAS proteins are frequently mutated in cancer. Across cancers as a whole, the prevalence of RAS mutations is difficult to accurately quantify but is somewhere between 15-30% (Prior IA; Lewis, 2012). Amongst the three proteins, mutations in KRAS are the most common, accounting for around 80% of all RAS protein mutations (Prior, Hood and Hartley, 2020). KRAS is most frequently mutated in pancreatic, colorectal (CRC) and non-small cell lung (NSCLC) cancers with estimated frequencies (in Western populations) of around 85%, 40% and 30% respectively (Moore *et al.*, 2020). Beyond these, KRAS mutations also occur in around 30% of cholangiocarcinoma and 10% of ovarian & endometrial carcinomas (Timar and Kashofer, 2020). Conversely NRAS is most commonly

mutated in melanoma and acute myeloid leukaemia (around 20% and 15% respectively) while HRAS shows predilection for bladder and head & neck cancers (around 5% each) (Prior, Hood and Hartley, 2020).

Most oncogenic mutations in RAS isoforms are missense gain-of-function mutations in codons G12, G13 or Q61 (Hobbs, Der and Rossman, 2016). Different RAS isoforms differ in their frequency of such alterations. In KRAS, G12 and G13 mutations predominate. In contrast, Q61 mutations are rare in KRAS but common in NRAS, while the frequencies in HRAS lie in between the other two isoforms. Furthermore, within a given isoform and codon, the frequency of amino acid substitutions varies by cancer type. For example, in lung cancer, the commonest KRAS G12 mutation is G12C, possibly associated with tobacco smoke exposure (Dogan *et al.*, 2012), while in colon and pancreas cancers, G12D is the commonest.

Impaired GTP hydrolysis, resulting in increased signalling through downstream pathways, is a key property of oncogenic RAS (Gibbs *et al.*, 1984; Scheffzek *et al.*, 1997). However, different mutations result in distinct biochemical and structural properties. Differences occur in (a) GTP binding affinity, (b) intrinsic and GAP-mediated GTP hydrolysis and (c) effector binding affinity (Hunter *et al.*, 2015). In fact, analysis of intrinsic GTP hydrolysis rates of various KRAS mutations showed that while G12A, G12R, Q61H and Q61L mutations resulted in 40–80% reduction compared to wild type, G12C was an outlier, with a rate almost comparable to wild type. This is consistent with observations that KRAS G12C isoforms maintain demonstrable GTP–GDP cycling, a phenomenon exploited by recently developed inhibitors (Patricelli *et al.*, 2016).

Though these different variants may affect signalling differently, several processes are affected by oncogenic RAS regardless of the variant in question (Pylayeva-Gupta, Grabocka and Bar-Sagi, 2011a). Canonically, oncogenic RAS promotes cellular proliferation. This effect occurs through several mechanisms including the transcriptional induction and stabilisation of the G1 cyclin, cyclin

D1 (Filmus *et al.*, 1994). The relationship between RAS and apoptosis is more complex, with studies demonstrating both pro and anti-apoptotic effects (Downward, 1998). Nonetheless, as discussed below, direct RAS inhibitors induce hallmarks of apoptosis in sensitive cells, suggesting an apoptosis-suppressing role for oncogenic RAS in these cells (Patricelli *et al.*, 2016). Oncogenic RAS also reconfigures metabolism, supporting the shift from oxidative phosphorylation to aerobic glycolysis. This process involves the upregulation of hypoxia inducible factor 1α and enhances the transport and glycolytic capture of glucose (Blum *et al.*, 2005). Beyond these effects on proliferation, survival and metabolism, oncogenic RAS also influences the processes of invasion and metastasis. Through a constellation of changes including; reduced expression of the cell-cell adhesion molecule E-cadherin; downregulation of integrins that promote matrix attachment; and polarisation of the cytoskeleton to generate the front-rear asymmetry necessary for motility, oncogenic RAS promotes invasion (Pollock *et al.*, 2005; Schmidt *et al.*, 2005). Of note epithelial-to-mesenchymal transition, a process involving downregulation of E-cadherin, is a feature of certain pre-clinical KRAS-mutant models and may suggest unique vulnerabilities of these cells in conjunction with direct KRAS inhibition, as discussed below (Solanki *et al.*, 2021).

1.1.3 Targeting KRAS

1.1.3.1 Historical efforts

Given the prevalence of RAS mutations in cancer, decades of research have focussed on attempts at inhibition of this pathway. Direct targeting of KRAS has proved challenging, in part because of its shallow surface with limited opportunity for allosteric binding, and its picomolar affinity for GTP (Mccormick, 2018). Initial approaches focussed on inhibiting RAS prenylation using farnesyl transferase inhibitors (FTIs) (Kohl *et al.*, 1995). This modification, at the c-terminus, influences membrane localisation and is essential for activity. However, clinical trials were initially disappointing because both KRAS and NRAS (but not HRAS) can also be prenylated by geranylgeranyltransferase

and, unfortunately, the clinical studies focussed patients with KRAS and NRAS mutations. Subsequently, focus on HRAS-mutated cancers has led to Breakthrough Therapy Designation by the FDA for the FTI tipifarnib for patients with HRAS-mutant head & neck squamous cell carcinoma (*Kura Oncology Receives FDA Breakthrough Therapy Designation for Tipifarnib in Head and Neck Squamous Cell Carcinoma*, 10/09/2021).

Beyond direct targeting of RAS, other efforts focussed on inhibition of downstream effectors within the RAF/MEK/ERK and PI3K/AKT/mTOR pathways fuelled by *in vitro* observations demonstrating sensitivity of KRAS-mutant cell lines to such inhibition (Garnett *et al.*, 2012). However, as monotherapy, such agents are poorly efficacious in patients. This can be partly explained by their mechanism of action. Following allosteric MEK inhibition, feedback reactivation of MEK by wild-type (WT) RAF can occur. While some MEK inhibitors can prevent this, clinically available inhibitors such as cobimetinib fail to do so, and thus lack utility in the WT RAF population (Hatzivassiliou *et al.*, 2013). Furthermore, BRAF targeting agents, in cells with oncogenic RAS and WT BRAF, also cause paradoxical activation of the MAPK pathway (Hatzivassiliou *et al.*, 2010). These nuanced pitfalls of MEK and BRAF-specific agents in RAS-mutated cells are compounded by complex parallel downstream signalling cascades influenced by RAS. Inhibition of one pathway (and suppression of negative feedback mediators) may simply increase flux through parallel pathways, maintaining the transformed cell state and meaning that even inhibitors that can prevent feedback reaction of MEK, for example, may lack efficacy. To compensate, one could attempt to target multiple pathways, but this is likely to increase the risk of toxicity even if doses are carefully optimised to maximise synergy.

1.1.3.2 Covalent KRAS inhibition

A much needed paradigm shift in RAS targeting came in 2013, when Shokat and colleagues developed ‘compound 12’, a covalent inhibitor of KRAS(G12C) (Ostrem *et al.*, 2013). They exploited both the ‘novel’ switch-II pocket (discovered close to the switch-II region and only accessible in the GDP-bound state) and also the presence of cysteine (an inherently reactive amino acid) in the mutant protein. Screening 480 tethering compounds, they discovered that compound 12 bound at the switch-II pocket and covalently modified the reactive cysteine. Subsequently, SOS-mediated nucleotide exchange and RAS-RAF interaction are both blocked such that the protein is effectively trapped in its inactive conformation (Ostrem *et al.*, 2013). The propensity of the drug to bind only in the GDP-bound state requires a sufficient concentration of cellular KRAS to be present in this conformation. As discussed above, biochemical studies indicate that KRAS(G12C) protein has an intrinsic hydrolysis rate similar to WT. This means that 25% of the protein is GDP-bound at steady-state compared to <5% for other common mutations (Hunter *et al.*, 2015; Mccormick, 2018).

These parameters were sufficient for robust effects on signalling as shown by development of ARS-853, an agent closely related to compound 12 (Patricelli *et al.*, 2016). Treatment of a panel of KRAS-mutant cell lines with ARS-853 demonstrated inhibition of downstream signalling specifically in G12C-mutant cells. Of note there was heterogeneity in the depth and durability this across lines, implying factors beyond the G12C mutation itself capable of modulating intrinsic sensitivity. In addition to effects on signalling, ARS-853 resulted in G1 arrest, reduced expression of cyclin D1 and hallmarks of apoptosis (e.g. PARP cleavage) in H358 cells (a human lung cancer line). Concomitantly, H358 growth *in vitro* was inhibited, and rescued by ectopic expression of KRAS(G12V).

While H358 cells were sensitive, when ARS-853 was tested across a panel of lines grown as monolayers (2D) some were insensitive to the drug. The same lines were also insensitive to siRNA-mediated KRAS knockdown despite

inhibition of RAF-RBD (Ras binding domain) pulldown in all lines tested (Patricelli *et al.*, 2016). This is consistent with previous data showing that some lines are independent of KRAS for growth in 2D culture systems (Singh *et al.*, 2009). Despite this, all G12C-containing lines were robustly inhibited in 3D culture, consistent with the increased dependence on KRAS in this format.

Following the study of ARS-853, ARS-1620 was developed; engineered for improved *in vivo* potency (Janes *et al.*, 2018). The authors again demonstrated that several KRAS(G12C) cell lines were relatively insensitive in 2D culture but sensitive in 3D systems. The same lines responded *in vivo* suggesting that 3D-spheroid systems best predict *in vivo* tumour responses. Since the description of ARS-1620, further compounds with enhanced drug-protein interaction (relative to compound 12) have been developed and described including AMG 510 (Canon *et al.*, 2019) and MRTX849 (Hallin *et al.*, 2019).

Like ARS-1620, AMG 510 is able to inhibit KRAS signalling and generate hallmarks of apoptosis *in vitro,* specifically in KRAS(G12C) lines, with heterogeneity in depth and durability of effect (Canon *et al.*, 2019). However, potency was higher than for ARS-1620 both in terms of signalling and effects on viability. This translated to its *in vivo* effect where the dose required to achieve regression of MIA PaCa-2 xenografts was over 3-fold lower than for ARS-1620. In addition, using subcutaneous CT26 tumours (murine colorectal carcinoma), these authors examined the effect of AMG 510 in an immunogenic KRAS(G12C) model. Intriguingly, durable remissions were seen only in mice with a replete lymphocyte compartment. The effect of KRAS (and its inhibition) on the antitumour immune response is discussed in a later section of this introduction.

Characterisation of MRTX849 included assessment of the difference in drug sensitivity across a panel of 17 KRAS(G12C) mutant lines in both 2D and 3D culture (Hallin *et al.*, 2019). While target engagement was comparable between the most and least sensitive lines, there was a difference in suppression of

downstream signals. The least sensitive lines showed only partial inhibition of phosphorylated ERK (pERK) and $pS6^{235/236}$ and no effect on the mTOR targets p70 s6 kinase (T412) or $pS6^{S240/44}$. This suggests maximising inhibition of KRAS-dependent ERK and S6 signalling may be required for optimal suppression of viability. Furthermore, *in vivo* analysis of 26 cell line or patient-derived xenografts (with a range of sensitivity to drug) showed that none of the genetic co-alterations tested (including TP53, STK11 and CDKN2A) correlated with response. Gene expression studies suggested that baseline expression of human epidermal receptor (HER) family receptor tyrosine kinases (RTKs) and early cell cycle regulators trended with tumour response. Together the data suggested that durable and robust ERK inhibition may associate with apoptosis induction and maximal treatment response (Hallin *et al.*, 2019).

To begin to understand what may drive therapeutic response or resistance beyond the correlative analyses above, the authors also performed CRISPR/Cas9 screens using the H2122 KRAS(G12C) model. Both *in* vitro and *in* vivo, depleted single guide RNAs (sgRNAs) included those for MYC, SHP2 and several cell cycle regulators. Enriched sgRNAs included those for KEAP1 and CBL – known tumour suppressor genes (TSGs). Intriguingly, objective response rate to both AMG 510 (sotorasib) and MRTX849 (adagrasib) in clinical trials appear lower in patients with KEAP1 co-mutations (Riely *et al.*, 2021; Skoulidis *et al.*, 2021). This data from clinical studies adds credence to this pre-clinical work on MRTX849 (Hallin *et al.*, 2019) suggesting that KEAP1 is important for maintaining response to treatment.

Following on from this pre-clinical work, both sotorasib and adagrasib are not only being studied in clinical trials, but the former has been approved by the UK Medicines and Healthcare products Regulatory Agency under project orbis for provision within the National Health Service (*Lung cancer patients to get breakthrough drug on NHS*, 2021). Adagrasib has been granted Breakthrough Therapy Designation by the US Federal Drug Administration (*Mirati Therapeutics' Adagrasib Receives Breakthrough Therapy Designation from*

U.S. Food and Drug Administration for Patients with Advanced Non-Small Cell Lung Cancer Harboring the KRASG12C Mutation, 2021). Both approvals concern patients with NSCLC who previously received platinum chemotherapy and checkpoint inhibitor therapy. Data showed that the agents could achieve an objective response rate (ORR) in this patient cohort of between 35 – 45% with a median duration of response of just under a year (Riely *et al.*, 2021; Skoulidis *et al.*, 2021). Of note, responses in other cancers are lower than for NSCLC (Hong *et al.*, 2020; Johnson, Ou and Barve, 2020). For example, ORR in colorectal cancer was between 5-20% in the phase I studies. This was particularly disappointing given the high prevalence of this disease. The reasons for the disparity are not fully understood but in one study, colorectal cancer cell lines were found to have higher basal receptor tyrosine kinase (RTK) expression than NSCLC lines (Amodio *et al.*, 2020). This affected pERK rebound following AMG 510 treatment and, though several RTKs contributed, EGFR had a dominant effect. Consistently, treatment of KRAS(G12C) patient derived organoids with AMG 510 alone had little or no effect while combination with cetuximab yielded significant suppression of proliferation. Indeed, the combination of adagrasib and cetuximab (EGFR inhibitor) yielded an ORR of 43% compared to 22% for adagrasib monotherapy (Weiss *et al.*, 2021) and is now being studied in a phase III trial in patients with CRC (NCT0479358). Since the initial trials with sotorasib and adagrasib, trials with other G12C inhibitors have commenced. Table 1 summarises some of the KRAS(G12C) inhibitors currently/previously in clinical development.

Drug	Manufacturer	Phase	Key trials	Combination partners
AMG510 (sotorasib)	Amgen	III	NCT04933695 NCT05054725 NCT05198934 NCT03600883	SHP2i, Cpi, EGFRi etc.
MRTX1257 (adagrasib)	Mirati	III	NCT04685135 NCT04613596 NCT04793958	CDK4/6i, Cpi, SOS1i, EGFRi etc.
GDC-6036	Roche/Genetech	I	NCT04449874	Cpi, EGFRi, VEGFAi, SHP2i
JNJ-74699157 (ARS-3248)*	Janssen	I	NCT04006301	
D-1553	Inventis Bio	I/II	NCT04585035	Several (not specified)
JDQ443	Novartis	I/II	NCT04699188	SHP2i, Cpi

Table 1. KRAS(G12C) inhibitors in clinical development Phase refers to phase of the most advanced trial. CDK4/6 = cyclin dependent kinase 4/6, Cpi = checkpoint inhibitor, EGFR = epidermal growth factor receptor, SHP2 = Src homology-2 domain-containing protein tyrosine phosphatse-2, SOS = son of sevenless, VEGFA = vascular endothelial growth factor A. *JNJ-74699157 has ceased clinical development

1.1.3.3 Intrinsic and acquired resistance to KRAS(G12C) inhibitors

Despite the encouraging efficacy of KRAS(G12C) inhibitors in second-line for NSCLC, most patients with objective responses to sotorasib in a phase II trial (including 4 with complete responses) eventually relapsed (Skoulidis *et al.*, 2021). Several studies, both pre-clinical and clinical, have generated hypotheses for how such resistance is generated. In terms of intrinsic resistance, studies have focussed on baseline characteristics of cells.

As already discussed, characterisation of MRTX849 included baseline gene expression studies suggesting that expression of HER-family RTKs or cell cycle

regulators may correlate with response (Hallin *et al.*, 2019). Consistently, their drug screen showed synergy with afatinib (EGFR inhibitor), palbociclib (cyclin dependent kinase (CDK) 4/6 inhibitor) and the Src homology region 2-containing protein tyrosine phosphatase (SHP2) inhibitor RMC-4550 in partially sensitive/refractory KRAS(G12C) models. Other studies have shown high basal PI3K/AKT signalling in KRAS mutated pancreatic cell lines that showed KRAS-independence after genetic knockdown (Muzumdar *et al.*, 2017). In support of this, another drug screen investigating synergy with ARS-1620 discovered that PI3K/AKT targeting provided the most consistent synergy across a panel of KRAS(G12C)-mutant lung cancer lines (Misale *et al.*, 2019). While inhibition of KRAS(G12C) and the PI3K/AKT/mTOR pathway can provide robust inhibition, more complete pathway shut-down can be achieved through concomitant targeting of IGF1R (Molina-Arcas *et al.*, 2019). This triple combination (KRAS, PI3K and IFG1R targeting) produced robust regression in several *in vitro* and murine models of KRAS(G12C)-mutant lung carcinoma. These effects are consistent with previous data showing that PI3K pathway activity is dependent on basal IGF1R signalling, specifically in KRAS-mutant lines (Molina-Arcas *et al.*, 2013).

As a separate approach to identifying intrinsic resistance mechanisms, gene expression profiling of both KRAS(G12C)-containing cell lines and human tumours revealed a baseline dichotomy between those expressing an epithelial versus a more mesenchymal signature (Solanki *et al.*, 2021). The latter expressed both high basal and feedback activation of FGFR and AXL, suggesting the possibility of biomarker-driven synergies in this population of EMT-high tumours. Other recent work on EMT and resistance to KRAS(G12C) inhibition reinforced the aforementioned KRAS-independent activation of PI3K by IGF1R, as mentioned above (Molina-Arcas *et al.*, 2019; Adachi *et al.*, 2020). In the more recent work, induction of EMT resulted in G12C inhibitor resistance, an effect partly mediated by IGF1R-activation of PI3K. These authors used also used a triple combination (using SHP2 instead of IGF1R inhibition) to drive synergy in various models.

Many cell lines with intermediate sensitivity or refractoriness to KRAS(G12C) inhibitors demonstrate rebound of pERK despite continued drug administration (Ryan *et al.*, 2020). This is associated with increased activation of several RTKs. While no single RTK inhibitor consistently provided synergy across the lines, inhibition of SHP2 (a protein tyrosine phosphatase that functions downstream of multiple RTKs to promote RAS activation (Nichols *et al.*, 2018)) synergised with G12C-inhibition to impair viability across all lines tested (Ryan *et al.*, 2020). In a more recent study, not only was this synergy reinforced but the combination was shown to result in profound tumour microenvironment (TME) remodelling, as discussed later (Fedele, Li, Teng, Connor J.R. Foster, *et al.*, 2021).

The studies above are likely to provide rational synergies to prevent intrinsic (or delay acquired) resistance. When acquired resistance does eventually occur, other strategies may be needed. Many clinical studies that have focussed on genetic mechanisms of acquired resistance have recently come to light (Awad, Liu and Arbour, 2021; Tanaka *et al.*, 2021; Zhao *et al.*, 2021). There are some recurrent themes across these. Firstly, despite careful profiling of tissue and/or circulating free DNA (cfDNA) many patients had no discernible resistance mechanisms. In one study of 38 patients who had initially responded and then relapsed on adagrasib, 21 had no putative resistance mechanisms identified by genomic profiling (Awad, Liu and Arbour, 2021). Of note, however, the original G12C mutation was not identifiable in 6/38 of these patients, all of whom had cfDNA (rather than tissue analysis). Thus, the sensitivity of this assay may be a limiting factor for detection. In a separate analysis of 43 patients treated with sotorasib, 16 had no identifiable treatment-emergent alterations (Zhao *et al.*, 2021). The second pervading theme was that resistance was associated with acquired mutations in MAPK pathway members. These included switch II pocket mutations including those that confer resistance to both inhibitors (e.g. Y96S) and those which result in heterogenous sensitivity between the two (e.g. R68M and H95D) (Awad, Liu and Arbour, 2021). The latter finding raises the

possibility of biomarker-driven switching of G12C inhibitors although this is unlikely to ever be formally studied in clinical trials. Thirdly, resistance mechanisms were heterogenous both across and even within patients, with some demonstrating alterations in several members of the pathway. This raises questions about the optimum strategy to both prevent and treat resistance when it occurs. Next, and intriguingly, many putative resistance mechanisms occurred at low variant allele frequencies (VAF). While this was in part attributed to the sensitivity of cfDNA, there is incomplete understanding of the extent to which the resistant clones drive the overall clinical picture and whether they may even be able to influence surrounding cells which do not harbour the same alterations (Zhao *et al.*, 2021). Finally, resistance with some patients was associated not with genomic alterations but with cell state changes (e.g. from adenocarcinoma to squamous cell carcinoma). There was a paucity of tissue biopsy at relapse (most patients had cfDNA analysis alone) so it is difficult to estimate the true prevalence of this change.

An intriguing study of a single patient who developed resistance to adagrasib demonstrated, amongst other variants, *de novo* occurrence of the resistant KRAS(Y96D) allele (Tanaka *et al.*, 2021). Using structural modelling, the authors demonstrated that this disrupts drug interaction with KRAS, allowing nucleotide cycling to proceed. In order to circumvent this resistance mechanism, they used the structurally and functionally distinct KRAS(G12C) inhibitor RM-018. This molecule forms a ‘tri-complex’ structure with the GTP-bound KRAS molecule, sterically occluding the interaction with downstream effectors. They showed that, in terms of viability, H358 cells bearing KRAS(G12C/Y96D) were 100-fold less sensitive to adagrasib relative to those harbouring KRAS(G12C) mutations alone. Conversely, KRAS(G12C) and KRAS(G12C/Y96D) cells were equally sensitive to RM-018. This suggests a potential therapeutic strategy to overcome this mechanism of resistance.

Thus, in conclusion, RAS proteins are important oncogenes across cancers. KRAS in particular is frequently mutated in tumours that are prevalent (lung and

colon) or highly lethal (pancreatic). Targeting KRAS has undergone a paradigm shift in recent years with the advent of covalent inhibitors against KRAS(G12C). This approach needs to be optimised but bears great potential for treatment of a significant proportion of patients with NSCLC in particular. Optimal synergies are required to maximise the benefit of this approach.

1.2 Antitumour immunity

1.2.1 Introduction

William Coley's observation in 1891 that injection of bacterial toxin was associated with regression of advanced sarcoma, is one of many examples of primitive cancer immunotherapies being used to induce tumour response (Hoption Cann, Van Netten and Van Netten, 2003). Since then, our understanding of the influence of the immune system on cancer behaviour has advanced considerably. One widely-regarded hypothesis, the immunoediting hypothesis, proposes that most clinically apparent tumours have progressed through three stages – elimination, equilibrium and escape (Schreiber, Old and Smyth, 2011). The theory surmises that throughout our lifetimes, we develop tumours that never become clinically apparent because our immune system eliminates them at an early stage. In some cases, immune elimination is incomplete, and the tumours enter a state of equilibrium where the rates of immune clearance and tumour growth are similar. Tumours may regress (immune elimination eventually prevails) or 'escape'.

Immune escape can occur through several mechanisms. One mechanism of 'escape' from immune control is by inducing an immunosuppressive state within the tumour microenvironment (TME). This can occur through recruitment of immunosuppressive cells or subversion of cells already present. Subversion may be secondary to tumour-intrinsic expression of surface and/or soluble mediators, metabolic factors, nutrient deprivation or altered pH amongst others. Therapeutic modulation of this tumour immune cross-talk can tip the balance of this interaction in favour of the immune system, facilitating tumour elimination. For example, tumour and tumour-associated immune cells can upregulate expression of programmed death-ligand 1 (PD-L1) a cell-surface molecule that can bind programmed cell death-1 (PD-1) which can be expressed on antigen-experienced T-cells. This interaction negatively regulates T cell activation, contributing to tumour immune evasion (Freeman *et al.*, 2000; Wei, Duffy and Allison, 2018). Consistent with its role in tumour immune evasion, antibodies

against programmed death-ligand 1 (PD-L1) or its receptor programmed cell death-1 (PD-1) have revolutionised the treatment of several malignancies (Robert, 2020). Nonetheless, such immunotherapy is ineffective in many cancers and where responses do occur, they are often incomplete and transient. Therefore, an improved understanding of tumour immune evasion mechanisms could help design novel synergies to improve the efficacy of immune targeting approaches, and ultimately improve patient outcome.

1.2.2 Components of the tumour immune microenvironment

1.2.2.1 Macrophages

Tumour associated macrophages (TAMs) are the most abundant immune type across several primary tumour sites, and generally correlate with worse prognosis (Gentles *et al.*, 2015). A summary of their role in the TME, and of other cells, is shown in Table 2. In a non-malignant context they may be either tissue-resident (TRM), undergoing self-renewal and adopting specialised local functions, or they may derive from circulating monocytes (MDM) usually under inflammatory conditions (Ginhoux and Guilliams, 2016). Ontogeny of macrophages in tumours is less well understood (Lahmar *et al.*, 2016). In some models of lung cancer at least, it appears that monocyte-derived macrophages form the majority of TAMs (Sawanobori *et al.*, 2008) and that impairment of CCR2-dependent monocyte recruitment can impair tumour growth (Cortez-Retamozo *et al.*, 2012). These studies, however, did not explore the temporal or spatial heterogeneity of TAM ontogeny. Using orthotopic KP tumours injected into *Map17-creER* transgenic mice crossed with the *Rosa26-LSL-tdTomato* strain (to label adult haematopoietic stem cells and their progeny), it has been shown that TRMs accumulate close to tumour cells early in tumour establishment, influencing their invasiveness and tumour immune composition (Casanova-Acebes *et al.*, 2021). However, as the tumours develop, TRMs move to the periphery while MDM accumulate within tumour stroma. Therefore, it is likely that in any given model TAM ontogeny varies temporally and spatially.

Type	Function
Macrophages	Pro-tumourigenic macrophages can inhibit T cell function, stimulate angiogenesis, liberate growth factors and remodel the ECM. Anti-tumour macrophages can stimulate Th1 and $CD8^+$ T cells responses and directly phagocytose tumour cells
Dendritic cells (DC)	Conventional type I DCs (cDC1) cross-present antigen to T cells and liberate cytokines contributing to their activation. cDC2 cells interact with $CD4^+$ T cells.
T cells	Exist as $\alpha\beta$ or $\gamma\delta$ T cells dependent on receptor structure. $\alpha\beta$ are predominantly $CD4^+$ or $CD8^+$. The latter are an important final effector mechanism of immune-mediated tumour killing.

Table 2. Major immune cell types in the TME

Phenotypically, TAMs are often described as either M1-like or M2-like. This nomenclature stemmed from studies of macrophage activation *in vitro* (Stein *et al.*, 1992; Dalton *et al.*, 1993). M1 macrophages, activated by a priming stimulus (IFN-γ) followed by a (microbial) trigger (lipopolysaccharide (LPS) or tumour necrosis factor alpha (TNF-α)), are often described as 'classically activated' macrophages. They liberate pro-inflammatory cytokines such as IL-1b and IFN-γ as well reactive oxygen and nitrogen species (ROS & RNI) in order to mount an effective response against intracellular pathogens, and tumours. M2 or 'alternatively' activated macrophages are a more heterogenous group, activated by diverse stimuli including the Th2 cytokines IL-4 and IL-13. They may express high levels of arginase and liberate IL-10 and transforming growth factor beta (TGF-β) (Martinez and Gordon, 2014). In the TME, however, TAM subtyping is complex and may not fit neatly into these categories. In a recent single cell analysis of human and mouse lung tumours, of nine human macrophage clusters and four murine macrophage clusters none exhibited an 'M1-like' gene

expression signature, suggesting limited utility of this paradigm *in vivo* (Zilionis *et al.*, 2019).

Macrophages are notoriously plastic cells and, correspondingly, have been ascribed diverse intratumoural functions which may be pro- or anti-tumoural in nature (Noy and Pollard, 2014; Cassetta and Pollard, 2018). Anti-tumoural macrophage function can be conceptualised into those relevant during tumour initiation, during local tumour progression and those during tumour metastasis.

Oncogene signalling or chronic inflammation (e.g. autoimmune, infective, irritant) can activate transcription factor networks (e.g. via NFkB) that result in tumour-intrinsic cytokine signalling that engages innate immunity from tumour initiation (Crusz and Balkwill, 2015). Specifically, macrophages may respond to such signals by secreting factors that initiate and/or promote tumor growth through mitogenic cytokines (e.g. TNF-α), growth factors (e.g. EGF/family members, WNT ligands) or mutagens (ROS and RNI) (Canli *et al.*, 2017; Cassetta and Pollard, 2018). Beyond this, macrophages can facilitate the angiogenic switch through production of vascular endothelial growth factor A (VEGFA), WNT7B, CXCL8 and other secreted factors (Lin *et al.*, 2006; Yeo *et al.*, 2014). In addition, macrophages are able to directly interact with the endothelial compartment. For example, expression of angiopoietin 2 receptor (TIE2) on monocytes facilitates binding to angiopoietin 2-expressing endothelial cells, and subsequent angiogenesis in a paracrine manner (De Palma *et al.*, 2005).

TAMs also play a role in tumour immune evasion and therefore local tumour progression. The ability of TAM to subvert the host immune response can occur via surface receptors, secreted factors or metabolic dysregulation. TAM expression of non-classical class I MHC, or co-inhibitory checkpoints including PD-L1, can negatively modulate natural killer (NK) and T cell activation (Kochan *et al.*, 2013; DeNardo and Ruffell, 2019). Immunosuppressive secreted factors include IL-10 and TGF-β, the latter being able to induce Treg formation

(Cassetta and Pollard, 2018), and chemokines such as CCL2 which can further recruit immunosuppressive myeloid cells via its receptor CCR2. A well-studied metabolic consequence of alternative macrophage activation is depletion of microenvironmental L-arginine via overexpression of the enzyme arginase 1 (Arg1). Using Lewis Lung carcinoma cells injected subcutaneously, it was shown that a subpopulation of TAM expressed high levels of Arg1, and that injection of an arginase inhibitor was able to block tumour growth (Rodriguez *et al.*, 2004). *In vitro,* these Arg1-expressing macrophages inhibited proliferation of antigen-specific T cells and blocked re-expression of the TCR CD3ζ chain. In a similar vein, TAM depletion of the amino acid tryptophan through expression of indoleamine 2,3-dioxygenase (IDO), can inhibit T cell proliferation and effector function (Viola *et al.*, 2019).

Finally, in some models, macrophages have been shown to aid the latter stages of metastasis formation – extravasation, seeding and subsequent tumour growth. In several models of breast cancer, tumour and stromal-derived CCL2 recruited inflammatory monocytes (which subsequently differentiated to MDM) to sites of lung metastases (but not primary tumours). Blocking CCL2/CCR2 interaction inhibited lung metastasis formation and prolonged survival. In addition, myeloid-derived VEGFA was important in enhancing endothelial permeability to facilitate extravasation (Qian *et al.*, 2011). In a separate study using Lewis lung carcinoma, tumour-secreted veriscan acted via macrophage TLR2 to facilitate metastases to distant sites (Kim *et al.*, 2009).

Given their association with poor prognosis and evidence of tumour-promoting activity, efforts have been made to target the TAM compartment. Conceptually this may be achieved by depleting or repolarising TAMs. Administration of a colony stimulating factor 1 receptor (CSF1R) inhibitor to patients with tenosynovial sarcoma, a tumour type characterised by high CSF1 and CSF1R, produced objective responses in the majority of patients (Tap *et al.*, 2015). This provides proof-of-concept that TAM-targeting, in a carefully selected cohort, is efficacious. This recently led to the first FDA approval in this tumour type (*FDA*

approves pexidartinib for tenosynovial giant cell tumor, 14/08/2021). CSF1R targeting, while effective in selected tumour types, potentially depletes the systemic macrophage repertoire, risking toxicity. Repolarisation of TAMs has the potential for reduced toxicity. To this end, several strategies have therapeutic potential including CD40 agonistic antibodies, toll-like receptor (TLR) stimulators and PI3K-γ inhibition (Kaneda *et al.*, 2016; Cendrowicz *et al.*, 2021). The most clinically successful strategy thus far, however, has been targeting the CD47-SIRPα interaction. CD47 is overexpressed on several cancer types and serves to protect against autophagocytosis while also affecting macrophage polarisation (Jaiswal *et al.*, 2009; Cassetta and Pollard, 2018). Early phase trials in haematological malignancy have been encouraging, leading to FDA orphan drug status and a current phase III trial for patients with myelodysplastic syndrome (Garcia-Manero *et al.*, 2021). Another agent, RRx-001, is a nongenotoxic alkylating agent whose anticancer mechanism is not well understood but partly involves inducing M1 to M2 repolarisation via a complex mechanism involving phagocytosis of drug-bound, oxidatively stressed, erythrocytes in hypoxic tumour (Oronsky *et al.*, 2021). It is being tested in a phase III trial for patients with small cell lung cancer (Oronsky *et al.*, 2019).

1.2.2.2 Dendritic cells

Several dendritic cell (DC) subsets exist based on ontogeny, phenotype and function (Wculek *et al.*, 2020). In both mice and humans, the first major division of these cells is into conventional vs non-conventional subtypes. In mice, conventional DCs (cDCs) can be subdivided into CD11b$^+$ vs CD11b$^-$ DCs. The latter (CD11b$^-$) subgroup is also known as the cDC1 subtype and include DCs that express the transcription factor BATF3. These have been shown to have a crucial role in antitumour immunity. DCs from Batf3$^{-/-}$ mice show defective cross-presentation and impaired antitumour responses to highly immunogenic syngeneic tumours (Hildner *et al.*, 2008). Non-conventional subsets include

B220^{+} plasmacytoid DCs and monocyte-derived DCs which differentiate from CCR2^{+} monocytes under inflammatory conditions.

On encountering specific cues, dendritic cells undergo maturation. Whilst this is a heterogenous process dependent on divergent environmental cues, it involves certain fundamental changes including enhanced antigen processing, migratory and co-stimulatory capacity plus liberation of various cytokines, influencing T cell differentiation (Dalod *et al.*, 2014). This process is a critical part of the cancer immunity cycle. For example, upon activation-induced CCR7 expression, DCs can enter tumour draining lymph nodes and effectively prime antitumour T cell responses (Chen and Mellman, 2013). The aforementioned cues which activate DCs can vary. For example, in one study, WT mice as well as those deficient for TLR4, TLR6 or MyD88 all generated spontaneous antitumour immune responses to subcutaneous (SC) B16.SIY melanoma tumours suggesting they are dispensable for DC activation. Conversely, those deficient in interferon regulatory factor 3 (IRF3) or stimulator of interferon genes (STING) did not, and further analysis *in vitro* and *in vivo* suggested failure of T cell priming by antigen presenting cells, including DCs, was responsible (Woo *et al.*, 2014). Conversely, immunogenic cell death, for example that elicited by chemotherapy, does require intact DC TLR4 signalling to generate a productive anti-tumour response (Kroemer *et al.*, 2013) suggesting that routes to DC activation differ according to external conditions.

Given their role in initiation of adaptive immune responses, tumours have evolved mechanisms to subvert DC recruitment or function. For example, in a BRAF^{V600E}/PTEN$^{-/-}$ melanoma model, introduction of a stabilising β-catenin mutation resulted in a lack of tumour CCL4 and consequent reduction in tumour-infiltrating Batf3^{+} DCs (Spranger *et al.*, 2017). These tumours lacked a T cell infiltrate and failed to respond to immune checkpoint blockade. Similarly, in a separate model of BRAF^{v600E} melanoma, Ptgs1/2 KO resulted in NK-mediated cDC1 recruitment in a CCL5 and XCL1 dependent manner (Böttcher *et al.*, 2018). In both studies, gene expression analyses of human tumours identified

analogous mechanisms of immune subversion suggesting that cDC targeting could be a viable strategy to synergise with checkpoint blockade. Beyond DC recruitment, the TME can subvert DC differentiation and activation thereby affecting function. Such mechanisms include tumour-intrinsic expression of CD47, veriscan, IL-10, lactic acid or induction of ER stress within DCs. In addition, a novel extracellular mechanism of DC modulation has recently been reported (Giampazolias *et al.*, 2021). This study showed that secreted gelsolin can inhibit the binding of cDC1-expressed DNGR-1 to F-actin (exposed on dead cell debris). Usually, DNGR-1 engagement by F-actin promotes cross-presentation, and hence $CD8^+$ T cell priming. Consistently, mice deficient in secreted gelsolin were able to better control the growth of various tumour models compared to WT mice and also responded better to treatment with various immunotherapy.

Several strategies have been used to exploit DCs for therapeutic purposes. The first group of strategies aim to stimulate DC maturation/activation. Imiquimod, a TLR7/8 agonist is used clinically for non-melanomatous skin cancers and has shown efficacy for the treatment of cutaneous breast cancer metastases although patient numbers were small (Adams *et al.*, 2012). An obvious limitation of such a strategy is route of administration, although oral agonists for TLR7 and other TLRs are being developed (Gardner, de Mingo Pulido and Ruffell, 2020). As mentioned previously, sensing of tumour DNA via the cGAS-STING pathway can activate DCs. It should be noted, however, that this pathway is active in other TME cells and so the precise mechanism of action will be context-specific. However, clinical activity has been limited so far; challenges include the metabolic stability of such drugs, concerns of systemic toxicity, their effect on effector T cells and mitigation of compensatory feedback loops following STING targeting (Amouzegar *et al.*, 2021). A separate group of strategies involves blocking inhibitory signals. As an example, it has been shown that DC TIM3 can interact with the alarmin HMGB1 and therefore interfere with the innate response to chemotherapy-induced cell death (Chiba *et al.*, 2012). TIM3 inhibition may therefore be an attractive strategy in combination

with chemotherapy. Finally, dendritic cell vaccines have been tested in over 200 clinical trials. Evidence of $CD8^+$ T cell responses have been seen, but these have rarely translated into meaningful clinical benefit (Wculek *et al.*, 2020). Nonetheless this is a strategy with huge potential. It is possible, perhaps even likely, that an optimal combination of DC subtype, targeted antigen, DC adjuvant and method of delivery will eventually be successful in the right patients.

1.2.2.3 T cells

T cells form a diverse group of cells of the lymphoid lineage. Those that express an $\alpha\beta$ T cell receptor (TCR) can broadly be subtyped into $CD8^+$ cytotoxic T cells, $CD4^+$ T helper cells and $CD4^+$ T regulatory cells (Tregs). Within each of these strata are yet further subtypes (differentiation fates) and transcriptional states.

Although tumour cells can be phagocytosed, for example by TAMs (Gordon *et al.*, 2017), $CD8^+$ T cells are often considered the most important final effector mechanism for immune-mediated cancer killing (Raskov *et al.*, 2021). This process requires $CD8^+$ T cell activation and proliferation. This involves: a) recognition of its cognate antigen in the context of class I MHC on a professional antigen presenting cell (APC), b) secondary (co-stimulatory) signals beginning with ligation of T cell CD28 with CD80/86 on the APC and c) liberation of cytokines, which may be autocrine, to enhance T cell proliferation and survival (Waldman, Fritz and Lenardo, 2020). Following activation in this way, the $CD8^+$ T cell is able to kill cognate antigen-expressing target cells.

Despite the potential for adaptive immunity to eliminate neoplastic cells, clinically apparent tumours have not succumbed in this way. Several mechanisms may be responsible, most of which ultimately affect the capacity of effector $CD8^+$ T cells to recognise, reach or kill tumour cells (Sharma, Hu-

Lieskovan *et al.*, 2017; Christian U. Blank, John B. Haanen, 2016). As a first requirement, tumours must present antigens likely to generate an adaptive immune response. Such antigens are either tumour-specific, being generated from somatic genomic alterations, viruses or cancer-germline gene products, or they are tumour-associated, including overexpressed proteins or differentiation antigens only expressed in the tumour cells and its tissue of origin (Coulie *et al.*, 2014). Presentation of such antigens requires intact antigen processing machinery. Thus, lack of immunogenic antigens or the machinery necessary to process them may prevent tumour immune rejection.

Nonetheless, many clinically apparently tumours do present potentially immunogenic antigens, yet escape $CD8^+$ T cell mediated destruction. One mechanism of tumour escape, involves the action of inhibitory checkpoint molecules that restrain/alter $CD8^+$ T cell activation, proliferation, effector function and metabolism (Waldman, Fritz and Lenardo, 2020). For example, ligation of $CD8^+$ T cell-expressed PD-1 with stromal or tumour cell-expressed PD-L1 can inhibit T cell proliferation and affect survival (Raskov *et al.*, 2021). As discussed later, PD-L1 upregulation on tumour cells can be secondary to oncogenic signalling (Coelho *et al.*, 2017) while PD-1 upregulation on T cells may be part of a broader hyporesponsive state in these cells (Philip and Schietinger, 2021). Such T cell dysfunction is still not completely understood in terms of its causes, molecular programs, phenotype and functional consequences. One theory proposes that early in tumorigeneses, low levels of tumour antigen combined with lack of co-stimulation lead to a dysfunctional state akin to anergy (early dysfunction). As the tumour progresses, the combination of a continuous antigen stimulation along with a hostile TME with immunosuppressive cells, cytokines, nutrient deprivation and metabolic stress results in a more profound, ‘late dysfunctional state’. Phenotypically, this is characterised by upregulation of various inhibitory immune checkpoints including PD-1, LAG3 and TIM3 while functionally, cells progressively lose effector abilities in a well-described hierarchical manner, including effector

cytokine secretion and proficiency in target cell killing (Philip and Schietinger, 2021).

Given the negative role of PD-1/PD-L1 signalling in T cell activation, inhibitors of this checkpoint have been used therapeutically with success in specific tumour types (Robert, 2020). Nonetheless, the precise mechanism and nature of the cells that execute the response is not known (Wei, Duffy and Allison, 2018). There is evidence to suggest that terminally dysfunctional T cells are epigenetically fixed, and therefore unable to reinvigorated by checkpoint blockade (Philip *et al.*, 2017). Nonetheless specific T cells, for example those in tumour draining lymph nodes (TDLNs) or that have recently entered the TME may be in a more progenitor-like state and therefore have capacity to increase effector function in response to checkpoint blockade (Philip and Schietinger, 2021). In support of this, a recent study extracted tumour infiltrating lymphocytes (TIL) from patients with NSCLC who had progressed on nivolumab (an anti-PD-1 antibody), expanded and activated them *ex vivo* before reinfusion (Creelan *et al.*, 2021). Several patients showed complete responses. Although the extracted and reinfused TIL products were heterogenous, it is possible that the cells that responded to IL2 *ex vivo* were the progenitor-like or 'less' dysfunctional T cells that had retained proliferating capacity.

Beyond $CD8^+$ T cells, the contribution of $CD4^+$ T helper cells (hereafter $CD4^+$ cells) to tumour immune responses cannot be overlooked. Indeed, the TIL products for many patients in the aforementioned NSCLC study contained tumour-specific $CD4^+$ cells, and a durable antitumour response was observed in a patient with cholangiocarcinoma after infusion of a tumour-specific $CD4^+$ product (Tran *et al.*, 2014). $CD4^+$ T cells are a heterogenous population. Their most studied role is in the provision of 'help' to $CD8^+$ T cells directly (e.g. through secretion of IL2) and indirectly (e.g. through the maintenance of cross-presenting DCs, for example by upregulation of CD40L). In addition, if polarised towards a T_H1 phenotype, they can liberate IFNγ and TNFα, both of which can

have direct antitumour effects. Furthermore, it has also been shown that these cells are capable of direct cytotoxicity, dependent on the transcription factor BLIMP1 (Śledzińska *et al.*, 2020). In this study, melanoma-specific (tryp-1-specific) $CD4^+$ cell transfer into lymphodepleted mice injected with the B16 melanoma line resulted in $CD4^+$ tumour infiltration and upregulation of GzmB in these cells. Loss of Blimp-1 prevented this expression while loss of T-bet prevented IFN-γ expression suggesting different transcriptional regulators of polyfunctionality.

In the study above, acquisition of $CD4^+$ cell cytotoxicity was restrained through the presence of regulatory T cells (Tregs). Tregs are a subset of $CD4^+$ cells characterised by the transcription factor FOXP3 and the high affinity IL2 receptor subunit CD25 which, in physiology, are indispensable for the maintenance of self-tolerance (Vignali, Collison and Workman, 2008). Such cells are able to exert immunosuppression via several mechanisms (Togashi, Shitara and Nishikawa, 2019). These include competition for IL2, inhibition of antigen presenting cells (e.g. through CTLA-4 expression), secretion of soluble factors including cytokines (e.g. IL10) and adenosine and even direct cytotoxicity against immune effectors through perforin and granzyme secretion. In support of this, lack of CTLA4 specifically in murine Tregs leads to fatal autoimmunity (Wing *et al.*, 2008). As further evidence for the importance of Tregs in cancer it is notable that the aforementioned study interrogating the ontogeny of TAM in lung cancer (Casanova-Acebes *et al.*, 2021) demonstrated that TRMs recruit Tregs early in NSCLC and that deletion of such TRMs not only reduced Treg numbers but likely also their immunosuppressive capacity as evidenced by reduced CTLA4 and CD73 expression.

1.2.2.4 Other immunosuppressive TME populations

The TME is of inordinate complexity and several other cell types including NK cells, neutrophils, B cells and non-immune types including cancer-associated fibroblasts (CAFs) and endothelial cells amongst others all mediate

immunosuppressive functions. It is likely that the relative importance of these cell types, and the ones previously mentioned, depend on diverse factors including the primary or metastatic tissue site, histology and stage of the cancer, systemic immune status, the microbiome, any anti-cancer treatment received and more (Christian U. Blank, John B. Haanen, 2016).

NK cells are strictly cells of the innate system, since their receptors are germline-encoded, however their effector mechanisms overlap profoundly with those of cytotoxic $CD8^+$ T cells. Discharge of their killing mechanisms depends on the balance between activation inflammatory signals mediated by diverse cell surface receptors (Miller and Lanier, 2019). In humans, activating receptors include CD16, NKp30, NKp44 and NKp46 while inhibitory receptors include certain killer inhibitory receptors (KIRs), NKG2A and LILRB1. Besides the activating receptors, co-activating receptors which enhance NK cell activation, include DNAM1, 4-1BB and 2B4. Co-inhibitory receptors including PD-1, LAG3 and TIM3 are also relevant (Cózar *et al.*, 2021). Many such inhibitory receptors recognise MHC class I whose genes are often downregulated in human melanoma and lung cancer, for example (Rodig *et al.*, 2018; Rosenthal *et al.*, 2019). NK cells are capable of eliminating some tumours that lack class I MHC (Karre *et al.*, 1986) however this mechanism is subverted in many tumours. Mechanisms of subversion include the immunoediting of activating NK ligands, the expression of alternative inhibitory receptors and a hostile TME leading to ineffective NK persistence after killing (Cózar *et al.*, 2021). Mechanisms to re-engage NK cells leading to effective killing include the use of antibodies against inhibitory receptors (e.g. anti-NKG2A), stimulation of ADCC by tagging tumour cells with IgG1-containing antibody, the use of bispecific antibodies able to ligate NK activating receptors and tumour antigen or therapies to upregulate stress-ligands on tumours (Miller and Lanier, 2019).

Like macrophages, neutrophils are plastic cells of the myeloid lineage. Much interest in the role of neutrophils in cancer has stemmed from the negative association between tumour associated neutrophils (TAN) and survival plus the

use of the neutrophil-lymphocyte ratio as a promising biomarker for checkpoint inhibitor therapy (Havel, Chowell and Chan, 2019). However, given their plasticity, neutrophils have been ascribed both anti and pro-tumourigenic function and, accordingly, been given the nomenclature N1 and N2 neutrophils respectively. As such, the relationship between neutrophils and cancer prognosis is complex. Although the majority of studies describe a negative association between TAN and overall survival, the relationship depends on diverse factors including the type of tumour and its stage, neutrophil phenotype and location within the tumour (Shaul and Fridlender, 2019). As an example of the anti-tumour effect of TAN, in a study of early NSCLC patients TAN interacted with T cells to induce T cell proliferation and IFNγ liberation suggesting that rather than being immunosuppressive, these TAN promoted anti-tumour responses (Eruslanov *et al.*, 2014). In a follow-up study, a neutrophil subset with APC characteristics, able to cross-present antigen, was found in patients with early-stage NSCLC dependent on the synergistic action of TME-derived IFNγ and GM-CSF (Singhal *et al.*, 2016). Conversely TAN can inhibit anti-tumour immunity by secreting chemokines (e.g. CCL17 recruiting Tregs and CXCL8 which recruits further neutrophils and promotes tumour cell proliferation), upregulating ARG1, promoting angiogenesis and metastases through MMP9 secretion and contributing to the metastatic niche through neutrophil extracellular trap (NET) formation (Shaul and Fridlender, 2019; Mukaida, Sasaki and Baba, 2020).

The role of B cells in cancer has not been as thoroughly studied as their T cell counterparts. However, recent publications focussing on tertiary lymphoid structures (TLSs) in melanoma showed that at the very least, B cell markers have the potential to be prognostic (Cabrita *et al.*, 2020; Helmink *et al.*, 2020). In one such study it was shown that co-occurrence of $CD8^+$ and $CD20^+$ cells in the TME of patients with metastatic melanoma independently predicted improved overall survival (Cabrita *et al.*, 2020). These tumours contained TLSs and increased numbers of $TCF7^+$ (naïve or memory) T cells compared to non-TLS bearing tumours, suggesting ongoing recruitment of such cells to the TLS-

bearing TME . Separately, a study looking at patients with metastatic melanoma who were treated with neoadjuvant checkpoint blockade, found that B cell markers (in bulk RNAseq) were the most differentially expressed between responders and non-responders and validated this in a renal cell carcinoma cohort. Histological analysis showed these B cells were part of TLS structures and single cell analysis of these cells revealed enrichment of class-switched memory B cells in responders suggesting direct contribution to the improved outcome (Helmink *et al.*, 2020). Beyond their positive influence within TLSs, B cells have also been shown to have immunosuppressive functions too (Michaud *et al.*, 2021). Mechanisms of B cell immunosuppression include the expression of inhibitory checkpoints such as PD-L1 and the liberation of immunosuppressive cytokines including IL-10 and IL-35. The signals which promote such immune regulatory function of B cells are still being explored.

1.2.3 Classification of the tumour immune microenvironment

Techniques that allow spatial profiling of tumours have resulted in classifications of different types of TME. In one such classification based on moderate-resolution TME analysis, three broad-classes were described (Binnewies *et al.*, 2018).

Name	Description
Infiltrated-excluded	Lack cytotoxic lymphocytes, poor response to immunotherapy
Infiltrated-inflamed	Activated lymphocyte infiltration. Often PD-L1 high
Tertiary lymphoid structure containing	Presence of cellular aggregates of lymphoid cells architecturally resembling lymphoid tissue

Table 3. Types of tumour immune microenvironment

Infiltrated-excluded TMEs (I-E) are those broadly populated with immune cells but void of cytotoxic lymphocytes. In such TMEs, cytotoxic cells are often located at the tumour periphery or within fibrotic nests. Such I-E tumours have

also been called ‘cold’, and demonstrate poor response to immunotherapy when compared with T-cell-infiltrated lesions (Daud *et al.*, 2016). In addition to the altered spatial distribution of T cells in this TME class, the T cells lack expression of activation markers such as granzymes and interferon-gamma (IFN-γ) (Binnewies *et al.*, 2018). Importantly, the presence of a ‘cold’ TME does not necessarily imply lack of immunogenic antigen expression by tumour. Instead, such a TME may be secondary to various tumour-intrinsic or extrinsic mechanisms which affect innate immune sensing, or modulate T cell recruitment, survival, proliferation or function (Gabrilovich and Nagaraj, 2009; Feig *et al.*, 2013; Beatty *et al.*, 2015; Spranger, 2016). In addition, in some tumours characterised by a desmoplastic stroma the physical barrier imposed by the matrix, plus fibroblast-secreted immunosuppressive factors, may be the primary mechanism of lymphocyte exclusion (Pickup, Novitskiy and Moses, 2013).

The next subtype of TME, infiltrated-inflamed (I-I), is characterised by infiltration of activation marker-expressing $CD8^+$ T cells into the tumour core. The co-existence of viable tumour with such T cells implies the presence of immune escape mechanisms. As evidence of this, tumour and stromal cells in many such tumours express high levels of PD-L1.

The third class of tumours, essentially a subclass of I-I tumours, have tertiary lymphoid structure (TLS)-bearing TMEs. TLSs are cellular aggregates primarily composed of lymphoid lineage cells such as naïve and activated T cells (including T follicular helper cells), B cells, plasma cells and follicular dendritic cells arranged in a manner architecturally similar to secondary lymphoid organs (Sautès-Fridman *et al.*, 2019). Evidence for the relevance of TLSs in human malignancies includes two recent studies which looked at separate cohorts of patients with melanoma or renal cancer and found association between improved overall survival and the presence of tertiary lymphoid structures (Cabrita *et al.*, 2020; Helmink *et al.*, 2020).

While alternative TME subtyping has also been described (Hegde, Karanikas and Evers, 2016), there is overlap with the classes above. Furthermore, there is consistent evidence that tumour immune composition (which reflects TME structure) can be both prognostic, and predictive of therapeutic response to anti-PD-1 or PD-L1 antibodies (Herbst *et al.*, 2014; Tumeh *et al.*, 2014). Therefore, an understanding of the factors influencing TME structure may suggest therapeutic targets that could be used to remodel the tumour contexture and generate clinical responses. Tumour intrinsic factors polarising the tumour microenvironment can be conceptualised in four (potentially related) categories: a) Antigen load/landscape, b) Antigen presentation, c) 'Genetic' T cell exclusion (e.g. oncogenic signalling altering the tumour secretome) and d) Resistance to (T cell) effector mechanisms (Sharma *et al.*, 2017) . The latter 3 may all be affected by oncogenes and TSGs some of which are discussed later.

The effect of antigenic load on microenvironment composition is illustrated well by the consensus molecular subtypes of colorectal carcinoma (CRC), a tumour type that is generally insensitive to checkpoint inhibition as monotherapy (Guinney *et al.*, 2015). Consensus subtype 1 of this international classification is characterised by microsatellite instability and a high mutational burden. This is hypothesized to explain the high expression of $CD8^+$ & T_H1 T cell genes and high PD-1 expression seen in these tumours. Consequently, this subtype of CRC is uniquely sensitive to anti-PD-1 therapy despite having poor survival after conventional therapies (Guinney *et al.*, 2015).

Tumour 'extrinsic' factors polarising the microenvironment include various immune-polarising cell types such as those of the myeloid lineage, regulatory T cells (Tregs), cancer associated fibroblasts and endothelial cells (Wong *et al.*, 2020; Arwert *et al.*, 2021). Of note, these 'intrinsic' and 'extrinsic' factors, rather than being independent, interact such that immunosuppressive cell types can modulate tumour cell-intrinsic signalling and vice-versa. As just one example, oncogenic STAT3 suppression can result in liberation of cytokines that induce activation of innate immune cells. These cells, in turn released further pro-

inflammatory mediators contributing to anti-tumour cytotoxicity (Wang *et al.*, 2004).

1.2.4 Tumour-intrinsic mechanisms of immune escape

1.2.4.1 Introduction

The TME consists of a variety of cell types which shape the immune response to the tumour. However, arguably the most important cell type in shaping immune responses are the tumour cells themselves. Tumour cells can influence tumour immunity in several ways. Firstly, these cells may harbour tumour-associated or tumour-specific antigens capable of activating adaptive immunity while conversely they may, often epigenetically, suppress expression of such molecules or the machinery required to present them on the cell surface. However, beyond the 'intrinsic' immunogenicity of a tumour cell, oncogene and tumour-suppressor gene (TSG)-mediated signalling pathways for example by KRAS (and other RAS family members), TP53, WNT, PI3K and STK11 amongst others have been shown to have diverse effect on TME immune polarisation (Nguyen and Spranger, 2020). This can be via a variety of mechanisms including alteration of cell-surface molecules (Coelho *et al.*, 2017), secreted factors (Luke *et al.*, 2019) or altered metabolism (Scharping *et al.*, 2021).

Given the clonal nature of many of these, it is likely that this influence extends throughout the disease course, from the earliest invasive (or even pre-invasive) lesion until metastatic dissemination to various sites. As an example, work in pre-invasive squamous cell lung cancer in patients demonstrated altered cancer cell-intrinsic antigen presentation and expression of 4-1BBL in lesions that progressed to invasive cancer versus those that regressed (Pennycuick *et al.*, 2020). Furthermore, a study in murine NSCLC demonstrated that early lesions co-opt alveolar macrophages to influence immunosuppressive cell composition (Casanova-Acebes *et al.*, 2021).

Here we describe some of the immune effects that oncogenes and TSGs can have.

1.2.4.2 KRAS and other RAS family members

Although the canonical roles for KRAS pertain to its influence on proliferation and survival, it is becoming clearer that it also influences the hallmarks of immune evasion and tumour-promoting inflammation (Hamarsheh *et al.*, 2020). The ability of oncogenic KRAS to produce these effects may not be surprising. Firstly, RAS family members including KRAS have been shown to activate NFkB signalling in the epithelial compartment; this influences transcription of various pro-inflammatory cytokines (Finco *et al.*, 1997; Kim *et al.*, 2002). Furthermore, MAPK signalling is responsible for many downstream effects of TLR signalling in macrophages, and AP-1 (a key downstream mediator of KRAS signalling) is necessary for proper T cell activation and cytokine production (Kawasaki and Kawai, 2014; Atsaves *et al.*, 2019). In wound healing, a process necessitating proliferation of the epithelial compartment, there is abundant epithelial-immune cross-talk and evidence that the epithelial compartment proliferates in response to cytokines such as IL6 (Kuhn *et al.*, 2014; Brazil *et al.*, 2019).

With this in mind, there is accumulating literature demonstrating the ability of oncogenic RAS to induce cytokine production that can influence tumorigeneses and antitumour immunity. One well-studied example is IL6. This is a pleiotropic cytokine most commonly associated with acute inflammation. Multiple studies have demonstrated that oncogenic RAS can liberate IL6 from various cell types and that this required for tumourigenesis (Ancrile, Lim and Counter, 2007). The direct mechanism of IL6 leading to this effect is likely to be context dependent and, indeed, in one study IL6 *deficiency* promoted tumour initiation through influx of iNOS-expressing macrophages (Qu *et al.*, 2015). In fact, the effects of most cytokines are difficult to summarise succinctly and will depend on whether the tumour is early or advanced, the concentration and temporal properties of

the cytokine, the cells present in the TME, their receptor expression patterns, other cytokines present etc. For this reason, with the exception of a few, most cytokines are capable of being both pro or anti-tumourigenic. Taking this into account, it is notable that while IL6 can act to directly stimulate tumour cell proliferation and angiogenesis, it can also remodel the TME to be more immunosuppressive. Studies in murine pancreas and lung cancer models have shown that the IL6/STAT3 axis increases influx of immunosuppressive myeloid cells, although it is not always clear upon which cell types the IL6 acts to mediate this effect (Fukuda *et al.*, 2011; Caetano *et al.*, 2016).

Beyond IL6, oncogenic RAS can affect expression of the ELR$^+$ CXC chemokines which generally recruit cells of the myeloid lineage. Across a variety of cell lines, it was shown that all RAS isoforms could induce secretion of the entire family of ELR$^+$ CXC chemokines although the extent of increase over control varied between the cell lines (O'Hayer, Brady and Counter, 2009). Furthermore, mice deficient in CXCR2 were resistant to spontaneous, typically RAS-mutated, skin tumours (O'Hayer, Brady and Counter, 2009). Thus, similar to IL6, CXCL chemokines have been implicated in RAS-driven tumorigeneses, for example by acting in the TME. Using subcutaneously injected HeLa cells it was shown that CXCL8 was tumorigenic by promoting myeloid cell recruitment and neovascularisation without direct tumour autonomous effect (Sparmann and Bar-Sagi, 2004). Similarly, in a lung carcinoma model, treatment with an anti-CXCR2 antibody affect tumour growth *in vivo* only (Wislez *et al.*, 2006).

Beyond IL6 and the ELR$^+$ CXC chemokines, RAS-mutated tumours have been linked to secretion of several further cytokines/chemokines with potentially immunomodulatory properties, including IL1β, IL10, TGF$-\beta$, CCL5 and recruitment of Th17 lymphocytes secreting tumour-promoting IL17 (Carvalho *et al.*, 2018). As usual, the quantity of liberated cytokines and their effects vary between models, and this has to be borne in mind when making generalisations about the potential for targeting the TME-modulating effects of RAS therapeutically. It is likely that a biomarker or tumour type-specific approach

would maximize the likelihood of therapeutic benefit. Lack of such patient selection may underscore the failure of these therapies thus far (Hamarsheh *et al.*, 2020). As mentioned above, given the pleiotropic nature of such cytokines, their effects may differ during the time course of the disease (e.g. be pro-tumourigenic or anti-tumourigenic at different times). Intriguingly, in an exploratory analysis of a trial in which the IL1β inhibitor canakinumab was used to prevent recurrent vascular events after myocardial infarction, patients who received the drug had a lower incidence and mortality rate from lung cancer than those who received placebo (Ridker *et al.*, 2017). Conversely, they had a higher rate of infections. This provides an intriguing hypothesis for the utility of IL1β inhibition early in the course of disease and, to this end, ongoing trials are taking place in early stage or adjuvant disease (NCT03968419, NCT03447769).

Beyond cytokines and chemokines, RAS-mutated tumours have also been shown to liberate various growth factors including GM-CSF. In the models studied, GM-CSF was shown to promote the expansion of immunosuppressive myeloid populations in the primary tumour (Bayne *et al.*, 2012; Pylayeva-Gupta *et al.*, 2012). Tumour secretion of GM-CSF was also shown to be important in a model of metastases from pancreatic adenocarcinoma where it influenced the differentiation of monocytes to immunosuppressive DCs capable of recruiting Tregs and suppressing $CD8^+$ T cells (Kenkel *et al.*, 2017). This data is somewhat paradoxical given the immunostimulatory effect of GM-CSF in other contexts. Indeed, it has been used as an adjuvant in anti-cancer vaccines. As with many cytokines, the pleiotropic nature of GM-CSF effect may depend on its relative concentration plus tumour and host tissue-intrinsic factors and therefore, once again, the context-specific effect of RAS' ability to liberate these cytokines needs to be borne in mind.

As well as secreted factors, membrane-bound molecules may influence tumour immune evasion. In various model systems, oncogenic RAS has been shown to upregulate PD-L1 expression. For example, transformation of human lung bronchial epithelial cells resulted in PD-L1 upregulation while blocking MEK

activity in this line or the human lung adenocarcinoma line H358 reduced PD-L1 expression (Chen *et al.*, 2017), consistent with work in H1373 and H441 KRAS-mutant lung adenocarcinoma lines (Sumimoto *et al.*, 2016). Our lab later demonstrated that this effect was, at least in part, due to the ability of oncogenic RAS to inhibit the RNA-destabilising function of tristetraprolin (TTP) (Coelho *et al.*, 2017). As a result, PD-L1 mRNA stability, and protein expression, increased. TTP and its ability to destabilise target mRNA is discussed later in this introduction.

Of note in the cell lines interrogated in the aforementioned studies, AKT inhibition did not have the same effect on PD-L1 expression as inhibiting MEK. However, other studies *have* shown a role for the PI3K/mTOR pathway in PD-L1 regulation (Lastwika *et al.*, 2016). This is consistent with work on an extensive panel of melanoma cell lines (with varying BRAF, NRAS or PTEN status) which showed variable effect of inhibitors against BRAF, MEK or AKT on PD-L1 expression, even when considering lines with common genetic alterations (Atefi *et al.*, 2014). This suggests that the genomic and epigenomic background likely modulates the effect of KRAS signalling on PD-L1 expression. Consistent with the pre-clinical data, there is also suggestion that KRAS upregulates PD-L1 in patients, although it is difficult to exclude smoking and tumour extrinsic PD-L1 induction by IFNγ as the predominant mechanism of PD-L1 upregulation (Huynh *et al.*, 2016; Ji *et al.*, 2016)

While many studies show the effect of oncogenic RAS in isolation, human lung tumours have a high tumour mutational burden and contain aberrations in multiple oncogenes and TSGs. As an example of the potential for co-operation between oncogenes to influence the TME, a study looking at co-activation of MYC in a lung model driven by KRAS(G12D) demonstrated dramatic TME alteration upon MYC activation (Kortlever *et al.*, 2017). This included CCL9-driven TAM recruitment, IL-23 mediated NK exclusion and a dramatic increase TAM-driven angiogenesis. More commonly, however, human KRAS-mutated lung cancer is partitioned according to aberrations in TSGs such as P53,

KEAP1 and STK11 so efforts on understanding how these co-operate with KRAS may be useful. To this end several studies have looked at STK11/LKB1 loss in KRAS-mutant lung adenocarcinoma models, fuelled by observations in patients that these tumours have a poor prognosis and have features of an excluded TME (Skoulidis *et al.*, 2018). Mechanistically, it has been suggested that STK11 loss results in enhanced epigenetic plasticity and, under selective pressure, silencing of STING (Kitajima *et al.*, 2019). STING silencing led to reducing IRF3-mediated transcription and increased NFkB signalling, including enhanced immunosuppressive myeloid cell recruitment.

Much previous data relating to the ability of RAS to influence tumour immunity relied on the ability to switch RAS on/off *in vitro*, or by studying the importance of identified RAS-targets by knockdown. Often, when such experiments were performed *in vivo*, the perturbation was instigated from the onset of tumour implantation (or spontaneous generation in GEMMs). As alluded to above, the effect of cytokines such as IL6 and, indeed, mechanisms that a tumour uses to evade immunity, may change as the tumour develops. So, while innate immune effects regarding IL6 and CXC chemokines may be important at tumour initiation there may be additional RAS-mediated immune effects in established tumours.

The advent of mutant-specific KRAS(G12C) inhibitors, as discussed above, has allowed us to flexibly inhibit tumour-specific oncogenic KRAS *in vitro* and *in vivo* giving the opportunity to study the immune-modulatory effects in manner not possible before. In five human xenograft models of NSCLC, inhibition of oncogenic KRAS using MRTX849 induced downregulation of CXCL1, CXCL8, NT5E and VEGFA mRNA, downregulation of CD274 (PD-L1) mRNA and upregulation of class I MHC (Briere *et al.*, 2019). In a syngeneic model (CT26, colon carcinoma), treatment reduced myeloid-derived suppressor cell infiltration, increased macrophage ‘M1’ polarisation, recruited dendritic cells and increased T cell number (including T regulatory cells). Furthermore, the magnitude and duration of response to MRTX849 treatment of CT26 tumours in

immune compromised mice was diminished relative to wild-type mice. This data suggests that even as monotherapy, therapeutic MRTX849 efficacy is partially due to the generation of an adaptive anti-tumour immune response.

In a separate study, long-term cures induced by AMG 510 in a subcutaneous CT26 model were also suggested to rely on anti-tumour immunity (Canon *et al.*, 2019). Similar to the experiments with MRTX849, only 1/10 mice had durable regression with AMG 510 alone, however combination with anti-PD-1 therapy resulted in complete responses in 9/10 mice. Again, KRAS(G12C) inhibitor treatment resulted in an increase of T cells, $CD103^+$ cross-presenting dendritic cell and macrophage infiltration while also increasing T-cell chemoattractant cytokines, such as CXCL9-11. MEK inhibitor treatment in the same model did not have this effect and furthermore, MEK inhibition but not AMG 510 was shown to impair T cell proliferation in a co-culture system in vitro. This may partly explain the lack of clinical success when combining MEK or BRAF inhibition with immunotherapy while also suggesting that use of mutant-specific inhibitors such as AMG 510 could overcome this.
Further evidence for the potential of KRAS(G12C) inhibition to reduce the immunosuppressive tumour microenvironment produced by oncogenic KRAS and potentially sensitize tumours to immune checkpoint blockade came from our lab, using the 3LL-ΔNRAS murine lung carcinoma model (van Maldegem *et al.*, 2021). Using imaging mass cytometry (IMC), significant changes in tumour immune contexture induced by KRAS inhibition were clearly evident. These included infiltration of $CD8^+$ cells which displayed PD-1 upregulation especially when in close proximity to tumour cells, suggesting tumour-driven activation.

In a pancreatic cancer model, KRAS(G12C) inhibition again resulted in an increase in T cell chemoattractants and reduction in myeloid-derived suppressor cells but intriguingly, these changes were more pronounced with SHP2/KRAS-G12C dual inhibitor treatment (Fedele *et al.*, 2021). Moreover, these effects were enhanced yet further when anti-PD-1 therapy was also

included, raising the intriguing possibility of using a triple combination of dual targeted therapy with checkpoint blockade in the clinic.

Consistent with the increase in T cell chemoattractants, class I MHC and PD-L1 mentioned in various studies above, in mouse models of pancreatic ductal adenocarcinoma KRAS-dependent evasion of NK and B cell responses was found to be due to (MYC-mediated) repression of the Type I Interferon pathway (Muthalagu *et al.*, 2020).

Based on such pre-clinical evidence, trials combining KRAS(G12C) inhibitors and immunotherapy are underway. CodeBreak 101, a multi-arm phase I trial, is investigating several combinations involving AMG 510, including a combination arm with checkpoint blockade. The combination of MRTX849 and pembrolizumab cleared the dose-limiting toxicity observation period in the phase I/II KRYSTAL-1 trial and is now formally entering the phase II stage, as the KRYSTAL-7 trial where MRTX849 will be combined with pembrolizumab in two arms, according to PD-L1 tumour proportion score. Finally, GDC-6036 is being combined with atezolizumab (anti-PD-L1) in a phase Ia/Ib trial and JDQ443 with the anti-PD-1 antibody spartalizumab in a phase Ib/II trial that opened in February 2021.

1.2.4.3 Other tumour intrinsic pathways influencing the immune TME

Besides RAS specifically, individual components of downstream signalling pathways can also affect tumour-intrinsic programs promoting immune evasion. For example, vemurafenib (an inhibitor of BRAF(V600E)) increases the expression of MHC class I in sensitive cells and thus renders them more susceptible to CD8-mediated killing (Boni *et al.*, 2010; Frederick *et al.*, 2013). Furthermore, BRAF inhibition in melanoma cell lines reduced production of IL6, IL-10 and VEGF (Sumimoto *et al.*, 2006). Following such preclinical data, trials have attempted to combine immunotherapy with BRAF and MEK inhibition. Recent early phase clinical trials have attempted the triple combination of

BRAF, MEK and PD-(L)1 inhibition in patients with advanced, untreated, melanoma (Ribas *et al.*, 2019, 2020). While this led to a high proportion of objective response (> 70%), the grade 3/4 toxicity rate was also very high (upto 73%). Thus, although potentially efficacious, the tolerability of such combinations will have to be assessed in larger scale trials. Furthermore, its benefit over and above sequencing the therapies is currently uncertain.

The next best studied RAS effector pathway is the PI3K/AKT/mTOR axis. Loss of PTEN, a negative regulator of PI3K signalling, in melanoma models inhibited T-cell mediated killing and trafficking into tumours (Peng *et al.*, 2016). The same authors showed that patients with melanoma and PTEN loss had reduced T cell infiltration within their tumours and, , *ex vivo*, their T cells were less likely to expand successfully. Functionally, they demonstrated that PTEN loss resulted in tumour-intrinsic upregulation of immunosuppressive cytokines including CCL2 and VEGFa. Other studies supporting the hypothesis for a role of PTEN in anti-tumour immunity include interrogation of The Cancer Genome Atlas (TCGA) sarcoma data set showing that PTEN deletion correlates with reduced expression of genes encoding T cell markers and second study showing PTEN loss in an isolated progressing tumour in a patient with uterine cancer on checkpoint inhibition (Kalbasi and Ribas, 2020).

The tumour suppressor p53 is mutated in 50% of all cancers and, like the RAS family, it is being increasingly appreciated that this profoundly affects tumour immune composition (Blagih, Buck and Vousden, 2020). Understanding its biology is especially important in lung cancer where tumours co-mutated in KRAS and p53 cluster separately, display higher expression of PD-L1 and markers of T cell infiltration and respond better to immune checkpoint inhibition than other KRAS-mutated tumours (Skoulidis *et al.*, 2015). Nonetheless, the knockout of P53 in pancreas and lung cancer models already carrying KRAS pathway mutations, resulted in further infiltration of immunosuppressive myeloid cells, Tregs and systemic T cell dysfunction (Blagih *et al.*, 2020). The same authors showed in another model, using doxycycline-inducible KRAS(G12D),

that removal of doxycycline reduced myeloid cell numbers but not Tregs suggesting that while KRAS and p53 co-operate to develop an immunosuppressive TME, some effects (at least in this model) are specific to p53.

Beyond the MAPK pathway and related components, the WNT-β-catenin pathway has also received attention for its ability to affect tumour immune responses (Kalbasi and Ribas, 2020). Its role in the CCL4-mediated recruitment of cross-presenting dendritic cells has already been discussed (Spranger, Bao and Gajewski, 2015) but beyond this, several studies have shown associations between activation of the pathway and the presence of an immune-excluded TME across several cancers (Kalbasi and Ribas, 2020). Furthermore, secretion of WNT-ligands by tumour cells can alter dendritic cell metabolism and affect T cell function (Zhao *et al.*, 2018).

As a separate strategy, several studies have studied the effect of cell-cycle checkpoints on tumour-intrinsic immunity. In one, the authors interrogate several murine models of breast and other solid tumours and found that CDK4/6 inhibitors were able to increase tumoural antigen presentation (Goel *et al.*, 2017). This was in part due to increased intracellular dsRNA stimulating production of type III interferons. Using a different approach, another group single-cell profiled 33 melanoma tumours and identified a tumour cell-intrinsic expression program that associated with T cell exclusion and predicted worse survival (Jerby-Arnon *et al.*, 2018). This program included many CDK target genes. Expression was suppressed by CDK4/6 inhibition both *in vitro* and *in vivo.*

Thus, in conclusion, several oncogenic and tumour suppressor cell-intrinsic programs are able to influence the tumour immune response through influencing the secretion of soluble factors, cell surface molecules or cell-intrinsic programs such as interferon response pathways. A deeper

understanding of the effect of such pathways will allow the development of rational synergies with the potential for clinical benefit.

1.3 Biology of tristetraprolin

1.3.1 RNA degradation and tristetraprolin

Gene expression profiles are often used to infer the functional state of a cell, driven predominantly by underlying transcriptional networks. However, steady-state gene expression reflects the net result of transcription *and* mRNA degradation. In relative terms, transcription is much slower than degradation. To this end, 'housekeeping' genes tend to have relatively long half-lives (stable mRNA) while gene groups such as transcription factors, cytokines and growth factors are enriched for short-half-life mRNAs (unstable) (Yang *et al.*, 2003). This instability gives the cell a mechanism of rapidly lowering mRNA levels by ceasing transcription. Conversely, increasing their stability can quickly increase their steady-state levels potentially more rapidly than may be achieved by stimulating transcription. In either case the cell is able to rapidly respond to external stimuli such as infection.

Mature mRNAs contain stability-promoting structures including the 5'-cap and 3' poly(A) tail. Degradation of mRNA must commence with disruption of one of these structures or endonucleolytic cleavage however, in eukaryotes, initiation by poly(A)-shortening is the commonest mechanism (Garneau, Wilusz and Wilusz, 2007). Regardless of the pathway through which degradation occurs, stability is primarily a function of the repertoire of proteins that associate with an mRNA, forming messenger ribonucleoprotein (mRNP). mRNP composition in turn, depends in large part on sequence-specific determinants found largely in the 5' and 3' untranslated regions (UTRs) of the message (Garneau, Wilusz and Wilusz, 2007). Of such sequence-specific determinants, AU-rich elements (AREs) are the most well characterised (Barreau, Paillard and Osborne, 2005). These consist of 50-150 nucleotide sequences rich in both adenine and uridine and, crucially, containing a core pentamer of AUUUA. Beyond the core pentamer, flanking A and U nucleotides are necessary for functional stabilisation or destabilisation by ARE-binding proteins although there is no consensus on the exact requirements here (Bakheet *et al.*, 2001; Bakheet, Hitti

and Khabar, 2018). Furthermore, while AREs were initially discovered and characterised in terms of their 3' UTR location, it has recently been discovered that they are also prevalent within intronic regions (Sedlyarov *et al.*, 2016).

Several proteins capable of binding to AREs have been described including tristetraprolin (TTP), human antigen R (HuR) and AU-rich element RNA-binding protein 1 (AUF1). TTP is the founding member of a family of CCCH tandem zinc finger-containing RNA binding proteins (Brooks and Blackshear, 2013a). Following binding to its target, TTP recruits deadenylase machinery to initiate the process of message degradation (Marchese *et al.*, 2010). Importantly, TTP binding does not guarantee destabilisation and therefore other factors are important, although these have not been well-defined at present (Sedlyarov *et al.*, 2016).

1.3.2 TTP regulation

TTP (gene name *ZFP36*) was first identified as an immediate early gene. Gene expression could be induced in response to a variety of stimuli including insulin, phorbol esters, serum and a variety of growth factors (Lai, Stumpos and Blackshear, 1990). Its gene locus is small, consisting of 2 exons (49/28bp & 962/932bp) and one intron (381/681bp) in the human (GRCh38) and mouse (GRCm10) genomes respectively (data from University of Santa Cruz genome browser). Despite this, its transcriptional and post-transcriptional regulation is complex.

Initial promoter analysis of TTP identified consensus elements for the transcription factors early growth response 1 (EGR-1), activator protein-2 (AP-2) and specificity protein 1 Sp1 which were all shown to contribute to serum induction of *Zfp36*, although absence of their putative binding elements did not completely abolish serum responsiveness, suggesting further mechanisms of regulation (Lai *et al.*, 1995). Further work indicated that Smad proteins downstream of TGF-$\beta 1$ could also induce TTP transcription via Smad-

responsive elements in the promoter (Ogawa *et al.*, 2003). In fact methylation of a CpG island within the TGF-$\beta 1$ responsive region results in epigenetic downregulation of TTP in a panel of hepatocellular carcinoma cell lines, and consequent stabilisation of c-Myc mRNA (Sohn *et al.*, 2010). Furthermore, a putative NF-κB binding site within the 5' regulatory region of *Zfp36* was shown to contribute to the LPS induced upregulation of TTP seen in macrophages.

As above, TTP can be induced via a variety of external stimuli mediated through various transcription factors. The example of epigenetic silencing of TGF$-\beta 1$-induced TTP expression in hepatocellular carcinoma suggests that heterogenous epigenetic modulation of the TTP promoter could modulate TTP responsiveness to external stimuli in different cell types. Beyond transcriptional regulation, TTP is extensively regulated at the post-transcriptional level. To this end, TTP is extensively phosphorylated. The best known phosphorylation sites are at serines 52 and 178 in the mouse (80 and 186 in humans) (Clement *et al.*, 2011). Phosphorylation at these sites, by the enzyme MAP kinase-activated protein kinase 2 (MK2 ,downstream of p38 MAPK), can inhibit deadenylase recruitment and thus the ability of TTP to destabilise its targets (Clement *et al.*, 2011). Simultaneously, such phosphorylation promotes nuclear export of TTP to the cytoplasm (where it will be ready to act once dephosphorylation occurs) and also mediates recruitment of protein 14-3-3, shielding TTP from proteasomal degradation (Brooks and Blackshear, 2013a). This triplet of effects (impaired function, nuclear export and stability) ensures accumulation of a cytoplasmic reservoir of TTP. This is important for resolution of an acute inflammatory response as discussed in the next section.

The importance of serines 52 and 178 has been shown through the generation of mice in which both are mutated to (nonphosphorylatable) alanine residues (*Zfp36*aa/aa mice) (Ross *et al.*, 2015). As discussed below, TTP is important in the destabilisation of various inflammatory cytokines, including those induced by LPS. To this end, *Zfp36*aa/aa mice appear healthy and are protected from the cytokine storm that normally occurs post-LPS challenge (consistent with

super-active ('non-phosphorylatable') TTP destabilising LPS-induced cytokines) (Ross *et al.*, 2015). Interestingly, TTPaa is expressed at a lower level than WT TTP for two reasons (Ronkina *et al.*, 2019). Firstly, as above, phosphorylation protects TTP from proteasomal degradation and secondly TTP destabilises its own mRNA. Hence, since TTPaa is more active than WT TTP, its mRNA (and protein) levels are lower (Lee *et al.*, 2020). Further evidence for the importance of these residues in TTP function came from a study which examined the response of bone marrow-derived macrophage (BMDM) derivatives to LPS (Ronkina *et al.*, 2019). These derivatives included WT, TTPaa, MAP kinase-activated protein kinase 2/3 (MK2/3) double KO (DKO) and TTPaa/DKO BMDMs. In this study, expression of various cytokines including TNFα, IL6 and CXCL1 was reduced in LPS-stimulated TTPaa, DKO or TTPaa/DKO BMDMs compared to wild-type. However, the reduction was more profound in DKO and TTPaa/DKO mice compared to TTPaa mice suggesting MK2/3 roles beyond phosphorylation at S52/S178. While this may be secondary to MK2/3 substrates other than TTP, the authors showed that MK2 can phosphorylate TTP at S316, an effect that has been shown to inhibit TTP interaction with de-adenylase machinery (Fabian *et al.*, 2013).

Finally, it should be noted that TTP has been shown to be phosphorylated at various other sites, but the functional outcome of this is unknown (Rezcallah, Al-mazi and Ammit, 2021). Furthermore, while many kinases have been predicted to phosphorylate TTP *in silico*, direct (*in vitro* or *in vivo*) evidence for this is lacking. Studies have suggested co-operation between ERK and p38 in phosphorylating (and inhibiting) TTP (Deleault, Skinner and Brooks, 2008; Brooks and Blackshear, 2013a) however a direct action of ERK on TTP has not been definitely ascribed in these. Thus, the effect of ERK inhibition or activation on TTP activity may be via its ability to affect p38 activation, as shown by our lab (Coelho *et al.*, 2017).

1.3.3 TTP function in physiology, including putative targets

As above, TTP is capable of destabilising target mRNA, and its action can be inhibited through p38/MK2-dependent phosphorylation. The p38-MAPK pathway is activated in macrophages following inflammatory stimuli, for example via LPS (Yi *et al.*, 2014), and indeed these are the cells in which TTP has been most studied. To this end, its function was first elucidated through observation of the phenotype of *Zfp36*-/- mice (Taylor *et al.*, 1996). These mice develop normally but later develop a spontaneous inflammatory phenotype including cachexia, arthritis and weight loss in a manner that phenocopies TNFα excess. Treatment with infliximab (anti-TNFα monoclonal antibody) abolishes much of the clinical syndrome. It was then shown that TNFα mRNA decays more slowly in TTP KO macrophages and that TTP could bind directly to TNFα mRNA (Carballo, Gilkeson and Blackshear, 1997). This was the first clue to the physiological role of TTP. Nonetheless, myeloid cells are not the sole effectors of the inflammatory phenotype in *Zfp36*-/- mice. This is evident given that mice with myeloid-specific TTP deficiency do not develop spontaneous inflammation, although they are hypersensitive to low doses of LPS (Qiu, Stumpo and Blackshear, 2012).

The dominant effect on TTP localisation, stability and activity by the p38-MAPK pathway led to a working model of TTP function and expression, which has been validated experimentally (Clark and Dean, 2016). This model proposes that pro-inflammatory stimuli such as LPS promote TTP expression but, simultaneously, synthesized TTP is phosphorylated (at serines 52, 178 and 316) in a p38-MAPK dependent manner. This phosphorylation stabilises TTP, ensures its cytoplasmic location and also renders it inactive. Thus, both inflammatory mRNA and a pool of inactive cytoplasmic TTP accumulate. As the inflammatory stimulus wanes the strength of p38 signalling falls such that the balance of phosphorylation/dephosphorylation of TTP swings in favour of the latter (e.g. through phosphatases such as protein phosphatase 2 PP2A). As TTP is dephosphorylated it becomes active, contributing to destabilisation of inflammatory mRNA such as TNFα, IL6 and IL-1β while also destabilising its

own mRNA until its level falls to resting values. A summary of this process is shown in Figure 2.

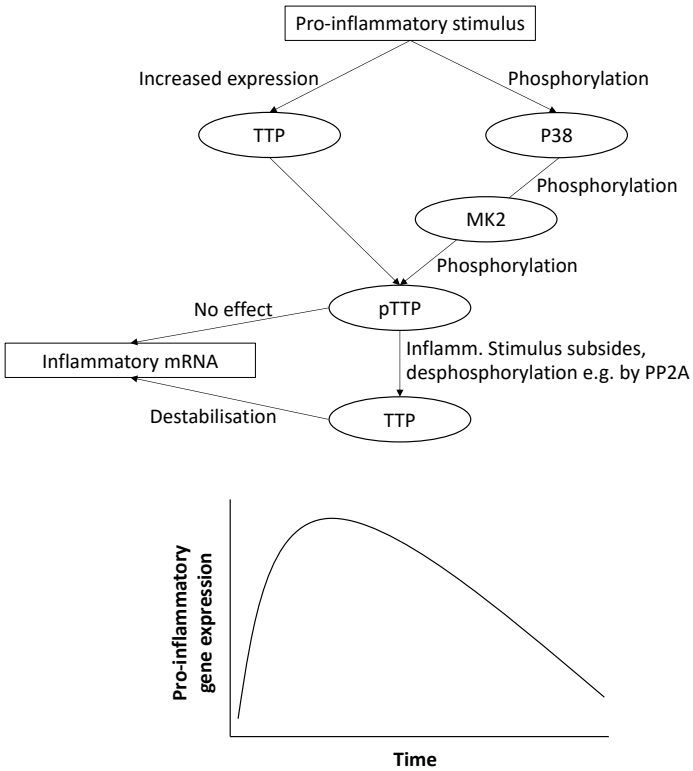

Figure 2. Schema of TTP effect Inflammatory stimuli result in increased tristetraprolin (TTP) expression, p38 phosphorylation and expression of inflammatory mRNA species (not shown). Expressed TTP is quickly phosphorylated by MAP kinase-activated protein kinase 2 (MK2), and accumulates (inactive) in the cytoplasm. Waning of the inflammatory stimulus allows phosphatases such as protein phosphatase 2 (PP2A) to shift the equilibrium toward dephosphorylated TTP resulting in destabilisation of inflammatory transcripts.

As described above, TNFα was the first TTP target identified but several more have been proposed since, both in human and murine macrophages but also fibroblasts, B cells, T cells and cancer cells (Brooks and Blackshear, 2013a). Thus, while the canonical function of TTP concerns the resolution of inflammation in macrophages, it is expressed and functional in several other cells and tissues.

Of note, most studies examining TTP and its targets have focussed on a single (or few) model systems and describe one (or few) TTP targets that seem to have dominant effects in that system. Therefore, it may be that the ability of TTP to degrade various target transcripts varies between models, contingent on factors including the genomics and epigenomics of the system (which may influence, for example, the expression of proteins that interact with TTP or of other RNA-binding proteins) and the stimulus being studied. Beyond this, however, several studies have interrogated TTP effects at a transcriptome-wide level.

The first such study to do this looked at TTP binding and its effect on gene expression in human embryonic kidney (HEK-293) cells (Mukherjee *et al.*, 2014). They used photoactivatable ribonucleoside-enhanced crosslinking and immunoprecipitation (PAR-CLIP) to interrogate TTP binding throughout the genome, and then RNAseq in the context of TTP overexpression to interrogate its effect on target destabilisation. Binding-site analysis demonstrated enrichment of known TTP target sequences (e.g. the AUUUA pentamer) although only 47% of targets contained this sequence suggesting added complexity in TTP binding specificity. Furthermore, many bound sites were intronic rather than located in the 3' UTR. Nonetheless, when correlation with gene expression studies were performed, downregulated genes correlated with presence of the octamer UAUUUAUU, suggesting its importance in functional binding. Pathway analysis of genes downregulated upon TTP binding showed enrichment for immune genes, but also those involved in proliferation and epithelial-to-mesenchymal transition.

Similar studies have been performed in murine bone marrow-derived macrophages (BMDMs) (Sedlyarov *et al.*, 2016; Tiedje *et al.*, 2016). Intriguingly, in one such study, only 32 of the 1587 binding positions identified for TTP overlapped with the 2731 positions from the aforementioned study in HEK-293 cells (Sedlyarov *et al.*, 2016). This considerable difference in TTP binding between model systems was hypothesized to be due to a combination of lack of

many immune targets in HEK-293 cells and differential regulation of TTP binding between the two systems. Nonetheless, it highlights the lack of understanding of factors that modulate TTP binding to its targets and whether such binding is 'functional' (i.e. causes destabilisation).

Beyond comparison to the previously established HEK-293 dataset, the two studies using murine BMDMs examined the effect of LPS stimulation on TTP binding and destabilisation at different phases of the inflammatory response. The findings corroborated the functional model of TTP described above (Clark and Dean, 2016) by confirming that TTP is unable to destabilise its targets early after an inflammatory stimulus, but becomes active later, when the inflammatory stimulus subsides.

1.3.4 TTP in cancer

TTP targets suggested in the literature include MYC, cyclin D1 (CCND1), IL6 and prostaglandin-endoperoxide synthase 2 (PTGS2), all of are associated with cancer. Given the ability of TTP to destabilise these messages, it is not surprising that it has been labelled as a tumour suppressor and investigated as such. To add support to this hypothesis, it has also been shown that TTP is directly transcriptionally repressed by Myc in a lymphoblastoid B cell line (Rounbehler *et al.*, 2012). ChIP assays showed direct binding of Myc to the regulatory region of the *Zfp36* gene while furthermore, Myc induction reduced nascent *Zfp36* mRNA expression. To support this observation, the authors also interrogated expression profiles across several human malignancies from Gene Expression Omnibus Series and found an inverse correlation between MYC and *ZFP36*. Conversely, the bona-fide tumour suppressor p53 has been shown to enhance TTP promoter activity, again suggesting that TTP may be repressed in cancer and function as a tumour suppressor (Lee *et al.*, 2013).

Further support for the labelling of TTP as a tumour suppressor relates to the plethora of studies showing suppression of TTP in various malignancies, either at the level of gene expression or protein (Saini, Chen and Patial, 2020). The causes of such suppression are not well described but individual studies have highlighted examples where TTP is suppressed through promoter methylation, microRNA-mediated deregulation or post-translational modification (Sohn *et al.*, 2010; Sun *et al.*, 2015; Coelho *et al.*, 2017). Furthermore, analysis of gene expression from TCGA lung adenocarcinoma and breast cancer datasets suggest that TTP is part of a 50 gene signature that predicts poor prognosis in low-expressors (Fallahi *et al.*, 2014). In this study, luminal A breast cancers (a more indolent subgroup) were enriched in the TTP-high cohort while in lung cancer, the TTP-high cohort was associated with earlier stage disease.

Beyond evidence showing that TTP expression is reduced in cancer, individual studies have demonstrated the ability of TTP to influence specific hallmarks of cancer. For example, in various systems, TTP has been shown to affect proliferation via targeting c-Myc, cyclin D1 and E2F1 while also being able to inhibit c-Jun expression through inhibition of the nuclear translocation of the p65 subunit of NF-κB (Marderosian *et al.*, 2006; Lee, Lee and Leem, 2014; Xu *et al.*, 2015) ; of note, although the canonical role of TTP is to destabilise target mRNA, it is appreciated that it also acts at the transcriptional level (Ciais, Cherradi and Feige, 2013). As well as its effect on proliferation, TTP also influences apoptosis. In one glioma model, it destabilised urokinase plasminogen activator (uPA) and urokinase plasminogen activator receptor (uPAR) while in another, it destabilised proto-oncogene serine/threonine-protein kinase pim1/2 and X-linked inhibitor of apoptosis proteins (XIAP) (Selmi *et al.*, 2012; Ryu *et al.*, 2015). In both cases the effects of TTP on these transcripts included induction of apoptosis.

Given the fairly recent installation of tumour-associated inflammation as an ‘enabling characteristic’ of cancer (Hanahan and Weinberg, 2011), the contribution of TTP to this process cannot be ignored. Indeed, the function of

TTP was discovered following observation of the phenotype of TTP KO mice, who develop a pervasive inflammatory phenotype (Brooks and Blackshear, 2013a). Several studies have described the importance of TTP and inflammation in cancer. Putative targets include CXCL1, CXCL2, IL-1β, IL-6, IL-8 and PTGS2 amongst others (Saini, Chen and Patial, 2020). Once again, these observations were made across many different model systems with most studies describing the modulation of just one or a few of these targets in each system. Besides inflammation, TTP has also been implicated in the regulation of angiogenesis through its targeting of VEGFa and epithelial to mesenchymal transition (EMT) via its effects on various EMT regulators including ZEB1, SOX9, TWIST1 and SNAIL1 (Montorsi *et al.*, 2016; Yoon *et al.*, 2016).

While various evidence points to TTP as a tumour suppressor, it is important to appreciate that it has many targets, not all of which are oncogenic. For example, the tumour suppressor LATS2 is a TTP target. However, in one model of colorectal cancer, TTP was shown to downregulate LATS2 but also E2F1 and inhibitor of apoptosis 2 (cIAP2) (Lee *et al.*, 2018). Thus, despite its effect on LATS2, the net effect of TTP activation was suppression of proliferation, invasion and metastasis. We also note that the studies above tended to focus on one, or just a few, TTP targets in a given system. Taking a broader approach, one study interrogated expression of ARE-containing mRNAs across multiple cancer types (Hitti *et al.*, 2016). They showed that ARE-mRNAs were over-expressed in tumours and that this correlated with TTP expression. In further analyses, a cluster of 11 overexpressed ARE-mRNAs that participate in the M phase of the cell cycle were interrogated and found to physically interact with TTP in validation experiments, suggesting direct regulation. Patients with high expression of these genes had worse survival. This suggests that while individual studies identify isolated TTP targets, TTP may act at a broader level within cancers, to modulate networks of targets and affect outcome.

1.4 Thesis objectives

Oncogenic KRAS has been shown to contribute to tumour immune evasion but the mechanisms behind such effects remained ill-defined (Cullis, Das and Bar-Sagi, 2018). Previous work from our lab explored a mechanism by which oncogenic KRAS signalling can result in immune polarisation; TTP was shown to be phosphorylated in a RAS-dependent manner resulting in stabilisation of PD-L1 mRNA with potential contributions to tumour immune evasion. In this thesis we aim to further elucidate the role of TTP, first by exploring its expression in human tumours, next by exploring the effects of its over-expression (at the transcriptomic level) in an immunogenic murine carcinoma model (CT26) and finally by further exploring its relationship to oncogenic KRAS using *in silico* and *in vitro* analysis.

The effects of oncogenic RAS are complex and diverse and likely to be mediated by more than simply its effect on TTP. Beyond understanding the mechanistic basis of oncogenic KRAS activity, further elucidation of its phenotypic effect will give us insight into the diversity of cell types affected and generate hypotheses for synergistic combinations with the recently developed KRAS(G12C) inhibitors. Using IMC, researchers from our lab have shown a profound spatial effect of KRAS inhibition on the myeloid repertoire of 3LL tumours (van Maldegem *et al.*, 2021). While IMC can generate detailed spatial characterisation and limited phenotypic information it lacks the ability to generate hypotheses about function characterisation through transcriptomic evaluation. In this thesis we aim to use CITE-seq to better understand phenotypic effects that KRAS inhibition has in this model and to generate hypotheses about the functional state of the immune repertoire with the aim of generating insights into potential therapeutic synergy. The 3LL model has a high neoantigen burden (edurne paper) yet is refractory to the effect of check-point inhibition making it an intriguing model for exploration of such synergy.

Chapter 2. Materials & Methods

2.1 *ZFP36* analysis from TCGA

Analysis was performed using R version 4.0.5. TCGA data was downloaded using TCGAbiolinks (version 2.18.0). Duplicated patient IDs were removed and genes with an average raw count of < 1 per sample were discarded. Data was normalised using variance stabilising transformation (VST) from the DESeq2 package (version 1.30.1). Log-fold changes (LFCs) of tumour vs. normal tissue were calculated as a difference of means from the normalised data while p-values were the result of corresponding t-tests. Boxplots were generated using default settings in base R and histograms of tumour versus normal log-fold changes (LFCs) were generated using ggplot2 (version 3.3.3).

In order to generate survival curves, VST-normalised samples were grouped according to *ZFP36* expression quantiles. Survival data was obtained from the TCGA Clinical Data Resource (Liu *et al.*, 2018) and Kaplan-Meier curves were plotted using the survival package (version 3.2-10) with log-rank tests conducted using the coin package (version 1.4-1).

Heatmaps were plotted using gplots (version 3.1.1). For annotation of correlation plots, the RAS activity group (RAG) annotations were provided by an inventor (Sophie De Carne) of the signature, a member of the lab. Mutation data was obtained from cBioPortal (https://www.cbioportal.org). Finally, the Venn diagram was generated using the VennDIigram package (version 1.6.20).

2.2 Cell culture

A summary of the cell lines used in this thesis is given in Table x. Further details regarding CT26 derivatives are given in the results section. Cells were grown in RPMI medium (CT26 and 3LL-ΔNRAS) or DMEM (KPAR(G12C)),

supplemented with 10% fetal calf serum, 4mM glutamine (Sigma), 100units/ml penicillin and 100mg/ml streptomycin (Sigma). Sub-culturing was performed by first removing the medium and then washing with PBS. Detachment was induced through application of trypsin (sigma) followed by re-seeding at a dilution appropriate for the given cell line. Passage number was recorded, and cells were not grown for more than 20 passages. Cells were kept in a humidified, 37°C incubator with 5% ambient CO_2.

Cell line	**Source**
CT26 (parental)	The Francis Crick Institute cell services
CT26 (TTP KO)	The Francis Crick Institute cell services (Coelho *et al.*, 2017)
CT26 (Tet-On TTP(WT))	The Francis Crick Institute cell services (Coelho *et al.*, 2017)
CT26 (Tet-On TTP(aamt))	The Francis Crick Institute cell services (Coelho *et al.*, 2017)
CT26 (G12C)	Mirati Therapetuics
3LL-ΔNRAS	The Francis Crick Institute cell services (Molina-Arcas *et al.*, 2019)
KPAR(G12C)	Downward lab (de Carné Trécesson *et al.*, 2020) produced KPAR1.3 (G12D) subsequently modified by Pablo Romero (Downward lab), who used PRIME-editing to generated KPAR(G12C)

Table 4. Cell lines and source

2.3 Quantitative real-time PCR (qPCR)

RNA was extracted using the RNeasy Mini Kit (QIAGEN), following manufacturer's instructions. RNA was eluted in 30μL. For in vivo tumour

samples, tumours were individually isolated from the lungs, lysed and homogenised using the QIAshredder (QIAGEN) following manufacturer's instructions prior to RNA extraction using the commercial kits described above. After quantification, 500ng of RNA was used to generate cDNA using SuperScript II Reverse Transcriptase (Life Technologies). Briefly, 3µl of RNA were incubated with 1µl of 50µM Random Hexamers and 0.5µl of 10mM pre-mixed dNTPs at 65°C for 5min. Subsequently, the reaction was incubated with 1µl of 0.1M DTT (ThermoFisher), 2µl of 5x First Stand Buffer (ThermoFisher) and 0.5µl (20 units) of the RNase inhibitor RNaseOUT™ (ThermoFisher) at 25˚C for 10min and 42˚C for 50min before reaction inactivation by incubating at 70°C for 15min. cDNA was diluted to 1.25ng/ml and real-time PCR (qPCR) reactions were performed using either Quantitect Primer Assays (QIAGEN) or custom-made primers (Table 5). For qPCR, 5ng of cDNA, 1µl of 2µM primer and 5µL of SYBR Green mastermix (Life technologies) were dispensed into 384 well plates. Relative gene expression was calculated using the ΔΔCT method with Gapdh and Hsp90 used as housekeeping genes.

Gene	Sequence	Source	Cat. No.
Areg	Fw: TGCCTTCTGGCAGTGAACTC Rev: CCTTGTCATCCTCGCTGTGA		
Cd274	Fw: CGCCACAGCGAATGATGTTT Rev: AGGATGTGTTGCAGGCAGTT		
Dusp5	Fw: GGATGCAGCTCCTGTAGTACC Rev: TCCGAGAAGCGTGATAGGCA		
Gapdh	Fw: CAAGCTCATTTCCTGGTATGACA Rev: GGATAGGGCCTCTCTTGCTC		
Hsp90	Fw: AGATTCCACTAACCGACGCC Rev: TGCTCTTTGCTCTCACCAGT		

Ier3	Fw: CGCGTTTGAACACTTCTCGC Rev: ATGTTGGGTTCCTCGGTTGG		
Lif	Fw: ACAACTGTGCAGACTGTGGA Rev: TGCAGGCCGTTTTCAGAAGT		
Myc	Fw: CCGGGGAGGGAATTTTTGTCT Rev: GAGGGGCATCGTCGTGG		
Plaur	Fw: GTGTTGCAACTACACCCACTG Rev: TGGAAGCCATTCGGTGGAAA		
Plk3	Fw: CGGTCATCCAGATGTCAGGC Rev: TGGCCACAGTCAAACCTTCT		
Ptgs2	Fw: TGGGTTCACCCGAGGACTG Rev: GGGGATACACCTCTCCACCAA		
Vegfa	Fw: CACTGGACCCTGGCTTTACT Rev: GCAGTAGCTTCGCTGGTAGA		
Zfp36		Qiagen	QT01060962

Table 5. Primer sequences for qPCR

2.4 Cytokine array

10^5 CT26(aamt) cells were plated in a 6 well plate followed by administration of doxycycline (1µg/ml) or DMSO (1µl/ml) 24 hours later. Twelve hours later, medium (including doxycycline or DMSO at appropriate concentrations) was changed. After a further 12 hours, supernatant from the wells was harvested and used in the Proteome Profiler Mouse Cytokine Array Kit, Panel A (R&D Systems), as per manufacturer's instructions. Briefly, pre-coated array membranes were blocked using 2ml of Array Buffer, rocking for 1h before addition of a pre-mixed solution containing a maximum of 1ml of each sample and 15µl of the detection antibody cocktail. Samples and antibodies were incubated overnight at 4°C on a rocking platform shaker. The following day,

membranes were washed using the Wash Buffer supplied before addition of Streptavidin-HRP. After adding the chemiluminescent substrate provided, membranes were developed using standard film techniques. Images were analysed using ImageJ (NIH).

2.5 ELISA

10^5 CT26(aamt) cells were plated in a 6 well plate followed by administration of doxycycline (1µg/ml) or DMSO (1µl/ml) 24 hours later. Twelve hours later, medium (including doxycycline or DMSO at appropriate concentrations) was changed. After a further 12 hours, supernatant from the wells was harvested and used in ELISA protocols. DuoSet ELISA, Mouse CXCL1/KC (R&D Systems) was used, following manufacturer's instructions. Briefly, 96-well polystyrene plates for ELISA (R&D) were coated overnight with the coating antibody provided by the Kit, diluted in 0.1M NaHCO3 buffer. The following day, plates were washed using a solution of 0.01% Tween (Sigma) in PBS. Plates were then blocked with a solution of 10% fetal calf serum (Sigma) in PBS for 1h. After washes as before, experimental samples and recombinant cytokines to be used as standards were added to the plate and incubated for 2h. Plates were then washed and a biotinylated detection antibody, diluted in blocking buffer, was added at the concentration instructed and incubated for 2h. After washing, plates were incubated with a solution of Streptavidin-HRP for 20 minutes before addition of a chemoluminescent substrate. After incubating for 10-20min (depending on signal intensity), absorbance at 450nm was measured using a Tecan microplate reader.

2.6 In vivo experiments

All studies were performed under a UK Home Office approved project license and in accordance with institutional welfare guidelines.

For subcutaneous experiments, CT26 (TTP KO or aamt) cells were harvested using trypsin and re-suspended in PBS at (10^5 cells/50µL) for injection. These cells were mixed 1:1 with GeltrexTM matrix (ThermoFisher) and injected in a total volume of 100µl subcutaneously in one flank of BALB/c mice. Injection was performed on day 0, and mice subsequently received either 2% sucrose control or doxycycline in 2% sucrose (50mg/L administered at a dose of 50mg/kg) via oral gavage. Treatment was given daily from day 3 onwards, with breaks at weekends. Tumour growth was followed twice a week by caliper measurements and tumours were left to grow not larger than 1.2cm in diameter following a UK Home Office approved project license. Mice were culled using an approved schedule 1 method when tumour diameter exceeded this set point, if protocol-defined endpoints were breeched or on day 20 of the experiment.

For orthotopic growth using 3LL-ΔNRAS cells, the cells were harvested as before, and 1 million 3LL-ΔNRAS cells were injected in PBS in a total volume of 100µl in the tail vein of C57Bl/6 mice. If mice were planned to receive treatment then, after 21 days, they were scanned using computed tomography (CT) and allocated into one of two groups. One group received MRTX1257 (Mirati Therapeutics) at 50mg/kg or 10% Captisol (Ligand) in 10mmol/L citrate buffer (pH 5.0) as vehicle control daily via oral gavage for a total of 7 days. Mice were culled (using an approved schedule 1 method) on the 7th day of treatment, within 4 hours of drug administration. Mouse weight was monitored regularly as a measure of tumour growth and mice were sacrificed (early than the 7th day of treatment) if weight loss was over 10% as per the UK Home Office approved project license.

Figure 3 below represents an overview of the experimental schema.

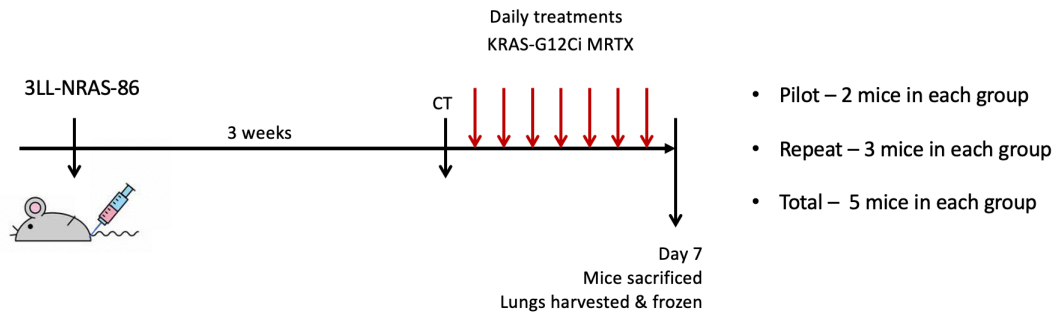

Figure 3. Experimental schema for orthotopic experiments

For CT scanning, mice were anaesthetised by inhalation of isoflurane (Abbott Labs) and scanned using the Quantum GX2 micro-CT imaging system (Perkin Elmer). Breathing rate and body temperature were measured throughout the scan using in-built physiological monitoring devices.

2.7 In vitro G12C treatment for RNAseq

For RNAseq experiments interrogating the transcriptome-wide effect of KRAS(G12C) inhibition, 3LL- ΔNRAS or KPAR(G12C) cells were treated with 100nM MRTX1257 or MRTX849 respectively, for 0, 8 or 28 hours (3LL-ΔNRAS) or 0, 8 or 24 hours (KPAR(G12C)) before extraction of RNA for RNA-sequencing. Experiments were performed by Edurne Mugarza (3LL- ΔNRAS) or Jesse Boumhela (KPAR(G12C))

2.8 Viability assay

For viability assay, the CellTiter-Blue assay (Promega) was used. CT26(KRAS(G12C)) cells were grown in 96-well plates and treated for 72 hours with varying concentrations of the appropriate agents (serial diltuions of

trametinib (LC labs), AZ-8037 (Astrazeneca) or MRTX1257 (Mirati Therapeutics) beginning at 2500nM for a total of 9 two-fold dilutions) for 72 hours. At the end of the experiment, 5µl of the CellTiter-Blue reagent was added to each well and the reaction was incubated for 90 minutes at 37°C. Fluorescence was subsequently measured using and EnVision plate reader (Perkin Elmer) with excitation/emission wavelengths of 560/590nm. For data analysis, medium containing wells were used as a background and subtracted from the values of the cell-containing wells.

2.9 Western blotting

10^5 CT26 (KRAS(G12C)) cells were cultured in 6-well plates for 24 hours before application of control (DMSO), 100nM MRTX1257 or 250nM AZ-8037 (both KRAS(G12C) inhibitors) for 6, 24 and 48 hours prior to protein isolation. At the end of the experiment, plates were placed on ice, medium was removed and cells were washed with ice cold PBS. Lysis buffer was prepared using 10X Cell Lysis Buffer (Cell Signaling Technologies), supplemented with EDTA-free protease inhibitor cocktail tablets (Roche), 1mM PMSF and 25mM NaF. Cells were de-attached using a rubber scraper and collected in tubes which were left on ice for approximately 10 minutes for lysis. Tubes were then centrifuged at 4°C for 15 minutes at 14,000rpm, after which the pellet was discarded and the supernatant was transferred to a new tube. Protein abundance was measured using the Lowry-based DC Protein Assay (BioRad) using bovine serum albumin as a standard. Equal amounts of protein were taken for each sample and NuPAGE LDS Sample Buffer (4X, Thermo Fisher) was added. Samples were incubated at 95°C for 5 minutes for protein denaturation and either stored at -20°C or loaded (20-30mg per sample) onto NuPAGE 4-12% Bis-Tris protein gels (Thermo Fisher). Protein transfer to PVDF membranes was performed using the Trans-Blot Turbo Transfer System (BioRad) or standard manual transferring techniques. For antibody detection, horseradish peroxidase

conjugated antibodies were used (GE Healthcare) and data was developed using standard film techniques. Primary antibodies used are listed in Table 6.

Target	Source	Cat. no
pAKT473	Cell Signalling Technology	4060
pERK	Cell Signalling Technology	9101
pS6	Cell Signalling Technology	2211
KRAS	Sigma	WH0003845M1
Vinculin	Sigma-Aldrich	V9131

Table 6. Antibodies for Western blots

2.10 Bulk RNA sequencing (RNAseq)

10^5 CT26 cells (all four derivatives, see results section 3.3) were plated in 6 well plates for 24 hours, before application of 1μg/ml of doxycycline or 1μl/ml DMSO. RNA was subsequently extracted using the RNeasy Mini Kit (QIAGEN). RNA quality was measured using the 2100 Bioanalyzer (Agilent). Libraries were prepared using the KAPA Hyper Prep kit (Roche). 25 million reads were sequenced per sample at a single read length of 75bp, in an Illumina HiSeq 4000 system. Library preparation and sequencing were performed by the Advanced Sequencing Facility at the Francis Crick Institute.

Fastq files generated from sequencing were processed using the nfcore RNAseq pipeline (https://github.com/nf-core/rnaseq) using the following command:

```
nextflow run nf-core/rnaseq \
   --genome GRCm38 \
   --reads '<path to directory containing reads>' \
   --singleEnd \
   --email <my_email> \
   -profile crick \
   -r 1.4.2 \
```

Following the generation of count matrices using the pipeline above, data was pre-processed by first removing genes expressed at a mean of <1 read per sample before normalisation using variance stabilising transformation (DESeq2, version 1.22.2). Differential expression was also performed using DESeq2, and results reported as the interaction term between Condition and Cell Line, thus representing the effect of treatment specifically in that line using CT26 (TTP KO) cells treated with DMSO as the baseline factors. Once differential expression was performed, shrinkage of log-fold changes were performed using the APEGLM method (Zhu, Ibrahim and Love, 2019). MA plots (M = log ratio and A = mean (average)) were made using the plotMA function from DESeq2 while Venn diagrams used the VenDiagram package (v1.6.20).

In order to perform gene set enrichment, we used the fgsea package (version 1.16.0) with msigdbr (version 7.2.1) used to derive murine equivalents of the hallmark gene sets. To derive the gene signature, genes significantly downregulated (adjusted $p < 0.1$) at a log-fold change <-0.5 after induction of TTP were extracted from the data and mapped to human homologues using information from Ensembl via the BioMart package (v 2.46.3). TCGA data for lung and colon adenocarcinoma was obtained from TCGAbiolinks (version 2.18.0). For each tumour type, a loess curve was fitted to the data and genes with a log-coefficient of variance below the curve or a VST-normalised expression level <7.5 were discarded. The remaining genes were used to cluster the data and partition for survival. Survival analysis was performed as described in section 2.1.

2.11 siRNA experiments

siGENOME siRNAs against murine *Zfp36* (Dharmacon) were dissolved in siRNA resuspension buffer (Dharmacon) and stored at -20°C. On the day of use, siRNAs were thawed on ice and diluted in HBSS (ThermoFisher) to reach a concentration of 250nM (10µl of siRNA per well). This solution was mixed with 10µl HBSS (Gibco) containing 0.1µl DharmaFECT 1 transfection reagent (Dharmacon) per well. The transfection complex was incubated for 20-40 minutes before adding dropwise (200µl per well) to freshly seeded cells (not more than 10 minutes prior to transfection). As a control, cells were either Mock-transfected (no siRNA) or transfected with a siGENOME non-targeting pool (siScr, Dharmacon). The procedure was repeated 24 hours later, for a total of two transfections.

2.12 Optimisation of antibody concentration for CITE-seq

C57Bl/6 mice were injected with 10^6 3LL-ΔNRAS cells and tumours harvested on day 28. Mice were untreated with the rest of the protocol being as previously described (section 2.6).

2.12.1 Tumour dissociation

2.12.1.1 Method 1

Tumours (on ice) were chopped into 2-4mm pieces and placed into 2.35mL of serum-free RPMI premixed with the appropriate quantities of proprietary digestion enzymes (Tumour Dissociation Kit, mouse; Miltenyi Biotec) in gentleMACS™ C tubes (Miltenyi Biotec). The tubes were then placed in a gentleMACS™ Octo Dissociator and the mixtures subjected to a hybrid

enzymatic/mechanical dissociation (programme 37C_m_TKD_1 (soft)). Following dissociation, RPMI was topped up to 5mL and 200U/ml DNase added (Sigma-Aldrich D4263) and left for 5 minutes at room temperature (RT). The suspension was then passed into a 15mL Falcon tube through a 70μm MACS® SmartStrainer, and washed with a further 10mL of RPMI. Cells were centrifuged at 300g (4°C) for 7 minutes before being resuspended in 5ml eBioscience™ red blood cell lysis solution for 5 minutes at RT before stopping the reaction with 5mL RPMI, this time with 2% FBS. Cells were then washed a resuspended in Cell Staining Buffer (BioLegend) at a concentration of 2 x 10^7 cells/ml.

2.12.1.2 Method 2

To optimise the protocol, the proprietary method above was compared to a dissociation method developed in house usually used for the study of immune cells. Tumours (on ice) were chopped into 2-4mm pieces and placed into 2ml of digestion solution consisting of 1mg/ml collagenase type I (Thermofisher) and 50 U/ml of DNase in HBSS (both Life technologies). The mixture was incubated at 37°C for 30min before homogenisation by passing through a needle. This was followed by further incubation at 37°C for 20 minutes. Cell were then filtered through a 70μm MACS® SmartStrainer and red blood cells were shocked using ACK lysing buffer (Life Technologies) and finally washed three times in fluorescence-activated cell sorting (FACS) buffer (2nM EDTA, 0.5% BSA in PBS pH 7.2) before resuspension at 2 x 10^7 cells/mL

2.12.2 Flow cytometry

First, FC receptors of dissociated cells in staining buffer or FACS buffer, as above, were blocked (BioLegend TruStain FcX™) at 4°C for 10 minutes. Subsequently, cells were co-stained with fluorophore-conjugated antibodies against the putative CITE-seq targets (in six-step serial dilution) and CD45 (Table 7). Finally, 4',6-diamidino-2-phenylindole (DAPI) was used as a viability dye and added immediately before cells were passed through the cytometer. Cytometry was performed on a BD LSRFortessa™ cytometer (BD Biosciences)

for antibody titration experiments and on a BD Influx™ (BD Biosciences) for sorting cells prior to CITE-seq (section 2.13). Cell sorting was performed by the Flow Cytometry science technology platform (STP) at the Francis Crick Institute. FlowJo (version 10, LLC) was used for analysis.

Target	Clone	Fluorophore	Concentration (μg/ml)	Source	Cat. no
CD103	2.00E+07	PE	16	BioLegend	121405
CD11b	M1/70	PE	4	BioLegend	101207
CD11c	N418	PE	40	BioLegend	117307
CD206	C068C2	PE	32	BioLegend	141705
CD223	C97BW	PE	40	BioLegend	125207
CD24	M1/69	PE	16	BioLegend	101807
CD25	PC61	PE	40	BioLegend	102008
CD274	MIH6	BV605	40	BioLegend	153606
CD279	RMP1-30	PE	20	BioLegend	109103
CD366	RMT3-23	PE	40	BioLegend	119704
CD4	RM4-5	PE	32	BioLegend	100511
CD44	IM7	PE	5	ThermoFisher	12-044
CD45	30-F11	APC	1 (not titrated)	BioLegend	103111
CD62L	MEL-14	PE	4	BioLegend	104407
CD64	X54-5/7.1	PE	32	BioLegend	139304
CD69	H1.2F3	PE	40	BioLegend	104507
CD73	TY/11.8	PE	16	BioLegend	127205
CD8	53-6.7	PE	32	BioLegend	100707
F4/80	BM8	PE	32	BioLegend	123109
Ly6C	HK1.4	PE	16	BioLegend	128007
Ly6G	1A8	PE	4	BioLegend	127607
MHCII	M5/114.15.2	PE	4	BioLegend	107607

Table 7. Antibodies used in flow cytometry Concentration refers to the highest concentration of the six-step serial dilution. APC = Allophycocyanin, BV605 = Brilliant Violet™ 605, PE = phycoerythrin

2.13 CITE-seq sample processing

Preparation of samples for CITE-seq was done in conjunction with Sophie de Carne (post-doctoral scientist, Francis Crick Institute).

Mice with orthotopic 3LL-ΔNRAS tumours were treated as described (section 2.6) and tumours dissociated (section 2.12.1.1). While tumours were dissociating, we prepared our TotalSeq™-A (BioLegend) antibody cocktail by adding individual antibodies at the determined concentrations (Table 8 and results section 4.3) in Cell Staining Buffer (BioLegend) to a total volume of 50μL kept on ice.

Following single cell dissociation of tumours, 10^6 cells were resuspended in 50μL of Cell Staining Buffer and FC receptors of cells were blocked (BioLegend TruStain FcX) for 10 minutes at 4°C while the antibody cocktail was centrifuged at 14000g also for 10 minutes at 4°C. Cells were then incubated with the antibody cocktail for 11.5 minutes at 4°C followed by 3 cycles of washes with Cell Staining Buffer.

Finally, cells were resuspended in 400μL for FACS. DAPI was added prior to FACS, and DAPI -ve cells were sorted, for further analysis. Of note, ensuring high cell viability prior to single cell sequencing is important for optimising data quality (Haque *et al.*, 2017). The decision to sort for viable cells was a considered decision made despite the trade-off of increased processing time.

Following cell sorting, DAPI -ve cells were washed once before resuspension at 1000 cells/μL in RPMI with 2% FBS, and submission to the Advanced Sequencing Facility at the Francis Crick Institute for processing. In brief this consisted of first confirming viability post-FACS. Next, both RNA and ADT libraries were prepared using the 10x 3' mRNA-Seq v3.1 with CITE-Seq for

TotalSeq™-A antibodies technique (10x genomics). Finally, libraries were sequenced using paired end sequencing (100 base pairs) on a HiSeq sequencer. Approximately 4000 cells per sample were sequenced to a depth of 50,000 gene expression and 5,000 ADT expression reads.

Target	Clone	Concentration (μg/ml)	Cat. No.
CD103	2E7	0.5	121437
CD11b	M1/70	0.0625	101265
CD11C	N418	5	117355
CD206	C068C2	1	95052
LAG3 (CD223)	C9B7W	2.5	125229
CD24	M1/69	4	101841
CD25	PC61	2.5	102055
PD-L1	MIH6	10	153604
PD-1 (CD279)	RMP1-30	2.5	109123
TIM3 (CD366)	RMT3-23	2.5	119729
CD4	RM4-5	0.5	100569
CD44	IM7	0.5	103045
CD62L	MEL-14	0.0625	104451
CD64	X54-5/7.1	8	139325
CD69	H1.2F3	1.25	104546
CD73	TY/11.8	0.5	127227
CD8	53-6.7	2.5	100773
F4/80	BM8	5	123153
Ly-6G/ly-6C	RB6-8C5	0.125	108459
Ly6G	1A8	0.125	127655
MHCII	M5/114.15.2	0.125	107653

Table 8. CITE-seq antibodies All antibodies were TotalSeq™-A (BioLegend)

2.14 CITE-seq data processing

FASTQ files had already been generated by the Advanced Sequencing Facility at the Francis Crick Institute. Alignment, filtering, barcode count and UMI counting were performed by using Cell Ranger (version 3.0.2, 10x Genomics) resulting in the generation of matrices containing either mRNA or ADT counts for each cell. Such processing was performed for each sample individually. Quality control metrics produced by Cell Ranger were interrogated to assess sample adequacy.

Matrices were then read using R (version 4.0.0).

2.14.1 Pilot sample analysis

Pilot matrices were read into R (version 4.0.0) and crude analysis was performed by normalising using log-transformation (mRNA) or Centred Log-Ratio (CLR) followed by PCA and t-distributed stochastic neighbourhood embedding (t-SNE) using Seurat (version 4.0.1). Low quality cells were not filtered out.

For comparison to bulk samples, bulk data was processed as above (section 2.10) while the single cell data was processed by combining counts from all cells per sample, and then processed using DESeq2 (version 1.30.1).

2.14.2 Cell-level quality control

Quality control metrics (including PCA and outlier detection) were generated using scater (version 1.18.6) while doublet detection was performed using scDblFinder (version 1.4.0). Visualisation was performed using Seurat (version 4.0.1).

The distribution of various QC metrics were visualised, whilst the same QC metrics were also overlaid on UMAP (Uniform Manifold Approximation and Projection) plots to look for clusters within UMAP space. Following interrogation of the various metrics in this way, it was decided to filter cells using the percentage of the transcriptome occupied by mitochondrial genes according to sample-specific thresholds. The cut-off range across samples varied from 12-16% with cells expressing mitochondrial genes above this level being removed.

2.14.3 Sample integration

Following cell filtering as above, the mRNA data from each sample was normalised using scTransform (SCT) (Hafemeister and Satija, 2019) after removing genes which were not expressed in any sample. ADT data was normalised using CLR.
In order to integrate the 10 samples we first used RNA expression alone. This was performed using Seurat (version 4.0.1). The steps involved:

1) Selecting a list of 3000 variable features common to as many of the datasets as possible
2) Performing pairwise joint dimension reduction using canonical correlation analysis (CCA) in a hierarchical manner determined by the pairwise distances between individual datasets. CCA finds shared gene-gene correlation structures between the datasets and uses this to embed cells within the dimension-reduced space (Stuart *et al.*, 2019) . Within CCA space, cell-cell anchors were then determined using the proximity of reference and query cells in this shared space, as well as their nearest neighbours. Anchors join analogous cell types between reference and query data sets, within the low dimensional space.
3) Anchors were used to determine a ‘correction matrix’ to correct for type-specific batch effects between the datasets (i.e. different correction vectors for different cell types) whilst preserving biological differences.

This produced an integrated expression matrix which can be treated as a single normalised scRNAseq matrix for downstream analysis.

Next, integration was performed for the same samples but this time using ADT expression values. Once integrated expression matrices were produced for both samples, we then needed to integrate information from both modalities to produce a joint definition of cellular state. This integration was performed using the weighted nearest neighbours (WNN) approach also from the Seurat package (Hao *et al.*, 2021). In brief, the algorithm:

1) Clusters the data using either RNA or ADT expression alone. Then, for each cell, it identifies how similar that cell is to its 20 closest neighbours (in RNA or ADT space).
2) This information is used to calculate cell-specific modality weights (i.e. assign a weighting for the relative importance of RNA vs. ADT information in that cell).
3) Use the weights to create a WNN graph.
4) Use this graph as input to downstream algorithms including clustering, UMAP and trajectory inference methods

In all analyses, clustering was performed using the FindClusters function from Seurat. The original Louvain algorithm was used to cut the graph and generate clusters. For clusters generated on the integrated dataset containing all cells, the resolution was set to 0.5. For other cell types, the resolution was set as indicated in the relevant results chapter. Where clusterings at different resolutions were displayed in a tree, the tree was generated using the Clustree package (version 0.4.4)

2.14.4 Automated assignment of cell identity

Automated assignment of identity was performed by using SingleR (version 1.4.1) and a reference dataset of single cell profiled $CD45^+$ cells from orthotopic

KP1.9 tumours (Zilionis *et al.*, 2019). The algorithm assigns identities via the following steps:

1) Calculate Spearman correlation between each cell from a cell in the query dataset and each cell from a given label in the reference dataset, using label-specific marker genes (determined by pairwise comparisons between labels in the refence).
2) Define the per-label score (of each query cell) as the 80th percentile Spearman correlation for that label.
3) Repeat for each label in the query
4) Fine-tune data by subsetting the reference data to only include cells of the top scoring labels, and re-defining label markers. The repeat the above process, iterating until only one label is left.
5) Repeat for all cells in the query

The table below contains a very brief description of some of the labels from the reference study (Zilionis *et al.*, 2019). In general, descriptions from the study focussed on tumour/normal tissue discrimination and marker genes, rather than making functional assumptions or assessment.

Label	**Description**
N1	Enriched in normal lung. High canonical neut markers (e.g. S100A8)
N2	Enriched in normal lung. Form subpopulation separate to rest. High type I IFN genes
N3	Exclusive to tumour. Siglecf low. Intermediate state between N1 and N4/5
N4	Tumour enriched
N5	Tumour enriched. Ctsb high
N6	Tumour exclusive. Adamdec1, Fcnb and Ngp high (differentiates from N4)
Dendritic cells (DC)	
DC1	Expressed classical DC1 markers e.g. Itgae). Lack Ccr7 expression
DC2	Express cDC2 markers (e.g. Lilrb4, H2-DMb2)
DC3	Markers of activated DCs including Ccr7

pDC	Cluster distinctly. Siglech and Ccr9 - expressing
Monocytes (and monocytic DCs)	
Mon1	Markers of classical monocytes (Ly6c1, Ly6c2, Ccr2)
Mon2	Markers of alternatively activated monocytes (Itgal, Ace)
Mon3	Expression of neutrophil-related genes (S100a8, S100a9, Il1b)
MonoDC	Some DC-related genes (Clec10a, MHC II) but low markers of mature DC (Xcr1, Cd1a, Tcf4)
Macrophages	
Mac1	Tumour exclusive. C1qb, Cd86
Mac2	Tumour exclusive. Gpnmb high
Mac3	Tumour exclusive. Alox15, Saa3 and Prg4 high
Mac4	Also present in normal tissue. Markers of alveolar macs. (Krt19, Krt79)
T and natural killer (NK) cells	
T1	CD8a high
T2	Foxp3 & Il2ra high
T3	Mki67 high
NK	High expression of several killer lectin-like receptor genes (Klrs)

Table 9. Automated cell labels (Zilionis *et al.*, 2019)

2.14.5 Differential abundance

Differential abundance testing was performed using EdgeR (version 3.32.1). For each cell type, a quasi-likelihood negative binomial generalised linear model (GLM) was fit using both condition (control vs treated) and batch (pilot vs. post-pilot) as coefficients in the model. Once model parameters had been estimated, empirical Bayes quasi-likelihood F-tests were used to generate FDR p-values to ascribe significance.

2.14.6 Manual annotation of clusters

For manual annotation of clusters, differential expression (DE) testing was performed between each cluster and all other clusters combined using the FindMarkers function from Seurat with the 'Wilcoxon' method. For pairwise differential expression between each cluster and all other clusters, DE testing was performed using the findMarkers function from scran (version 1.18.7) with t-tests, Wilcoxon signed rank sum tests and binomial tests all being used to find appropriate markers. The results of each test were inspected to find the most appropriate markers. In general, we tried to find markers with a high log-fold change between the cluster of interest and all other clusters and/or a high log-fold change between the proportion of cells expressing said marker in the cluster of interest vs. all other cells.

Where cell cycle phase was used to guide manual annotation, this was calculated using Seurat (version 4.0.1). In brief, the algorithm took a list of s-phase and g2m-related genes (provided by Seurat) and calculated their average expression. From that average expression, the algorithm then subtracted the average expression of 100 control genes. The control genes were selected by first assigning all genes in the genome into one of 25 bins according to their average expression in the entire dataset. Next, for each gene in the s-phase and g2m-related sets, 100 control genes were selected from the same bin. The average expression of these control genes in the cell of interest was calculated, and it was this value that was subtracted from the average expression of the s-phase or g2m-related genes.

2.14.7 Differential expression between conditions

Differential expression between conditions within a cluster was performed using the FindMarkers function from Seurat, this time using the Model-based Analysis of Single-cell Transcriptomics (MAST) method corrected for batch (pilot vs. post-pilot). As sensitivity analysis, we also used the likelihood ratio test after

performing batch-corrected logistic regression, also via Seurat. Where indicated, DE between conditions within a cluster was also performed using the findMarkers function from scran, using t-tests, Wilcoxon signed rank sum tests and binomial tests.

To determine *specific* DE within a cluster, we used scran (version 1.18.7). In brief, the function created a pseudo-bulk dataset for each unique combination of cluster and treatment and then tested the null hypothesis that, for any given gene, the log fold-change between treated and control conditions lay between zero and the average log-fold change of that gene (treated vs control) in all other clusters.

Gene set enrichment analysis (GSEA) on the lists of DE genes was performed using the fgsea package (version 1.16.0) while murine gene sets were obtained from the msigdbr package (version 7.4.1).

Chapter 3. Results 1: Role of TTP in regulation of gene expression and growth in RAS mutant tumours

3.1 Introduction

While there is increasing appreciation of the final effectors that mediate tumour immune evasion, the cell-intrinsic programs that control production of such effectors are less well understood. In human cancers, tumour-intrinsic expression of TTP is generally suppressed relative to normal tissue counterparts. In murine models, modulation of TTP has been associated with altered expression of specific immune effectors with immune-evasive properties. Despite such reports of TTP modulation on individual immune effectors, there is little understanding of the transcriptome-wide effects of TTP modulation in an immunogenic carcinoma model system.

Here, we interrogate the effects of TTP overexpression in an immunogenic murine KRAS-mutant colon carcinoma model (CT26). Using analysis of gene expression, secreted cytokine profiles and subcutaneous *in vivo* tumour growth we show that TTP overexpression in this model has broad transcriptomic effects and results in reduced tumour growth *in vivo*. Later, using other RNAseq datasets, we examine whether the genes affected by TTP overexpression are also associated with KRAS modulation before looking for evidence of co-regulation of these genes by TTP and KRAS.

Of note, to avoid confusion, it is worth stating that the gene for TTP is *ZFP36*. There are some contexts in this chapter where either term is appropriate for use and thus the terms were used interchangeably in these cases.

3.2 TTP expression across human malignancies

TTP has been labelled as a tumour suppressor, in part due to studies demonstrating that its gene expression is reduced (relative to normal tissue counterparts) in several malignancies (Saini, Chen and Patial, 2020). Most such

reports describe individual tumours types, so we sought to systematically investigate this across several malignancies using gene expression data from TCGA. We interrogated *ZFP36* expression in 9 primary tumour types including bladder urothelial carcinoma (BLCA), breast invasive carcinoma (BRCA), colon adenocarcinoma, head and neck squamous cell carcinoma (HNSC), renal clear cell carcinoma (KIRC) lung adenocarcinoma (LUAD), lung squamous cell carcinoma (LUSC), pancreatic adenocarcinoma (PAAD) and prostate adenocarcinoma (PRAD). As shown in Figure 4, *ZFP36* expression was reduced relative to normal tissue counterparts in several malignancies. This was most pronounced for BLCA where malignant tissue demonstrated a 3 log-fold reduction in *ZFP36* gene expression compared to normal. The only tissue type where there was no significant different was PAAD, although the sample size was small (4 patients). Similarly, Figure 5 shows that except for pancreas cancer, *ZFP36* is consistently amongst the most downregulated genes in tumour vs normal tissue. This is most pronounced for BLCA and BRCA but also for HNSC, KIRC, LUAD and LUSC.

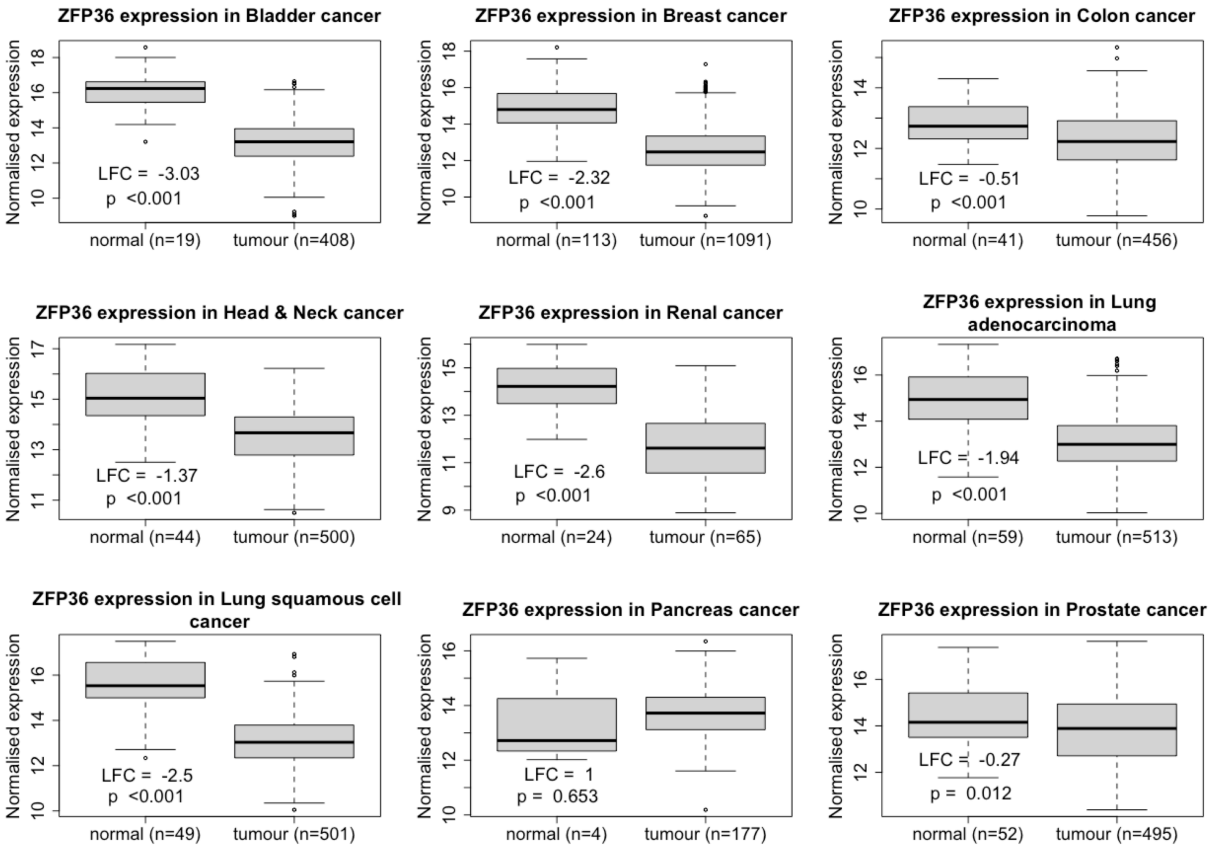

Figure 4. TTP expression in malignant and normal tissue counterparts

Boxplots denoting *ZFP36* expression in normal tissue counterparts vs. tumour tissue, across primary sites (TCGA data). Thick black lines within boxes represent median expression, box edges set at interquartile range (IQR) while whiskers extend to maximum and minimum values not exceeding a distance of 1.5*IQR from median. Log-fold change (LFC) and corresponding p-value refer to tumour vs. normal tissue. P-values calculated using unpaired T-tests.

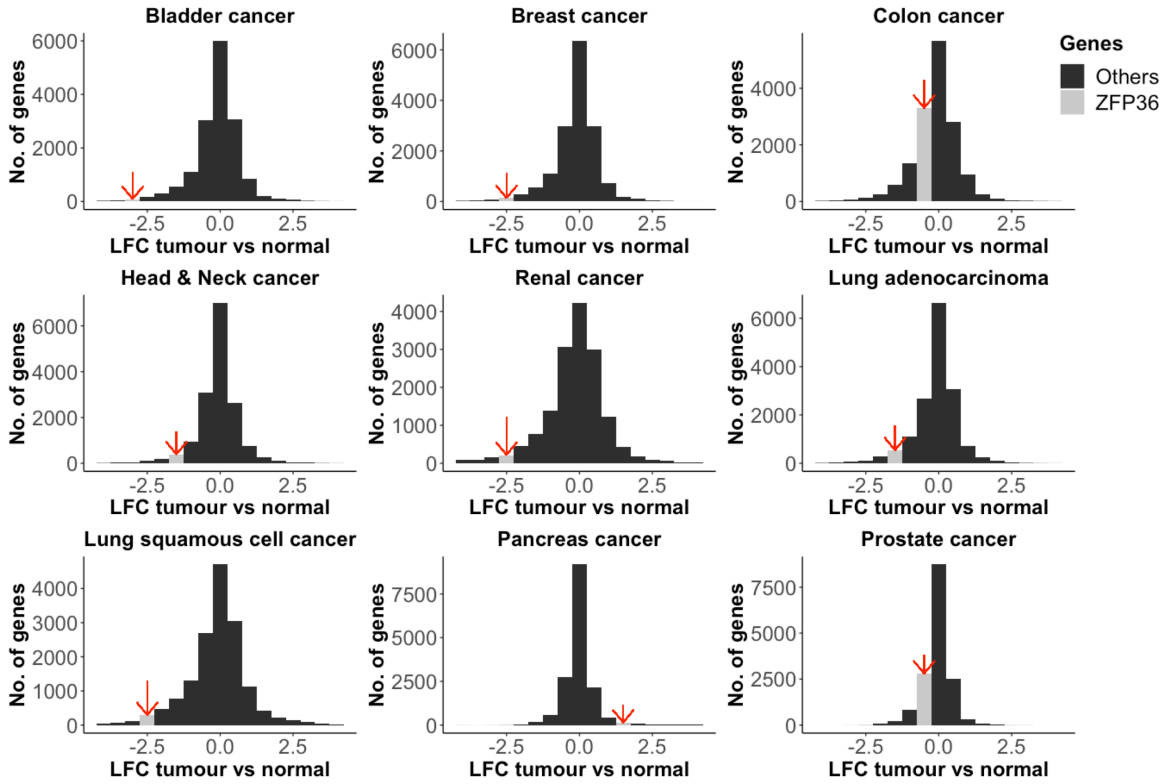

Figure 5. Log-fold change distributions of tumour vs. normal *ZFP36* expression across cancers (TCGA)For each tumour type, log-fold changes (LFC) for every gene (tumour vs normal tissue) were calculated and plotted as histograms. Grey bars with red arrows denote *ZFP36*-containing bin

Given the propensity for *ZFP36* to be underexpressed across a variety of tumour types, we next examined the effect of *ZFP36* expression on survival. If *ZFP36* is indeed a TSG, and if its gene expression correlates with its protein activity, then downregulation of *ZFP36* may predict worse survival. Surprisingly, as per Figure 6, across our 9 tumour types, there was no consistent association between *ZFP36* expression and survival

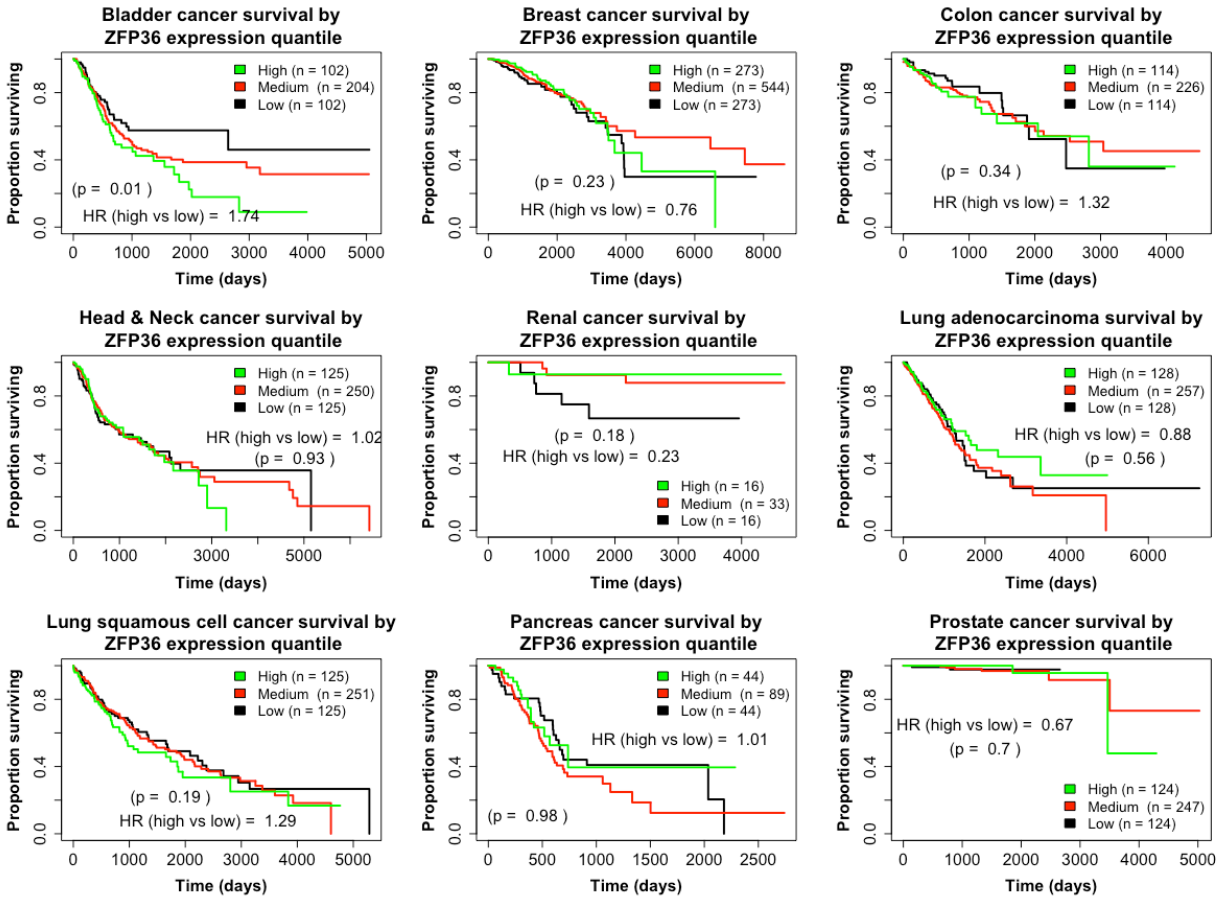

Figure 6. Overall survival by *ZFP36* expression quantile (TCGA)For each tumour type, samples were split into low (bottom 25%), medium (middle 50%) or high (top 25%) *ZFP36*-expressing tumours. HR = hazard ratio. P-value represents log-rank test of high vs low quantiles.

Given the lack of consistent association between *ZFP36* expression and survival we looked at whether *ZFP36* expression may actually be an unreliable indicator of its activity. For each cancer, we looked at log-fold change of established TTP targets (Brooks and Blackshear, 2013a) between *ZFP36* high and low-expressing quantiles. Because TTP destabilises its targets, high ZFP36 expression would be expected to associate with low expression of its targets (if indeed *ZFP36* expression correlates with its activity). Contrary to expectation, TTP targets tended to be more highly expressed in *ZFP36*-high quantiles and had lower expression in the *ZFP36*-low quantiles as shown in Figure 7.

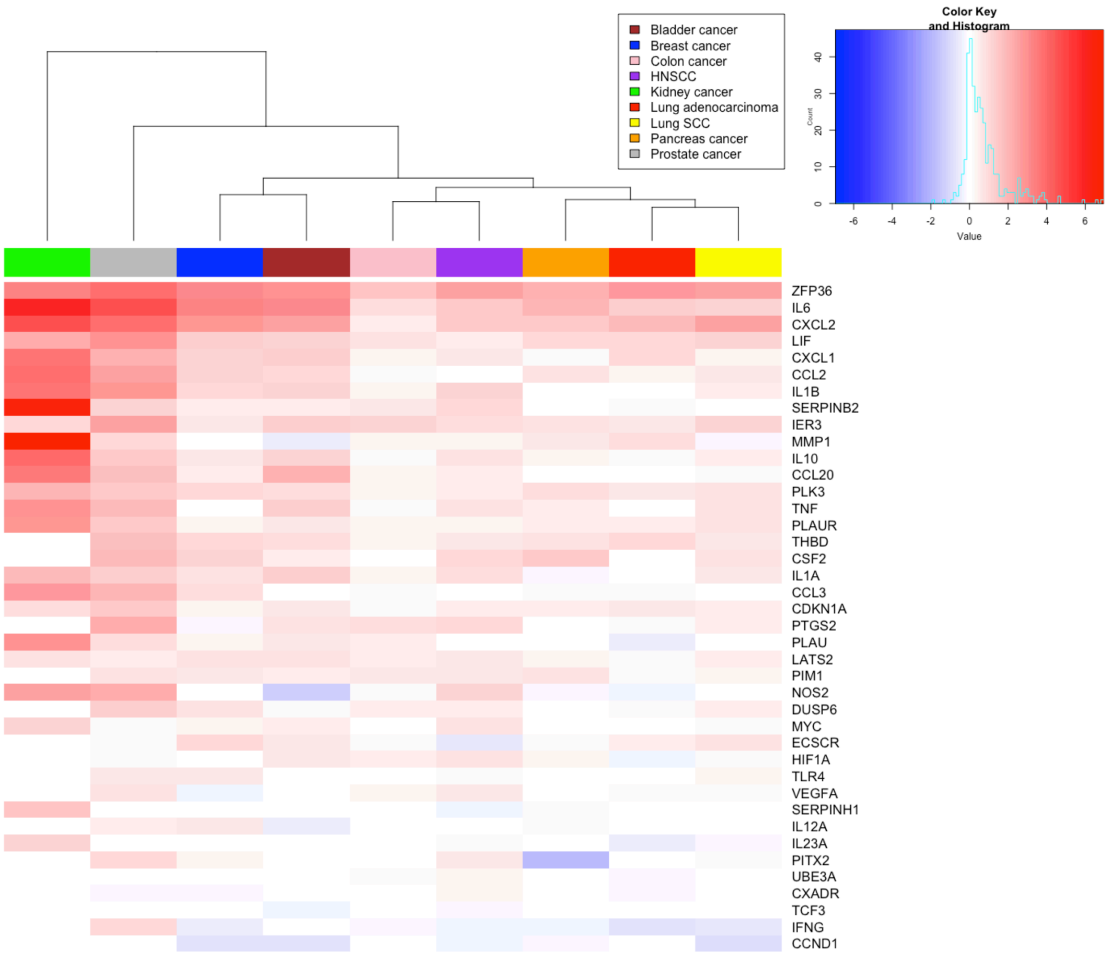

Figure 7. Log-fold change of established TTP targets between *ZFP36* expression quantiles (TCGA)Heatmap showing the log-fold change of TTP targets between high and low *ZFP36*-expressing quantiles. Red indicates upregulation in *ZFP36*-high quantile. HNSCC = head & neck squamous cell carcinoma.

Given the paradox that many TTP-targets appeared positively rather than negatively correlated with its gene expression, we looked more closely at which genes were most strongly positively correlated with *ZFP36*. As an example, in LUAD, several immediate early genes (Bahrami and Drabløs, 2016) were highly correlated with *ZFP36* gene expression across samples (Figure 8). Furthermore, these same genes were repressed across primary tumour sites (relative to normal tissue) in a manner similar to ZFP36 (data not shown).

We also used the 'RAS84' gene set, a transcriptomic signature of RAS activity developed in our lab by Sophie De Carne and Philip East (East *et al.*, 2021), we identified tumours with the lowest RAS activity - RAS activity group 0 (RAG-0) and then superimposed this annotation on the plots (Figure 8). As shown, these tumours have low of expression of *ZFP36* and its correlated genes. While *ZFP36* is a component of the RAS84 signature, it is evident that the other positively correlated genes, while not all part of the signature, also show association with low RAS84 index. As support of this link, when examining the mutational spectra between *ZFP36* expression quantiles, it is evident that the frequency of various oncogene or TSG aberrations show trends across the quantiles (Figure 9). In particular, KRAS mutations are almost three times more frequent in the highest *ZFP36*-expression quartile (45.67%) versus the lowest (15.75%).

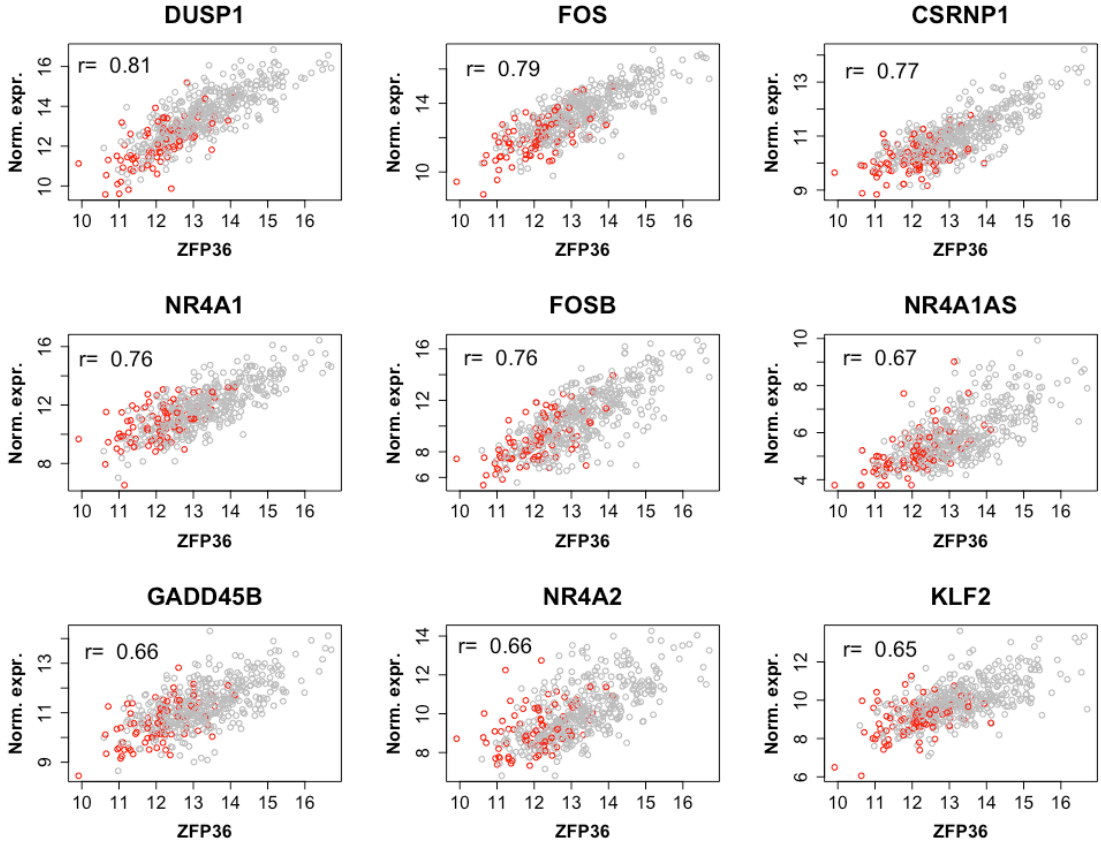

Figure 8. Most strongly positively correlated genes with *ZFP36* in LUAD Plots show the most highly correlated genes with *ZFP36* in LUAD (TCGA), using VST-normalised data. Red circles indicate samples belonging to RAS activity group 0 (lowest RAS transcriptional activity, (East *et al.*, 2021))

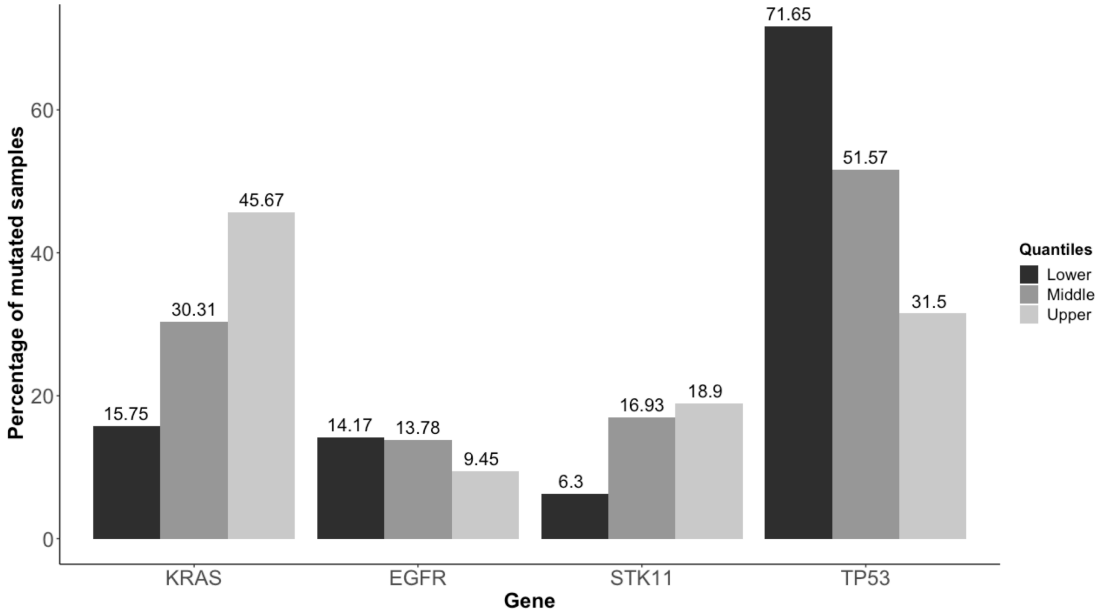

Figure 9. Mutation frequencies across *ZFP36* expression quantiles in LUAD

For each tumour type, samples were split into low (bottom 25%), medium (middle 50%) or high (top 25%) *ZFP36*-expressing tumours. Oncogenic or TSG mutations per quantile were plotted as bars.

We next looked for overlap in the module of genes that are highly correlated with *ZFP36*, between four tumour types; LUAD, COAD, PAAD and BLCA. Of the 50 genes most highly correlated with *ZFP36* in the individual tumour types, 22 overlapped between all four (Figure 10).

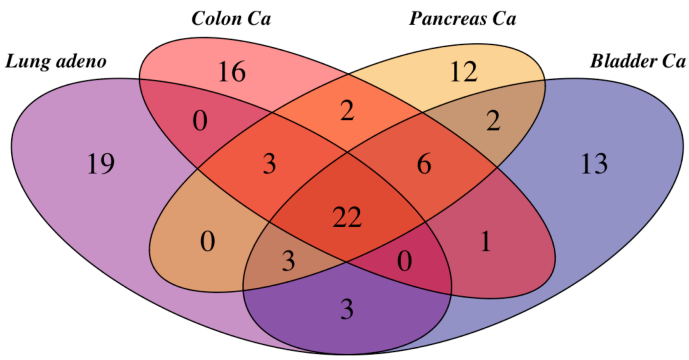

Intersect genes	
ZFP36	ATF3
DUSP1	PPP1R15A
FOS	RHOB
CSRNP1	SOCS3
NR4A1	HBEGF
FOSB	EGR3
GADD45B	JUN
NR4A2	MCL1
EGR1	KLF6
JUNB	IER2
NR4A3	ITPRIP

Figure 10. Overlapping *ZFP36*-correlated genes across cancers

The 50 most-highly correlated genes with ZFP36 in four TCGA tumour types are shown in the Venn diagram. Intersect genes refer to the 22 overlapping genes across all four types.

Given the failure of *ZFP36* expression to reliably predict survival when used in isolation, we instead looked at whether expression of this '*ZFP36* co-expression' module (of 22 genes correlated with *ZFP36* expression across 4 different tumour types) may be predictive instead. Across the four tumour types in which the genes were selected, there was no consistent nor significant association with survival.

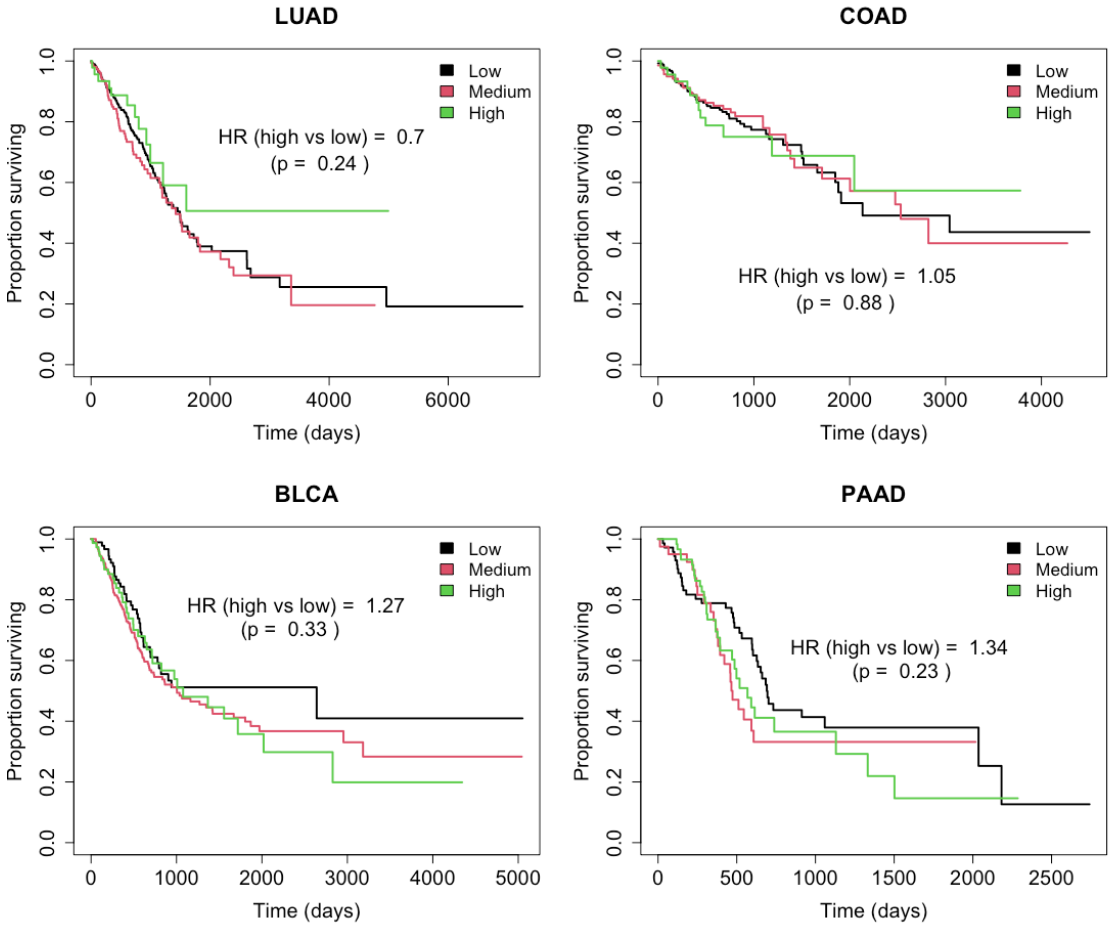

Figure 11. Survival by *ZFP36* co-expression module cluster For each tumour types, samples were clustered into three groups according to mean expression of the *ZFP36* co-expression module (low, medium or high). Survival for each was plotted along with the hazard ratio (HR) between high and low-expressors. P-value indicates significance of log-rank test between high and low cohorts.

To conclude this section, *ZFP36* gene expression is reduced across a broad range of malignancies relative to normal tissue. Nonetheless, its expression alone does not predict survival. Furthermore *ZFP36*, rather than being anticorrelated with its targets, shows a positive association instead. In fact, several genes including various immediate early genes, are positively correlated with *ZFP36* across malignancies. These genes tend to associate with RAS transcriptional activity (according to the RAS84 gene signature) suggesting that RAS may transcriptionally drive TTP and related gene expression. To this end, tumours with mutations in KRAS had higher TTP expression than wild-type KRAS LUAD. Even when all these genes are considered together, there was no obvious impact on patient survival. Given that *ZFP36* shows tumour suppressor characteristics in pre-clinical studies, it is unlikely that *ZFP36* gene expression in isolation (nor as part of a simple correlated gene module) is a reliable surrogate of its activity. Instead, a better surrogate of TTP activity, for example looking at its targets directly, may be more likely to predict survival in cancers where inhibition of TTP activity is an important tumour-suppressive mechanism.

3.3 TTP modulates gene expression in CT26 cells

While *ZFP36* expression in human tumours was not able to predict survival nor appeared a good surrogate of its activity, there is still pre-clinical evidence of tumour-suppressive activity of TTP warranting further study. Despite this, its global transcriptomic effect in tumour cells is not well described. In order to assess the ability of TTP to regulate tumour-intrinsic expression of immunomodulatory genes in an immunogenic model, we used CT26 (murine colon carcinoma) derivatives that had previously been generated in the lab (Figure 12) (Coelho *et al.*, 2017). These included:

1) Parental CT26 cells transfected with ‘empty’ Cas9 (hereafter called ‘parental’ cells)

2) CT26 cells where *Zfp36* had been functionally knocked out using CRISPR/Cas9 (hereafter called 'TTP KO' cells)

3) TTP KO cells transduced with doxycycline-inducible, wild-type, murine *Zfp36* (hereafter 'Tet-On TTP(WT)' cells)

4) TTP KO cells transduced with doxycycline-inducible murine TTP with serine to alanine mutations at positions 52 and 178, precluding phosphorylation at these sites (hereafter 'Tet-On TTP(aamt)' cells)

As alluded to in the introduction, TTP is phosphorylated at serines 52 and 178 by p38 MAPK. This phosphorylation stabilizes the protein but inhibits its function. Mutation of these residues from serine to alanine precludes phosphorylation, rendering TTP constitutively active. Mice with constitutional serine to alanine mutations at these residues are protected from certain inflammatory pathology (Ross *et al.*, 2015).

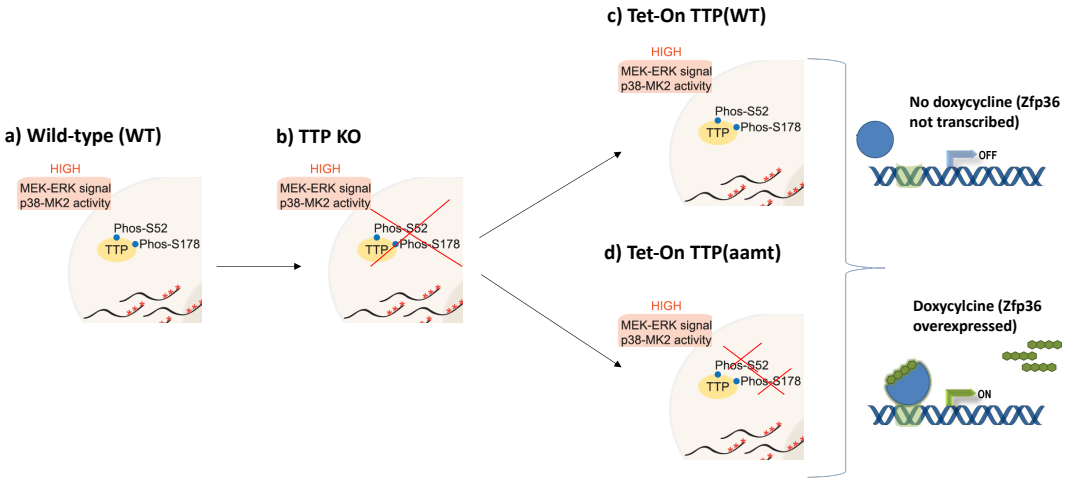

Figure 12 CT26 derivatives Figure adapted from (Coelho *et al.*, 2017). Derivatives include a) parental CT26 cells; b) parental cells with CRISPR/Cas9-mediated knockout of *Zfp36*; c) as per b) but reconstituted with doxycycline-inducible wild-type TTP; d) as per b) but reconstituted with doxycycline-inducible phosphosite-mutant TTP

We validated the system by measuring induction of *Zfp36* mRNA and its effect on *Cd274* upon stimulation of cells with 1μg/μl doxycycline. *Cd274* acted as our positive control given the established effect of TTP on its stability (Coelho *et al.*, 2017). As below, application of doxycycline resulted in robust induction of *Zfp36* mRNA only in derivatives with doxycycline-inducible TTP. In the same lines, *Cd274* mRNA was reliably reduced (Figure 13).

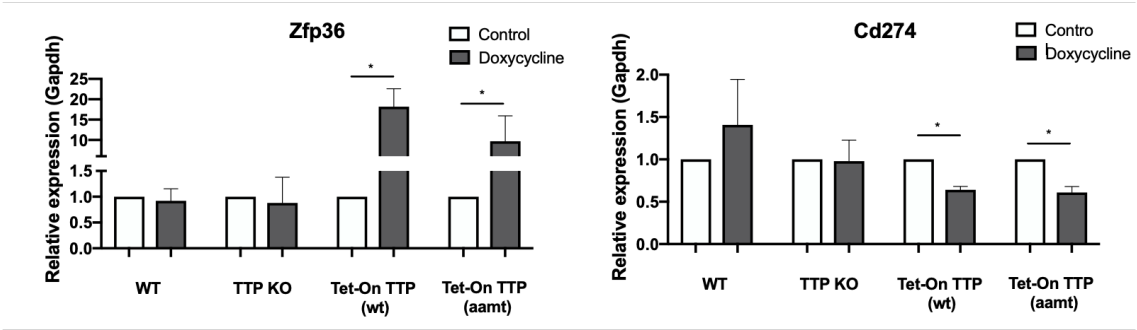

Figure 13. Validation of CT26 derivatives 10^5 cells were plated per well of a 6-well plate for 24 hours before adding doxycycline (1μg/ml) or vehicle (DMSO). After a further 24 hours, cells were harvested and RNA was extracted for qPCR. Data represent means ± SD of three biological replicates. Statistical comparisons performed using independent t-tests.

To test the effect of TTP induction beyond *Cd274* we performed qPCR on putative TTP targets, as described by Brooks et al.(Brooks and Blackshear, 2013a), specifically focussing on those with known roles in tumour immune evasion. We showed that induction of TTP resulted in downregulation of *Ptgs2* and *Vegfa* mRNA, but not *Myc* (Figure 14).

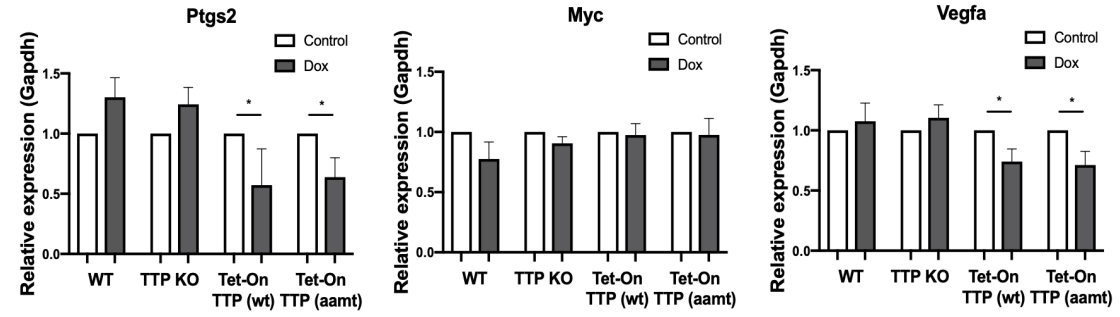

Figure 14. Effect of TTP induction beyond *Cd274* 10^5 cells were plated per well of a 6-well plate for 24 hours before adding doxycycline (1μg/ml) or vehicle (DMSO). After a further 24 hours RNA was extracted for qPCR. Data represent means ± SD of three biological replicates. Statistical comparisons performed using independent t-tests.

The canonical function of TTP involves regulation of the resolution phase of the inflammatory response, where it contributes to destabilisation of cytokine mRNA. We tested the effect of TTP induction on the levels of various cytokine mRNA in CT26 cells. The effect of TTP on cytokine mRNA levels was difficult to appreciate due to the low expression of many such mRNA species in this model (data not shown). Nonetheless, the relationship between cytokine mRNA and liberated protein levels is complex. Therefore, in order to examine the breadth of TTP effect on the cell secretome, we performed a cytokine array (Figure 15)

A.

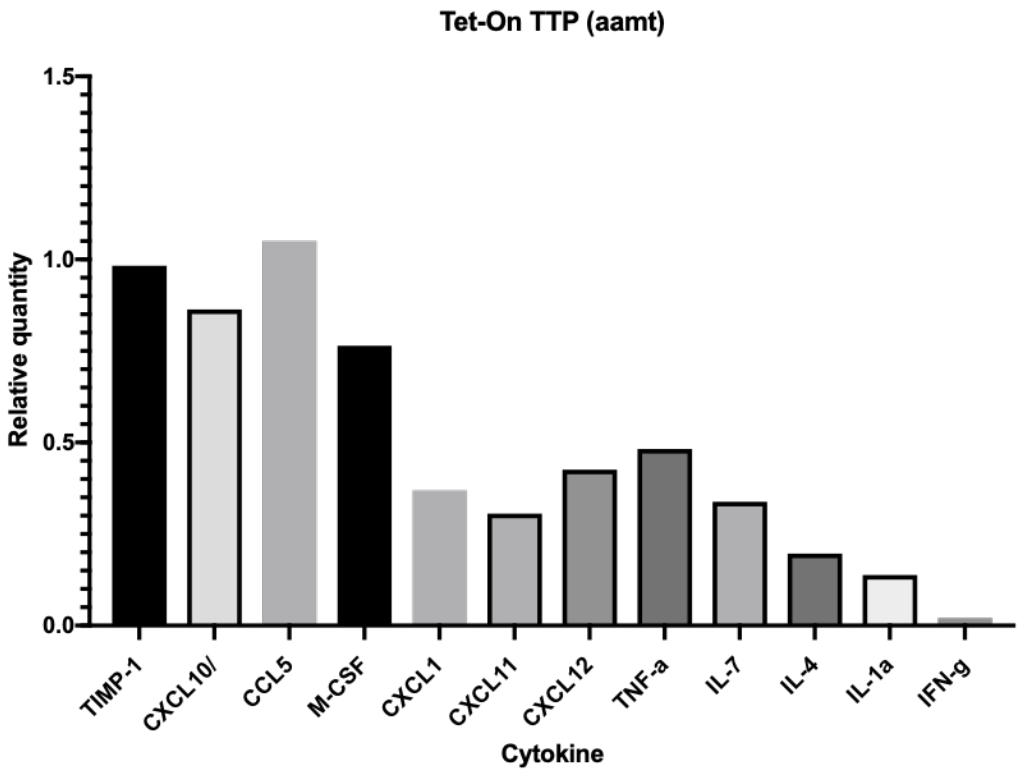

B.

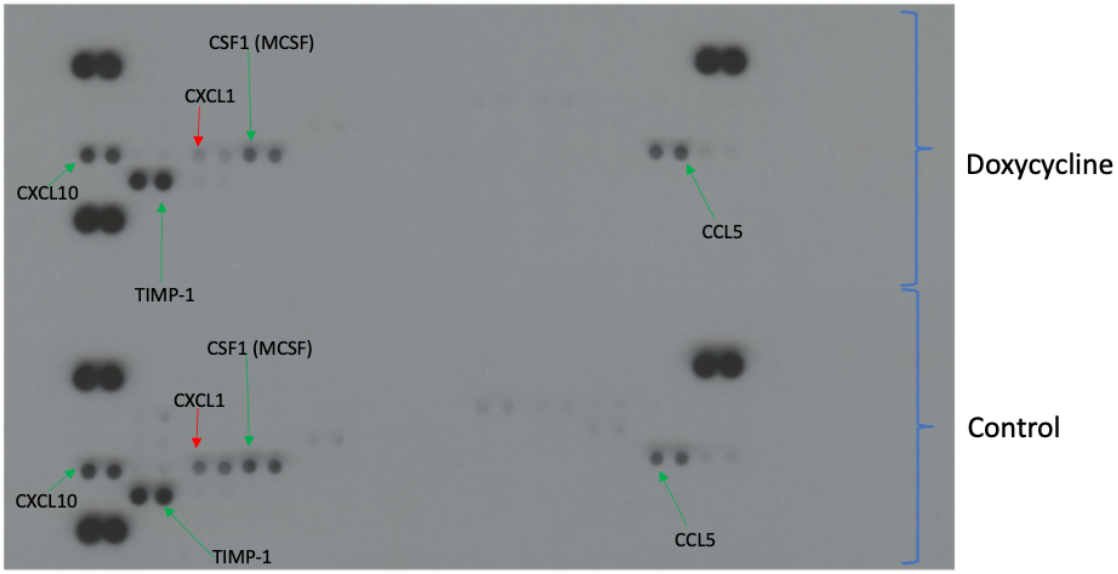

Figure 15. Cytokine array: effect of TTP induction in CT26 Tet-on TTP(aamt)

A. Cytokine array; Tet-On TTP(aamt) cells were treated with doxycycline (1 µg/ml) or vehicle control (DMSO) for 24 hours prior to supernatant harvest. Fresh medium (with doxyxcyline or control) was added overnight prior to harvest. Data

represented as relative pixel density of treatment/control for the 5-minute exposure time, x-axis ordered by control pixel density. **B.** Exposure film at 10-minute time-point. Red arrows: CXCL1; green arrows: representative molecules not affected by TTP induction.

Although TTP induction appeared to have a broad effect, reducing levels of several secreted molecules, many were not expressed very strongly. Conversely, many which were expressed at higher levels (e.g. CXCL10, CCL5 and CSF1) were relatively unaffected. However, we identified CXCL1 as downregulated by TTP overexpression and also liberated at relatively high quantities. Interestingly, CXCL1 is also a known KRAS target (Cullis, Das and Bar-Sagi, 2018).. Its expression in all four CT26 derivates following doxycycline exposure was validated by ELISA Figure 16). CXCL1 expression was reduced in the TTP-inducible lines, but not in the parental or TTP KO lines. Therefore, TTP overexpression is able to modulate the secreted levels of CXCL1 in our system.

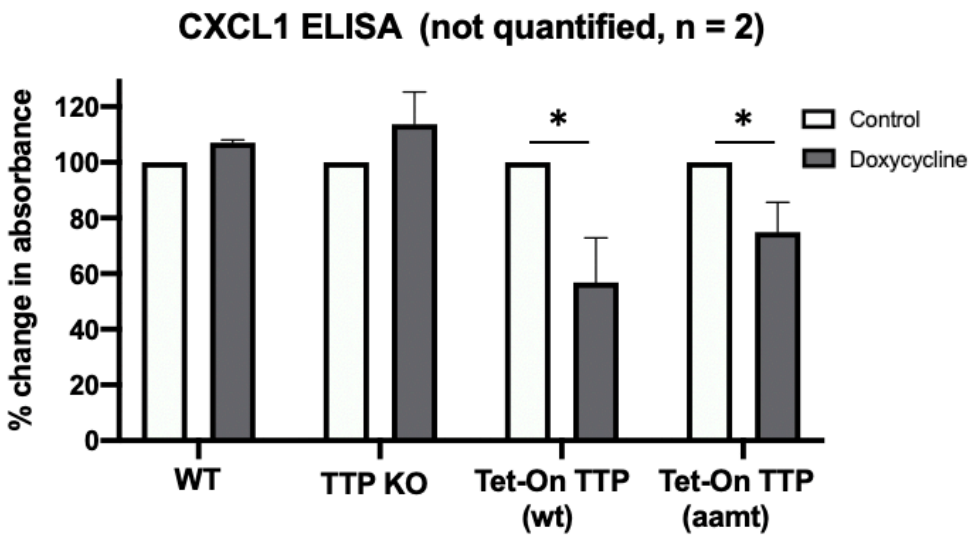

Figure 16. CXCL1 ELISA ELISA for CXCL1 following treatment of CT26 cells with doxycycline (1 µg/ml) or vehicle control (DMSO) for 24 hours prior to supernatant harvest. Fresh medium (with doxycycline or control) was added overnight prior to harvest. (n=2). Data represented as means and SD. Bars represent significant different in means ($p < 0.05$) using t-test.

While TTP can influence transcription, its major mechanism of action on gene expression is through destabilisation of target mRNA. To examine the effect of TTP on transcript half-life, actinomycin-D was used to block transcription after TTP overexpression. While *Vegfa* transcript half-life was not clearly different between doxycycline and control-treated conditions, half-life of *Ptgs2* mRNA was reduced following TTP induction, consistent with the notion that TTP affects steady-state expression by reducing transcript stability.

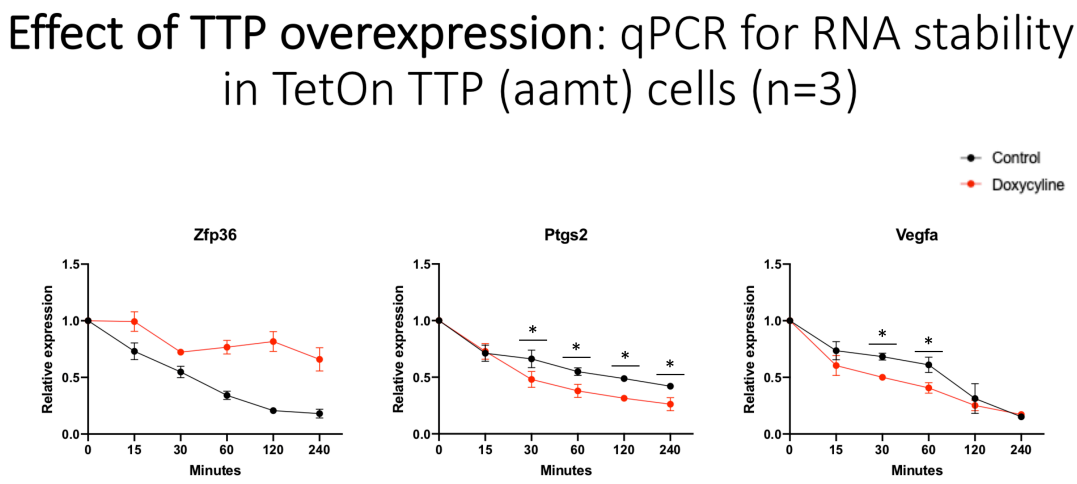

Figure 17. Zfp36 induction increases Ptgs2 instability Tet-On TTP(aamt) cells were treated with doxycycline (1 µg/ml) or vehicle control (DMSO) for 24 hours prior to administration of 5 µg/ml of actinomycin D. RNA was harvested at 0, 30, 60, 120 and 240 minutes after administration. For Ptgs2 and Vegfa, ANOVA was used to test all time points together ($p < 0.05$ for both) and then t-tests used for individual time-points ($p < 0.05$ denoted by asterisks)

Thus, TTP overexpression modulates gene expression in CT26 cells. Across three previously-described TTP targets – Ptgs2, Vegfa and Myc – expression of the former two was reduced in response to induction of the TTP gene, Zfp36. Furthermore, in a cytokine array panel, CXCL1 expression was reduced upon TTP induction, and effect confirmed with ELISA. The effect (on Ptgs2 at least) was likely due to transcript destabilisation, as shown by time course experiments after application of actinomycin D to block transcription.

In order to gain a broader understanding of the transcriptomic effect of TTP overexpression in this system we conducted an RNAseq experiment, as discussed next.

3.4 TTP induces downregulation of gene modules involved in oncogenic processes

CT26 derivatives were treated with either doxycycline (1μg/ml) or DMSO (1μl/ml) for 24 hours before RNA extraction. Experiments were done in triplicate and validated for Ptgs2 effect, as a positive control (Figure 18) before submission for RNA sequencing.

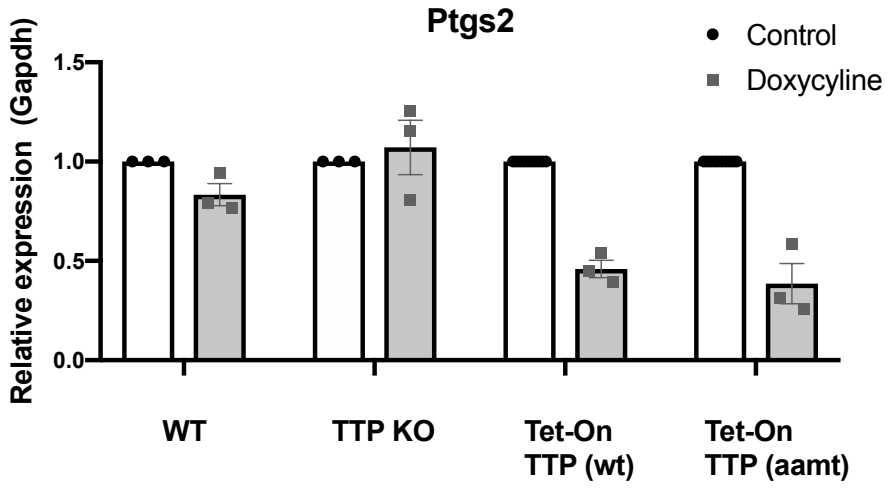

Figure 18. qPCR: validation of samples submitted for RNA sequencing 10^5 cells were plated per well of a 6-well plate for 24 hours before adding doxycycline (1μg/ml) or vehicle (DMSO). After a further 24 hours RNA was extracted. Data represent means ± SD of three biological replicates.

Following library preparation, sequencing and pre-processing (see methods), data was first screened using principal component analysis (PCA). Data from CT26 Tet-on TTP(aamt) cells, where phosphosite-mutant TTP is inducible upon

addition of doxycycline, showed separation by treatment (doxycycline vs control) along principal component 2 (PC2) in contrast to CT26 WT cells, where no obvious separation by treatment effect was obvious in the first two PCs (Figure 19).

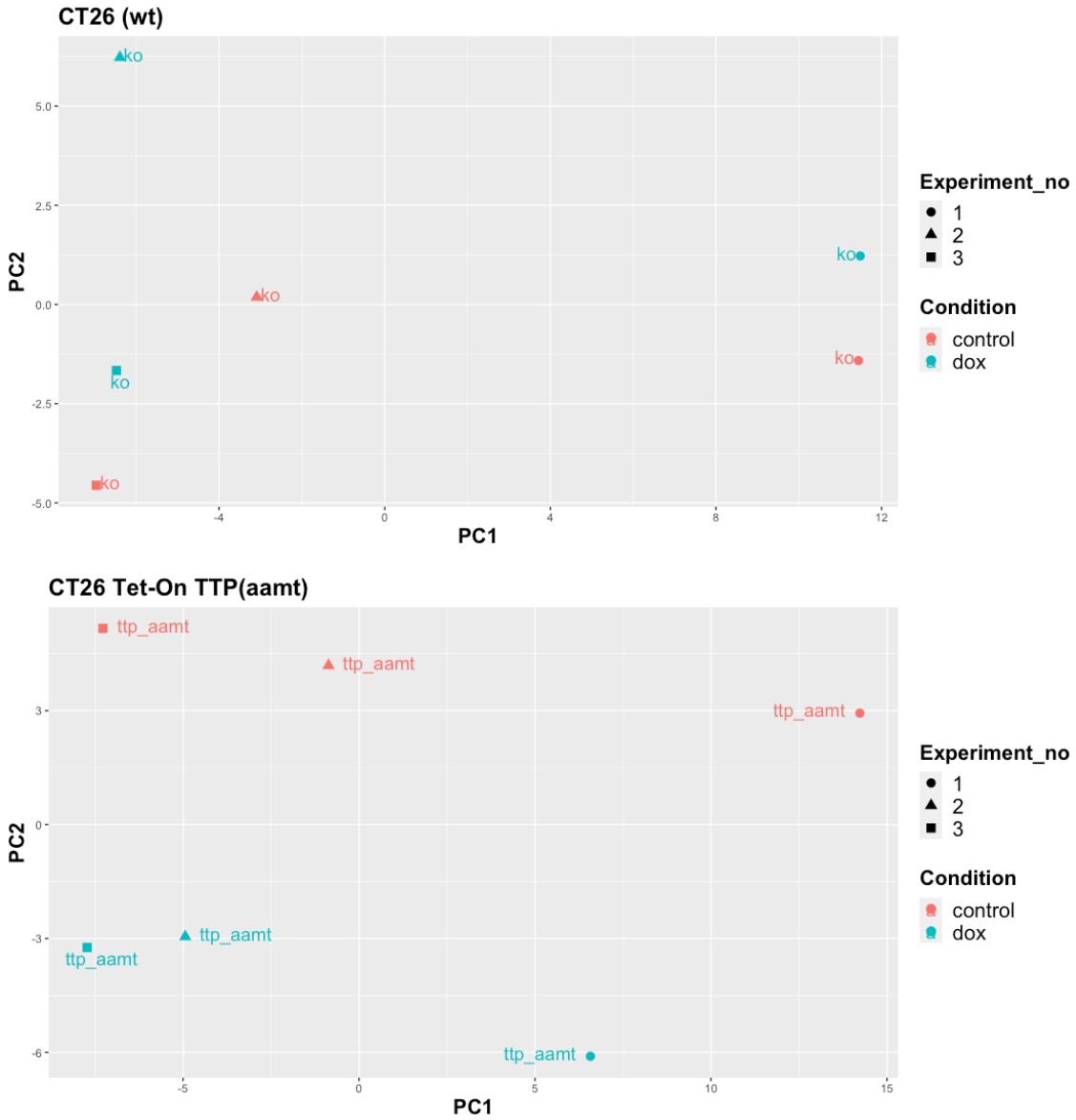

Figure 19. Principal component analysis of RNAseq data. PCA plots of CT26 (wt) and Tet-on (aamt) lines showing separation by treatment in PC2 for the latter.

Next, differential expression analysis was performed to specifically look at the genes downregulated upon TTP induction in both CT26 Tet-On TTP(wt) and CT26 Tet-On TTP(aamt) lines. As shown below, 116 and 105 genes were

significantly downregulated below an LFC of < -0.5 (equivalent to approximately ≥30% reduction) upon TTP induction, in the Tet-On TTP(wt) and Tet-On TTP(aamt) lines respectively. Only 15 and 10 genes respectively were significantly decreased by more than 50%.

	CT26 Tet-On TTP (wt)		**CT26 Tet-On TTP (aamt)**	
LFC	**Number**	**%**	**Number**	**%**
>2	9	0.06	8	0.05
>1.5	13	0.09	12	0.08
>1	24	0.16	31	0.21
>0.5	108	0.72	136	0.91
> 0	514	3.44	509	3.41
< 0	761	5.09	727	4.87
<-0.5	118	0.78	106	0.70
<-1	15	0.10	10	0.07
<-1.5	2	0.01	2	0.01
<-2	0	0.00	0	0.00

Table 10. Summary of Log Fold Changes upon TTP induction in Tet-On TTP(wt) and Tet-On TTP(aamt) lines. For each $\log_2$ fold change (LFC) the number of genes under or overexpressed upon induction of TTP is shown. Percentages refer to the percentage of all genes tested. All genes had an adjusted p value of < 0.1.

A graphical summary these changes is given by the MA plot in Figure 20. Fortuitously, Ptgs2 (which had been our positive control previously) was the most strongly downregulated gene in the Tet-On TTP(aamt) line and the 3rd most strongly downregulated in the Tet-On TTP(wt) line. Exact values for the most strongly downregulated genes in either line, are shown in Table 11

CT26 (Tet-On TTP(wt)

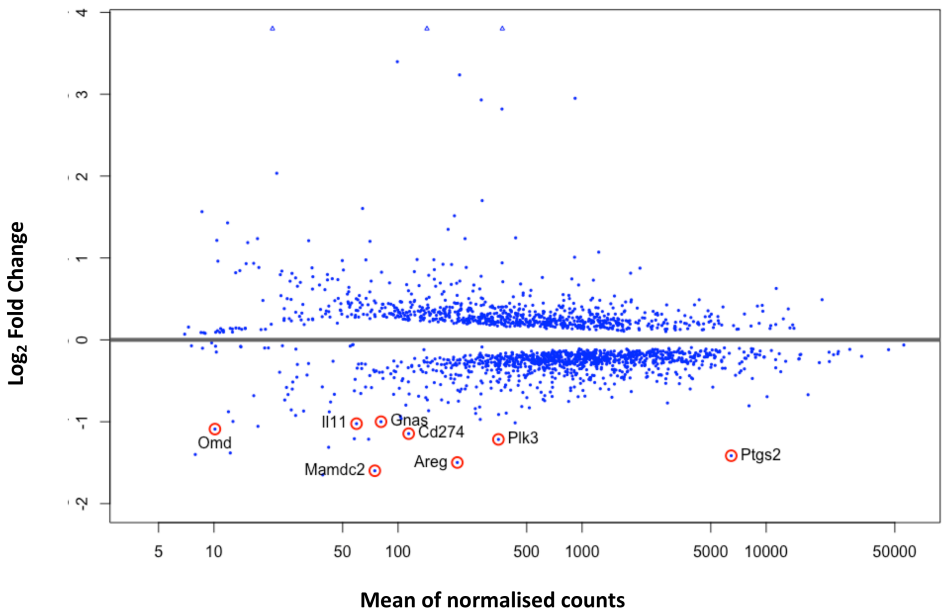

CT26 (Tet-On TTP(aamt)

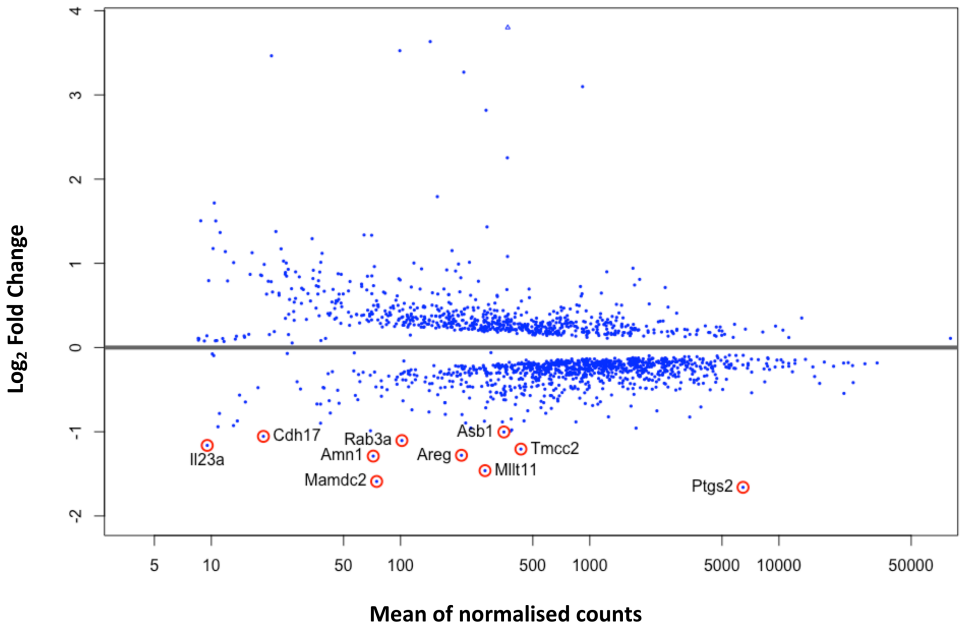

Figure 20. MA plot displaying effects of TTP induction in Tet-On TTP(wt) and Tet-on TTP(aamt) lines Here, the $\log_2$ fold change for each gene is plotted against its mean expression. Only genes with an adjusted p value of <0.1 are shown, and the 10 most strongly downregulated genes are highlighted.

	CT26 Tet-On TTP (wt)				CT26 Tet-On TTP (aamt)		
Name	**Mean expr.**	**LFC**	**Adj. p val.**	**Name**	**Mean expr.**	**LFC**	**Adj. p val.**
Mamdc2	74.8	-1.6	0.014	**Ptgs2**	6457.5	-1.66	<0.001
Areg	209.9	-1.5	<0.001	**Mamdc2**	74.8	-1.59	0.016
Ptgs2	6457.5	-1.42	<0.001	**Mllt11**	279.6	-1.46	<0.001
Plk3	351.1	-1.22	<0.001	**Amn1**	71.7	-1.29	<0.001
Srrm4	69.2	-1.21	<0.001	**Areg**	209.9	-1.28	<0.001
Cd274	114.2	-1.15	0.002	**Tmcc2**	432.6	-1.21	<0.001
Omd	10.1	-1.09	0.023	**Il23a**	9.5	-1.16	0.025
Il11	59.46	-1.02	<0.001	**Rab3a**	101.6	-1.1	<0.001
Tmcc2	432.57	-1.01	<0.001	**Cdh17**	18.9	-1.05	0.005
Gnas	80.82	-1	<0.001	**Asb1**	351.8	-1	<0.001

Table 11. Most strongly downregulated genes upon TTP induction

The 10 most strongly downregulated genes following TTP induction (adjusted p-value < 0.05) are shown for each line.

We next looked at the overlap between genes downregulated in both lines. Of 118 and 106 genes significantly downregulated below a LFC of -0.5 in Tet-On TTP(wt) and Tet-On TTP(aamt) lines respectively, 39 overlapped between the two groups (Figure 21). The 10 genes with the strongest mean reductions are shown in Table 12. Of note, several established RAS targets including Ptgs2, Areg, Lif and Plk3 appeared in this overlap.

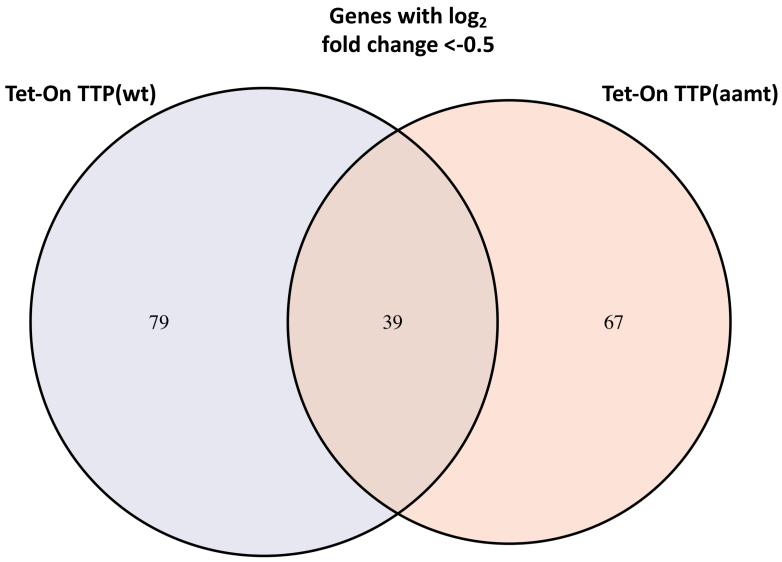

Figure 21. Overlap of downregulated genes Genes downregulated by <-0.5 (adjusted p-value < 0.1) following TTP induction

		Tet-ON TTP (WT)		Tet-ON TTP (aamt)	
	Mean expression	**Log_2 fold change**	**Adjusted p value**	**Log_2 fold change**	**Adjusted p value**
Ptgs2	6457.52	-1.42	<0.001	-1.66	<0.001
Mamdc2	74.77	-1.60	0.014	-1.59	0.016
Areg	209.86	-1.50	<0.001	-1.28	<0.001
Mllt11	279.64	-0.97	<0.001	-1.46	<0.001
Tmcc2	432.57	-1.01	<0.001	-1.21	<0.001
Hist1h2bc	41.97	-1.31	<0.001	-0.63	0.022
Asb1	351.83	-0.91	<0.001	-1.00	<0.001
Lif	387.00	-0.89	<0.001	-0.98	<0.001
Amn1	71.75	-0.58	0.004	-1.29	<0.001
Plk3	351.12	-1.22	<0.001	-0.50	0.032

Table 12. Top genes underexpressed in both datasets Results (adjusted p < 0.05) are ordered by mean log_2 fold change across the two lines

We next wanted to see whether the genes identified in our dataset are consistent with those known to be validated by TTP. We used the manually curated TTP-target genes list from Brooks et al (Brooks and Blackshear, 2013a). Table 13 shows these putative TTP targets and their $\log_2$ fold changes in our TTP-inducible cell lines. Highlighted in bold are those that were significantly underexpressed in our dataset. The table shows that many known TTP targets were significantly downregulated. A Fischer's exact test looking for enrichment of TTP targets in amongst the downregulated genes in our dataset was highly significant ($p < 0.0001$). The distribution of these literature-curated targets for the Tet-On TTP(aamt) line is shown in an MA plot (Figure 22). As shown, most genes are downregulated, and many are significant (fall within the red points on the graph) at an adjusted p-value of < 0.1.

		Tet-ON TTP (WT)		**Tet-ON TTP (aamt)**	
	Mean expression	**Log2 fold change**	**Adjusted p value**	**Log2 fold change**	**Adjusted p value**
Ccnd1	7290.5	0.00	0.991	-0.10	0.292
Ptgs2	**6457.5**	**-1.42**	**<0.001**	**-1.66**	**<0.001**
Serpinh1	6140.1	-0.02	0.827	-0.08	0.356
Myc	2782.4	-0.18	0.165	-0.22	0.064
Hif1a	**2746.7**	**-0.19**	**0.007**	**-0.16**	**0.021**
Cdkn1a	**2697.3**	**-0.43**	**0.009**	-0.26	0.076
Vegfa	**2591.9**	**-0.35**	**0.002**	**-0.47**	**<0.001**
Ube3a	2526.2	-0.23	0.071	-0.27	0.069
Dusp6	1828.1	-0.17	0.123	-0.11	0.335
Plaur	**1651.9**	**-0.39**	**<0.001**	**-0.70**	**<0.001**
Lats2	1157.0	-0.29	0.010	-0.27	0.019
Tcf3	794.0	0.04	0.800	0.10	0.438
Ier3	**571.1**	**-0.59**	**<0.001**	**-0.65**	**<0.001**
Lif	**387.0**	**-0.89**	**<0.001**	**-0.98**	**<0.001**
Tlr4	355.0	0.12	0.317	0.22	0.139

Plk3	**351.1**	**-1.22**	**<0.001**	**-0.50**	**0.032**
Pim1	122.1	-0.39	0.016	-0.33	0.032
Cd274	**114.2**	**-1.15**	**0.002**	-0.05	0.675
Thbd	74.2	-0.05	0.511	-0.47	0.057
Ecscr	**49.8**	**0.97**	**<0.001**	**0.64**	**0.005**
Cxcl1	11.0	0.00	0.972	0.05	0.405
Il23a	9.5	-0.03	0.407	-1.16	0.025
Il6	6.7	0.00	0.667	-0.01	NA
Clmp	6.2	0.03	NA	0.02	NA
Nos2	3.6	-0.02	NA	0.00	NA
Ccl2	2.2	-0.02	NA	-0.03	NA
Csf2	1.2	-0.01	NA	-0.03	NA

Table 13. Literature-curated TTP targets Data shows $\log_2$ fold change (and adjusted p-values) after 24 hours of *Zfp36* induction for the two cell lines as indicated. Bold entires indicate thoe with am adjusted p-value < 0.01.

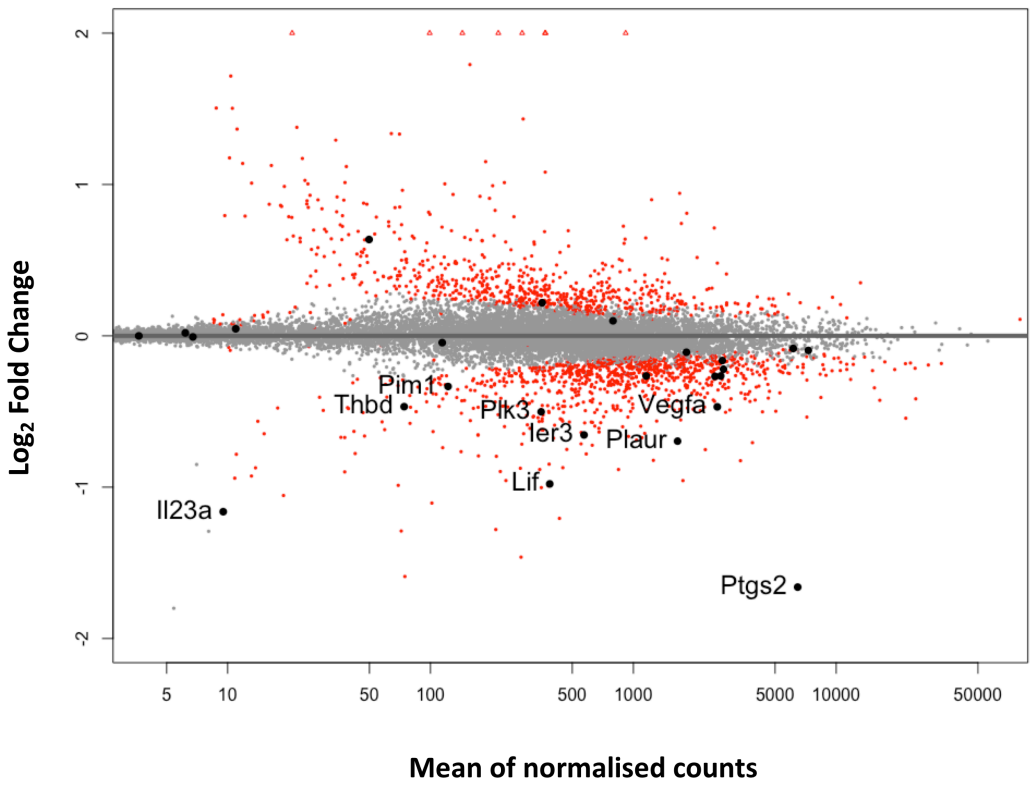

Figure 22. MA plot showing distribution of literature-curated TTP targets in Tet-On TTP(aamt) cells TTP targets shown in black. Those with a $\log_2$ fold change <-0.3 are annotated. Grey dots indicate genes that are not significantly changed (adjusted p value > 0.1), red dots are significant

Significant enrichment of TTP targets within the downregulated compartment of our data suggested that our system was performing as intended. In order to further interrogate the nature of the underexpressed genes, we performed gene set enrichment analysis looking at Tet-On TTP(wt) and Tet-On TTP(aamt) lines. We initially looked at hallmark gene sets from the Molecular Signatures Database (MSigDB). Given the canonical role of TTP in destabilising TNFα, it was reassuring that the gene sets pertaining to "TNFα signalling via NFκB" and the "inflammatory response" were high amongst the most significantly downregulated gene sets for both lines (Table 14, Figure 23). MYC target genes, genes in the PI3K/AKT/mTOR pathway and genes involved in the unfolded protein response were also amongst those with the lowest normalised enrichment scores

	Tet-ON TTP (WT)			Tet-ON TTP (aamt)		
Hallmark Pathway	**Rank**	**NES**	**Adj. p val.**	**Rank**	**NES**	**Adj. p val.**
MYC_TARGETS_V1	1	-1.880	0.000	2	-1.844	0.000
UNFOLDED_PROTEIN_RESPONSE	4	-1.901	0.000	1	-2.072	0.000
TNFA_SIGNALING_VIA_NFKB	3	-1.836	0.000	4	-1.677	0.003
MTORC1_SIGNALING	7	-1.676	0.001	3	-1.856	0.000
INFLAMMATORY_RESPONSE	10	-1.721	0.002	6	-1.600	0.013
MYC_TARGETS_V2	8	-1.852	0.002	10	-1.517	0.100

Table 14. Gene set enrichment analysis Table shows the most significantly downregulated gene sets following TTP induction. Sets were ordered by their adjusted p value in each line and ranks were then averaged between lines. The 6 highest mean ranks are displayed.

Of note, when gene sets were overlaid on MA plots, other patterns emerged. For example, while the MTORC1 gene set was significantly down-regulated according to its normalised enrichment score (NES), only few genes displayed a $\log_2$ fold change of <-0.5. Conversely, while the NES for "TNFα signalling via NF$\kappa\beta$" was similar, many more genes showed a $\log_2$ fold change of <-0.5. A similar distribution was seen for genes within the "Hallmark inflammatory signalling" gene set (several genes with <-0.5 $\log_2$ fold change) vs. the "Hallmark Myc targets v1" (only one gene with $\log_2$ fold change <-0.5 despite low NES, data not shown). Thus, in the sets related to signalling, a high percentage of genes were downregulated but the magnitude of this effect was small. Conversely, with the inflammatory gene sets, a smaller percentage was downregulated ($\log_2$ fold change <0) but there were more genes with a relatively higher magnitude of downregulation ($\log_2$ fold change < -0.5) (Figure 24).

a) Tet-On TTP(wt)

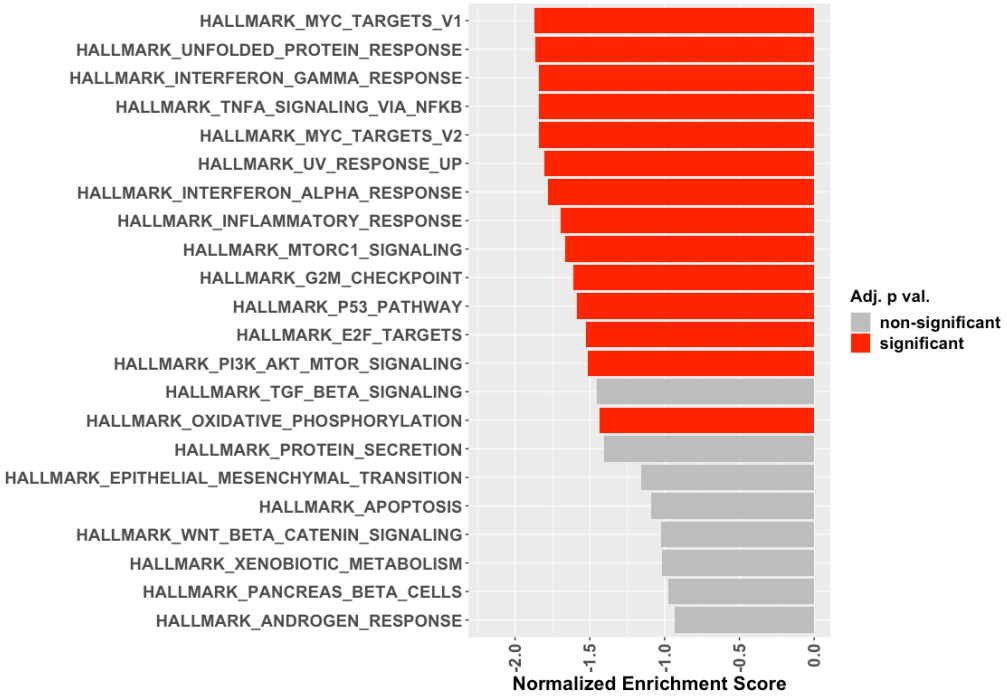

b) Tet-On TTP(aamt)

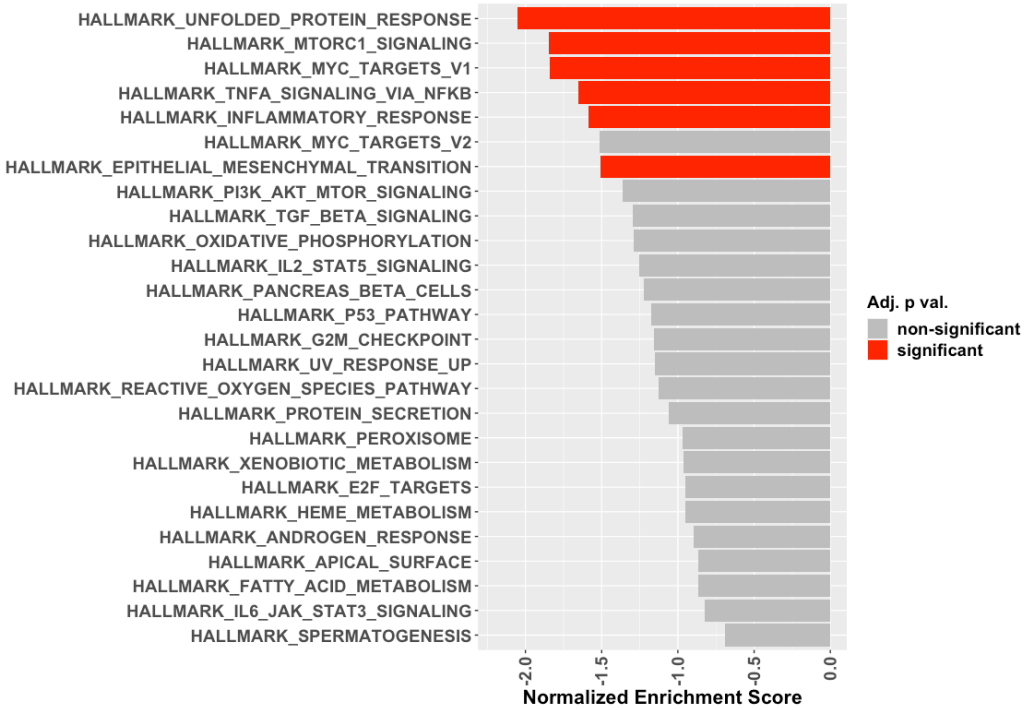

Figure 23. Gene set enrichment analysis - all downregulated sets All downregulated gene sets in a) Tet-On TTP(wt) and b) Tet-On TTP(aamt) lines, following TTP induction. Red bars indicate an adjusted p value < 0.05.

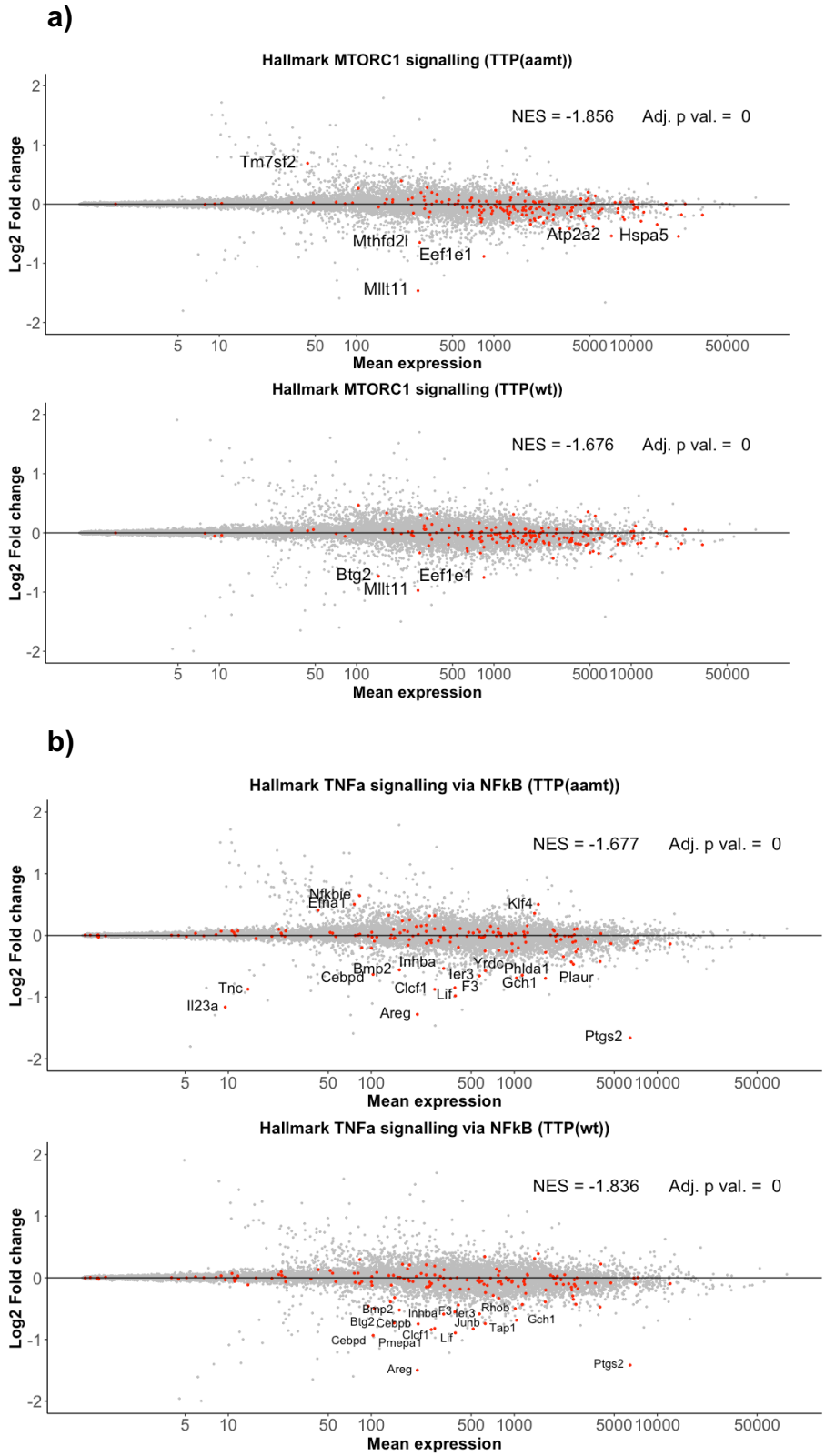

Figure 24. MA plots: selected gene sets MA plots for a) Hallmark MTORC1 genes and b) Hallmark TNFα signalling via NF$\kappa\beta$. Red dots represent genes belonging to pathway. Genes with an *absolute* $\log_2$ fold change >0.5 are annotated.

Given the importance of these downregulated gene sets in oncogenic processes, we next looked to see whether such TTP-downregulated genes may be important in human cancers. To this end, we attempted to build a signature of genes, and examine whether such a signature may be prognostic. We first selected genes with a $\log_2$ fold change of < -0.5 and an adjusted p-value of < 0.1 after induction of TTP in Tet-On TTP(aamt) cells. In order to only keep genes that varied sufficiently we plotted the mean of each gene in the TCGA LUAD dataset against its log coefficient of variation (ratio of standard deviation to mean). To this data, a smooth 'best fit' curve was fit using local regression (loess procedure). Genes which lay above the best fit line, are those with a high variability in the dataset (relative to their mean). These genes are more likely to be informative in terms of outcome metrics like prognosis. Genes with a low coefficient of variation vary little between patients and thus may not inform much yet could add noise to the data, as may genes with low expression. Therefore only genes which lay above the loess curve and had an arbitrarily high enough expression were retained in the signature.

Retained genes for each tumour type were used to cluster TCGA samples into three groups, which were labelled according to average expression of genes in each group (Figure 26).

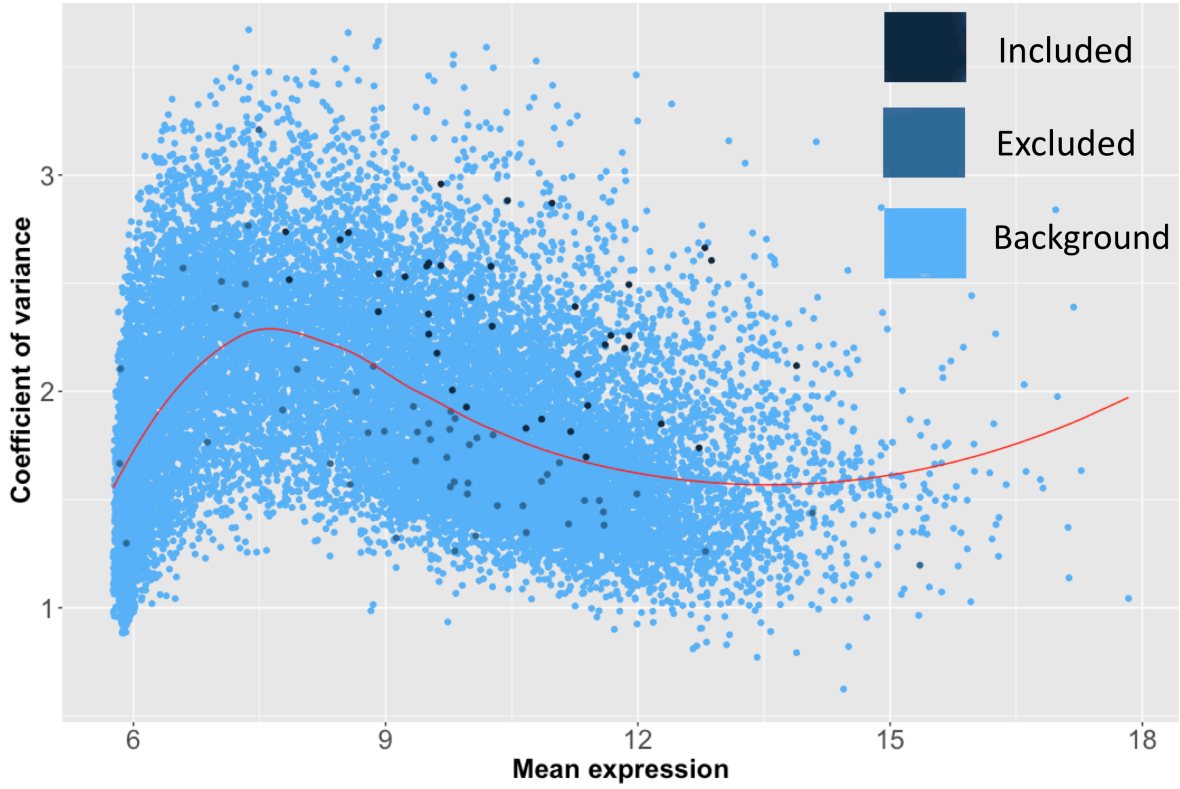

Figure 25. Selection of genes for signature Each dot represents a gene from the TCGA LUAD data set. The darker dots are those downregulated with an Log_2 fold change < -0.5 after induction of TTP in Tet-ON TTP(aamt). The darkest dots are those with sufficient expression and variance to be included in the signature. Similar analysis was done for the TCGA COAD dataset

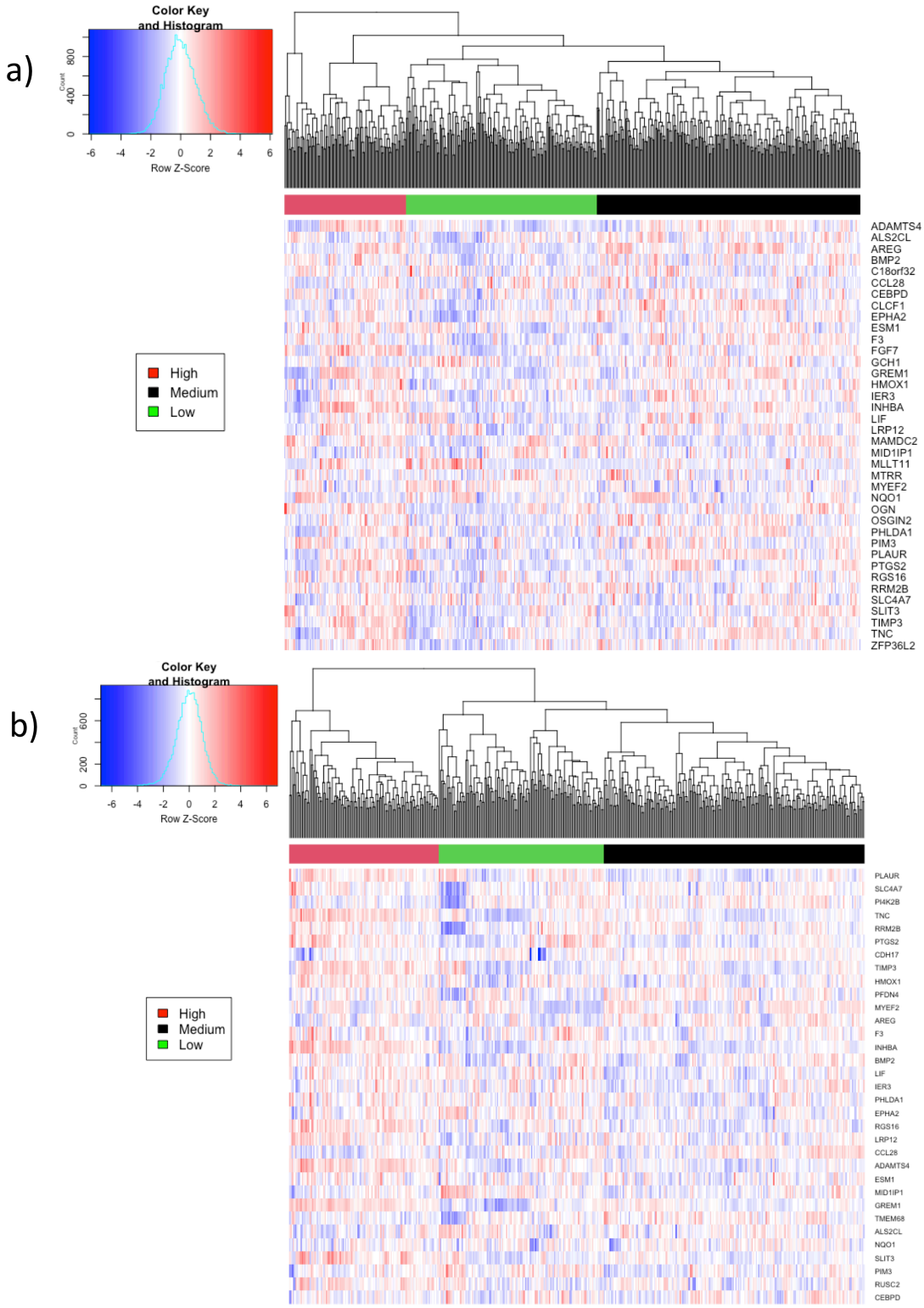

Figure 26. Clustering on 'TTP signature' genes Heatmaps demonstrating clustering of a) LUAD and b) COAD samples on 'TTP signature' genes. Clusters were annotated according to mean expression of signature genes.

Using such cluster annotations, we next looked at survival. As shown in Figure 27, samples with a high expression of signature genes had worse overall survival than those with lower expression. Those with a high expression of TTP signature genes had a 54% and 63% higher risk of death in LUAD and COAD respectively than those in the cluster with the lowest expression.

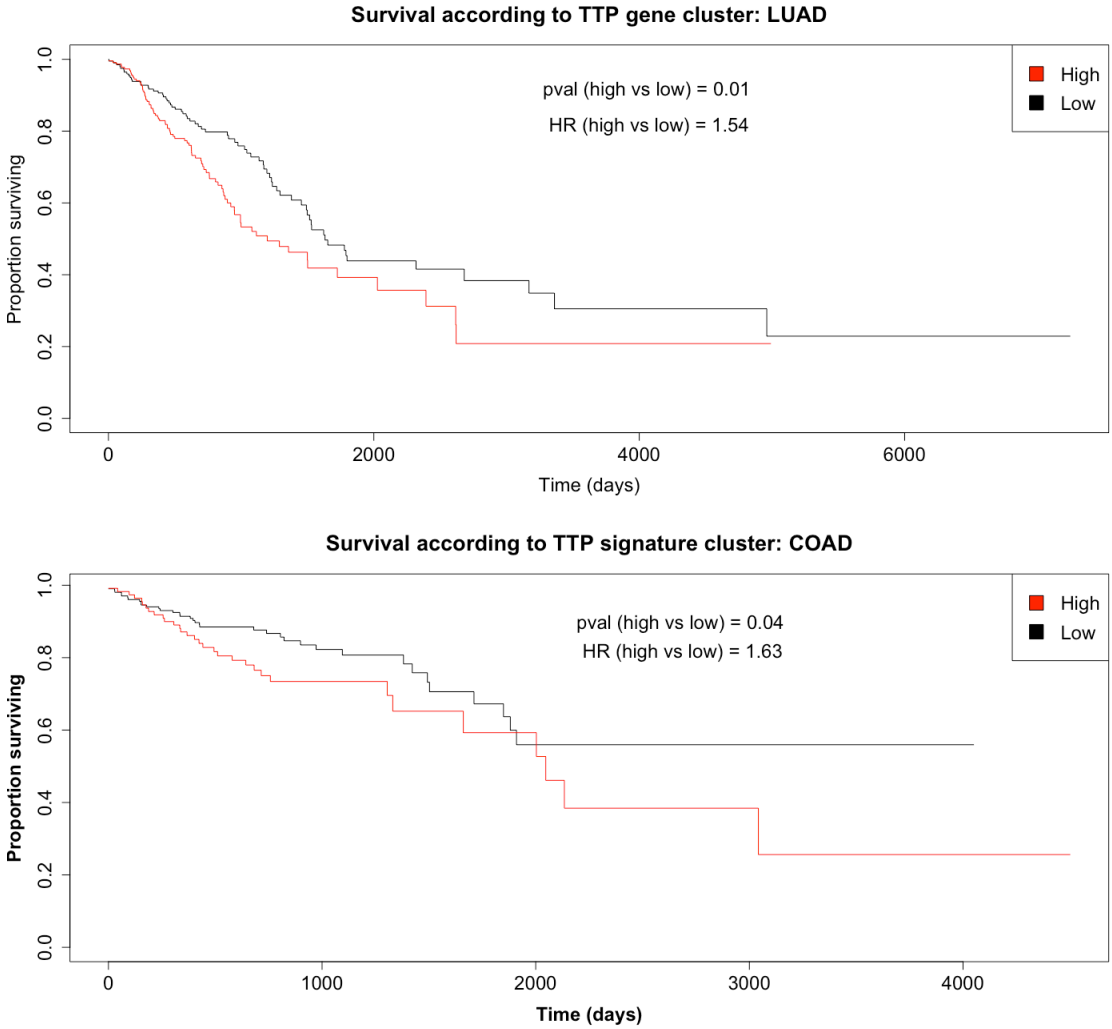

Figure 27. Overall survival by signature cluster For each tumour type samples were split into high and low groups depending on mean expression of TTP signature genes. Hazard ratios (cox proportional hazards model) and p-values (log-rank) between the two groups are shown

Thus, overexpression of TTP in CT26 cells results in downregulation of a number of gene sets including those related to MYC and mTOR signalling and in inflammatory pathways. Individual gene targets included known RAS-related

genes such as *Ptgs2*, *Areg* and *Lif*. Patients with LUAD and COAD who cluster in groups with lower expression of some of these TTP 'targets' exhibit better survival than those with higher mean expression of these genes. Although various factors could (and likely do) contribute to reduction in expression of our signature genes, the association of low expression of these genes with improved survival is nonetheless consistent with the pre-clinical evidence suggesting the putative role of TTP as a tumour suppressor.

3.5 TTP overexpression modulates CT26 tumour growth *in vivo*

Given the ability of TTP to downregulate genes known to be important for oncogenesis, we investigated whether overexpression of TTP may modulate tumour growth *in vivo*. CT26 TTP KO and CT26 TetOn TTP(aamt) cells were injected subcutaneously into BALB/c mice and, after tumours were established, mice were administered doxycycline (50mg/kg) or vehicle control daily, by oral gavage (see methods for details). Tumour growth was measured with callipers three time per week. In the TTP KO cells, addition of doxycycline had no effect on tumour growth dynamics. Conversely, in the Tet-On TTP(aamt) group, addition of doxycycline resulted in and approximately 40% reduction in tumour growth (768 mm^3 vs. 465mm^3 at the final time point). Induction of TTP therefore appears to slow tumour growth in this SC model.

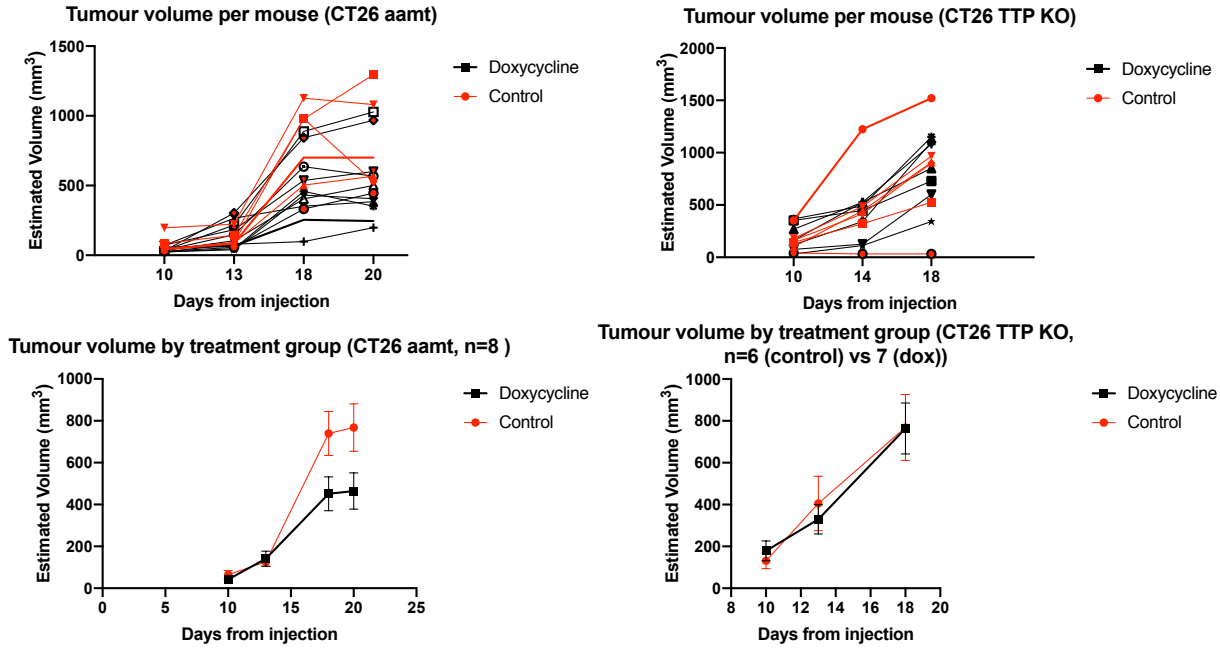

Figure 28. Effect of TTP induction on SC CT26 growthSC injection of $1x10^5$ CT26 cells followed by control (water) or doxycycline (50mg/kg) treatment by oral gavage (OG). Tumours injected on day 0 and doxycycline was administered from day 3, five days per week. Error bars represent 95% confidence intervals

3.6 TTP and KRAS targets overlap but TTP fails to modify KRAS effect during simultaneous perturbation

Given the observed overlap between TTP and KRAS targets, both from published TTP targets (Brooks and Blackshear, 2013a) and our own data, we sought to investigate this more formally. We began by interrogating *in vitro* RNAseq data from our lab, where the KRAS(G12C)-mutated 3LL-ΔNRAS or KPAR(G12C) lines were treated with the KRAS(G12C) inhibitors MRTX1257 or MRTX849 respectively. Details of the experimental schema are given in section 2.7. We sought to compare the set of downregulated genes after KRAS inhibition in these lines, with the genes downregulated by TTP induction in CT26 cells, specifically asking whether the overlap was significantly higher than that expected by chance. As shown in Figure 29 and Table 15, there was a significant overlap in the genes downregulated by KRAS inhibition and TTP overexpression. For example, at a $\log_2$ fold-change of <-0.5 (and an adjusted p value of <0.1) the overlap between these genes was around 4 times higher than

that expected by chance when considering KPAR1.3 versus CT26 Tet-ON TTP(aamt), and almost 12 times higher than that expected by chance when considering 3LL-ΔNRAS versus CT26 Tet-ON TTP(aamt).

3LL-ΔNRAS

Log_2 fold change	DE in 3LLs	DE in CT26 (TTPaamt)	DE in both	p-val.	Odds ratio	DE in CT26 (TTPwt)	DE in both	p-val.	Odds ratio
< -1	88	10	3	0.000	74.85	15	3	<0.001	43.68
< -0.5	514	106	29	0.000	11.83	118	17	<0.001	4.96
< 0	1669	986	344	0.000	5.91	1094	310	<0.001	4.07
> 0	1591	719	181	0.000	4.10	851	143	<0.001	1.96
> 0.5	825	139	33	0.000	6.02	112	19	<0.001	3.75
> 1	288	31	0	1.000	0.00	24	0	1.000	0.00

KPAR1.3

Log_2 fold change	DE in KPAR1.3	DE in CT26 (TTPaamt)	DE in both	p-val.	Odds ratio	DE in CT26 (TTPwt)	DE in both	p-val.	Odds ratio
< -1	187	10	2	0.008	17.64	15	5	0.000	35.82
< -0.5	637	106	17	0.000	3.99	118	16	0.000	3.27
< 0	2459	986	384	0.000	3.72	1094	376	0.000	3.01
> 0	2372	719	214	0.000	2.43	851	204	0.000	1.78
> 0.5	755	139	19	0.000	2.78	112	18	0.000	3.37
> 1	229	31	3	0.016	6.18	24	1	0.341	2.49

Table 15. Overlap between genes differentially expressed after KRAS inhibition and TTP overexpression 3LL-ΔNRAS cells and KPAR1.3 cells were treated with MRTX1257 or MRTX849 for **8 hours** *in vitro* before RNA extraction. Differential expression reported relative to control (DMSO) treatment. CT26 cells treated as previously described. Odds ratios and p-values calculated using Fischer's exact test.

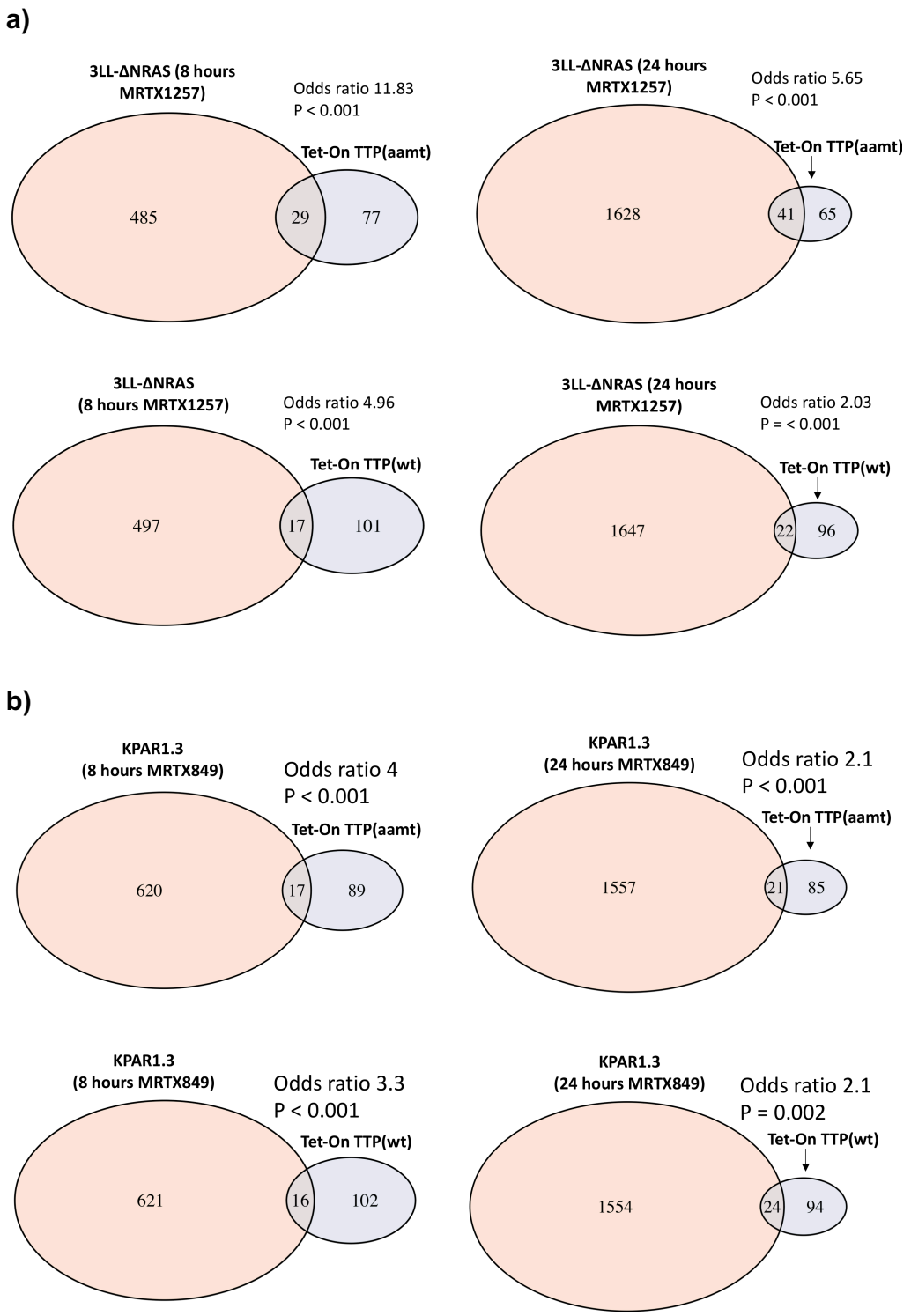

Figure 29. Venn plots: overlap between genes differentially expressed after KRAS inhibition and TTP overexpression a) 3LL-ΔNRAS cells and b) KPAR1.3 cells were treated with MRTX1257 or MRTX849 *in vitro* before RNA extraction. Differential expression reported relative to control (DMSO) treatment. CT26 cells treated as previously described. Odds ratios and p-values calculated using Fischer's exact test.

Individual genes downregulated with a $\log_2$ fold-change of <-0.5 (adjusted p value <0.1) in at least one KRAS(G12C) line and one CT26 derivative are shown in Table 16. These include genes encoding growth factors (e.g. Areg and Ereg), inflammatory/immunoevasive mediators (e.g. Ptgs2), cell cycle regulators (e.g. Plk3), transcription and translation mediators (e.g. Eef1e1, Zc3h8), Stat3 inducers (e.g. Il11 and Lif) and an ECM re-modeller (Plaur).

Gene	3LL-ΔNRAS	KPAR1.3	CT26 Tet-On TTP(wt)	CT26 Tet-On TTP(aamt)	Mean LFC
Areg	-3.65 (0)	-2.66 (0)	-1.5 (0)	-1.28 (0)	-2.27
Ptgs2	-1.92 (0)	-1.58 (0)	-1.42 (0)	-1.66 (0)	-1.64
Plk3	-2.26 (0)	-1.3 (0)	-1.22 (0)	-0.5 (0.03)	-1.32
Eef1e1	-1.2 (0)	-0.64 (0)	-0.75 (0)	-0.88 (0)	-0.87
Zfp36l2	-0.65 (0)	-1.1 (0)	-0.54 (0)	-0.83 (0)	-0.78
Zc3h8	-0.68 (0.01)	-0.54 (0.02)	-0.56 (0.01)	-0.96 (0)	-0.68
Il11	-0.14 (0.43)	-2.49 (0)	-1.02 (0)	-0.62 (0)	-1.07
Lif	0.14 (0.33)	-1.71 (0)	-0.89 (0)	-0.98 (0)	-0.86
Mllt11	-0.76 (0)	-0.15 (0.27)	-0.97 (0)	-1.46 (0)	-0.84
Ier3	-1.02 (0.01)	-0.46 (0)	-0.59 (0)	-0.65 (0)	-0.68
Plekha3	-0.92 (0)	-0.39 (0)	-0.6 (0)	-0.82 (0)	-0.68
Inhba	0.07 (0.68)	-1.53 (0)	-0.59 (0)	-0.54 (0)	-0.65
F3	-0.68 (0)	-0.3 (0)	-0.55 (0)	-0.85 (0)	-0.59
Clcf1	-0.67 (0)	0.05 (0.83)	-0.82 (0)	-0.87 (0)	-0.58
Slc25a25	-0.55 (0.04)	-0.1 (0.48)	-0.66 (0)	-0.72 (0)	-0.51
Tmem68	-0.61 (0)	-0.04 (0.82)	-0.6 (0)	-0.6 (0)	-0.46
Ereg	-2.56 (0)	-1.68 (0)	-0.63 (0.01)	-0.48 (0.04)	-1.34
Phlda1	-1.97 (0)	-1.19 (0)	-0.43 (0)	-0.64 (0)	-1.06
Gdf15	-0.82 (0.04)	-1.48 (0)	-1.4 (0.02)	-0.06 (NA)	-0.94
Pim3	-0.91 (0)	-0.78 (0)	-0.45 (0)	-0.75 (0)	-0.72
Yrdc	-0.98 (0)	-0.58 (0)	-0.24 (0.02)	-0.57 (0)	-0.59
Epha2	-0.88 (0)	-0.61 (0)	-0.35 (0.01)	-0.5 (0)	-0.58
Polr3d	-0.67 (0)	-0.53 (0)	-0.43 (0)	-0.57 (0)	-0.55
Dimt1	-0.72 (0)	-0.51 (0)	-0.27 (0.02)	-0.61 (0)	-0.53
Mak16	-0.64 (0)	-0.52 (0)	-0.42 (0)	-0.56 (0)	-0.53

Sele	-5.47 (0)	-0.01 (NA)	-0.17 (0.19)	-0.54 (0)	-1.55
Dynap	-0.01 (NA)	-1.67 (0)	-0.87 (0)	-0.04 (0.71)	-0.65
Plaur	-1.02 (0)	-0.41 (0)	-0.39 (0)	-0.7 (0)	-0.63
Ctgf	-0.02 (NA)	-1.33 (0)	-0.58 (0.02)	-0.43 (0.05)	-0.59
Slc4a7	-0.9 (0)	-0.42 (0)	-0.19 (0.08)	-0.6 (0)	-0.52
Hspa5	-0.35 (0.1)	-0.89 (0)	-0.27 (0.06)	-0.54 (0)	-0.51
Cbwd1	-0.53 (0)	-0.31 (0)	-0.35 (0)	-0.78 (0)	-0.5
Atp2a2	-0.52 (0)	-0.49 (0)	-0.4 (0)	-0.54 (0)	-0.49
Mtrr	-0.57 (0.01)	-0.44 (0)	-0.28 (0.01)	-0.58 (0)	-0.47
Pfdn4	-0.66 (0.02)	-0.38 (0)	-0.25 (0.03)	-0.55 (0)	-0.46
Mafk	-0.51 (0.01)	-0.39 (0)	-0.52 (0)	-0.35 (0.01)	-0.44
Syt4	0 (NA)	-0.99 (0.02)	-0.65 (0.01)	-0.08 (0.36)	-0.43
Bpnt1	-0.68 (0)	-0.14 (0.32)	-0.24 (0.05)	-0.64 (0)	-0.42
Tmem158	-0.11 (0.64)	-0.61 (0)	-0.58 (0)	-0.25 (0.13)	-0.39
Tmed5	-0.17 (0.17)	-0.53 (0)	-0.54 (0)	-0.11 (0.34)	-0.34

Table 16. Genes modulated by KRAS inhibition and TTP overexpression
Numbers show the $\log_2$ fold changes (LFCs) after 8 hours of KRAS inhibition (3LL-ΔNRAS or KPAR1.3) or 24 hours of TTP overexpression (CT26 derivatives). Adjusted p-values are in brackets. Genes grouped according to whether LFCs were: all <-0.5 (top), < -0.5 in both CT26 derivatives and one KRAS(G12C) line (second), <-0.5 in both KRAS(G12C) lines and one CT26 derivate (third) or <-0.5 in exactly one KRAS(G12C) and CT26 line each (bottom).

In addition, we looked at genes in the RAS84 signature and assessed whether they were downregulated upon TTP overexpression in our CT26 cells. The normalised enrichment score (NES) following GSEA was -1.48 for the Tet-On TTP(aamt) line (Figure 30) indicating that downregulated genes were enriched in this gene set. Leading edge genes (those that contributed the most to the NES) common to both lines included Lif, Clcf1, Plaur, Ier3, Bmp2, Epha2, Ereg, Slc20a1 and Junb. The significant NES in the GSEA analysis again adds support to the hypothesis that TTP targets are enriched in the set of KRAS-modulated genes. Note that the normalised enrichment score (NES) is a metric of enrichment which is normalised for the size of the gene set. High values indicate that genes in the gene set are enriched in the over-expressed portion of one's data, while low (negative) scores indicate that genes in the gene set are enriched in the under-expressed portion of one's data.

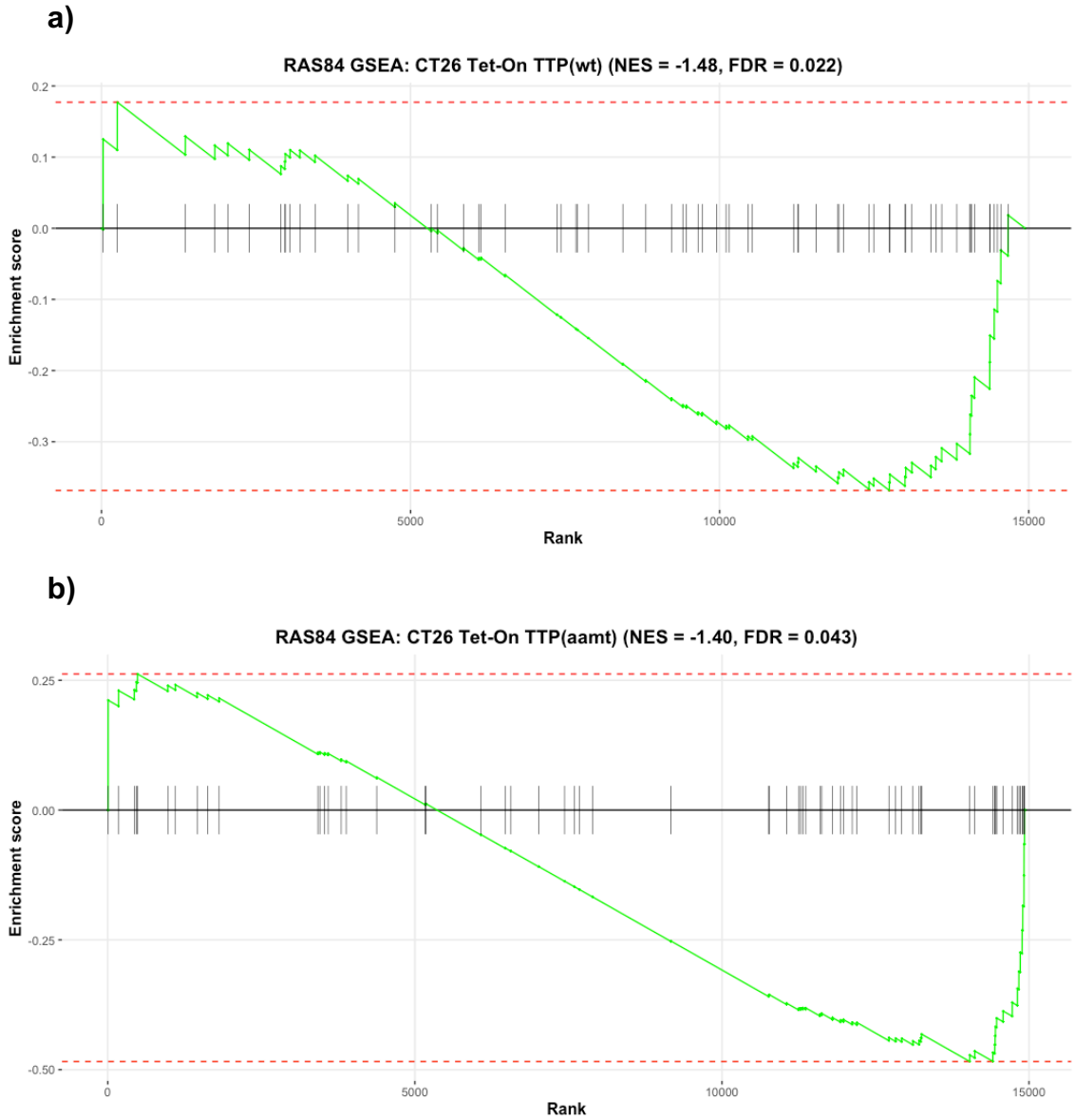

Figure 30. RAS84 GSEA Differentially expressed genes following Zfp36 overexpression in a) CT26 Tet-On TTP(wt) or b) CT26 Tet-On TTP(aamt) were ranked according to their shrunken $\log_2$ fold-change (most positive to most negative) and then used as input to GSEA against the RAS84 gene set

Given the overlap between genes related to KRAS inhibition and TTP overexpression, even across different models, we sought to perturb both KRAS and TTP in the same system to explore whether modulation of TTP could abrogate the effect of KRAS inhibition. We used a CT26(G12C) cells which enabled us to directly inhibit KRAS with the specific inhibitor MRTX1257. These cells were a gift from Mirati Therapeutics where the homozygous KRAS(G12D)

alleles had been edited to KRAS(G12C) alleles using CRISPR-CAS9 technology.

We first validated the ability of MRTX1257 to affect proliferation and MAPK signalling in these cells. Initially we assessed inhibition of signalling using Western blot (Figure 31). Cells were treated with MRTX1257 or, for comparison, the G12C inhibitor AZ8037 for 6, 24 or 48 hours. With both drugs, phospho-ERK levels at 6 and 24 hours were suppressed, with rebound starting to emerge by 48 hours. Phospho-S6 remained suppressed even at 48 hours.

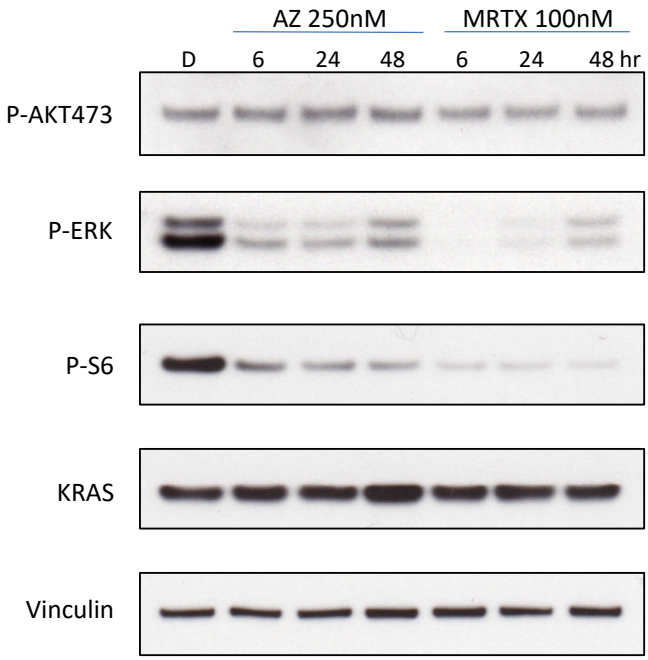

Figure 31. CT26(G12C) Western blot Cells were treated with the indicated drugs (250nM AZ8037 (AZ) or 100nM MRTX1257 (MRTX)) for varying durations.

To examine the impact of treatment on viability, parental or CT26(G12C) cells were treated with serial dilutions of either the MEK inhibitor trametinib (positive control), AZ8037 or MRTX1257 and viability was measured 72 hours later. Trametinib resulted in a 50% reduction in viability in both the WT and CT26(G12C) lines, while AZ8037 and MRX1257 affected viability only in the latter. MRTX1257 appeared more potent, with maximal effect on viability

occurring at just 10nM, consistent with the stronger pathway inhibition observed in the Western blot.

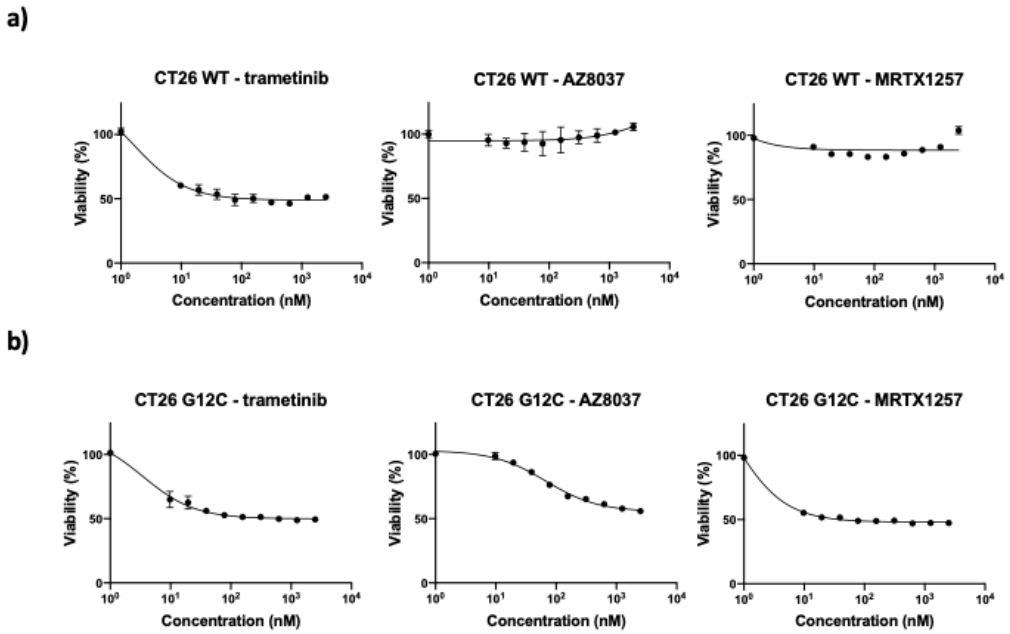

Figure 32. Viability: effect of MEK or KRAS(G12C) inhibitors CT26(G12C) cells treated with trametinib, AZ8037 or MRTX1257 at concentrations between 10 and 5000nM before viability was measured following addition of CellTiter-Blue. Viability is given as percentage of control.

Once we had established the effect of KRAS(G12C) inhibition on signalling and viability in CT26(G12C), we next assessed the effect of MRTX1257 monotherapy on the expression of selected genes identified as being potentially regulated by both KRAS and TTP in our RNAseq analyses Figure 33. This effect was compared to the analogous effect in 3LL-ΔNRAS cells. As expected, most genes were downregulated with inhibition of KRAS(G12C).

a)

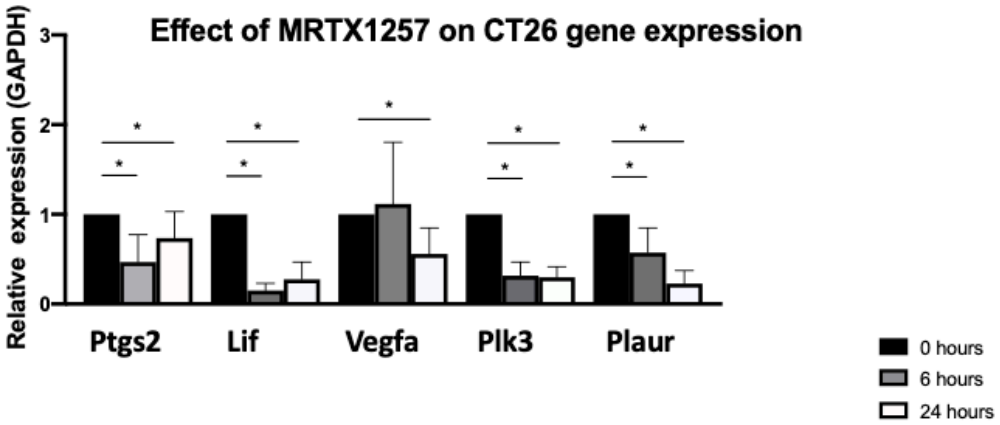

b)

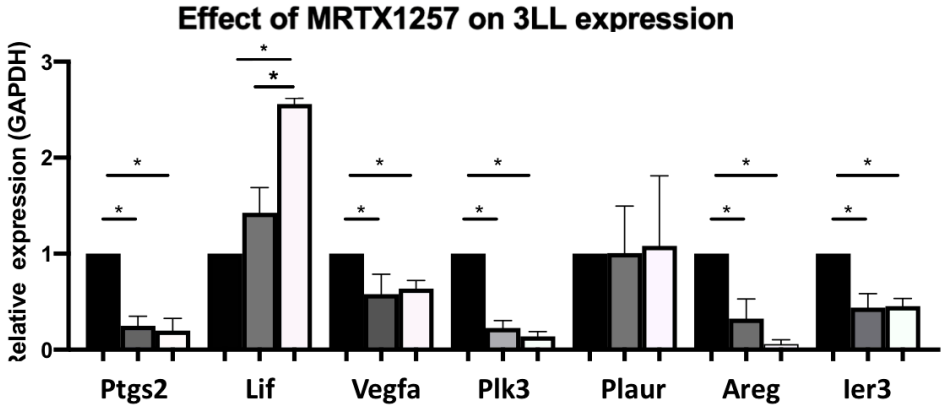

Figure 33. Effect of MRTX1257 monotherapy on selected gene expression a) CT26(G12C) or b) 3LL-ΔNRAS cells were treated with MRTX1257 for 0, 6 or 24 hours before harvest of RNA and analysis with qPCR. Means compared with independent t-tests. Significance bars indicate $p < 0.05$ (t-tests).

We next assessed whether knockdown of TTP using siRNA- could abrogate the effect of KRAS(G12C) inhibition. As shown by our lab, oncogenic KRAS can induce inhibitory phosphorylation of TTP via activation of the P38-MAPK pathway (Coelho *et al.*, 2017). Therefore, inhibition of oncogenic KRAS may, at least partly, result in downregulation of KRAS targets through dephosphorylation and subsequent activation of TTP. Through such a mechanism, the ability of KRAS inhibition to downregulate common TTP/KRAS

targets, including Ptgs2, may be abrogated if TTP is knocked down prior to KRAS inhibition.

To this end, we treated cells with siRNA against TTP and subsequently inhibited KRAS(G12C) (Figure 34). Knockdown of Zfp36 was robust, resulting in gene expression that was around 30% that of controls. In the presence of DMSO, Zfp36 suppression with siRNA against TTP (siTTP) resulted in a modest, but significant 25% rise in Ptgs2 mRNA compared to mock treated cells. When treated with MRTX1257, mock-treated cells showed a 38% relative decrease in Ptgs2 expression ($p = 0.02$) while the 15% decrease in Ptgs2 expression upon KRAS(G12C) inhibition in siTTP treated cells was not significantly different ($p = 0.51$). As a comparison, in the presence of DMSO, Myc expression was not increased upon addition of siTTP, compared to mock treated cells. Furthermore, the addition of MRTX1257 had a similar magnitude of effect regardless of whether cells were pre-treated with 'mock' or siTTP suggesting the inability of siTTP to abrogate the inhibition of Myc by MRTX1257.

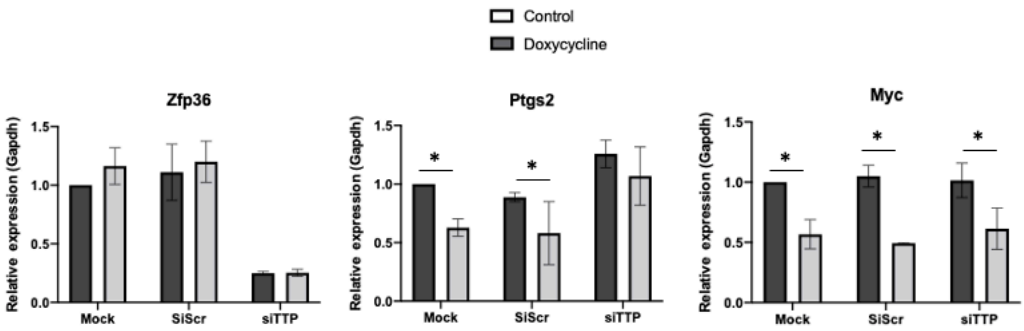

Figure 34. Perturbation of TTP and KRAS(G12C) within same system Cells were treated with mock mixture (HBSS alone), non-targeting siRNA (siScr) or siRNA against Zfp36 (siTTP) for 48 hours before the addition of 100nM MRTX1257 or DMSO control. ($n = 4$). Groups compared with independent T-tests, asterices indicate $p < 0.05$

3.7 Concluding remarks

In conclusion, *in silico* analysis using disparate models suggested a significant enrichment between KRAS and TTP targets, including known pro-tumourigenic transcripts such as *Areg, Ereg, Ptgs2, Lif and Plaur.* Knockdown of *Zfp36* using siRNA resulted in a modest rise in *Ptsgs2* mRNA and partially abrogated the effect of KRAS inhibition on the downregulation of this transcript although the magnitude of this effect was variable between replicates possibly because of the powerful and diverse transcriptional effects of KRAS inhibition. The fact that KRAS inhibition was able to downregulate *Ptgs2* even in the presence of siTTP suggests other mechanisms by which KRAS affects *Ptgs2* expression, or insufficient knockdown of TTP. Further work would require looking in other models and validating this result, for example using CRISPR-Cas9 technology to knock out the endogenous TTP locus and potentially lead to a more profound and durable suppression of *Zfp36*. This is alluded to in the discussion.

Chapter 4. Results 2: Using Cellular Indexing of Transcriptomes and Epitopes (CITE-seq) to interrogate gene expression and cell identity in an orthotopic KRAS(G12C) model

4.1 Introduction

While it's possible that some actions of KRAS are mediated through its effect on TTP, there are several other mechanisms through which KRAS operates and which result in diverse tumour-cell and microenvironmental change. Interrogation of both of these compartments at the single cell level would deepen our understanding of the effects of KRAS inhibition *in vivo* and potentially generate hypotheses concerning additive or synergistic combinations.

CITE-seq is a fairly novel technique, allowing simultaneous profiling of transcriptomes and surface protein expression from single cells (Stoeckius *et al.*, 2017). In CITE-seq, antibodies are attached to an nucleotide barcode (antibody-derived tag – ADT) which is specific for its target (e.g. all CD4 antibodies have the same tag). Single cells are then stained with such antibodies before further processing where cells are encapsulated within an emulsion droplet and subsequently lysed such that both antibody-derived tags (ADTs) and cellular mRNA are captured on a bead within the droplet. The ensuing chemical reaction adds a cell-specific barcode to each mRNA and ADT molecule from a given cell before the droplet is dissolved and all barcoded mRNA and ADTs mix together. This is followed by several rounds of amplification via PCR. Finally, this amplified library is size-separated to produce separate mRNA and ADT libraries for sequencing.

Because of the sequencing depth limitation, single-cell RNA sequencing suffers from the problem of 'drop-out' whereby lowly expressed RNA are not detected. This can impact on clustering and, potentially, cellular identification. Because of this, CITE-seq has the potential to increase resolution of cell states above that

achieved through single-cell RNAseq alone since the ADT signal is less subject to drop-out because of the reduced number of targets to sequence

We sought to use CITE-seq to understand the cell type-specific effects of KRAS(G12C) inhibition in an orthoptic murine lung carcinoma model. In this chapter we describe selection of our antibody panel, determination of antibody concentrations, quality control (QC) of our data and an overview of the landscape of cell types within our chosen system.

4.2 Antibody panel selection

As previously mentioned, data from our lab using IMC has shown that KRAS(G12C) inhibition of orthotopic 3LL-ΔNRAS tumours results in remodelling of the tumour immune microenvironment (van Maldegem *et al.*, 2021). Using detailed phenotypic characterisation and preserved tissue architecture, this enabled an understanding of the baseline and post-inhibition location of various cell types/states, and work is ongoing to understand the effect of KRAS inhibition on cell-cell interaction patterns using neighbourhood analysis. To complement this approach, CITE-seq would give us an insight into the transcriptional changes within the various types/states and thus may allow us to infer functional effects, something not possible with IMC alone.

To this end, we used the same model system (orthotopic 3LL-ΔNRAS tumours) and treatment schema (section 2.6) that was adopted in the IMC experiments. The murine Lewis lung carcinoma line (LL/2 or 3LL) was derived from a spontaneous lung carcinoma in the C57Bl/6 mouse, and serially passaged via SC implants of tumour fragments (Mayo, 1972). Data from our lab has shown that it possesses a very high non-synonymous mutation burden (over 2000 predicted) of which many are expressed and predicted to bind H2-Db (H2-Kb is not expressed in the 3LL cells used in our lab) (Mugarza *et al.*, 2021). This suggests potential for immune recognition. Data from our lab also established that alongside the homozygous KRAS(G12C) variants, 3LL cells possess an

NRAS(Q61H) variant capable of inducing resistance to KRAS(G12C) inhibition (Molina-Arcas *et al.*, 2019). Molina-Arcas et al. edited out the oncogenic NRAS using CRISPR/Cas9 technology, generating a 3LL-ΔNRAS line sensitive to KRAS(G12C) inhibition.

We designed a custom antibody panel aiming to overlap as much as possible with the IMC panel while taking into account various factors. Firstly, intracellular antibodies used in IMC could not be used for CITE-seq, where the cells are intact. Secondly, some antibodies were unable to be validated for use in IMC but could be used for CITE-seq characterisation. Finally, financial cost (up-front purchase plus any additional sequencing required per antibody) was a limiting factor as to how many antibodies could be selected. The overall goal was to represent the most diverse range of cell types possible, bearing in mind the aforementioned caveats.

The final selection of antibodies is detailed in Table 17. Thus, marker selection included a range of markers for various T cell types/states, monocytes, macrophages, dendritic cells and miscellaneous markers. These were chosen given the importance of T cells as final effectors of certain antitumour immune responses and the predominance of myeloid infiltrate in 3LL tumours (Waldman, Fritz and Lenardo, 2020; van Maldegem *et al.*, 2021). Given the caveats previously mentioned, and their low abundance within 3LL tumours, markers for B cells, natural killer cells and gamma-delta T cells were omitted as were certain intracellular markers present in the IMC panel including CD68, CXCL9, α-smooth muscle actin, vimentin, type I collagen, forkhead box P3 (FOXP3), pAKT, pS6, cleaved caspase 3 and Ki-67. Broadly staining markers such as CD45 and CD3 were felt to be redundant given our inclusion of more specific markers, and hence were also omitted. Finally, certain markers useful for T cell characterisation or monocytes/neutrophils were not present in the IMC panel, but added to the CITE-seq repertoire (CD25, CD62L, CD69, LAG3 and Ly6C/Ly6G).

Target	Main cell type	In IMC?	In CITE-Seq?
T cell			
CD3	Pan T cell	Yes	No
CD4	$CD4^+$ lymphocytes	Yes	Yes
CD8a	$CD8^+$ lymphocytes	Yes	Yes
FoxP3	T_{reg}	Yes[1]	No
CD25	T_{reg}, T activation	No	Yes
CD279 (PD-1)	Activated/exhausted T cells	Yes	Yes
TIM3	T cell, macrophage	Yes	Yes
LAG3	T exhaustion	No	Yes
CD62L	Naïve T	No	Yes
CD69	T activation (acute)	No	Yes
Monocyte/macrophage			
Ly-6C/Ly-6G	Classical Monocytes/neutrophils	No	Yes
CX3CR1	Alternative monocytes	Yes	No
F4/80	Macrophages	Yes	Yes
CD68	Macrophages	Yes[1]	No
CD206 (MMR)	Macrophages (‘M2’-like)	Yes	Yes
CD274 (PD-L1)	Tumour, myeloid	Yes	Yes
CD11c	Macs (peripheral)	Yes	Yes
Dendritic cell			
CD103	Conventional dendritic cells 1	Yes	Yes
MHC-II (IA-IE)	Antigen presenting cells (APCs)	Yes	Yes
CD80 (B7-1)	APCs	Yes	No
CD86 (B7-2)	APCs	Yes	No
CD24	Dendritic, T cell activation	Yes	Yes

Miscellaneous			
CD44	Tumour stemness, T cell activation	Yes	Yes
PVR	Various	Yes	No
CD335 (Nkp46)	NK	Yes	No
CD45R (B220)	B cells	Yes	No
CD31 (PECAM-1)	Endothelial	Yes	No
EpCAM	Epithelial	Yes	No
CD73	Several	Yes	Yes
CD45	All immune	Yes	No

Table 17. Comparison of IMC and CITE-seq antibody selection Table crudely split according to cell types likely to express highest levels of given markers, although many markers extend beyond the cell types indicated. Superscript 1 = intracellular markers

4.3 Antibody titration

Overabundance of an antibody-derived tag (ADT - i.e. the oligonucleotide conjugated to the antibody) in a CITE-seq experiment has the potential to consume a lot of reads, therefore reducing signal from other ADTs. Hence, titration of antibody concentrations is important. It has been shown that oligo-conjugated antibody signal is similar to fluorochrome-conjugated antibodies (of the same clone) in terms of the signal-noise ratio and the ‘saturation plateau’ (Stoeckius *et al.*, 2018).

Thus, in order to identify the optimum concentrations for use in CITE-seq experiments, antibodies were titrated using flow cytometry. As far as possible, antibodies used in flow cytometry (section 2.12.2) were the same clones as the

antibodies available for CITE-seq. Furthermore, most antibodies were conjugated to PE. As a 'bright' fluorophore providing a clear, strong, signal the use of PE helps mitigate the risk of choosing unsuitably high antibody concentration for CITE-seq purposes. In addition to titrating antibodies to obtain concentrations for use in CITE-seq, we also sought to compare two methods of tumour dissociation (section 2.12.1). Our in-house method (2.12.1.2) employs a manual mechanical dissociation step (dissociating cells via repeated passages through a fine bore needle) and there were concerns over maintenance of tumour cell viability. We therefore compared this method to the use of a commercial kit (Tumour Dissociation Kit, mouse; Miltenyi Biotec, section 2.12.1.1) which contains a proprietary enzymatic mix that has been proposed to preserve the majority of cell surface epitopes (Miltenyi Biotec, 2016) and employs an automatic mixed mechano-enzymatic dissociation step.

In order to obtain tumours for antibody titration, orthotopic 3LL-ΔNRAS tumours were grown in untreated mice and harvested after 28 days (section 2.6). Tumours were dissociated using one of the two methods discussed above, and results compared. Antibody concentrations were obtained through serial dilution. The concentration range over which serial dilutions were performed was decided using prior experience of flow cytometry in our lab and evidence from the literature (Buus *et al.*, 2020).

As shown in Figure 35, our in-house method of tumour dissociation resulted in a higher percentage of events being labelled as debris/non-cellular (74.5%) compared to the commercial method (54.8%). Furthermore, of those events that were retained after this step, viability was 96% with the commercial dissociation method compared to 87.8% with our in-house dissociation protocol. For this reason, we opted to take forward the commercial method to dissociate tumours for use in CITE-seq experiments.

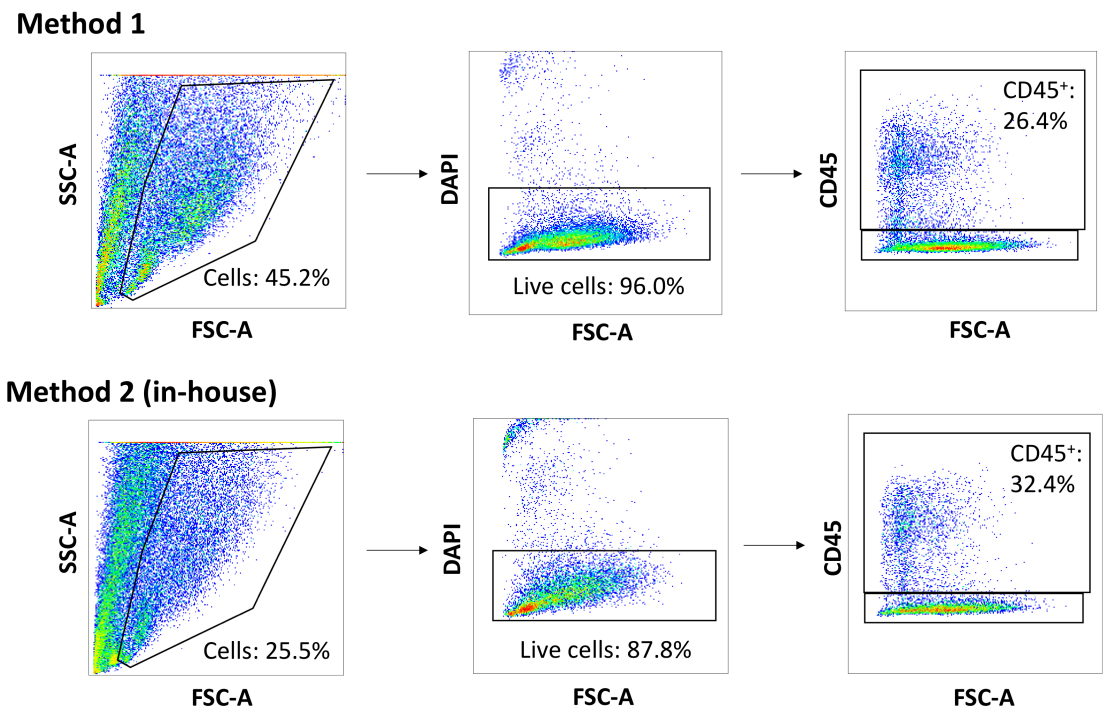

Figure 35. Comparison of tumour dissociation methods using flow cytometry3LL tumours grown for 7 days in untreated mice were processed and then dissociated with a proprietary (1) or in-house (2) mechano-enzymatic technique (section 2.12.1)

Following selection of the dissociation protocol, antibodies were titrated using flow cytometry to determine an optimum concentration to take forward for CITE-seq. An example of data used to optimise antibody concentrations is shown for CD11b (Figure 36). Two clearly distinct populations are seen. As the antibody concentration falls, signal from the ‘positive’ population falls, and moves close to that of the ‘negative’ population. Nonetheless, the two are still distinguishable even at the lowest antibody concentration. In this example, the lowest antibody concentration would be taken forward for use in CITE-seq analysis. Similar titration was performed, and concentrations determined, for all antibodies (section 2.13).

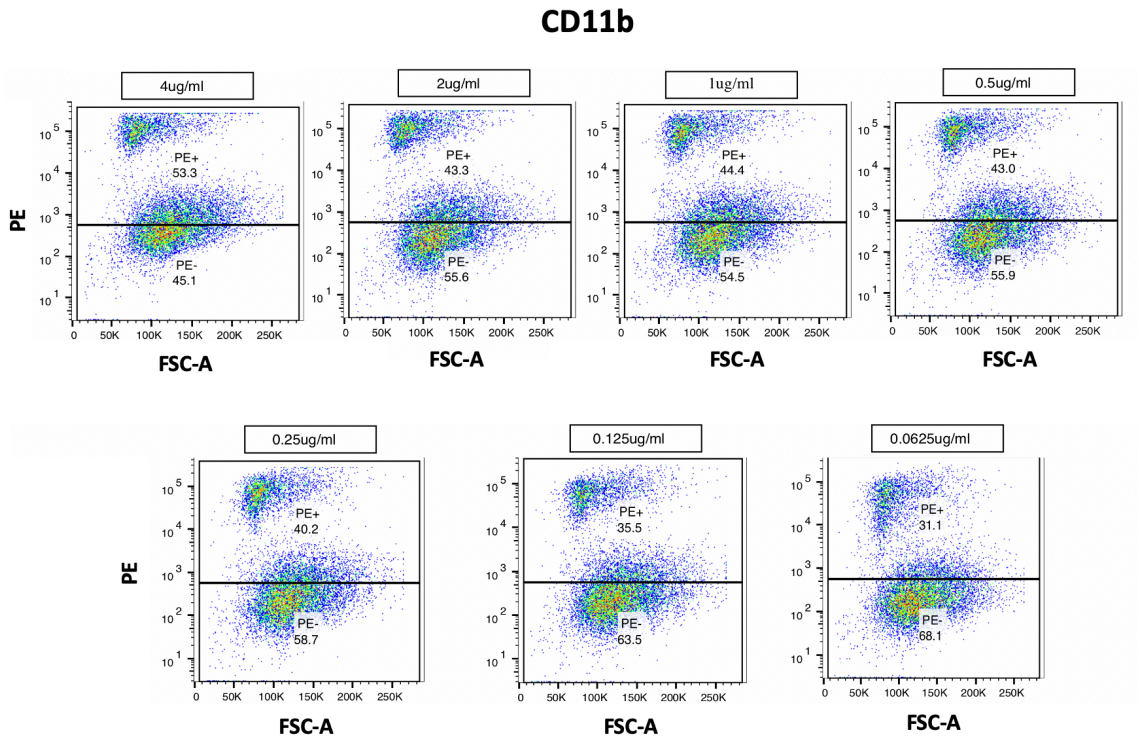

Figure 36. Antibody titration example - CD11b 3LL Cells were stained with CD11b antibodies at various concentrations (0.0625-4 ug/ml). Plots show percentage of CD11b^{+} cells per concentration with gating based on unstained controls (not shown).

4.4 CITE-seq pilot

In order to generate sufficient power, enabling robust detection of the effects of KRAS(G12C) inhibition, we chose to treat five mice with vehicle and five mice with MRTX1257. Given that the technique was new to our lab, and to generate biological replicates, we initially performed the protocol using four mice (two in each group, the 'pilot' experiment) and subsequently using three mice in each group (post-pilot) generating a total of ten samples for the final analysis.

Mice were treated as described (section 2.6). In brief, mice were injected with 3LL-ΔNRAS cells via their tail vein and, after 21 days of tumour growth, were treated with MRTX1257 or vehicle control for 7 days before tumours were then dissociated and processed for CITE-seq.

Parameters for the dissociation and sorting process are shown in Table 18. As shown, viability post-FACS was high indicating successful sorting.

Treatment	**No. of sorted cell**	**% of cells sorted**	**Viability(%)**
Control	201,301	56.4	86
Control	220,502	74.4	87
MRTX1257	221,789	74.5	87
MRTX1257	230,346	76.8	87

Table 18. Parameters for pilot CITE-seq protocol
Following dissociation and sorting of live events (DAPI +ve), cells were processed for sequencing of mRNA and ADTs (section 2.13). Cells were initially sequenced at a shallow depth, enabling estimation of cell number to guide deeper sequencing. Given that this was a novel technique in our lab, we also used this shallow sequencing of pilot samples to interrogate our data to ensure that antibody binding had worked and to obtain sample QC characteristics.

As shown in Table 19 below, QC characteristics were acceptable and generally consistent between samples. Of note, dead or dying cells can leak mRNA, resulting in high ambient RNA concentrations that can both increase sequencing cost and create noise. Reassuringly, in our pilot, the majority of mRNA reads were found in cell-containing droplets (rather than empty droplets) suggesting good quality cells. The background for ADTs was higher with around 70% of ADTs being found in cell-containing droplets in three out of the four samples. This is however an acceptable level and should still allow detectable

signal. One sample, however, had notably fewer ADTs in cells (38.4%, in a control sample). Given this was isolated to one sample, it was not a protocol-related issue. In our protocol, we stained cells with CITE-seq antibodies before washing three times and then performing FACS (which also acts to wash the cells). Upon troubleshooting, no reason for the spurious finding was elucidated. Furthermore, when clustering samples using ADT information alone, we were able to resolve expected populations in all samples (e.g. $CD4^+$ and $CD8^+$ cells, see below - Figure 39).

	Control	**Control**	**MRTX1257**	**MRTX1257**
Sequencing				
Number of reads	61,870,663	72,710,549	70,108,425	81,213,275
Valid Barcodes	98.80%	98.80%	98.90%	98.80%
Mapping				
Reads Mapped to Genome	89.70%	90.00%	90.40%	89.70%
Reads Mapped Confidently to Transcriptome	71.80%	72.50%	72.60%	72.00%
Cells				
Estimated Number of Cells	3,459	3,391	5,071	4,077
Fraction Reads in Cells	96.20%	96.30%	96.60%	95.60%
Mean Reads per Cell	17,886	21,442	13,825	19,919
Median UMI Counts per Cell	5,953	9,784	5,648	8,079
Antibody Sequencing				
Antibody: Number of Reads	5,843,960	11,206,099	8,044,252	4,908,389
Antibody: Mean Reads per Cell	1,689	3,304	1,586	1,203
Antibody: Valid Barcodes	99.30%	99.20%	99.30%	99.20%
Antibody application				
Antibody: Antibody Reads in Cells	71.80%	38.40%	74.10%	73.90%

Table 19. QC characteristics of pilot samples Single cell analysis of 3LL tumours treated with vehicle control or MRTX1257. QC characteristics of pilot samples were generated using Cell Ranger.

In addition to inspection of sample QC, we also analysed the shallow-sequenced pilot samples to check that results were as expected. We first looked at the distribution of ADT counts in our samples (Figure 37) and its dynamic range (Figure 38). ADT count distribution was similar between samples, with a peak at around 100 counts/cell. A plot of the dynamic range of our antibody repertoire showed very few reads occupied by T cell markers (e.g. CD4, CD8, CD69) and a cDC1 marker (CD103). This is consistent with our knowledge that these tumours have a paucity of these immune subtypes and that expression of these markers is fairly cell-type specific. Furthermore, as shown later (e.g. Figure 39), binding of these antibodies was still sufficient to identify 'positive' clusters.

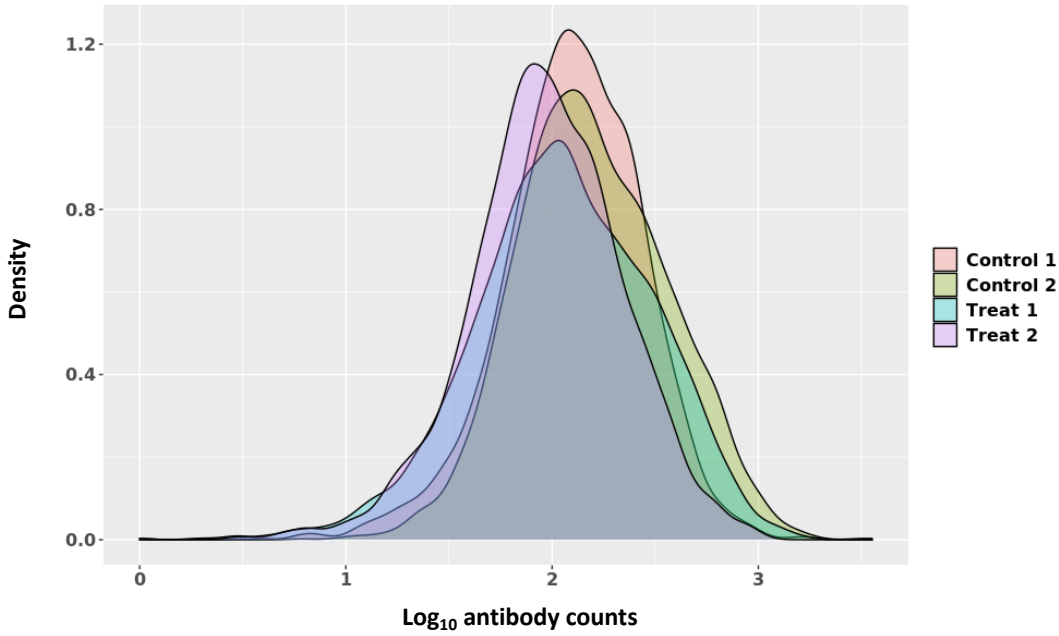

Figure 37. Distribution of ADT counts – QC check3LL tumours were treated with vehicle control or MRTX1257 and processed for CITE-seq. For each sample, the ADT counts per cell are represented as a density plot.

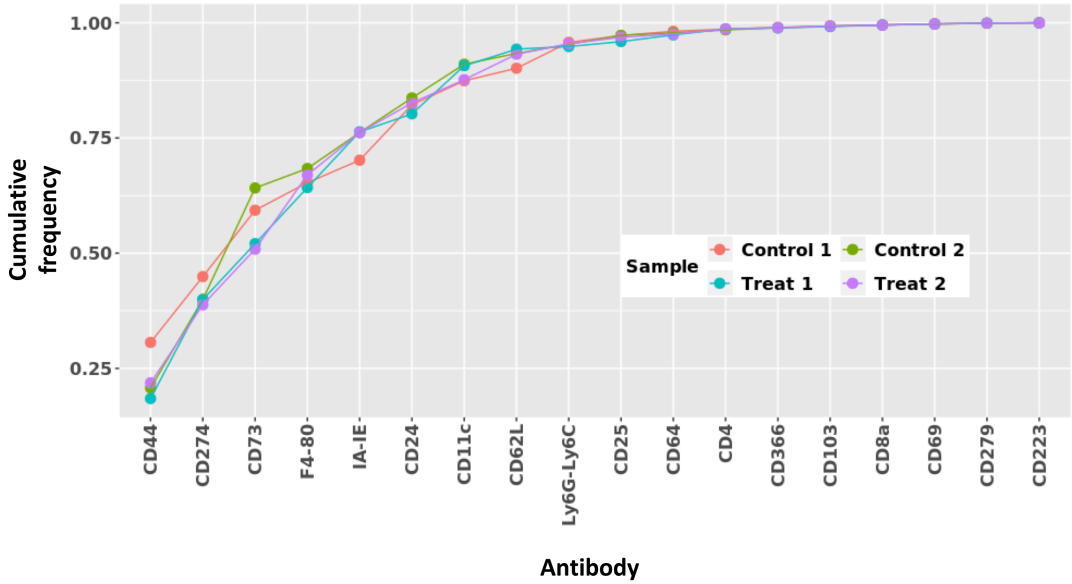

Figure 38. Dynamic range of ADT proportion 3LL tumours were treated with vehicle control or MRTX1257 and processed for CITE-seq. For each sample, the percentage of ADT reads occupied by each target antibody was calculated and plotted on a cumulative frequency plot. The x-axis is arranged by highest mean frequency.

We then generated tSNE plots for each sample in one of two ways - using either mRNA or ADT expression. We then overlaid expression of CD4 and CD8a ADTs onto these tSNE plots to visualise how cells expressing high levels of these tags ('expressing' cells) were embedded in the plot (Figure 39). When we overlaid CD4 or CD8a ADT expression on the tSNE plots generated using mRNA expression alone, cells that expressed high levels of these tags were embedded closely in tSNE space, but within this area there was clear separation of CD4 and CD8a expressing cells. When we overlaid the same ADTs on the tSNEs generated using ADT expression, CD4 and CD8a-expressing cells were embedded distinctly. This is both because ADT binding is more robust, and because there are far fewer ADT markers compared to genes. Thus, despite shallow sequencing, both mRNA and ADT expression resulted in biologically plausible embeddings using tSNE and, furthermore, performing tSNE using ADT expression values alone led to distinct separation of CD4 and C8a expressing cells in tSNE space suggesting utility of this modality in distinguishing the two cell types.

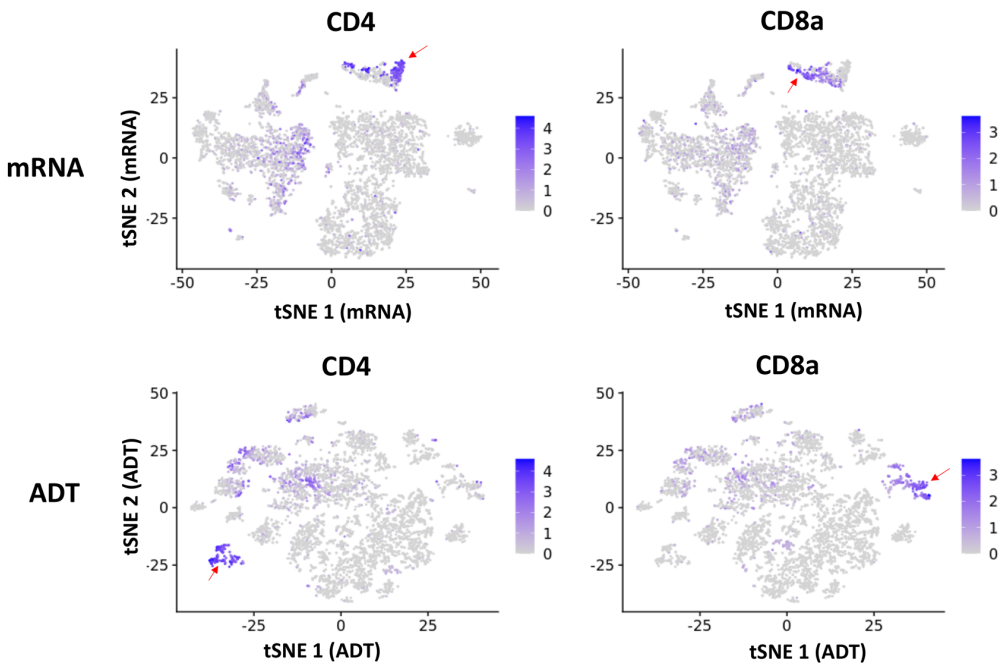

Figure 39. CD4 and CD8a ADTs in tSNE space 3LL tumours were treated with vehicle control or MRTX1257 and processed for CITE-seq. tSNE plots were generated using either mRNA or ADT expression. CD4 and CD8a ADT values were then overlaid. Red arrows indicate highest expressing cells.

As a final screen of our pilot data, we created a 'pseudo-bulk' dataset from the single cell data, and compared this to previously generated bulk RNAseq data from our lab, where mice with orthotopic 3LL-ΔNRAS tumours were treated with MRTX1257 for 28 hours or 8 days, or vehicle control (Mugarza *et al.*, 2021). We reasoned that, if successful, our pilot data would overlap significantly with bulk data. Reassuringly, the correlation between gene expression from the single cell and bulk *in vivo* datasets was high in both untreated and (8 day) treated samples (

Figure 40). Nonetheless correlation was not perfect, an effect partly expected given technical differences between the two experiments, batch effects and differences in processing of raw counts (filtering and alignment).

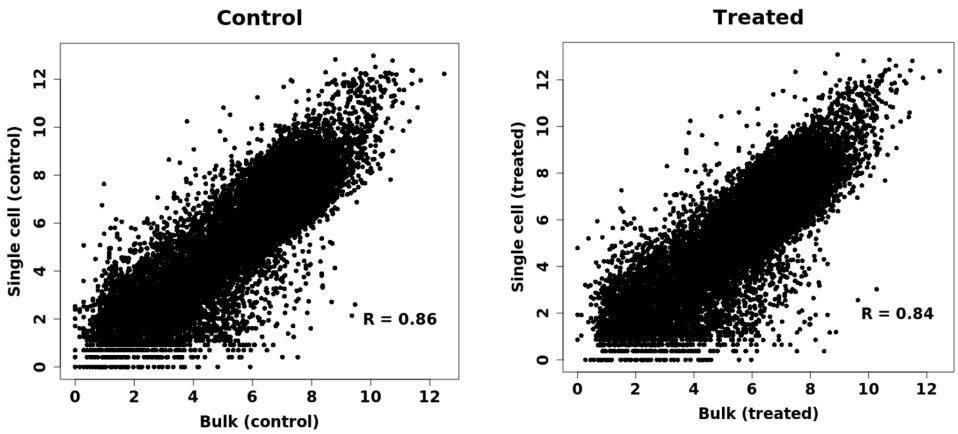

Figure 40. Correlation between bulk and single cell data of control or MRTX1257-treated 3LL tumours Expression values for untreated (n = 2 & 3 for single cell & bulk respectively) and treated (n = 2 & 3 for single cell & bulk respectively) mice were averaged by taking the mean expression values for each gene.

We next looked at the set of differentially expressed genes after treatment with MRTX1257 and asked whether these genes in the single cell dataset significantly overlapped with those genes downregulated after MRTX1257 in the bulk data. Indeed, there was significant enrichment between the two (Table 20). For example, the overlap between genes with a $\log_2$ fold change <-1.5 was far higher than that expected by chance (odds ratio 48.1).

$\log_2$ fold change	Single cell	Bulk (*in vivo*)	Changed in both	Background	p-value	Odds Ratio
< -1.5	182	137	34	14985	< 0.001	48.06
< -1	264	273	70	14985	< 0.001	28.59
< -0.5	316	800	121	14985	< 0.001	14.76
< 0	316	1779	124	14985	< 0.001	5.15
> 0	305	1716	176	14985	< 0.001	11.75
> 0.5	305	1174	156	14985	< 0.001	17.24
> 1	239	585	94	14985	< 0.001	28.19
> 1.5	138	291	54	14985	< 0.001	78.46

Table 20. Enrichment of up and downregulated genes in bulk and single cell data for control or MRTX1257-treated 3LL tumours Table shows number of genes with a given differential expression after MRTX1257 treatment.

As a final screen of consistency with previous lab data, we examined bulk RNAseq from *in vitro* 3LL-ΔNRAS cells (generated by Edurne Mugarza and Miriam Molina-Arcas) and looked at the genes most strongly downregulated after 28 hours of MRTX1257 treatment (Table 21).

Gene	Mean expression	Log_2 fold change	Adjusted p value
Sele	53.29	-7.50	< 0.001
Etv4	889.83	-7.08	< 0.001
Etv5	956.57	-6.70	< 0.001
Prkg2	280.60	-6.33	< 0.001
Dusp6	569.68	-5.59	< 0.001
Prkcb	10.34	-5.44	< 0.001
Ccl2	1385.97	-5.32	< 0.001
Areg	64.24	-4.99	< 0.001
Styk1	183.66	-4.73	< 0.001
Spry4	465.21	-4.68	< 0.001

Table 21. Differential expression after 28 hours of MRTX1257 treatment of 3LL cells grown in vitro

We reasoned that these tumour-intrinsic genes should also be downregulated (upon MRTX1257 treatment) within the tumour compartment of the single cell space. We thus identified tumour clusters by visualisation of the sTSNE plot (generated using mRNA expression), as the H2-K1 (gene for H2-Kb) negative clusters given the lack of H2-K1 expression in this tumour model. An example of this, for the first control sample, is shown in Figure 41.

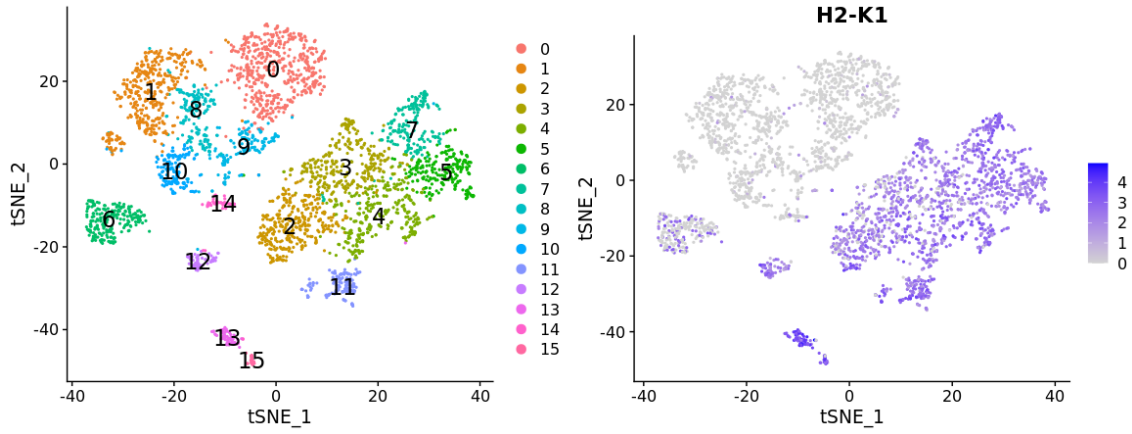

Figure 41. Identification of putative tumour clusters for a control sample 3LL tumour treated with vehicle control and clustered using Seurat.In this example, clusters 0, 1, 8, 9, 10 and 14 were identified as tumour clusters through absence of H2-K1 expression

By amalgamation of such clusters, we generated tumour meta-clusters in each sample. Within these meta-clusters, expression of *Sele*, *Etv4* and *Etv5*, the three most strongly downregulated genes in the bulk *in vitro* data, were clearly reduced in the mice treated with MRTX1257 (Figure 42). As shown in this figure, the $\log_2$ fold change of these genes in the single cell pilot was very similar to the $\log_2$ fold change in the bulk *in vivo* data. Furthermore, the expression and $\log_2$ fold change specifically in the tumour compartment was very similar to the $\log_2$ fold change of *all* cells in the single cell dataset suggesting that the effect of MRTX1257 on these genes is driven by its suppression of expression in tumour cells. This is illustrated on the tSNE plots for *Etv4* (Figure 43). In these plots, one can also appreciate that downregulation of *Etv4* appears restricted to a subset of tumour cells suggesting some tumour cell-intrinsic heterogeneity in response to drug.

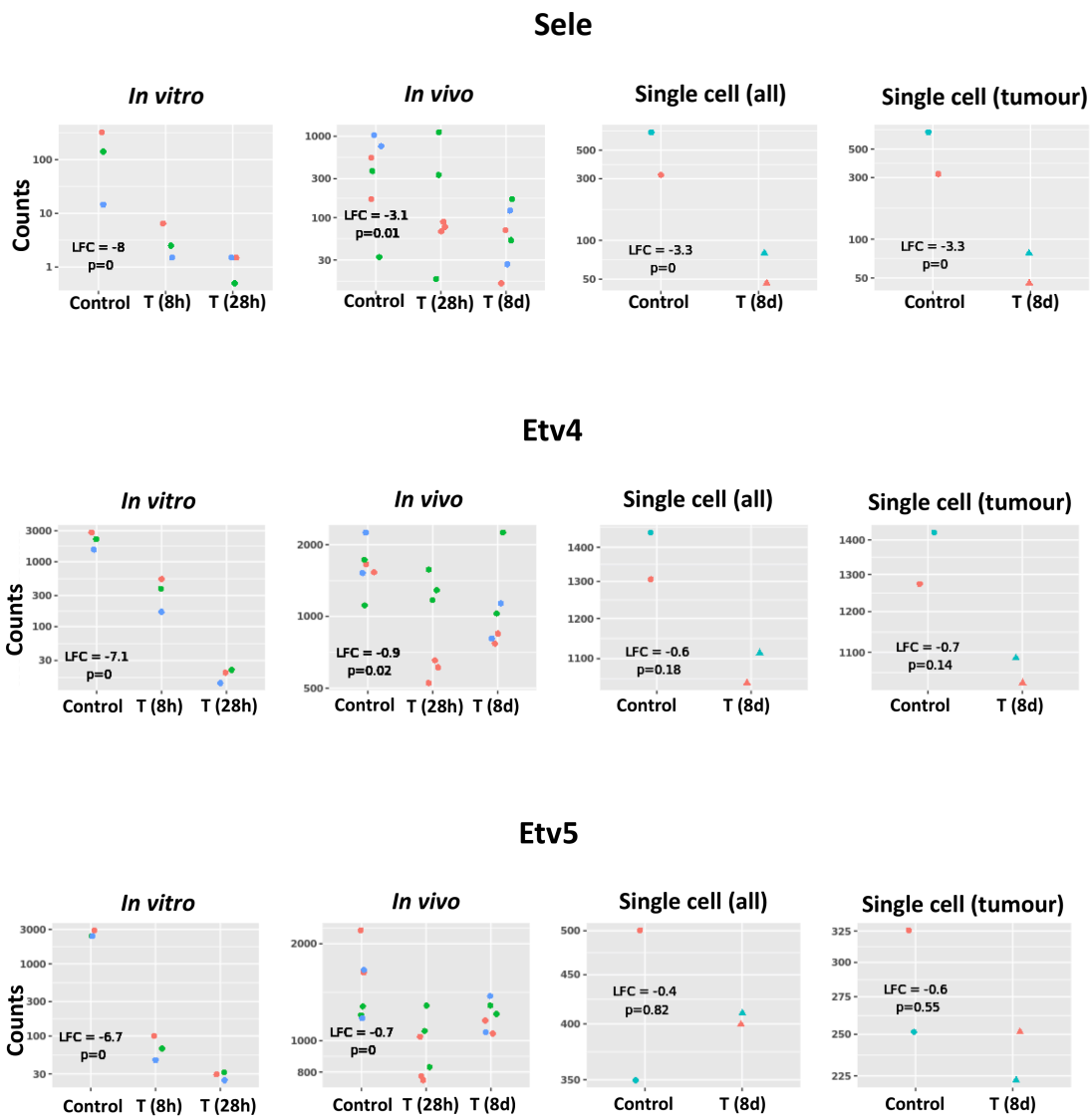

Figure 42. Effect of MRTX1257 on selected genes in 3LL cells/tumours Plots show effect of MRTX1257 on expression of different genes. T = treatment (for given hours/days). Colours represent different replicates (*in vitro* or single cell) or different mice (bulk *in vivo*). Note, for bulk *in vivo*, several tumours were harvested per mouse, and sequenced individually.

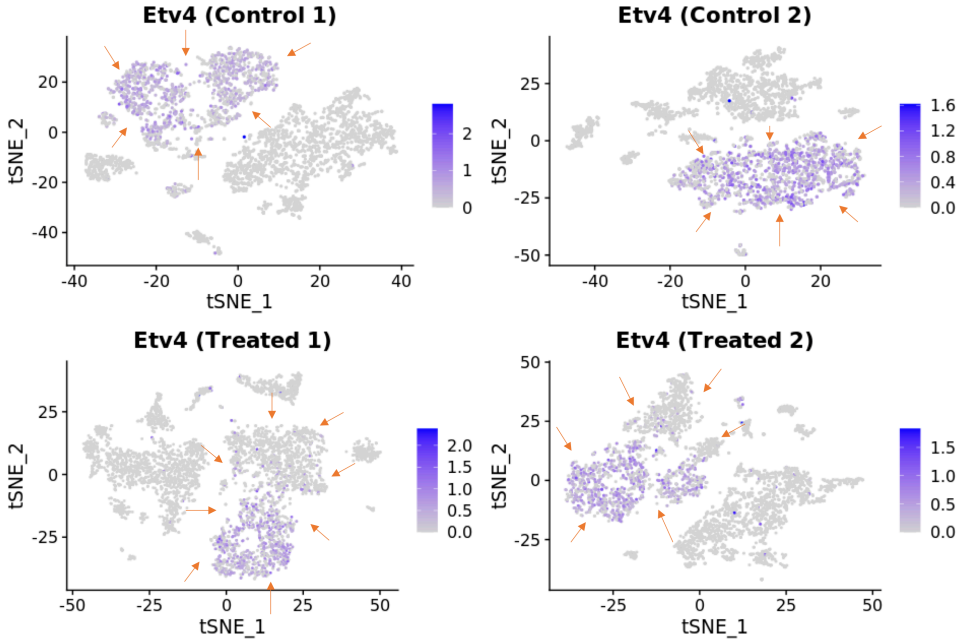

Figure 43. Tumour Etv4 expression in 3LL tumours treated with control or MRTX1257 Data clustered using Seurat. Red arrows indicate all tumour cell clusters

4.5 Characterisation of orthotopic 3LL-ΔNRAS tumours using CITE-seq

Given the acceptable QC of pilot samples and consistency with bulk RNAseq data, a further three mice were treated in each group, and all samples were sequenced to an increased depth. Once all samples had been acquired, processed and sequenced in this way, the data was analysed. Analysis began with a more thorough quality control of the data, aiming to identify poor quality cells to remove from further analysis. We then integrated samples using both mRNA and ADT information before aiming to characterise the landscape of the tumours using both automated and manual annotation of cells. For the following text, the following nomenclature applies

Name	Batch	Alias
Control 1	Pilot	Sample 1
Control 2	Pilot	Sample 2
Control 3	Post-pilot	Sample 3
Control 4	Post-pilot	Sample 4
Control 5	Post-pilot	Sample 5
Treated 1	Pilot	Sample 6
Treated 2	Pilot	Sample 7
Treated 3	Post-pilot	Sample 8
Treated 4	Post-pilot	Sample 9
Treated 5	Post-pilot	Sample 10

Table 22. Sample nomenclature of 3LL samples Control samples treated with vehicle control for 7 days, treated samples with 50mg/kg MRTX1257 for 7 days.

4.5.1 Removal of poor-quality cells

Poor quality cells, for example those that were dying during processing, add no information and can mislead downstream analysis. Thus, filtering is advised. Various per cell metrics can be informative when deciding which cells to filter out. Low quality cells often have a low transcript count, a low transcript diversity and a high percentage of transcripts from the mitochondrial genome. In addition to poor quality cells, doublets can also confound analysis. These cells may have an abnormally high transcript count and/or express an unusual combination of genes not found in singlets (for example genes specific to both myeloid and lymphoid cells). There is no ‘gold standard’ threshold of identifying poor quality cells or doublets, therefore individual samples need to be carefully interrogated and manual thresholds set (Luecken and Theis, 2019).

We looked at various metrics in the ten samples submitted for CITE-seq. As an example, one can see the distribution of some of these in Control 1. There was a trimodal distribution in the number of expressed genes and, similarly, in the

unique molecular identifier (UMI) count per cell, likely indicating three dominant populations in the sample. Also evident, is the fact that most cells have <10% of their transcriptome made up from mitochondrial genes, with a population of outliers above this. The distribution for ribosomal genes was similar, but with a higher peak.

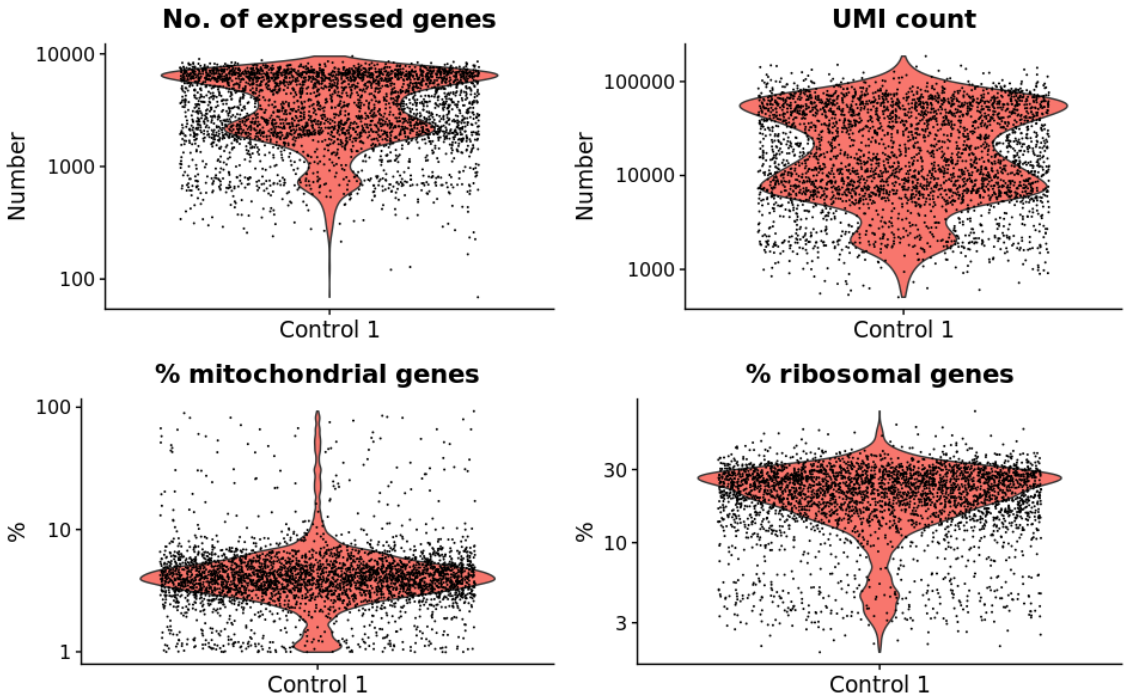

Figure 44. Violin plot showing distribution of QC metrics in single cell analysis of a control sample (3LL tumours)

In order to make clearer the appropriate threshold for filtering, these metrics can be plotted against one another. Poor quality cells with a high percentage of transcripts from the mitochondrial genome are likely to have few reads per cell and have a low transcriptional diversity. The latter can be quantified by looking at the percentage of the transcriptome occupied by the 50 most highly expressed genes. Good quality cells with a broad transcriptome are likely to have a low percentage of their transcriptome occupied by the 50 most highly expressed genes. Of note, however, tumours are likely to be heterogenous and therefore what constitutes ‘normal’ for one cell type may be abnormal for another.

In order to visualise key metrics together, we interrogated samples using a by plotting combinations of QC metrics against one another. Two such examples are shown in Figure 45, for two control samples (1 and 2). As is seen on the left-hand side, most cells had a low percentage of mitochondrial genes however in both samples there were outlier cells which lay above the bulk of the distribution. These outlier cells, with a higher percentage of mitochondrial genes, also tended to have a low gene count (number of different genes expressed). On the right, one can see that those cells with a high percentage of the transcriptome from the mitochondrial genome also had a low transcript diversity (a high percentage of the transcriptome occupied by just 50 genes). Of note, the plots on the right-hand side also show a population of cells with low gene counts, low transcript diversity and a *low* percentage of mitochondrial genes. When looking at the most highly expressed genes in this subpopulation of cells (those with >50% of their transcriptome from the top 50 genes and a mitochondrial gene percentage of <5%), neutrophil-associated genes (e.g. *Cxcl2, S100a8, S100a9 and Il1b)* highly expressed. This is consistent with evidence that neutrophils are relatively transcriptionally silent with a low diversity (Zilionis *et al.*, 2019) and exemplifies the heterogeneity of our sample with variations in ‘normal’ QC parameters between subpopulations. Thus, filtering all cells with low gene counts (without regard to other metrics such as mitochondrial percentage) would risk excluding neutrophils, for example.

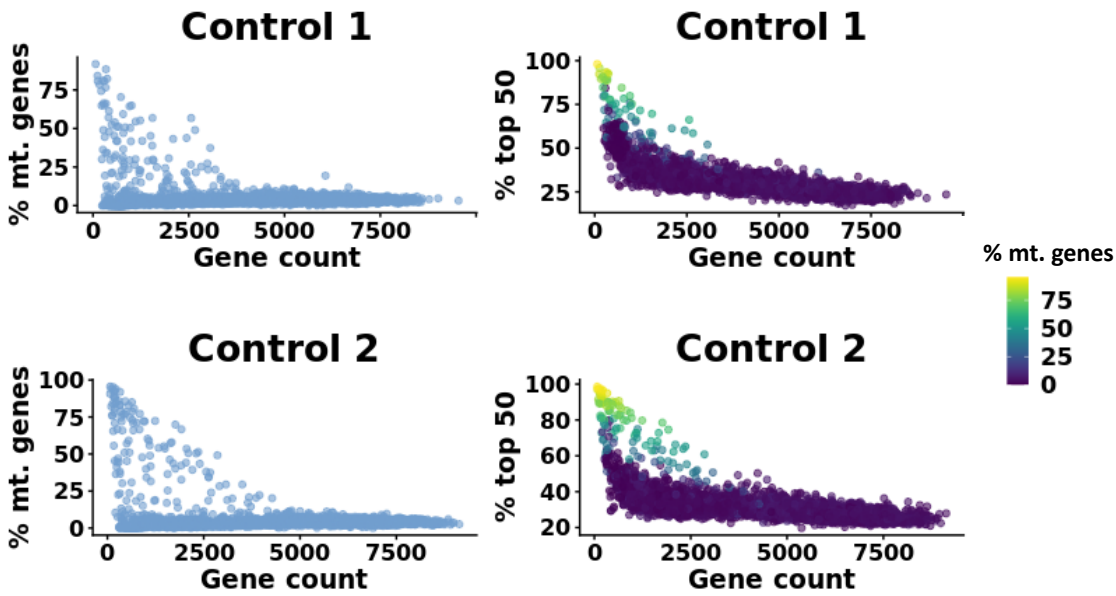

Figure 45. QC plots with multiple parameters of two 3LL tumours treated with vehicle control Cells processed for CITE-seq. The left-most plots simply show the percentage of the transcriptome occupied by mitochondrial reads versus the number of different genes detected, per cell. The right-most plots show the percentage of the transcriptome occupied by the 50-most highly expressed genes versus gene count. In addition, cells are coloured according to mitochondrial gene percentage.

As a final screen for outlier cells, we performed principal component analysis (PCA) using four metrics – read count, the number of different genes expressed, the percentage of the transcriptome made up of mitochondrial genes and the percentage of the transcriptome occupied by the 50 most highly expressed genes. An example of a PCA plot using these metrics is shown in (Figure 46). The plot is annotated with ‘outliers’ that were detected using an automated method that takes into account the distribution of the dataset with respect to all 4 QC metrics (rather than looking at them individually) (section 2.14.2). The plot on the right gives an intuition of parameter values for the outliers. As shown, many but not all ‘outlier’, cells had a high percentage of mitochondrial genes. Conversely, some cells called as outliers had a low mitochondrial gene percentage but appeared to have high transcript counts.

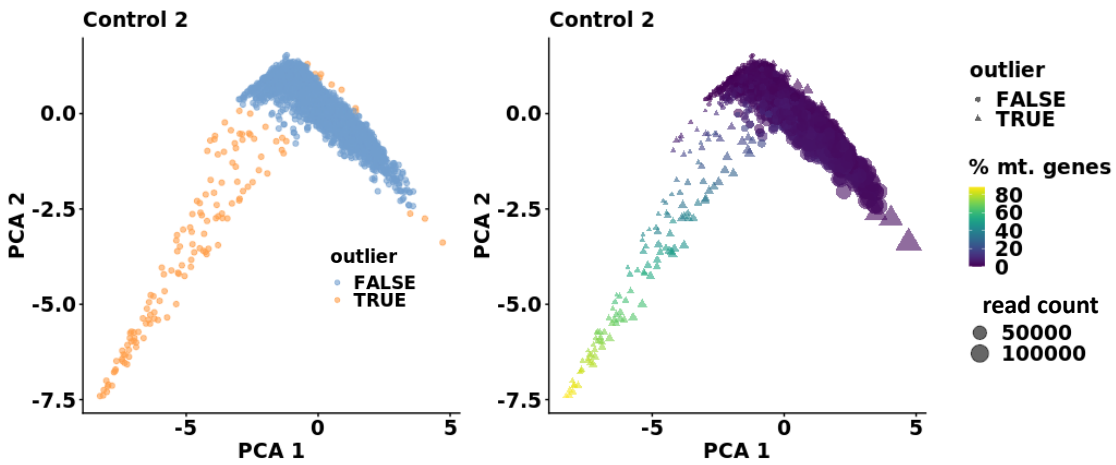

Figure 46. PCA on QC metrics, example for control 2 3LL tumours were treated with vehicle control and processed for CITE-seq. Four metrics (read count, the number of different genes expressed, the percentage of the transcriptome made up of mitochondrial genes and the percentage of the transcriptome occupied by the 50 most highly expressed genes) were used to generate PCA plots. An automatic outlier-detection algorithm was used to identify putative outliers (coloured orange on left-most plot). On the right, outliers are shown as triangles while cells are coloured by the % of the transcriptome made up of mitochondrial genes while the size of the dot represents read count.

Thus, in the final step before deciding which cells to filter out, doublet detection was attempted using an algorithm that simulated synthetic doublets. Real cells in the data were then classified as singlets or doublets according to how the simulated doublets clustered within the real data (section 2.14.2). This algorithm estimates the number of doublets as a function of the total number of cells in one's dataset. It then automatically labels this many cells (corresponding to the highest doublet scores) as being doublets.

Once we had assigned said doublet scores to the cells, we then proceeded to decide how to filter the data. In order to decide which cells to exclude from the final analysis, it is useful to visualise the cells (labelled with QC metrics) on a two-dimensional plot. Poor quality cells or doublets may cluster together, and this would add credence to the decision to exclude these cells from downstream analysis.

Shown below is a UMAP visualisation of two control samples annotated with certain QC metrics in a step-wise fashion (Figure 47). The plots on the left show all cells and highlights those with a high percentage of mitochondrial genes (threshold was set sample-wise) *and* a low transcript diversity (more than 50% of the transcriptome from the 50 most highly expressed genes). These cells cluster together, supporting their removal. Once removed, cells with a mitochondrial count above the sample specific threshold (regardless of transcript diversity) were visualised (middle panel). As shown, many of these cells occupied a similar area in UMAP space (i.e. compared to the previously removed cells) and were thus also removed. Finally, cells that had been labelled as outliers by the automated detection method described above were highlighted. Most automated 'outlier' cells would have been removed in the preceding filtering steps. The few cells that remained (coloured blue in the right-sided panels below) did not cluster discretely. It was therefore decided that they were not to be removed as they were unlikely to significantly affect downstream analysis and may not be true 'outliers' given the heterogenous nature of our sample. (Of note, the automated outlier detection method used does not take into account sample heterogeneity. Thus, suggested 'outliers' may in fact be normal cells representative of sample heterogeneity).

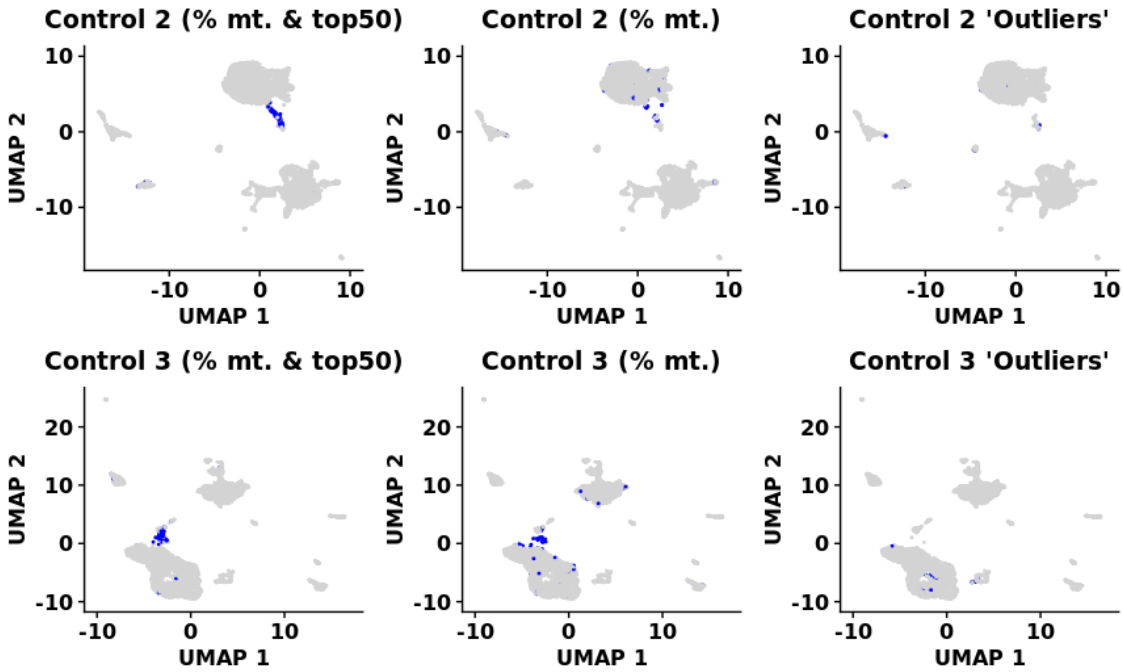

Figure 47. UMAP: removal of poor-quality cells On the left, cells with a high percentage of mitochondrial genes (>12% or 16% respectively for control 2 & 3) *and* >50% of the transcriptome from the 50 highest genes are highlighted. After removal, remaining cells with a high percentage of mitochondrial genes (regardless of transcript diversity) are highlighted (middle). Finally, after removal of these cells, automated 'outliers' are highlighted (right).

Finally, we visualised cells that had been labelled as doublets (not shown). Once again, these cells did not form a discrete cluster. Often, true doublets will form a cluster occupying space intermediate to two singlet clusters (Luecken and Theis, 2019). Given that we did not see this in our data, we could not be confident that we would not be throwing away valuable data, and these cells were retained. As mentioned, the doublet detection tool we used is mandated to call a certain number of cells as doublets (based on the 'expected' doublet rate, itself a function of the total number of cells sequenced). Therefore, the true doublet rate may be lower than this, and over-calling could result in loss of signal. In addition, as shown later, the majority of cells in our data were either tumour or myeloid cells. Thus, homotypic doublets, which are difficult to detect, would make up a significant number of the doublet population. We thus decided not to filter doublets at this stage, with the potential to revisit this in downstream analysis should issues arise.

4.5.2 Sample integration

Once data had been filtered as above, the filtered data set was normalised before samples were integrated (section 2.14.3). In brief, the 10 samples were first integrated using RNA expression and then using ADT expression. Finally, these two integrated datasets were used to create a weighted nearest neighbour (WNN) graph in order to enable joint definitions of cell state. A visual schematic of this procedure is shown in Figure 48.

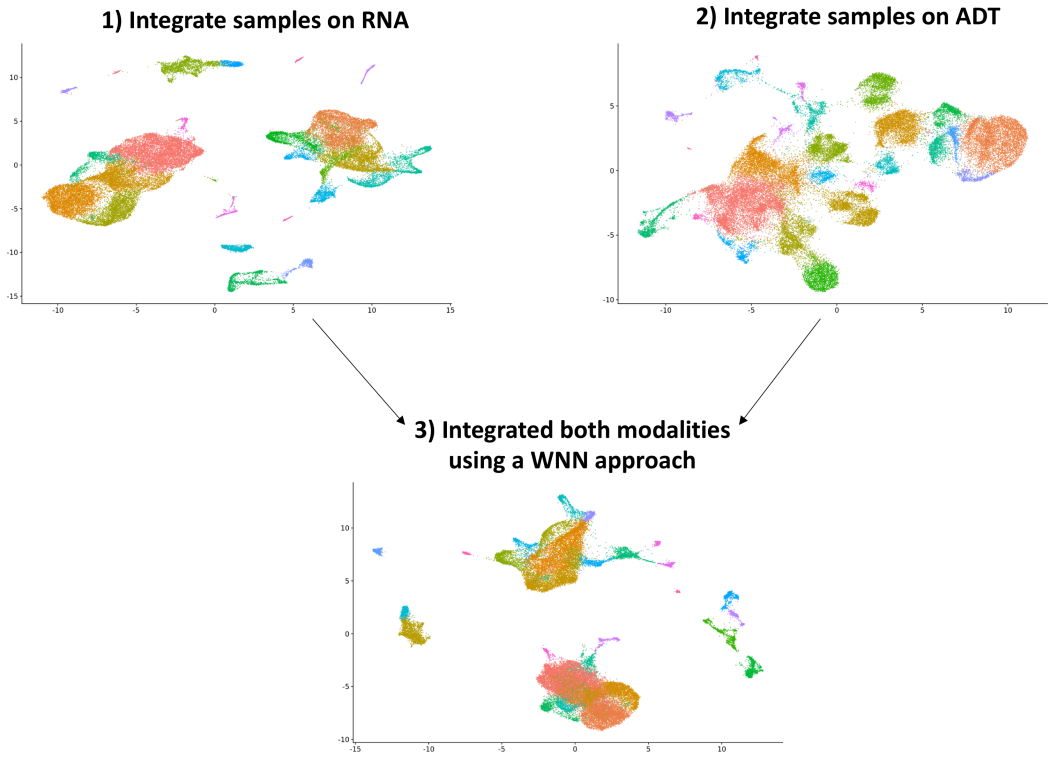

Figure 48. Schematic of integration procedure 3LL tumours from 10 mice (5 control, 5 treated with MRTX1257). The first step involves integrating all samples using their RNA expression, to produce an integrated matrix that is projected in the UMAP shown in 1). Next a similar procedure is done for ADT expression, shown in 2). Finally, both of these integrated representations are themselves integrated, to generate a 'WNN graph'. Such a graph can be used to cluster the cells and represent them in UMAP space, as is shown in 3).

As an illustration of the utility of such weighting, Figure 49 shows UMAP projections of integrated data using RNA expression alone, ADT expression alone or the WNN approach. Using RNA expression alone, CD4 and CD8a cells project very close to one another in UMAP space while when using ADT information alone they project distinctly. Likewise, using a WNN approach (and thus information from both RNA and ADTs), the cells project distinctly in UMAP space. Indeed, when we applied a clustering algorithm using RNA alone, one of the resulting clusters (number 9) contained both CD4 and CD8a positive cells. Conversely, applying a clustering algorithm using ADT alone or a WNN approach yielded distinct clusters for these cell types (e.g. clusters 19 and 22 for CD4 positive cells and cluster 9 for CD8a positive cells using a WNN approach). Thus, certain information (e.g CD4 and CD8a positivity) is not optimally captured using RNA sequencing alone. Conversely, other information (e.g. for intracellular markers such as Foxp3) would not be captured at all by ADTs yet would be informed by RNA. Thus, a WNN approach allows us to capture and use both sources to gauge cellular state.

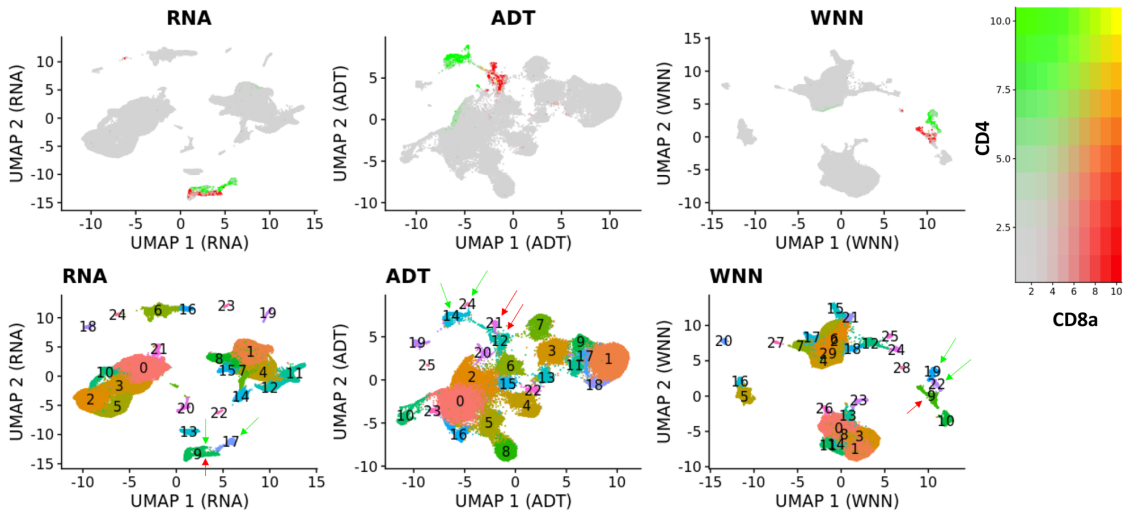

Figure 49. T lymphocyte representation across modalities 3LL tumours from 10 mice (5 control, 5 treated with MRTX1257). The top panels show UMAPs generated from RNA expression alone, ADT alone or from the WNN graph created using both RNA and ADT expression. The UMAPs are coloured according to their expression of CD8a (red) or CD4 (green) ADTs, with amber indicating both ADTs expressed within a cell. For the bottom panels, green arrows indicate $CD4^+$ cell-containing clusters while red indicates $CD8a^+$ cell-containing.

Once the data were integrated in this way, we were able to learn about the tumour landscape. Initially we overlaid manually curated gene sets representing broad cell types (Table 23) in order to gain an appreciation for the composition of our sample (Brown *et al.*, 2019; Zilionis *et al.*, 2019; Goveia *et al.*, 2020; Muhl *et al.*, 2020). As shown in Figure 50, myeloid cells including macrophages, monocytes and DCs made up a significant proportion of our landscape. Neutrophils, NK cells and T cells were present at lower frequencies while B cells, endothelial cells and mesenchymal cells were very uncommon. The remaining large cluster, which did not express any of the aforementioned markers was the tumour cell cluster as evidenced by its lack of expression of Ptprc (gene for CD45) and specific lack of H2-K1 expression (Figure 41).

Neutrophils	NK cells	Monocytes	Macrophages	DCs
Cxcl8	Gzma	Ly6c2	Apoe	Clec9a
G0s2	Klrb1c	Vcan	Mrc1	Ccr7
Cxcr2	Ncr1	Ace	C1qa	Batf3
S100a8	Klra4	Fcgr4	Fn1	Itgae
S100a9	Eomes	Chil3	Gpnmb	Irf4
Csf3r	Fasl		Cd68	H2-DMb2
Ffar2	Klrk1		Saa3	
Lymphocytes	**B cells**	**Endothelial**	**Mesenchymal**	
Cd3d	Ms4a1	Pecam1	Col1a1	
Cd3e	Cd19	Cdh5	Col1a2	
Cd3g	Bank1			
Cd28	Cr2			

Table 23. Gene sets for manual annotation used to name single cell clustersDCs = dendritic cells

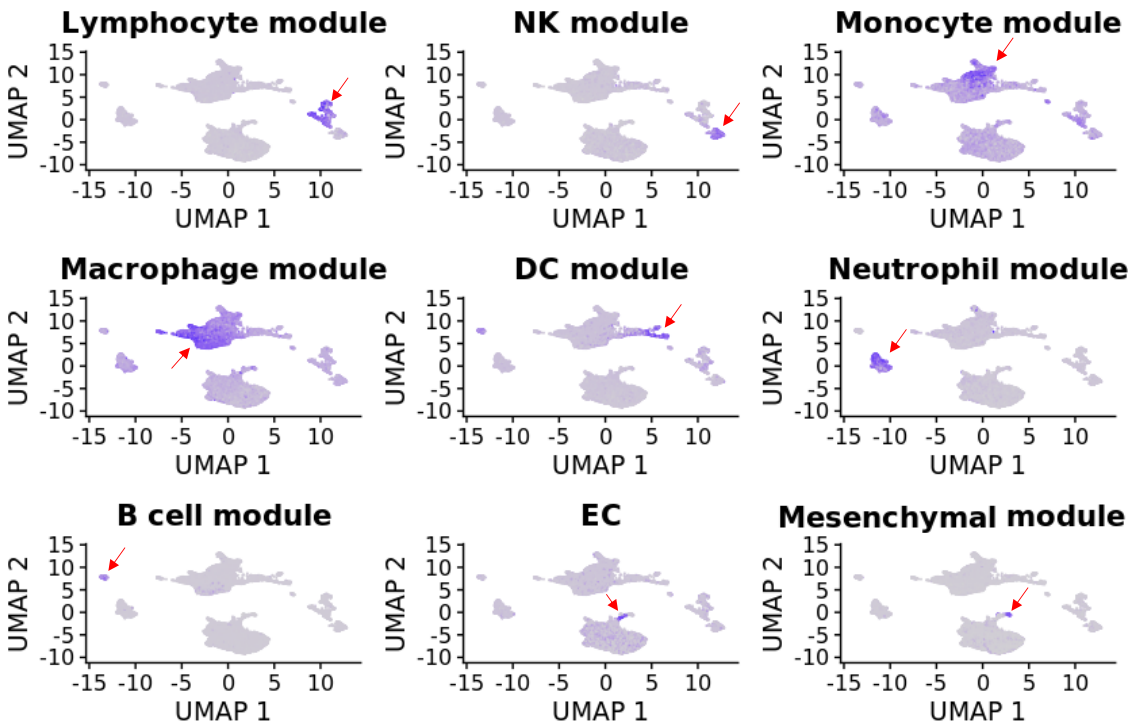

Figure 50. Marker genes sets expression in integrated 3LL data Marker gene lists were manually curated. Per cell scores were calculated (see methods) and projected onto UMAP plots using the WNN graph. Red arrows indicate highest expressing cells. NK = natural killer, DC = dendritic cell, EC = endothelial cell

Following overlay of marker gene sets as above, we sought to initially annotate cell types using an automated approach. We used single cell data from the literature (Zilionis *et al.*, 2019) where mice were injected with the KP1.9 tumour cell line and CD45^{+} cells were isolated for single cell sequencing. In this study, cells were first ascribed a broad identity using a Bayesian classifier and previously annotated transcriptional states from the IMMGEN consortium (Heng *et al.*, 2008). Following this, cells were subclustered and manually annotated. Brief descriptions of some labels from this study are shown in Table 9. We used the labels from this study and assigned each cell in our dataset to one of these labels using SingleR (version 1.4.1). In brief, the algorithm uses Spearman correlation to assess similarity between our data and labels in the reference dataset followed by fine tuning to resolve labels with similar scores (section 2.14.4).

Labels obtained by this method are overlaid on the WNN UMAP in Figure 51. Of note, the labels only apply to immune cells, so putative tumour, endothelial cell and mesenchymal cell clusters were excluded from labelling.

As shown in Figure 51, automated labelling largely agreed with the structure suggested by our overlay of manually curated genes. Furthermore, automated labelling suggested further substructure to the data. For example, alternatively activated monocytes (Mono2) occupied a distinct part of UMAP space from classically activated cells (Mono1). For macrophages, alveolar macrophages (Mac4) were seen to cluster separately. Substructure was also evident in the dendritic cell population with conventional type I (DC1) and II (DC2) dendritic cells and activated dendritic cells (DC3) all projecting distinctly within the space.

Nonetheless, some differences were also evident. For example, when our data was used to drive clustering (Seurat v 4.1.0, resolution = 0.5), DC2s and monocytic DCs were merged into a single cluster. Conversely there was more substructure in the macrophage/monocyte metacluster than was suggested by automated labelling. Of note, such substructure is somewhat dependent on parameters of the clustering algorithm however the current substructure seen was robust to reduction of the resolution parameter of said algorithm. Myeloid clusters are explored in Chapter 5.

In essence, the congruence of cells in our WNN UMAP space with literature-curated labels suggested that we had a robust and reproducible dataset, thus adding credibility to insights drawn from downstream analysis.

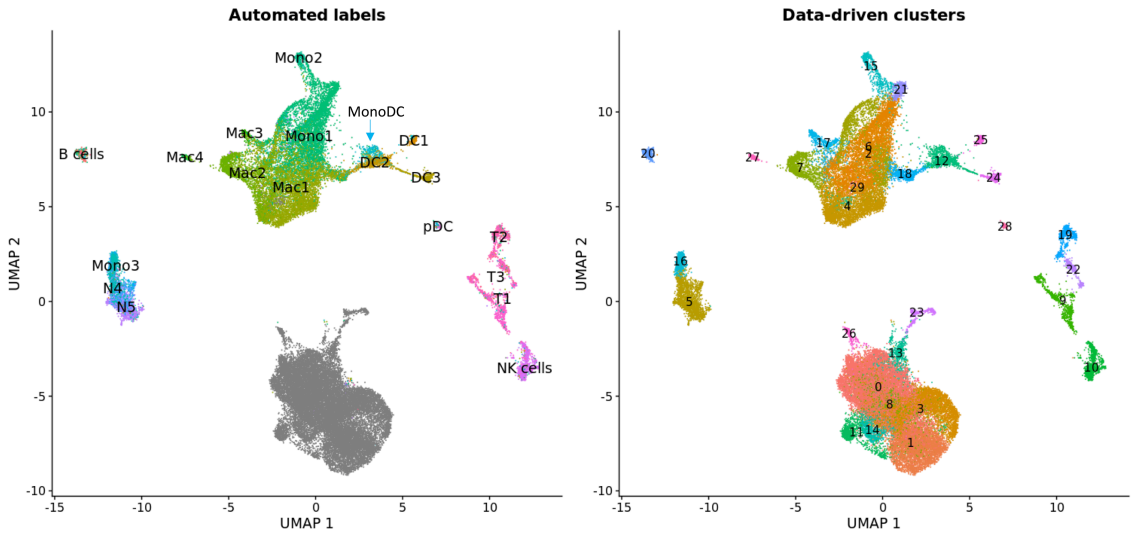

Figure 51. Automated cell labels and data-driven clusters

3LL tumours from 10 mice (5 control, 5 treated with MRTX1257). Data integrated using weighted nearest neighbours (Seurat). The left panel shows automated annotation of clusters using the SingleR package and reference data from Zilionis et al.

4.5.3 Composition analysis of integrated data

Once our data was integrated, we sought to identify the composition of the dataset, specifically observing this by sample and treatment. We did this for all cells, and separately for the immune compartment. For immune cells, we used the labels from automated annotation (and amalgamated cell types as indicated) whilst for non-immune cells (tumour, endothelial and mesenchymal) we manually annotated clusters based on marker expression (Figure 52).

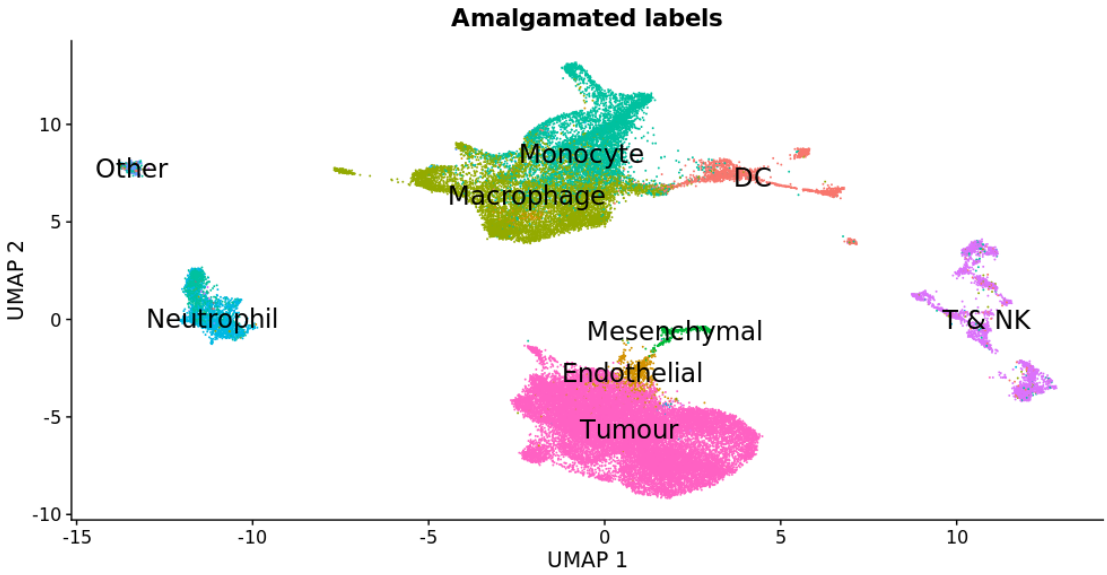

Figure 52. Amalgamated cell labels of integrated 3LL data Immune labels from automated analysis were combined while tumour, endothelial and mesenchymal clusters were annotated based on marker expression. ‘DC’ = DC1-3, pDC & monoDC; ‘Macrophage’ = Mac1-4; ‘Monocyte’ = Mono1-3; ‘Other’ = B cells & basophils; ‘Neutrophil’ = N1-5; ‘T & NK’ = T1-3 & NK.

As shown in Figure 53 there was per sample heterogeneity in composition, but some patterns emerged when looking at immune cells specifically.

a)

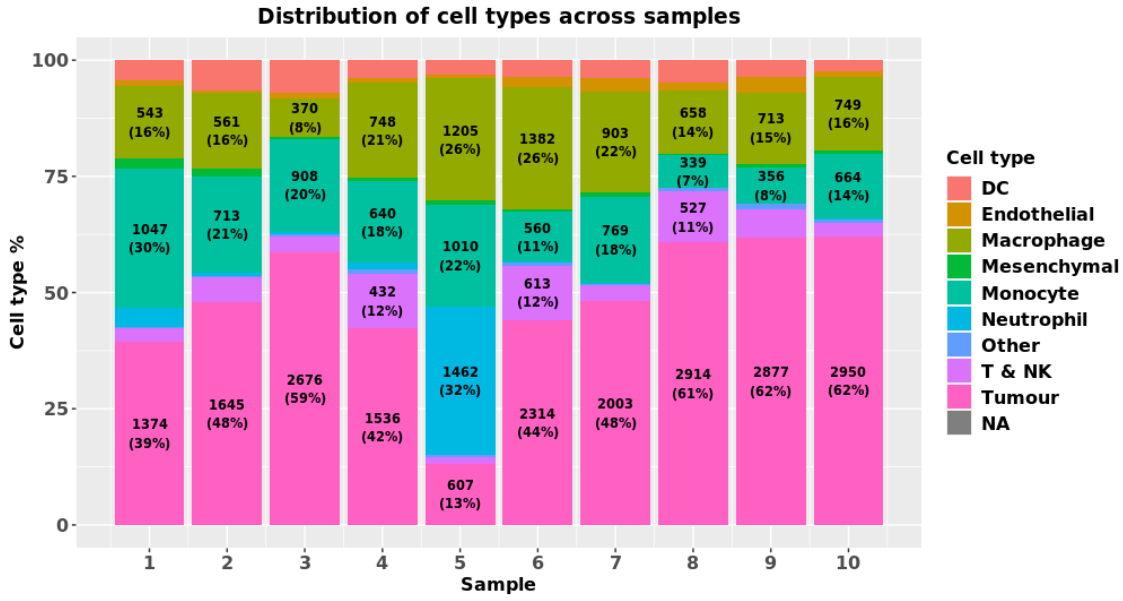

b)

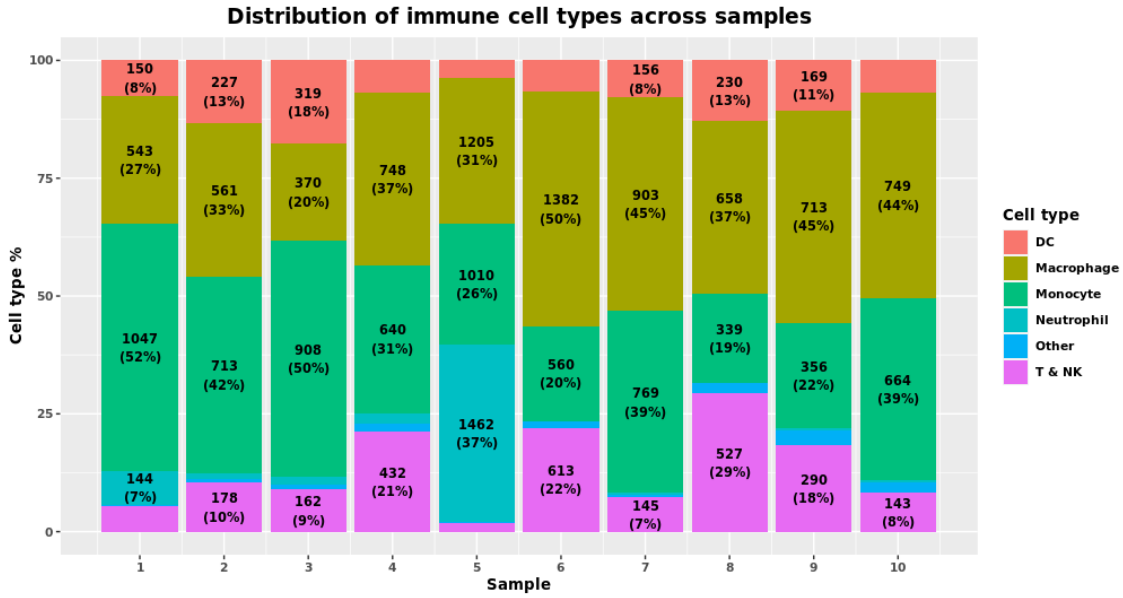

Figure 53. Distribution of cell types across samples Samples are arranged from 1-10 on the x-axis, with samples 1-5 representing 3LL control samples while 6-10 represent MRTX1257-treated samples. Samples 1,2 & 6,7 are pilot samples. Figures are labelled for cell types with a >7% composition. Top-panel includes all cells. Bottom panel only includes immune cells.

Of note, sample five was an outlier with few tumour cells and a much higher proportion of neutrophils compared to the other samples. This sample was not

noted to be macroscopically different during sample preparation. The high proportion of neutrophils suggests the presence of necrosis. We did not feel that it would be valid to simply exclude this sample from further analysis, however where relevant (for example during composition analysis below) sensitivity analysis was performed by excluding this sample and verifying that results were consistent.

When looking at all cells, there was a higher percentage of tumour cells in the treated samples than the control samples. There may be several reasons for this observation. Firstly, when allocating mice into treatment groups, the distribution of tumour volumes in the control arm was lower than those in the treatment arm. Furthermore, observations in our lab indicate that MRTX1257 has a cytostatic effect on 3LL-ΔNRAS tumours rather than being obviously cytotoxic. In addition, some mice in the control arm showed indications of tumour progression (weight loss, behavioural change, laboured breathing) and were culled according to protocol stipulations. Therefore, the remaining control mice (including those sampled) were those whose intrinsic tumour growth rate was, by definition, not sufficient to warrant culling of the mice prior to the experiment end point. Finally, the treated samples are likely to have had a different consistency to control samples and therefore may have been easier to dissociate, accounting for the higher proportion of these cells seen. These caveats are properties of the tumour model and are borne in mind during the discussion.

When looking at immune cell distribution specifically, the percentage of macrophages (within the immune compartment) was generally higher in the five treated samples (range 37% to 50%) than the five control samples (range 20% to 37%). Conversely, the percentage of monocytes was generally lower in the treated samples (range 19% to 39%) than the control samples (range 26% to 52%). This was consistent with previous data from the lab (Mugarza *et al.*, 2021). Exact figures for compositional changes are shown in Table 24. In this table, composition is also given per condition (in addition to per sample).

	1	2	3	4	5	6	7	8	9	10	All control	All treated
DC	150 (4.3)	227 (6.6)	319 (7)	139 (3.8)	146 (3.2)	184 (3.5)	156 (3.7)	230 (4.8)	169 (3.6)	119 (2.5)	**981 (5)**	**858 (3.6)**
Endothelial	43 (1.2)	15 (0.4)	63 (1.4)	37 (1)	34 (0.7)	118 (2.3)	125 (3)	80 (1.7)	156 (3.3)	57 (1.2)	**192 (1)**	**536 (2.3)**
Macrophage	543 (15.6)	561 (16.4)	370 (8.1)	748 (20.6)	1205 (26.3)	1382 (26.4)	903 (21.7)	658 (13.7)	713 (15.3)	749 (15.7)	**3427 (17.4)**	**4405 (18.6)**
Mesenchymal	75 (2.1)	53 (1.5)	25 (0.5)	24 (0.7)	39 (0.9)	30 (0.6)	43 (1)	9 (0.2)	41 (0.9)	34 (0.7)	**216 (1.1)**	**157 (0.7)**
Monocyte	1047 (30)	713 (20.8)	908 (19.9)	640 (17.6)	1010 (22)	560 (10.7)	769 (18.5)	339 (7.1)	356 (7.6)	664 (13.9)	**4318 (21.9)**	**2688 (11.4)**
Neutrophil	144 (4.1)	24 (0.7)	31 (0.7)	45 (1.2)	1462 (31.9)	5 (0.1)	8 (0.2)	2 (0)	7 (0.2)	7 (0.1)	**1706 (8.7)**	**29 (0.1)**
Other	7 (0.2)	12 (0.3)	17 (0.4)	37 (1)	18 (0.4)	35 (0.7)	10 (0.2)	39 (0.8)	50 (1.1)	38 (0.8)	**91 (0.5)**	**172 (0.7)**
T & NK	107 (3.1)	178 (5.2)	162 (3.5)	432 (11.9)	67 (1.5)	613 (11.7)	145 (3.5)	527 (11)	290 (6.2)	143 (3)	**946 (4.8)**	**1718 (7.3)**
Tumour	1374 (39.4)	1645 (48)	2676 (58.5)	1536 (42.2)	607 (13.2)	2314 (44.2)	2003 (48.1)	2914 (60.7)	2877 (61.7)	2950 (61.9)	**7838 (39.8)**	**13058 (55.3)**
Not assigned	0 (0)	1 (0)	2 (0)	0 (0)	0 (0)	0 (0)	2 (0)	1 (0)	4 (0.1)	1 (0)	**3 (0)**	**8 (0)**
Immune only												
DC	150 (7.5)	227 (13.2)	319 (17.7)	139 (6.8)	146 (3.7)	184 (6.6)	156 (7.8)	230 (12.8)	169 (10.7)	119 (6.9)	**981 (8.55%)**	**858 (8.69%)**
Macrophage	543 (27.2)	561 (32.7)	370 (20.5)	748 (36.6)	1205 (30.8)	1382 (49.7)	903 (45.4)	658 (36.7)	713 (45)	749 (43.5)	**3427 (29.88%)**	**4405 (44.63%)**
Monocyte	1047 (52.4)	713 (41.6)	908 (50.2)	640 (31.4)	1010 (25.8)	560 (20.2)	769 (38.6)	339 (18.9)	356 (22.5)	664 (38.6)	**4318 (37.65%)**	**2688 (27.23%)**
Neutrophil	144 (7.2)	24 (1.4)	31 (1.7)	45 (2.2)	1462 (37.4)	5 (0.2)	8 (0.4)	2 (0.1)	7 (0.4)	7 (0.4)	**1706 (14.87%)**	**29 (0.29%)**
Other	7 (0.4)	12 (0.7)	17 (0.9)	37 (1.8)	18 (0.5)	35 (1.3)	10 (0.5)	39 (2.2)	50 (3.2)	38 (2.2)	**91 (0.79%)**	**172 (1.74%)**
T & NK	107 (5.4)	178 (10.4)	162 (9)	432 (21.2)	67 (1.7)	613 (22.1)	145 (7.3)	527 (29.4)	290 (18.3)	143 (8.3)	**946 (8.25%)**	**1718 (17.41%)**

Table 24. Compositional change across samples 3LL tumours across 10 mice were treated with control (1-5) or MRTX1257 (6-10). Numbers in cells indicate the number of cells classified as the given cell type in the given sample (percentages in brackets).

In order to discern whether compositional changes across samples were significant, we used edgeR (version 3.32.1) to model the dispersion of cell abundance between samples and perform statistical testing for differential abundances (DA) between conditions. As shown in Table 25, when all cell types were included, neutrophils were the most significantly differentially abundant population, being reduced by a $\log_2$ FC of -5.6 ($p < 0.001$). Monocytes were also significantly reduced, by a $\log_2$ FC of -0.95 ($p = 0.04$) while endothelial cells more than doubled with treatment ($\log_2$ FC of 1.25, $p = 0.04$).

Of note, tumour cells were abundant within our samples, and were numerically more common in treated compared to control samples. Given their abundance, changes in tumour cell proportion per sample can affect the outcomes of compositional analysis on other cells even in the absence of 'true' (biological) changes. One approach to dealing with this is to repeat the DA analysis after removing the offending population. To this end, the analysis was re-run on non-tumour cells alone. As shown below, the change in neutrophils and endothelial cells was still significant. Conversely, while monocytes were still less common after treatment ($\log_2$ FC -0.57) this was no longer significant ($p = 0.199$). Meanwhile, the increase in macrophages became more apparent ($\log_2$ FC 0.52) although the result was not statistically significant ($p = 0.16$).

Finally, given the outlier nature of sample 5 (control 5), we performed a sensitivity analysis by repeating the above with sample removed. Despite its removal, the downregulation of neutrophil abundance with treatment was still evident ($\log_2$ FC = -3.53) and significant ($p = 0.002$).

	Log_2 FC	p-value	Adj. p (FDR)
Neutrophil	-5.61	0.00	0.01
Endothelial	1.25	0.01	0.04
Monocyte	-0.95	0.01	0.04
Other	0.65	0.15	0.32
Mesenchymal	-0.61	0.19	0.32
DC	-0.45	0.21	0.32
Tumour	0.45	0.27	0.35
T & NK	0.51	0.41	0.46
Macrophage	0.06	0.88	0.88
No tumour			
Neutrophil	-4.87	0.00	0.01
Endothelial	1.58	0.01	0.03
Other	1.01	0.04	0.12
Macrophage	0.52	0.08	0.16
Monocyte	-0.57	0.12	0.20
T & NK	0.81	0.23	0.30
DC	-0.18	0.68	0.70
Mesenchymal	-0.19	0.70	0.70

Table 25. Differential abundances of cell populations Log_2 fold changes represent change in abundance in treated 3LL tumours (MRTX1257) vs. control mice. Analysis repeated after removing tumour cells (bottom table). p-value adjustment performed using the Benjamini Hochberg method.

Therefore, we can conclude that treatment results in significant reductions in neutrophil abundance. Furthermore, although endothelial cells were uncommon, they appear to increase with treatment. Macrophages, T & NK cells appear to increase with treatment and monocytes appear to decrease, but the effects were not significant (at an adjusted p threshold of < 0.05) with evident sample-sample variability. Much of this is reassuringly consistent with previous data from the lab, adding credibility to any inferences drawn from downstream analysis (Mugarza *et al.*, 2021). While tumour cell abundance increased slightly with treatment (log_2 fold change of 0.19) this may be an artefact of tumour volume at initiation of treatment/control and because some mice in the control group were culled after triggering endpoints in the protocol. The transcriptional effect of treatment on the tumour cell compartment is discussed later.

4.6 Concluding remarks

We were able to generate a CITE-seq dataset of an orthoptic murine KRAS(G12C)-mutant lung carcinoma model treated with MRTX1257. We optimised the dissociation procedure by using a commercial dissociation method and, after sorting for viable cells, we obtained a good quality dataset where only a minority of the data appeared to be of poor quality. Analysis of the remaining cells revealed congruence with bulk sequencing experiments previously done by the lab, increasing confidence of inferences from downstream analysis. This includes both gene expression data and composition analysis where we saw a significant reduction in neutrophil proportion and an increase in endothelial percentage. In addition, through the example of Etv4, we saw an example of a gene downregulated by treatment but in only a subset of tumour cells, exemplifying the potential for single cell methods to characterise the behaviour of subpopulations in a way not possible with bulk methods.

Chapter 5. Results 3: Analysis of specific cell types in an orthoptic KRAS(G12C) model of lung cancer using CITE-seq

5.1 Introduction

Following sample acquisition, data pre-processing and interrogation of the tumour landscape, we sought to understand the cell type-specific effects of MRTX1257 in orthotopic 3LL-ΔNRAS tumours.

In this chapter we subset and analyse two individual cell types within these tumours, aiming to understand how treatment with MRT1257 specifically affects myeloid cells and tumour cells.

5.2 Myeloid cell effects

5.2.1 Subsetting and clustering

According to our preliminary analysis of the tumour landscape, myeloid cells are the dominant immune type within the orthotopic 3LL-ΔNRAS TME. In order to analyse myeloid cells specifically, marker genes (Table 23) were overlaid on an integrated WNN UMAP representation and cells within clusters expressing myeloid genes were subsetted. Of note, to maintain congruence with any downstream publications, the integrated WNN UMAP representation used here was pre-processed in a modified way from the pre-processing described in section 4.5.1. Pre-processing for the integrated WNN UMAP representation used here was performed by Phil East from the Bioinformatics Science Technology Platform at the Francis Crick Institute. The same principles were used (using QC metrics such as mitochondrial gene percentage and transcript diversity to subset cells) however the exact thresholds used varied from the examples given in chapter 4. This integrated dataset, and the overlay of myeloid genes within it, is shown in Figure 54.

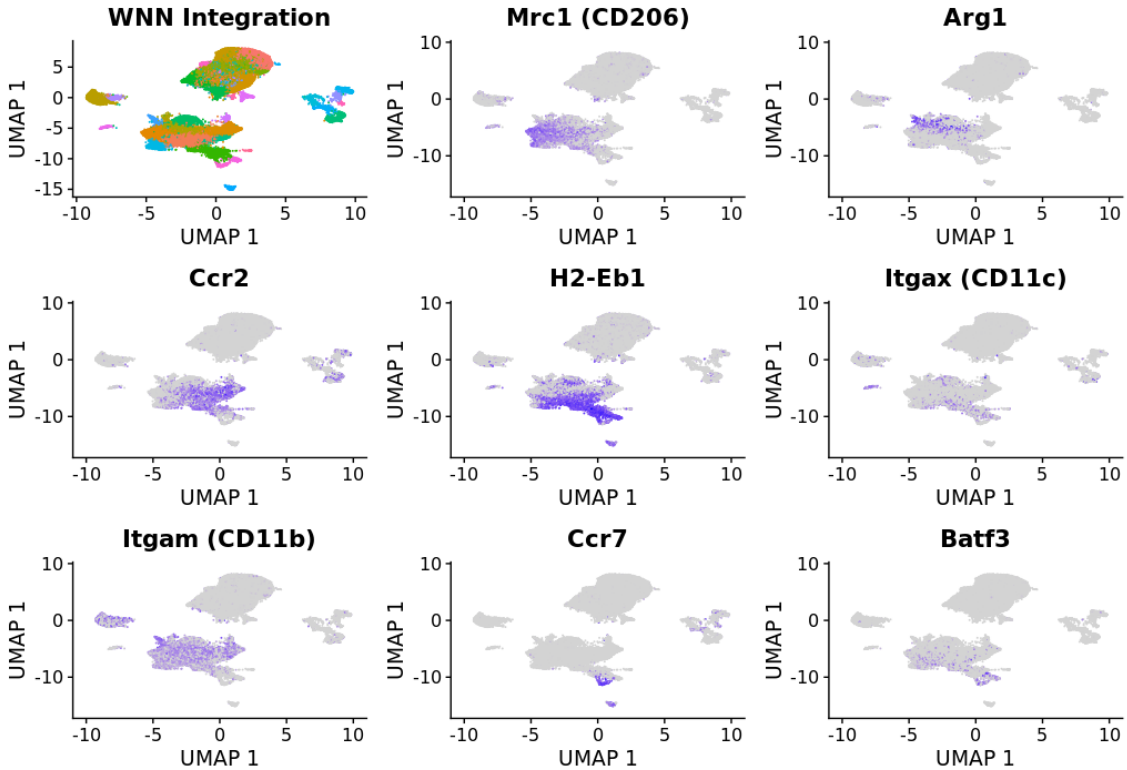

Figure 54. WNN integrated dataset and overlay of myeloid genes3 10 mice with 3LL tumours were treated with control (5 mice) or MRTX1257 (5 mice). Data integrated using WNN (Seurat). Overlay of myeloid genes, including but not limited to the ones shown here, were used to subset cells for downstream analysis.

Subsetted cells were then split by sample (i.e. according to their membership of the 5 control or 5 treated samples) before normalisation, scaling and variable feature selection was performed again (section 2.14). This was followed by the same schema for integration as used previously (i.e. integrating each sample on SCT-normalised mRNA expression, then separately on CLR-normalised ADT expression before finally creating an integrated WNN representation of the data). A schema for this workflow is shown in Figure 55.

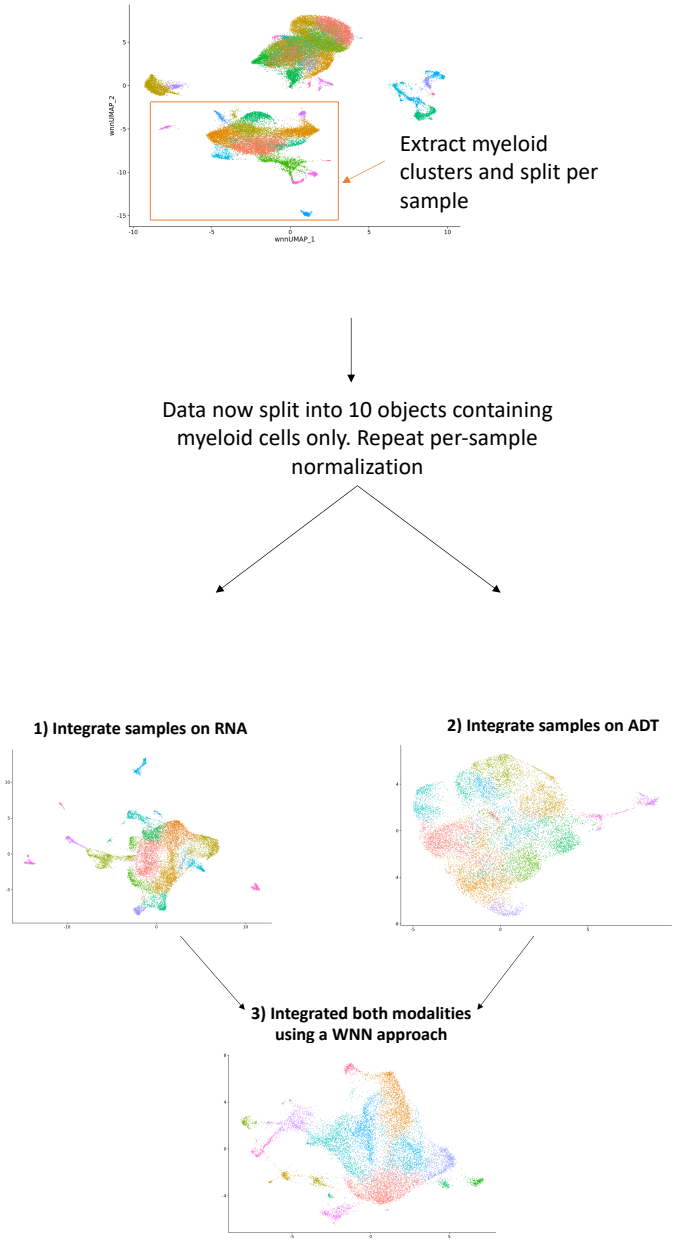

Figure 55. Subsetting and integration of the myeloid compartment 10 mice with 3LL tumours were treated with control (5 mice) or MRTX1257 (5 mice). Data integrated using WNN (Seurat). Myeloid cells were extracted from the integrated dataset containing all cells, split by sample and then re-integrated (after selection of variable features) using both mRNA and ADT information separately. Finally, the mRNA and ADT integrated objects were used to generate a WNN representation of the myeloid compartment that takes into account information from both mRNA and ADT expression.

Once cells were subsetted and reintegrated, clustering was performed. The algorithm used for clustering takes a ‘resolution’ parameter which affects the granularity of clustering. Low resolutions lead to coarse larger clusters while higher resolutions result in smaller, finer groups. There is no ‘correct’ number of clusters and one may use *a priori* biological knowledge along with inspection of the data to decide.

In order to help decide on a suitable number of clusters we used a sequence of different clustering ‘resolutions’ and interrogated the results graphically (Figure 56). In this tree, each horizontal line of nodes represents the clusters at a given resolution. Edges (arrows) represent where the cells from that cluster end up at the next resolution.

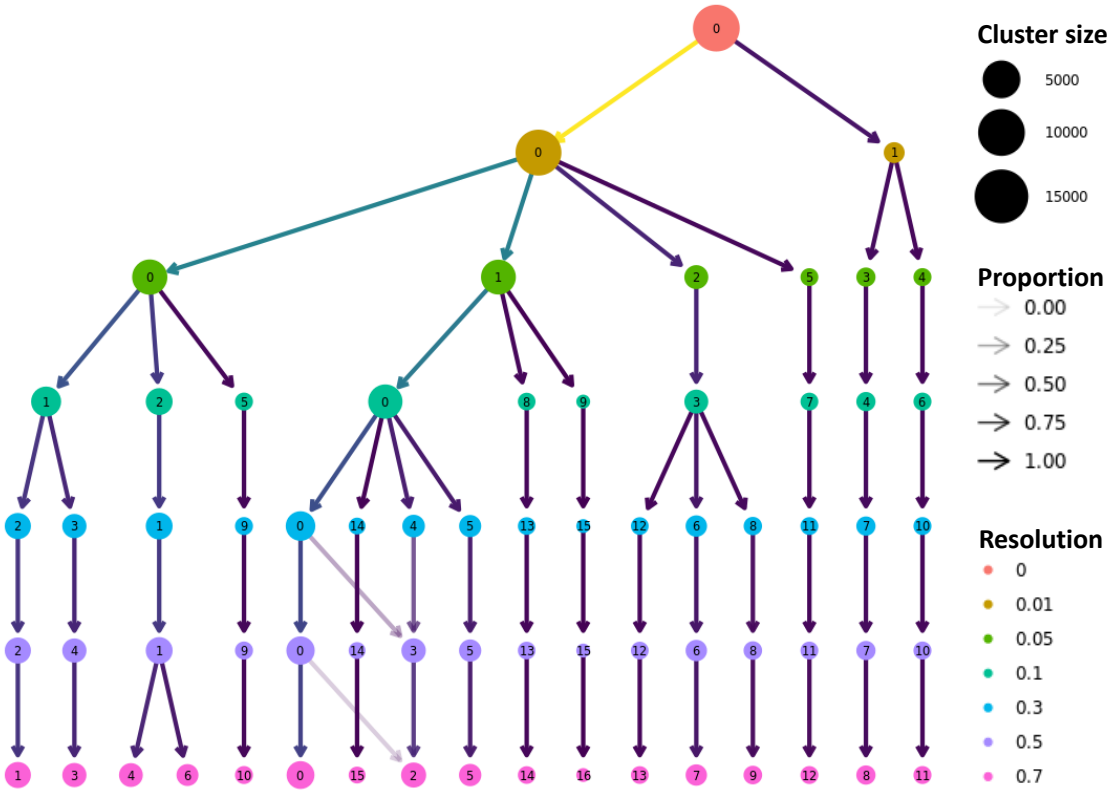

Figure 56. Effect of varying resolution on generation of clusters 10 mice with 3LL tumours were treated with control (5 mice) or MRTX1257 (5 mice). Data integrated using WNN (Seurat) and myelod cells extracted using myeloid-specific markers. Myeloid data re-integrated and interrogated with different clustering resolutions (Clustree package) as shown above

As shown, as the resolution was increased, clusters tended to split fairly 'cleanly' with little mixing of cells (i.e. cells that were in different clusters at a lower resolution did not tend to merge at higher resolutions). This suggested that we were not 'overclustering' our data. We decided to us a resolution of 0.5 to annotate our data. There were 16 clusters at this resolution, a number consistent with what one may expect from the literature (Brown *et al.*, 2019; Zilionis *et al.*, 2019). A visual intuition of how clusters evolved with increasing resolution is shown in Figure 57.

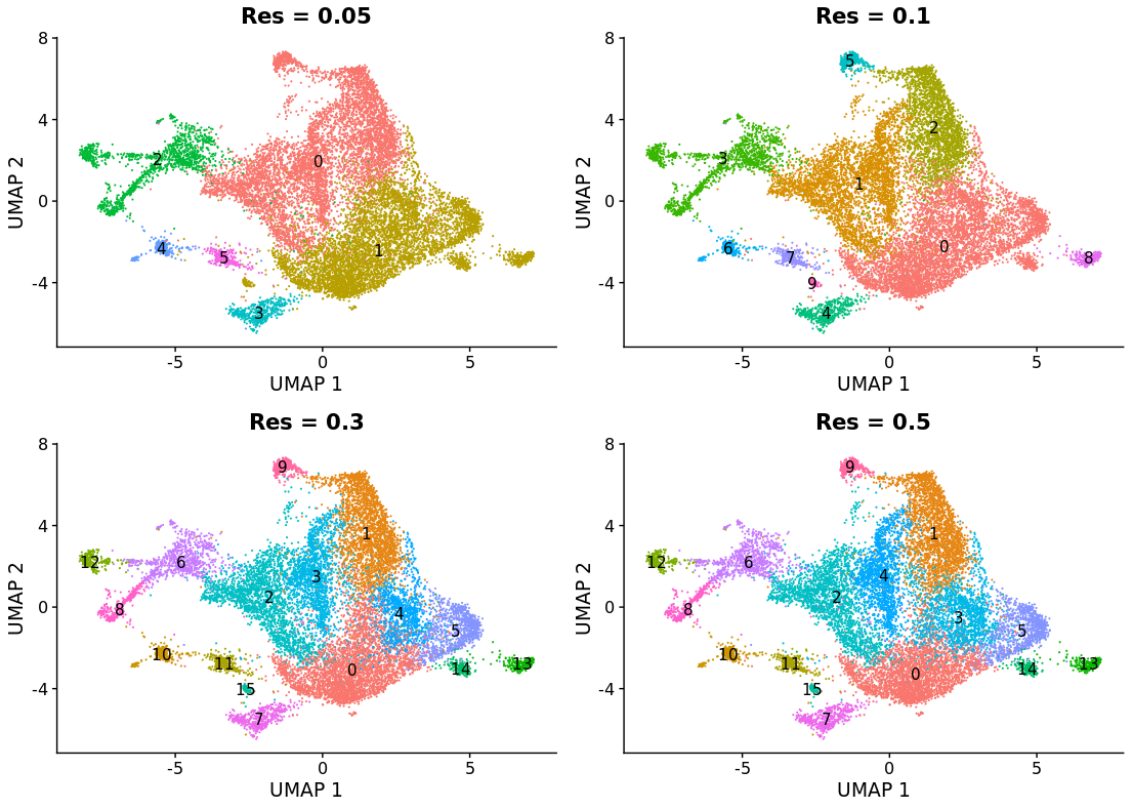

Figure 57. Evolution of clusters with increasing resolution

10 mice with 3LL tumours were treated with control (5 mice) or MRTX1257 (5 mice). Data integrated using WNN (Seurat). Different clustering resolutions were interrogated to ascertain optimal resolution for downstream analysis.

5.2.2 Cell-type annotation

Once this provisional cluster resolution had been set, we sought to annotate the clusters. In order to do this, we performed differential expression (DE) testing. For each cluster, we performed DE testing between that cluster and all other clusters combined. We then also performed pairwise DE between each cluster and every other cluster. For each cluster, DE was performed using different pairwise tests (t-tests, Wilcoxon signed rank sum tests or binomial tests) to give enough information to optimally select ‘marker’ genes.

The marker genes selected, and notes about the various clusters, are shown in Table 26 while a heatmap depicting expression of said markers over all myeloid cells is shown in Figure 58.

Cluster no. (brief description)	Genes expressed	Notes
0 (Chemokine-expressing macrophages)	Ccl7, Ccl8, Ccl12, Selnop	High expression of chemoattractant molecules (Ccl7, Ccl8, Ccl12) and 'M2'-like markers e.g. Mrc1 (CD206), Folr1 & Gas6
1 (Classical monocytes)	Vcan, Ly6c2, Hp, Ccr2, Chil3	Expression of classical monocyte markers
2 (Antigen Presentation high macs)	H2-Ab1 (and other MHC II gens), Cd74	Clusters 6 and 12 also express these, however they lack macrophage genes (e.g. C1qa). Conversely, cluster 2 lacks DC genes (e.g. Cd209a)
3 (Arg1 high macs)	Arg1, Cxcl3, Inhba, Vegfa, Ptgs2	Subset of this cluster express high Hsp1a/b (HSP70 family).
4 (ISG high mon/macs)	Cxcl10, Ifit1, Irf7, Isg15	Mixture of monocyte and macrophage markers. Uniquely high expression of IFN-stimulated genes
5 (Gpnmb high)	Gpnmb, Fabp5, Creg1, Syngr1	Gpnmb is specific to this cluster except for expression in a fraction of cluster 13 cells.
6 (cDC2 -like)	Cd209a, Ifitm1, Klrd1, H2-DMb2	Expression of known cDC2 markers
7 (Cycling macs)	Stmn1, Top2a, Mki67, Birc5	Uniquely expresses cell cycle genes. Also express some markers of cluster 0 cells. No monocyte genes
8 (Activated DCs)	Ccr7, Ccl5, Fscn1, Ccl22	Expresses markers of DC maturation
9 (Alt monocytes)	Ace, Cd300e, Itgal, Treml4	Expresses markers of alternatively activated monocytes

10 (Mesenchymal)	Cald1, Col3a1, Krt8, Sparc	Expresses mesenchymal genes. Also express the TF Rhox5. Express high levels C1qa and Apoe.
11 (mt. genes)	mt-Nd2, mt-Atp6, mt-Nd3	Small cluster with high mitochondrial gene counts
12 (cDC1-like)	Batf3, Itgae, Naaa, Clec9a	Expresses canonical cDC1 markers without markers of maturation
13 (Alveolar mac-like)	Marco, Ear2, Chil3, Lpl	Expresses markers of alveolar macrophages
14 (Saa3 high macrophage)	Saa3, Alox15, Serpinb2, Prg4	Striking similarity to the mac3 cluster from Zilionis et al.
15 (Unknown)	Mrc1, Cxcl3, Hspa1a	Expresses genes from clusters 0 (Mrc1), 3 (Cxcl3) & 1 (Vcan). No specific markers detected. Both treated and untreated cells & cells from all samples represented

Table 26. Myeloid cluster labels, markers and notes 10 mice with 3LL tumours were treated with control (5 mice) or MRTX1257 (5 mice). Data integrated using WNN (Seurat) and subsequently clusterd. Clusters were manually annotated – nomenclature as above. DC = dendritic cell, IFN = interferon, ISG = interferon-stimulated genes, HSP = heat shock protein, macs = macrophages, mt. = mitochondrial, TF = transcription factor

Thus, we identified 8 macrophage clusters (0,2,3,5,7,10,13,14), 2 monocyte clusters (1,9), 3 dendritic cell clusters (6,8,12) 1 cluster containing both macrophages and monocytes (4) and 1 cluster which could not be defined (15). Distinct cells within cluster 15 expressed either macrophage (Mrc1 and Cxcl3) or monocyte (Vcan) genes. It was a small cluster of only 63 cells with some cells from each sample, and both conditions (37 control and 26 MRTX1257). Cells within this cluster were not outliers for mRNA count, ADT count or the percentage of mitochondrial genes. Overall, no marker nor metadata characteristic was found to distinguish this cluster.

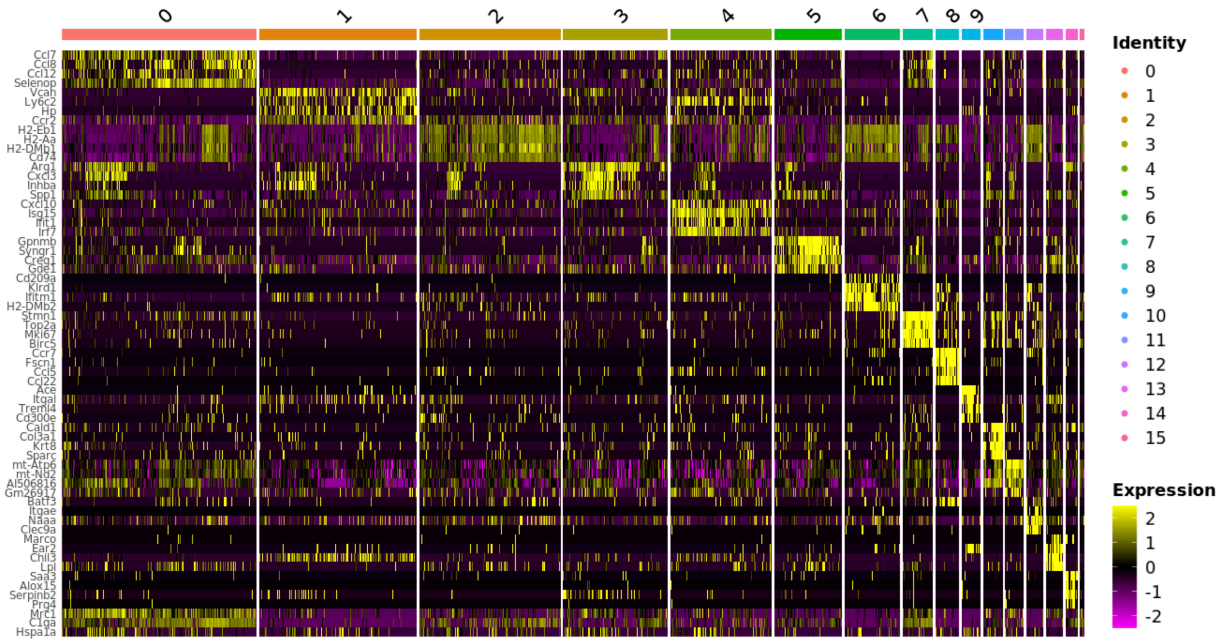

Figure 58. Heatmap showing expression of myeloid cluster markers10 mice with 3LL tumours were treated with control (5 mice) or MRTX1257 (5 mice). Myeloid cells were extracted and clusters. Cluster markers generated using manual Seurat and manual selection. Normalised expression values of cluster markers. Numbers above map indicate clusters.

Once clusters had been annotated in this way, we looked for effects of treatment. To this end, we looked at the compositional effects of treatment and also performed DE testing per cluster.

5.2.3 Composition distribution and analysis

The compositional distribution of clusters per sample and per condition is shown in Figure 59 with the breakdown also shown in

Table 27. As shown within the figure and table, there were certain differences apparent. For example, the proportion of myeloid cells labelled as macrophages with a high expression of antigen presentation machinery (AP-hi-mac) was higher in the treated samples (17%) than in the control samples (12%). Conversely the proportion of cells labelled as arginase 1-high macrophages (Arg1-hi mac) was higher in control samples (14%) than in treated samples (8%).

a)

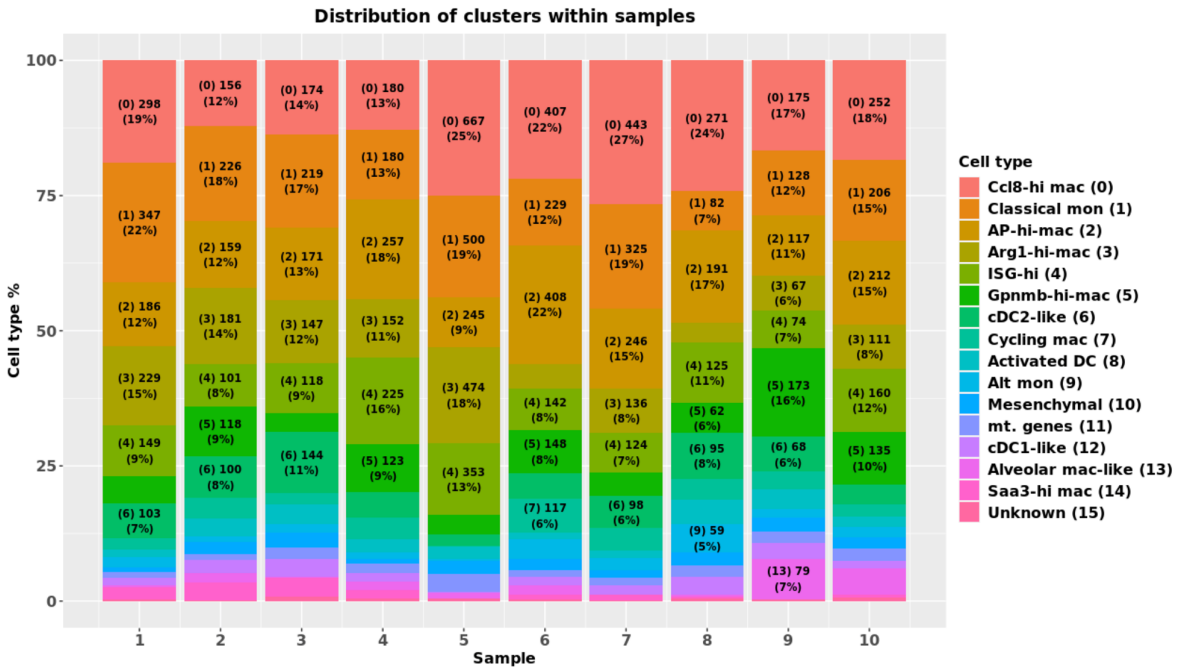

b)

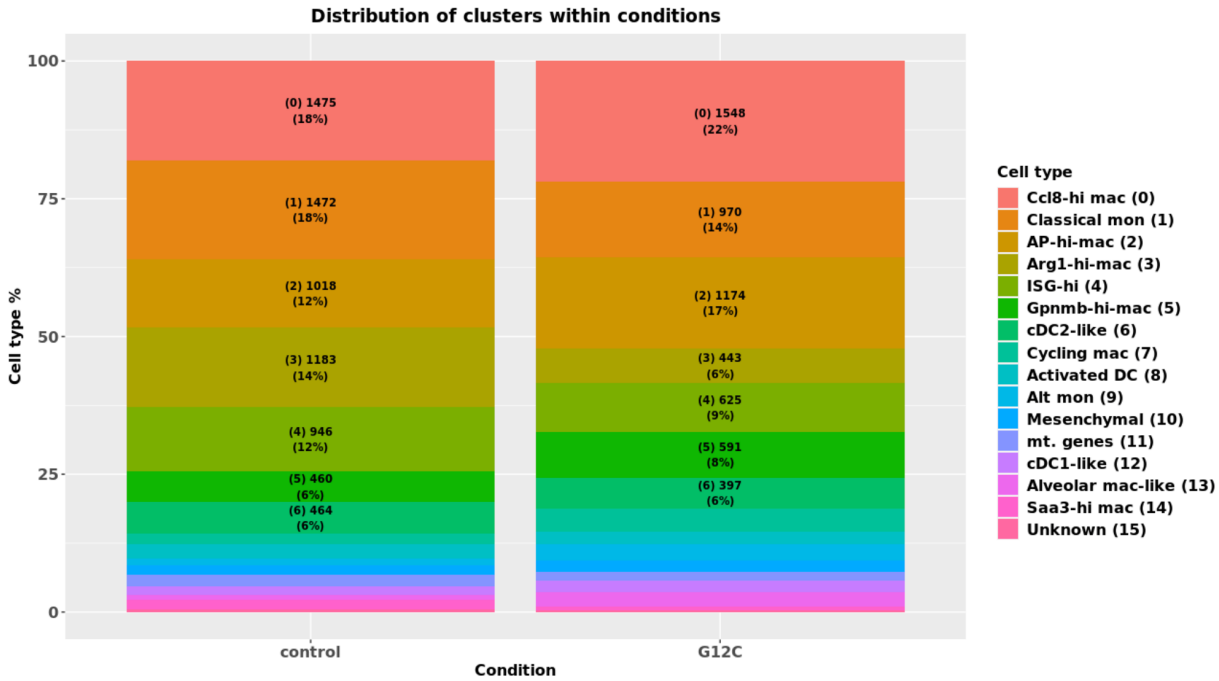

Figure 59. Distribution of clusters per sample & condition 10 mice with 3LL tumours were treated with control (5 mice) or MRTX1257 (5 mice). Myeloid cells were extracted, clustered and a manual nomenclature applied. Numbers inside the bars = (cluster number) number of cells (% of subset occupied by that cluster). Samples 1-5 are control, 6-10 are MRTX1257-treated.

	1	2	3	4	5	Control
Mac (Ccl8-high)	298 (19)	156 (12.1)	174 (13.7)	180 (12.9)	667 (25.1)	**1475 (18)**
Mon (classical)	347 (22.1)	226 (17.6)	219 (17.2)	180 (12.9)	500 (18.8)	**1472 (18)**
Mac (AP-high)	186 (11.8)	159 (12.4)	171 (13.5)	257 (18.4)	245 (9.2)	**1018 (12.4)**
Mac (Arg1-high)	229 (14.6)	181 (14.1)	147 (11.6)	152 (10.9)	474 (17.8)	**1183 (14.4)**
ISG-high	149 (9.5)	101 (7.9)	118 (9.3)	225 (16.1)	353 (13.3)	**946 (11.6)**
Mac (Gpnmb-high)	78 (5)	118 (9.2)	44 (3.5)	123 (8.8)	97 (3.6)	**460 (5.6)**
cDC2-like	103 (6.6)	100 (7.8)	144 (11.3)	65 (4.6)	52 (2)	**464 (5.7)**
Mac (cycling)	31 (2)	48 (3.7)	27 (2.1)	57 (4.1)	7 (0.3)	**170 (2.1)**
DC (activated)	24 (1.5)	42 (3.3)	46 (3.6)	33 (2.4)	59 (2.2)	**204 (2.5)**
Mon (alternative)	30 (1.9)	15 (1.2)	21 (1.7)	19 (1.4)	11 (0.4)	**96 (1.2)**
Mac (mesenchymal)	13 (0.8)	29 (2.3)	34 (2.7)	10 (0.7)	66 (2.5)	**152 (1.9)**
mt. genes high	17 (1.1)	13 (1)	27 (2.1)	25 (1.8)	85 (3.2)	**167 (2)**
cDC1-like	20 (1.3)	32 (2.5)	42 (3.3)	23 (1.6)	6 (0.2)	**123 (1.5)**
Mac (alveolar-like)	8 (0.5)	22 (1.7)	2 (0.2)	21 (1.5)	25 (0.9)	**78 (1)**
Mac (Saa3-high)	33 (2.1)	42 (3.3)	44 (3.5)	23 (1.6)	3 (0.1)	**145 (1.8)**
Unknown	6 (0.4)	2 (0.2)	11 (0.9)	6 (0.4)	12 (0.5)	**37 (0.5)**
	6	**7**	**8**	**9**	**10**	**MRTX1257**
Mac (Ccl8-high)	407 (21.9)	443 (26.5)	271 (24.2)	175 (16.6)	252 (18.4)	**1548 (21.9)**
Mon (classical)	229 (12.3)	325 (19.4)	82 (7.3)	128 (12.1)	206 (15)	**970 (13.7)**
Mac (AP-high)	408 (21.9)	246 (14.7)	191 (17)	117 (11.1)	212 (15.5)	**1174 (16.6)**
Mac (Arg1-high)	87 (4.7)	136 (8.1)	42 (3.7)	67 (6.4)	111 (8.1)	**443 (6.3)**
ISG-high	142 (7.6)	124 (7.4)	125 (11.1)	74 (7)	160 (11.7)	**625 (8.8)**
Mac(Gpnmb-high)	148 (8)	73 (4.4)	62 (5.5)	173 (16.4)	135 (9.9)	**591 (8.3)**
cDC2-like	87 (4.7)	98 (5.9)	95 (8.5)	68 (6.5)	49 (3.6)	**397 (5.6)**
Mac (cycling)	117 (6.3)	70 (4.2)	43 (3.8)	34 (3.2)	32 (2.3)	**296 (4.2)**
DC (activated)	23 (1.2)	24 (1.4)	51 (4.5)	39 (3.7)	26 (1.9)	**163 (2.3)**
Mon (alternative)	67 (3.6)	37 (2.2)	59 (5.3)	17 (1.6)	26 (1.9)	**206 (2.9)**
Mac (mesenchymal)	40 (2.1)	24 (1.4)	28 (2.5)	27 (2.6)	28 (2)	**147 (2.1)**
mt. genes high	21 (1.1)	21 (1.3)	22 (2)	21 (2)	32 (2.3)	**117 (1.7)**

cDC1-like	30 (1.6)	29 (1.7)	37 (3.3)	31 (2.9)	18 (1.3)	**145 (2)**
Mac (alveolar-like)	34 (1.8)	2 (0.1)	5 (0.4)	79 (7.5)	67 (4.9)	**187 (2.6)**
Mac (Saa3-high)	14 (0.8)	17 (1)	3 (0.3)	1 (0.1)	8 (0.6)	**43 (0.6)**
Unknown	7 (0.4)	2 (0.1)	6 (0.5)	3 (0.3)	8 (0.6)	**26 (0.4)**

Table 27. Composition of clusters within sample & conditions Numbers indicate how many cells in that sample fall within the given cluster (percentage in brackets). Samples 1-5 are control, 6-10 are MRTX1257-treated.

Similar to the analysis performed prior to subsetting macrophages (section 4.5.3), we performed differential composition analysis to assess whether the differences in composition were unlikely to be due to chance (Table 28). As shown, after adjustment for multiple hypothesis testing, only the change in the Arg1-hi-mac group remained significant. While Saa3-hi-mac and classical monocytes reduced in number, the changes were not significant after p-value adjustment. Likewise, the increase in AP-hi-mac with treatment was not significant either. As previously, given the outlier nature of sample 5, we performed a sensitivity analysis with this sample removed. Reassuringly, the reduction in Arg1-hi-mac remained significant after p-value adjustment ($\log_2$ FC -1.01, FDR 0.037) while the reduction in Saa3-hi macrophages was more pronounced ($\log_2$ FC = -2.23) and significant (FDR = 0.002).

	Log_2 FC	p-value	Adj. p (FDR)
Mac (Arg1-hi)	-1.15	0.00	0.048
Mac (Saa3-hi)	-1.99	0.02	0.146
Mon (alternative)	1.19	0.03	0.146
Mon (classical)	-0.43	0.16	0.482
Mac (alveolar-like)	1.36	0.18	0.482
Mac (Ccl8-hi)	0.37	0.23	0.482
Mac (cycling)	0.69	0.23	0.482
Mac(Gpnmb-hi)	0.52	0.27	0.482
ISG-hi	-0.30	0.27	0.482
Mac (Arg1-hi)	0.29	0.33	0.523

Table 28. Differential abundance testing of myeloid clusters 10 mice with 3LL tumours were treated with control (5 mice) or MRTX1257 (5 mice). Myeloid cells were clustered and a manual nomenclature applied. Log_2 FC represents the differential abundance, in the given cluster, after treatment with MRTX1257. p-value adjustment performed using the Benjamini Hochberg method.

Given the significant reduction in the proportion of Arg1-hi macrophages with treatment, and the immunosuppressive effect of arginine depletion within the TME, we describe this cluster in more detail here. When performing DE between this cluster and all other clusters combined, Arg1, Cxcl3, Vegfa and Cxcl2 were amongst the 12 most significantly upregulated genes in this cluster versus all others. Three of these genes are visualised on a UMAP plot in Figure 60.

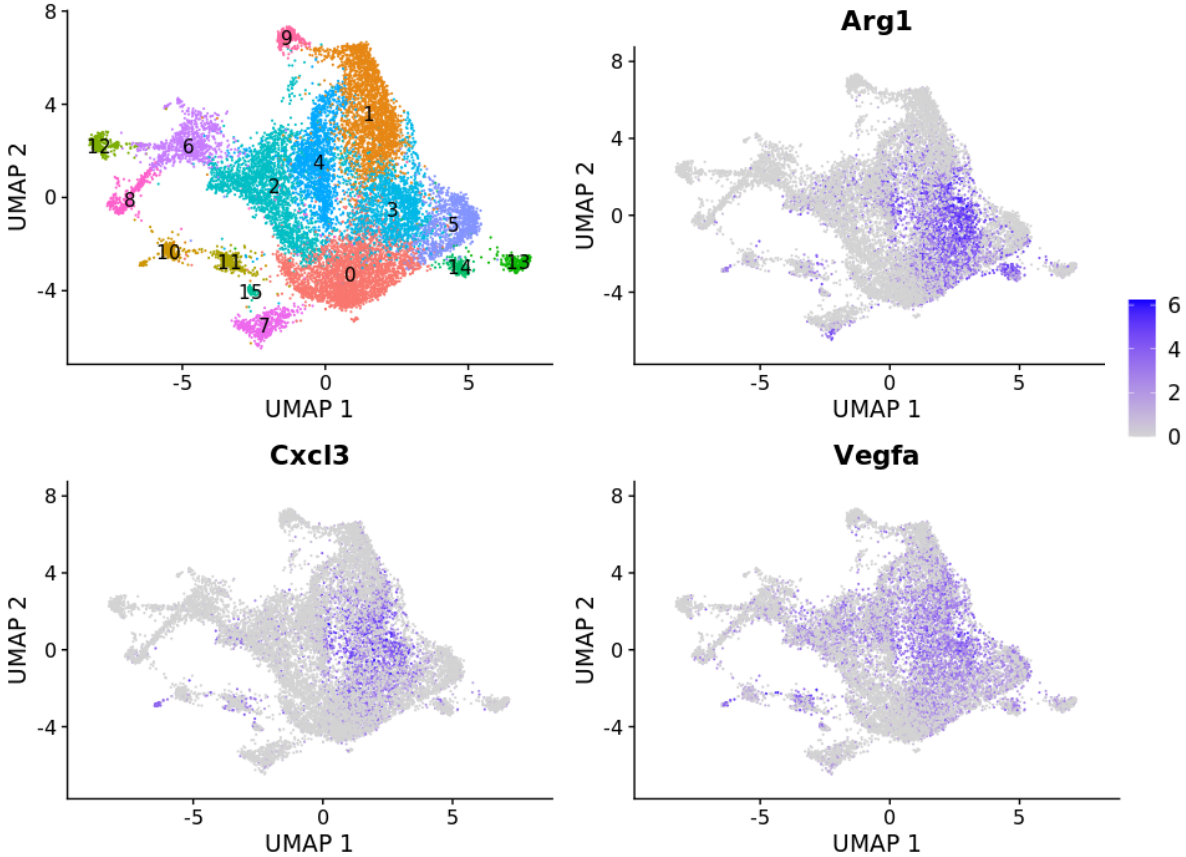

Figure 60. UMAP visualisation of cluster 3-high genes 10 mice with 3LL tumours were treated with control (5 mice) or MRTX1257 (5 mice). Myeloid cells were clustered separately. UMAP shows gene expression in cluster 3 myeloid cells (Arg-1 high myeloid cells). Scale represents log-normalised expression values

Other significantly upregulated genes included Spp1 (secreted phosphoprotein 1), Ptgs2, Nt5e, Ccl6, Ccl9, Tnfrsf9 (4-1BB), Mif (macrophage inhibitory factor) and Nos2 (nitric oxide synthase 2). Downregulated genes included class II MHC genes (e.g. H2-Eb1, H2-Ab1, H2-Aa), Cd74, Ccl8, Ccl5 and Cxcl9 and Cxcl10. The ten most significantly up and downregulated genes are shown in Table 29.

Upregulated			Downregulated		
Name	**Log_2 FC**	**Adj. p**	**Name**	**Log_2 FC**	**Adj. p**
Arg1	2.38	< 0.001	**Cst3**	-1.05	< 0.001
Fn1	1.52	< 0.001	**H2-Aa**	-1.59	< 0.001
Cxcl3	2.10	< 0.001	**H2-Eb1**	-1.77	< 0.001
Spp1	1.79	< 0.001	**Tmem176b**	-0.97	< 0.001
Vegfa	1.14	< 0.001	**Psmb8**	-0.75	< 0.001
Gapdh	0.67	< 0.001	**Tmem176a**	-0.91	< 0.001
Hilpda	1.33	< 0.001	**Fcgrt**	-0.68	< 0.001
Mif	0.85	< 0.001	**Samhd1**	-0.86	< 0.001
Pgk1	0.82	< 0.001	**H2afz**	-0.74	< 0.001
Thbs1	1.00	< 0.001	**H2-DMb1**	-0.97	< 0.001

Table 29. The most significantly DE genes in cluster 3 (Arg1-high) 10 mice with 3LL tumours were treated with control (5 mice) or MRTX1257 (5 mice). Myeloid cells were clustered separately. Log_2 fold-change refers to myeloid cluster 3 vs all other myeloid clusters combined (pseudocount = 1). Adjusted p value based on Wilcoxon signed rank sum test, Bonferroni correction.

In order to provide a more objective assessment of the differentially expressed genes in this cluster, we performed GSEA. Using the MSigDB hallmark gene sets (Liberzon *et al.*, 2015) the most upregulated genes related to hypoxia (e.g. Vegfa, Slc2a1) and epithelial to mesenchymal transition (e.g. Cxcl3, Spp1, Inhba). Amongst the most downregulated sets were those related to the interferon response (both alpha and gamma e.g. Ifit3, Rsad2, Cxcl10) and proliferation.

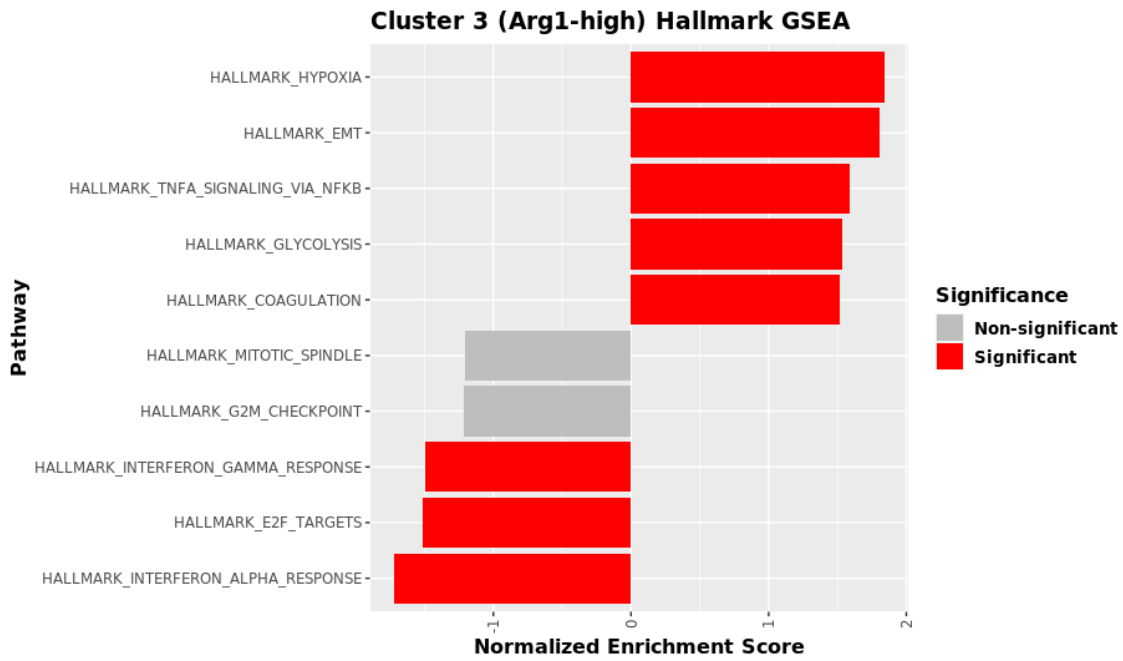

Figure 61. Most up and downregulated hallmark gene sets in myeloid cluster 3 (Arg1-high) 10 mice with 3LL tumours were treated with control (5 mice) or MRTX1257 (5 mice). Myeloid cells clustered separately. Log_2 fold changes for gene expression in cluster 3 compared to all other clusters combined were calculated and then ranked from highest to lowest for GSEA. Significance refers to adj. p-value < 0.05.

Given that Arg1, a marker of M2-like macrophages, was upregulated in cluster 3, we next looked at other M1 and M2-related genes. We obtained M1 and M2 gene signatures from a meta-analysis of published data (Orecchioni *et al.*, 2019) and used these as input to GSEA. This time, as input to the GSEA algorithm, we calculated log_2 fold-change between gene expression in cluster 3 and all other macrophage clusters combined (0, 2, 5, 13, 14). Thus, we are essentially asking whether cluster 3 is more M1 or M2-like than other macrophage clusters rather than whether it is M1/M2-like per se. The results of the procedure are shown in Figure 62. Surprisingly, given its high expression of Arg1 and Vegfa, overexpressed genes in this cluster were enriched in gene sets pertaining to classical (M1) macrophage activation. For example, the 'classic_vs_untreated' gene set represents those genes upregulated after classical macrophage activation *in vitro*. Overexpressed genes in cluster 3 that were part of this gene set included Nos2, Cxcl3, Ihnba and Ptgs2. Conversely, the 'alt_vs_classic_up' gene set represents genes upregulated in alternatively

activated macrophages (M2, activated by IL-4) vs. classically activated (M1, by LPs) *in vitro*. Genes downregulated in cluster 3, that were enriched in this gene set, include Ccl8, Mgl2 and Fcrls.

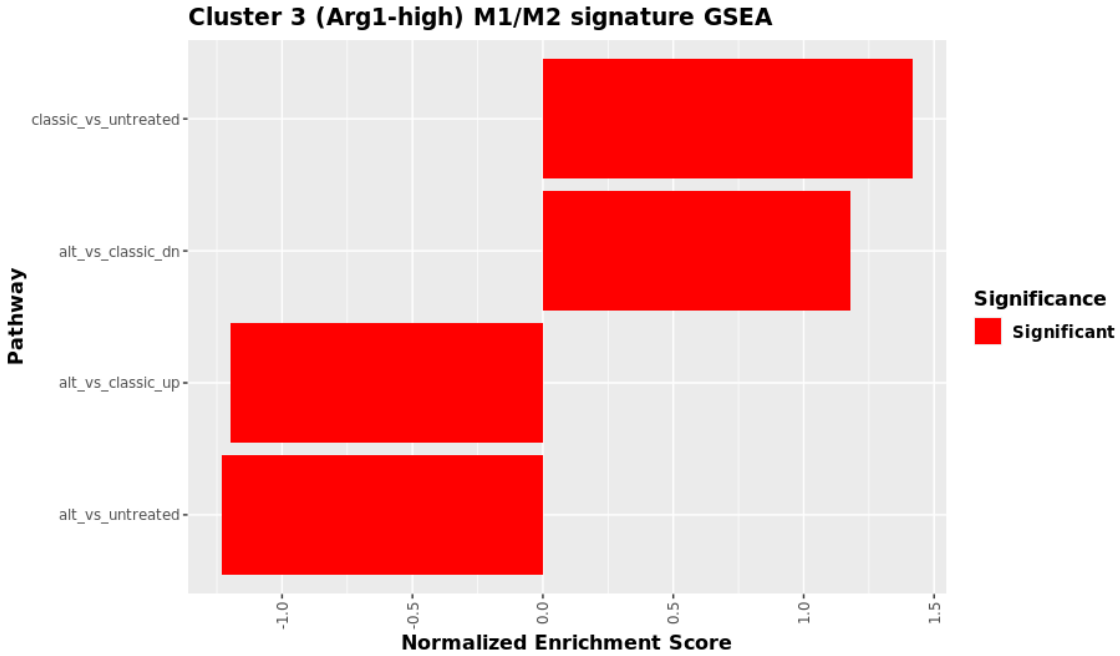

Figure 62. M1/M2 signature GSEA (cluster 3 vs. other macrophage clusters) 10 mice with 3LL tumours were treated with control (5 mice) or MRTX1257 (5 mice). Myeloid cells extracted and clustered separately. Macrophage clusters manually selected based on marker gene expression. Log_2 fold changes for gene expression in cluster 3 compared to all other macrophage clusters (0,2,5,13,14) combined were calculated and then ranked from highest to lowest for GSEA. Significance refers to adj. p-value < 0.05.

Despite the GSEA results above, the enrichment plot below illustrates the dichotomy of differential gene expression in cluster 3 (Figure 62). The illustrated gene set represents genes upregulated in alternatively activated macrophages compared to untreated macrophages *in vitro*. As shown, some such genes are upregulated in cluster 3 compared to other macrophage clusters (and these included Arg1, Ccl24 and Mmp12) while others are downregulated (e.g. Ccl8, Lpl and Mrc1).

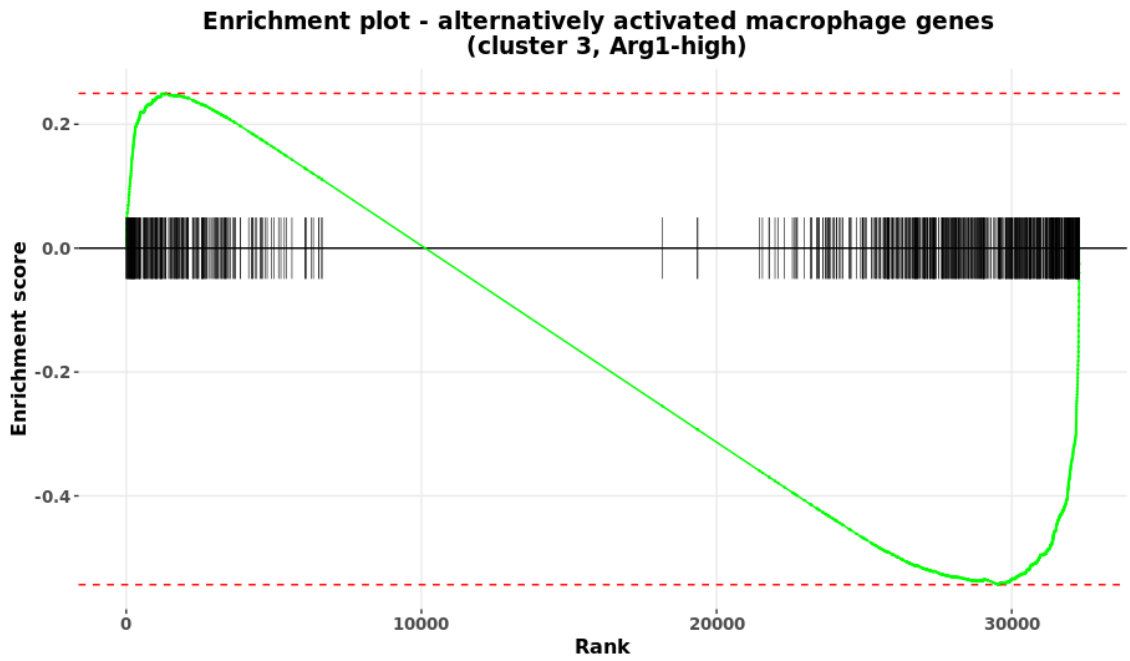

Figure 63. Alternatively activated macrophage enrichment plot (cluster 3, Arg1-high) 10 mice with 3LL tumours were treated with control (5 mice) or MRTX1257 (5 mice). Myeloid cells were extracted and clustered separately. Log_2 fold changes for gene expression in myeloid cluster 3 compared to all other macrophage clusters (0,2,5,13,14) combined were calculated and then ranked from highest to lowest for GSEA against the 'alt_vs_untreated' gene set. Significance refers to adj. p-value < 0.05.

The other cluster whose composition was significantly altered, was cluster 14, which we termed the 'Saa3-high' cluster. This represented a small proportion of cells in each condition (1.8% in untreated vs 0.6% for treated samples). However, given its significant change in frequency upon treatment, its distinct projection in UMAP space and its presence in the Zilionis dataset as their 'Mac3' cluster (Zilionis *et al.*, 2019), illustrating conservation across model systems, we felt it was worthy of further attention. This cluster was specific in its expression of Saa3, Prg4, Alox15 and Cd5l. The 10 most up and down-regulated genes are shown in Table 30.

Upregulated			Downregulated		
Name	**Log_2 FC**	**Adj. p**	**Name**	**Log_2 FC**	**Adj. p**
Prg4	3.97	< 0.001	**Lst1**	-2.03	< 0.001
Selp	1.59	< 0.001	**Coro1a**	-1.47	< 0.001
Fcna	2.67	< 0.001	**Marcks**	-1.58	< 0.001
Garnl3	1.30	< 0.001	**Lcp1**	-1.11	< 0.001
Lbp	1.21	< 0.001	**Ms4a6c**	-1.41	< 0.001
Ptgis	1.66	< 0.001	**Aif1**	-1.68	< 0.001
Cd5l	3.15	< 0.001	**Ms4a6b**	-1.51	< 0.001
Padi4	1.31	< 0.001	**Anxa5**	-1.06	< 0.001
Mlxipl	0.70	< 0.001	**Plbd1**	-1.57	< 0.001
Wnt2	0.48	< 0.001	**Malat1**	-1.13	< 0.001

Table 30. The most significantly DE genes in myeloid cluster 14 (Saa3-high) 10 mice with 3LL tumours were treated with control (5 mice) or MRTX1257 (5 mice). Myeloid cells were clustered separately. Log_2 fold-change refers to myeloid cluster 14 vs all other clusters combined (pseudocount = 1). Adjusted p value based on Wilcoxon signed rank sum test, Bonferroni correction.

The gene sets most enriched for up or downregulated genes in this cluster are shown in Figure 64.

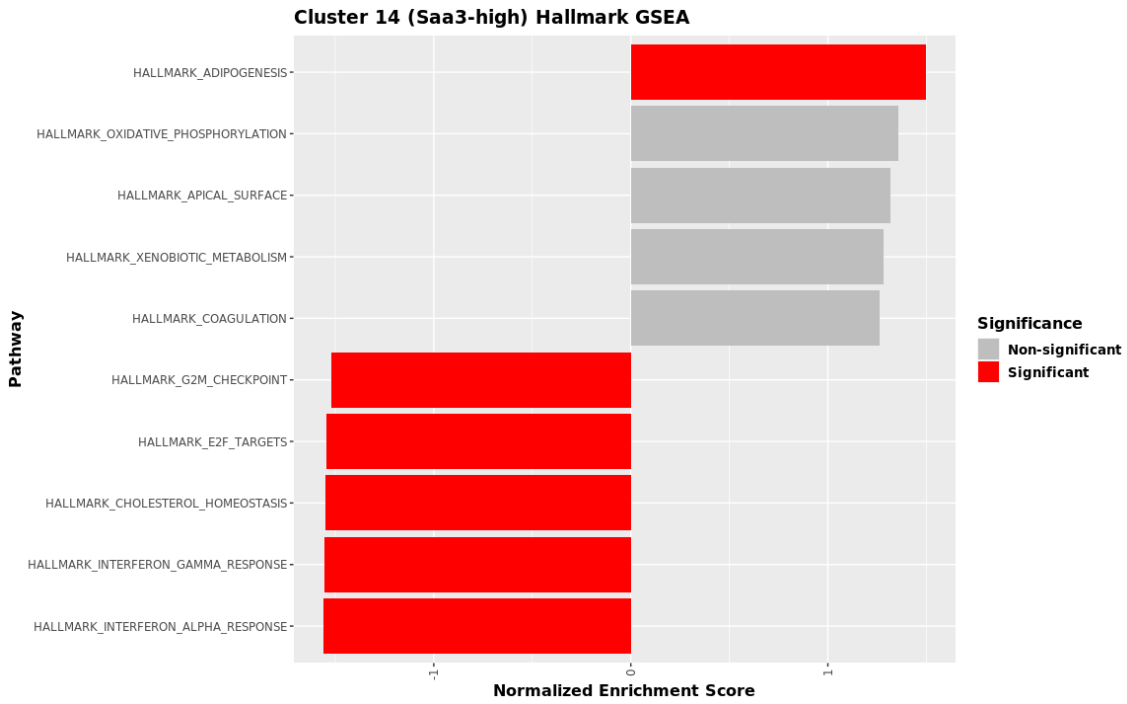

Figure 64. Most up and downregulated hallmark gene sets in myeloid cluster 14 (Saa3-high) 10 mice with 3LL tumours were treated with control (5 mice) or MRTX1257 (5 mice). Myeloid cells were clustered separately. Log_2 fold changes for gene expression in cluster 14 compared to all other clusters combined were calculated and then ranked from highest to lowest for GSEA. Significance refers to adj. p-value < 0.05.

Adipogenesis genes that were significantly upregulated included Ltc4s (leukotriene C4 synthase), Acly (ATP citrate lyase) and Idh1 (7-dehydrocholesterol reductase). While not significant, the oxidative phosphorylation gene set was also enriched for upregulated genes, including Idh1 (isocitrate dehydrogenase 1). Conversely, the cholesterol homeostasis gene set was enriched for downregulated transcripts including Fabp5 (fatty acid binding protein 5) and Cxcl16 which has been shown to influence high-density lipoprotein uptake and cholesterol efflux in macrophages (Barlic, Zhu and Murphy, 2009). Thus, this cluster appeared to have an altered metabolic phenotype relative to other cells in the myeloid compartment, specifically demonstrating an increased propensity for adipogenesis.

5.2.4 Per-cluster differential expression

After performing differential abundance testing, we next looked at differential expression between MRTX1257-treated and control cells, per cluster. A summary of these results is shown in Table 31.

LFC	Ccl8-hi mac	Classical mon	AP-hi-mac	Arg1-hi-mac	ISG-hi	Gpnmb-hi-mac	cDC2-like	Cycling mac
< -2	10	3	4	12	7	2	0	2
< -1.5	22	7	9	19	13	4	3	5
< -1	63	36	23	48	38	13	6	5
< -0.5	215	141	118	178	142	74	47	65
< -0.25	618	344	340	343	304	204	93	181
> 0.25	383	337	200	350	229	85	60	31
> 0.5	113	54	58	98	65	21	14	21
> 1	25	5	11	16	17	4	1	4
> 1.5	8	3	3	9	5	1	0	1
> 2	4	0	0	4	0	0	0	0
LFC	**Activated DC**	**Alt mon**	**Mesenchymal**	**mt. genes**	**cDC1-like**	**Alveolar mac-like**	**Saa3-hi mac**	
< -2	1	0	13	6	0	3	5	
< -1.5	2	0	37	8	4	5	12	
< -1	8	0	60	15	9	20	24	
< -0.5	29	6	139	15	31	61	41	
< -0.25	30	8	274	15	33	109	45	
> 0.25	10	0	605	5	12	53	13	
> 0.5	6	0	163	5	9	20	13	
> 1	2	0	23	4	2	1	9	
> 1.5	1	0	7	2	0	0	2	
> 2	0	0	1	1	0	0	2	

Table 31. Summary of myeloid per cluster differential expression (MRTX1257 vs control)10 mice with 3LL tumours were treated with control (5 mice) or MRTX1257 (5 mice). Myeloid cells were clustered separately. Figures refer to numbers of genes exceeding the given $\log_2$ FC at an FDR of < 0.1. Note, consistent with

previous figures/tables, clusters are ordered by size (Ccl8-hi macs the largest, Saa-hi macs the smallest).

As shown in the table, there were many differentially expressed genes in the larger clusters, with numbers tending to become smaller as cluster sizes reduced.

In order to gain better intuition for the distribution of effect sizes and the nature of up and down-regulated genes, we plotted gene expression, per cluster, split by condition. Examples are shown for some of the macrophage clusters (Figure 65) and some of the DC clusters (Figure 66).

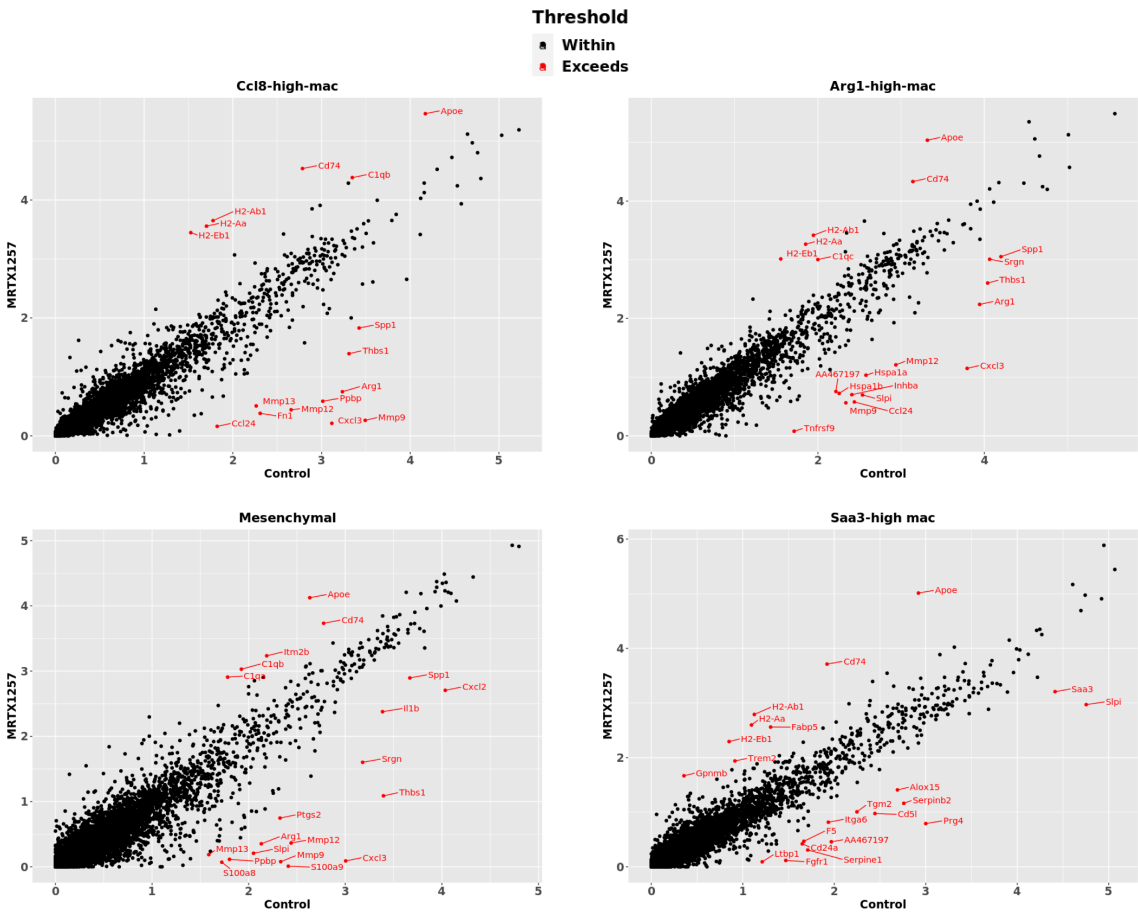

Figure 65. Selected macrophage cluster gene expression (MRTX1257 vs. Control) 10 mice with 3LL tumours were treated with control (5 mice) or MRTX1257 (5 mice). Myeloid cells were clustered separately and macrophages annotated within these clusters. Expression values represent $\log_2$ normalised values (pseudocount 0.5) using library sizes to calculate normalisation factors. Red dots indicate genes with an absolute $\log_2$ FC of > 1.

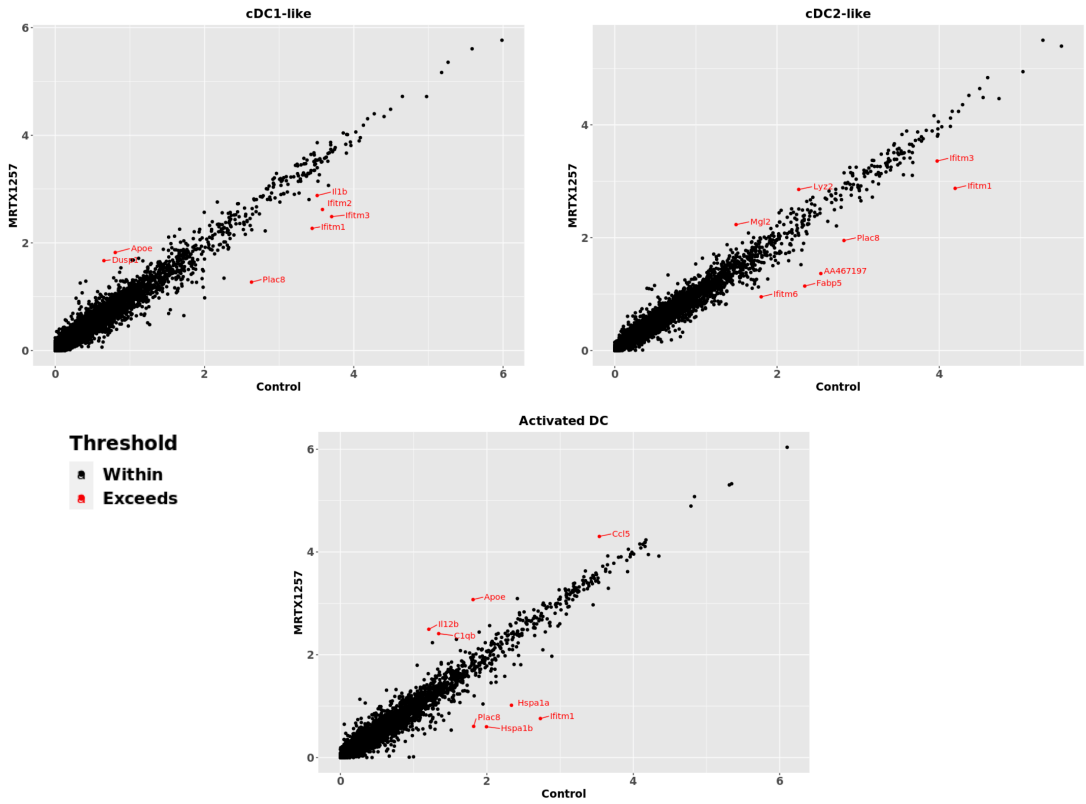

Figure 66. Selected dendritic cell cluster gene expression (MRTX1257 vs. Control) 10 mice with 3LL tumours were treated with control (5 mice) or MRTX1257 (5 mice). Myeloid cells were clustered separately. Expression values represent $\log_2$ normalised values (pseudocount 0.5) using library sizes to calculate normalisation factors. Red dots indicate genes with an absolute $\log_2$ FC of > 0.5

As shown, the effect of treatment on macrophage gene expression was more pronounced than that on DCs, consistent with the summary shown in Table 31. Furthermore, many of the over and underexpressed genes in the macrophage compartment were consistent across different macrophage clusters. As shown in the plots, class II MHC and complement genes were frequently upregulated while Arg1, Cxcl3, Ccl24, Mmp9/12/13 and Spp1 were consistently downregulated in these clusters. A similar pattern was seen in the cluster 1 (classical monocytes) cells and the other macrophage clusters (not shown).

Despite analysis to look for genes specifically differentially expressed in one cluster versus another (method in 2.14.7) we were unable to detect many genes whose differential expression was obviously specific to one cluster. We therefore manually interrogated the lists of DE genes, first focussing on the macrophage clusters (0,2,3,4,5,7,13,14) and the classical monocyte cluster (1). In this way, we were able to identify several genes, known to affect the tumour-immune interaction, that were DE upon treatment (Figure 67). This figure displays the macrophage clusters, along with the classical monocyte cluster, and shows the impact of treatment within each.

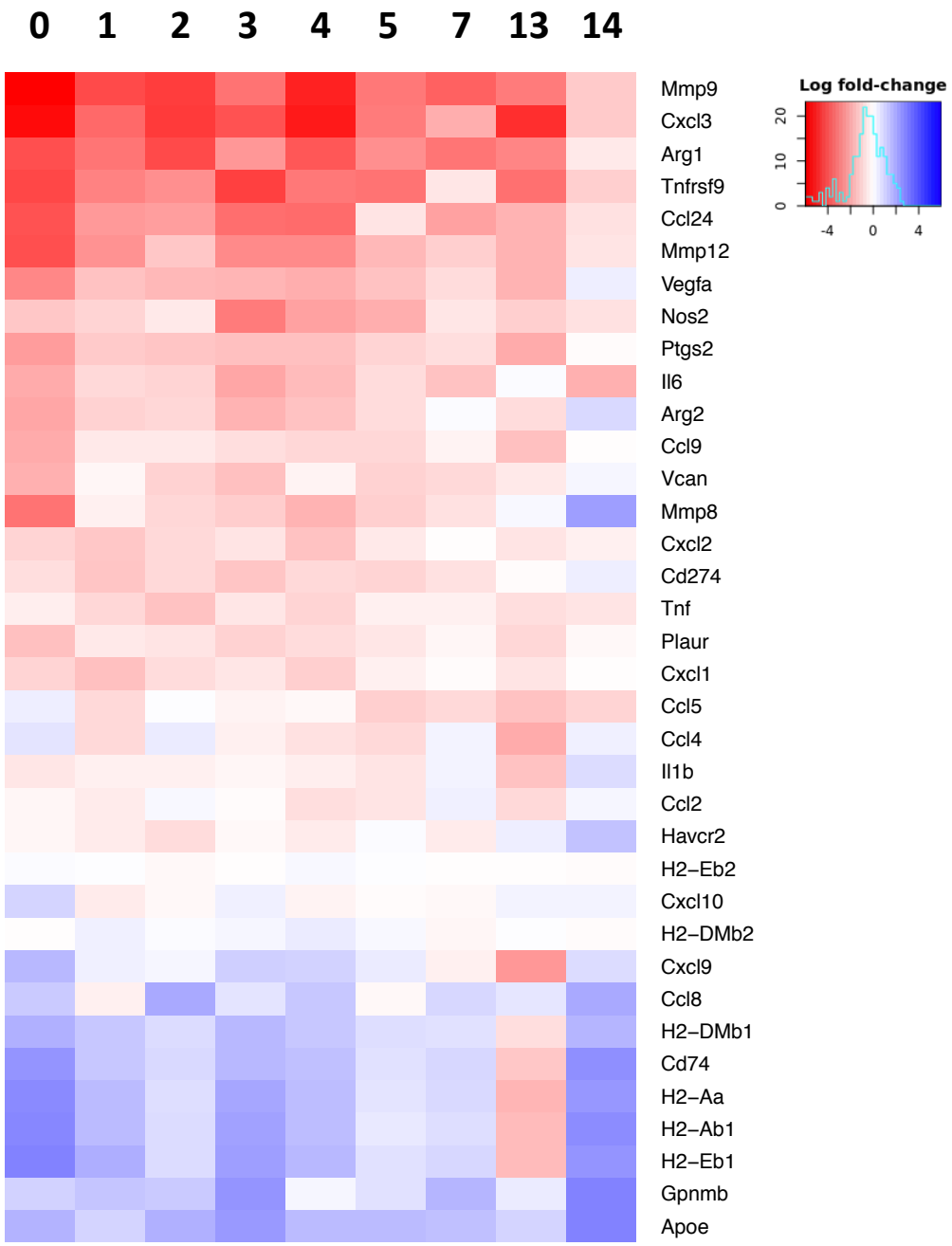

Figure 67. Log fold-change of selected genes in monocyte/macrophage clusters 10 mice with 3LL tumours were treated with control (5 mice) or MRTX1257 (5 mice). Myeloid cells were extracted and sub-clustered. Pseudo-bulk datasets were created per-cluster and $\log_2$ fold-change (pseudocount 0.1) was calculated between treated and non-treated cells. Cluster 0 = 'Ccl8-high', 1 = 'Classical monocytes', 2 = 'Antigen presentation-high', 3 = 'Arg1-high', 4 = 'Interferon-stimulated-genes-high', 5 = 'Gpnmb-hi', 7 = 'Cycling macrophages', 13 = 'Alveolar macrophages', 14 = 'Saa3-high'

As shown, in general, genes whose protein products are purported to be tumourigenic, were downregulated. Along with those mentioned above, we saw downregulation of Vegfa, Vcan (veriscan), Tnfrsf9 (4-1BB) and Ptgs2. Upregulated genes tended to be antitumorigenic and, in addition to those aforementioned, included Cxcl9 and (less strongly) Cxcl10.

Following interrogation of the lists of DE genes as above, we performed GSEA using the list of per-cluster DE genes as input to the algorithm. When tested against the hallmark gene sets, most gene sets showed a negative NES score across the clusters. The most negative scores were related to genes involved in TNFα and inflammatory signalling. The most downregulated genes within these sets (across the clusters) included Hbegf, Cxcl3, Lif and Il1a. Gene sets with generally positive NES scores included those related to adipogenesis and fatty acid metabolism. Upregulated genes, across clusters, in these sets included Apoe, Cd302 and Lpcat.

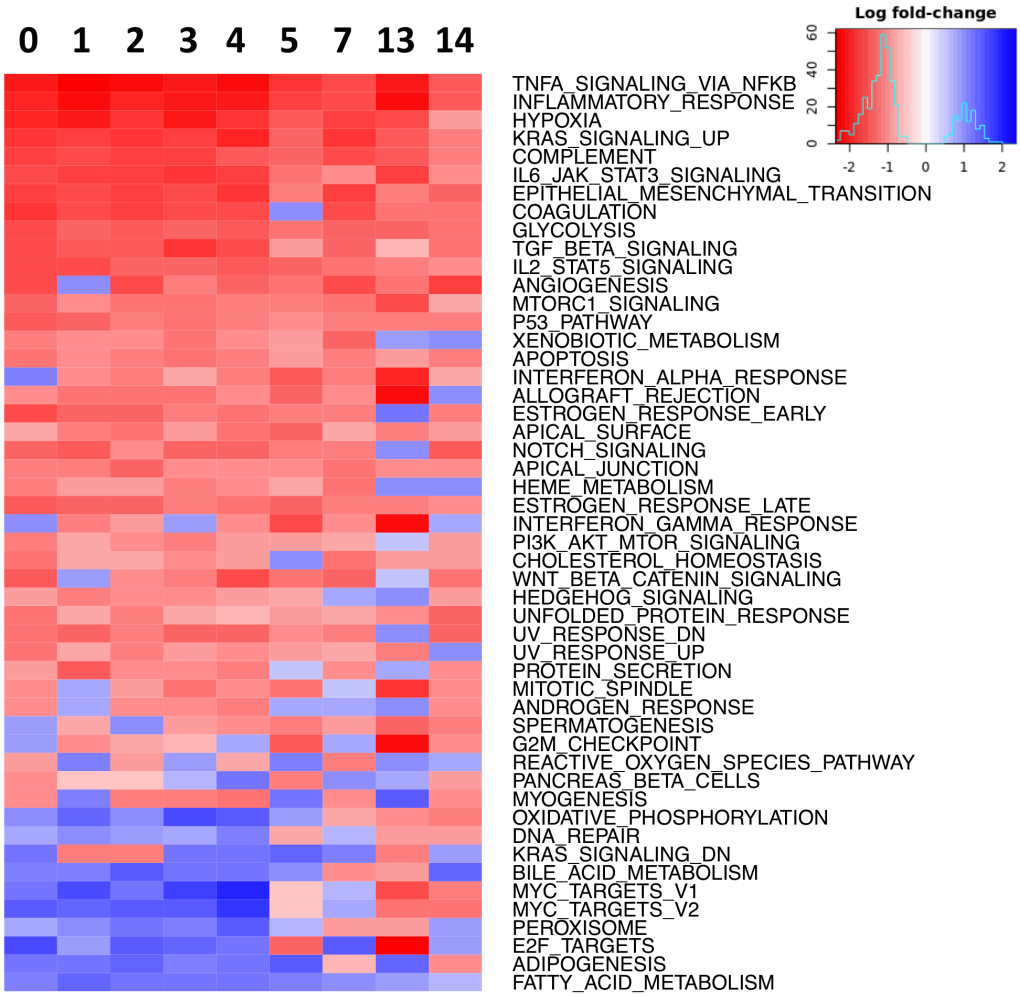

Figure 68. Heatmap of GSEA NES scores per myeloid cluster for hallmark sets 10 mice with 3LL tumours were treated with control (5 mice) or MRTX1257 (5 mice). Myeloid cells were extracted and sub-clustered. GSEA was performed per-cluster using the $\log_2$ fold-changes between MRTX1257 and control treated cells. NES scores displayed as a heatmap. Gene sets are arranged by mean NES score across the clusters. Cluster 0 = 'Ccl8-high', 1 = 'Classical monocytes', 2 = 'Antigen presentation-high', 3 = 'Arg1-high', 4 = 'Interferon-stimulated-genes-high', 5 = 'Gpnmb-hi', 7 = 'Cycling macrophages', 13 = 'Alveolar macrophages', 14 = 'Saa3-high'

Next, we used the previously mentioned gene sets pertaining to M1 and M2 macrophage polarisation *in vitro* (Orecchioni *et al.*, 2019) to interrogate the effect of MRTX1257 in the macrophage clusters. Surprisingly, genes downregulated by MRTX1257 were enriched in the 'classic_vs_untreated' gene set (mean NES across the clusters = -1.57, FDR < 0.01 in 7/9 macrophage clusters) suggesting that MRTX1257 downregulates classically activated

macrophage genes. When looking at the ‘leading edge’ of this gene set (the downregulated genes that most strongly contributing to the NES) they included Cxcl3, Vegfa, Ptgs2 and Il1a. While these genes may be part of this gene set, they are known to have anti-tumourigenic functions, and this is alluded to in the discussion. Other genes downregulated by MRTX1257 and part of this gene set include Slpi, Serpinb2 and Inhba, which have less clear functions in the tumour microenvironment. Conversley, when we looked at the NES scores for the ‘alt_vs_untreated’ cluster, the scores were closer to 0 suggesting that MRTX1257 does predominantly up or downregulates alternative monocyte genes. When we looked at genes in this set, those that were most strongly downregulated included Arg1, Mmp9, Mmp12 and Ccl24. Those that were most strongly upregulated include Tmem176a and Tmem176b. The effect of Mrtx1257 on these two genes, Arg1 and Vegfa is shown in Figure 69.

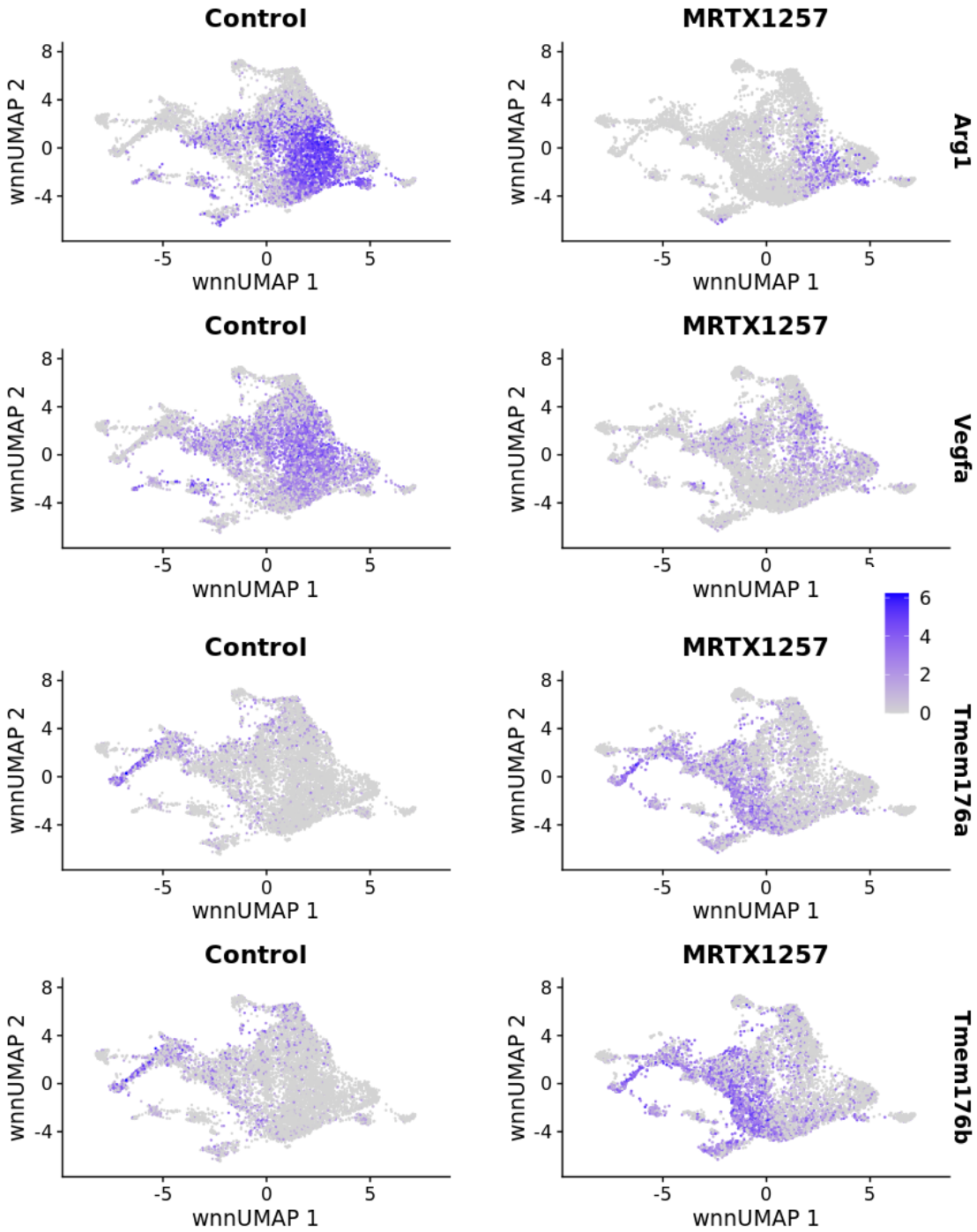

Figure 69. Effect of MRTX1257 on selected myeloid genes

10 mice with 3LL tumours were treated with control (5 mice) or MRTX1257 (5 mice). Myeloid cells were extracted and sub-clustered. Figure shows a UMAP representation of control (left) and treated (right) myeloid cells overlaid with given gene expression.

Beyond the macrophage compartment, we also looked at DCs. The repertoire of gene differentially expressed in the dendritic cell clusters was much narrower

than that in macrophages, but nonetheless distinct. As shown in (Figure 66) interferon-induced transmembrane (Ifit) genes were downregulated across the DC clusters. Conversley, upregulated genes in the activated DC subset included Il12b and Ccl5. The former is important for the generation of Th1-polarised immune response including the production of IFNγ while Ccl5 is known to act as a cDC1 chemoattractant (Böttcher *et al.*, 2018). Lyz2 and Mgl were specifically upregulated on cDC2 cells. The latter is a C-type lectin receptor that functions as a carbohydrate recognition molecule. As well as serving to recognise pathogens, it may also recognise alternatively-glycosylated tumour antigens (Saeland *et al.*, 2007). Changes in these Mgl2 and Il12b are visualised in Figure 70.

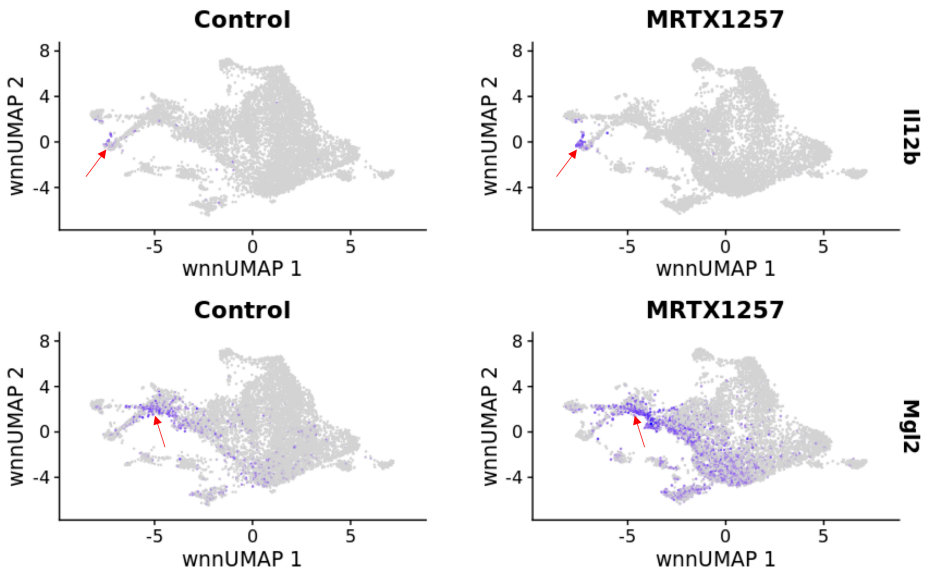

Figure 70. Effect of MRTX1257 on selected DC genes 10 mice with 3LL tumours were treated with control (5 mice) or MRTX1257 (5 mice). Myeloid cells were extracted and sub-clustered. Red arrows in top panels indicate location of the activated-DC cluster where Il12b was expressed. Arrows in bottom panel indicate location of cDC2-like cells.

5.3 Tumour cell effects

While myeloid cells make up the bulk of the immune infiltrate, MRTX1257 acts directly on tumour cells. For this reason, we next sought to understand the specific effects the drug was having in this compartment.

To begin to understand this effect, tumour cells were subsetted from the overall dataset. Tumour cells were identifiable by their lack of expression of H2-K1. These cells projected together in UMAP space (Figure 71) facilitating their segmentation.

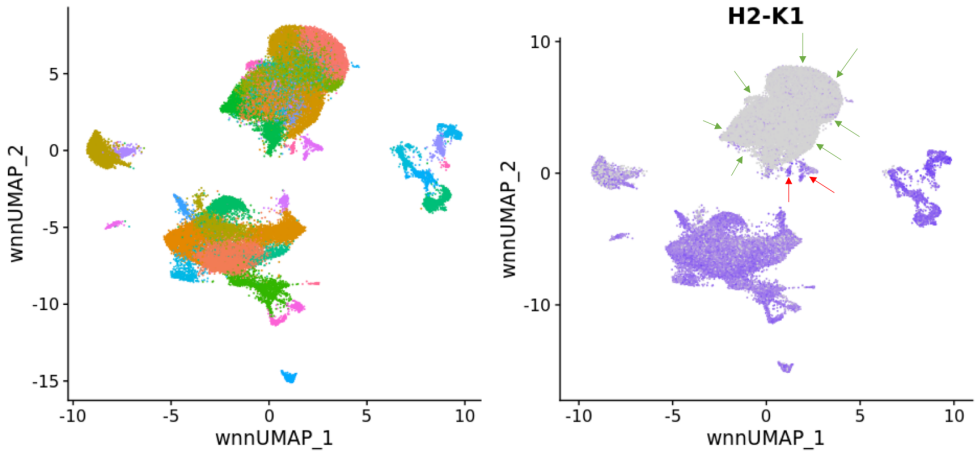

Figure 71. Lack of expression of H2-K1 in tumour clusters 10 mice with 3LL tumours were treated with control (5 mice) or MRTX1257 (5 mice) and cells projected in UMAP space after WNN integration (Seurat). Green arrows indicate tumour cell clusters. H2-K1-expressing cells (red arrows) projected nearby in UMAP-space expressed endothelial or mesenchymal markers and were not subsetted

Once cells were subsetted, they were integrated using the schema described for myeloid cells (Figure 55). Of note, often, cell cycle effects are not informative to the question being asked of a single-cell experiment, and they can be regressed out during data pre-processing. However, in this case, the drug was expected to have an (informative) effect on the cell cycle in tumour cells, and therefore its effects were not removed during pre-processing.

This resulted in a WNN graph representation incorporating all 10 samples and information from both mRNA and ADT, that was used to generate clusters and a UMAP representation (Figure 72).

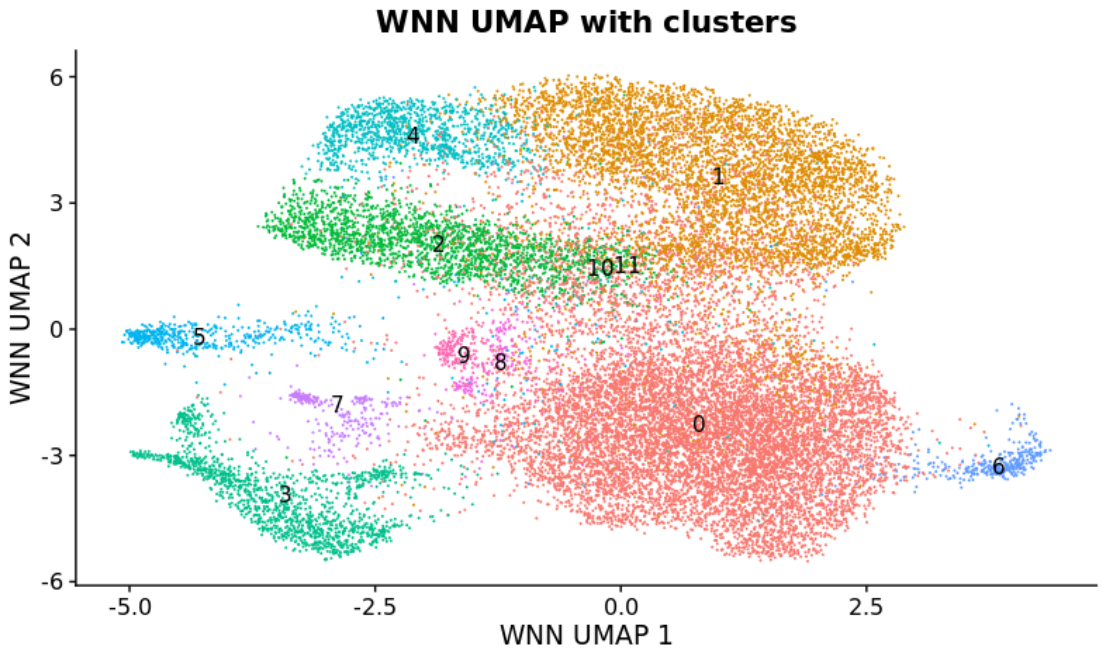

Figure 72. UMAP representation of tumour cells 10 mice with 3LL tumours were treated with control (5 mice) or MRTX1257 (5 mice). Tumour cells were extracted and subclustered as above. Both the UMAP representation and clusters (resolution 0.2) were generated based on the WNN graph

Once integration had been performed and clusters assigned, we sought to manually annotate the clusters. During such annotation it was discovered that cells in cluster 3 all had a high expression of mitochondrial genes (Figure 73a) while also having a low gene counts (not shown) consistent with poor quality/dying cells. Cells in cluster 5 expressed myeloid-specific genes including Lyz2, class II MHC and complement genes amongst others (Figure 73b,c). These cells likely represented doublets. When these cells were annotated on the original WNN UMAP representation containing all cells (Figure 73d) it was evident that they had not clustered separately, and instead were dispersed within the tumour clusters. This is possibly because the tumour cells were more transcriptionally active (higher read counts) and therefore dominated cluster

assignment. Only when sub-clustering these cells did their myeloid gene expression become apparent as a separate cluster.

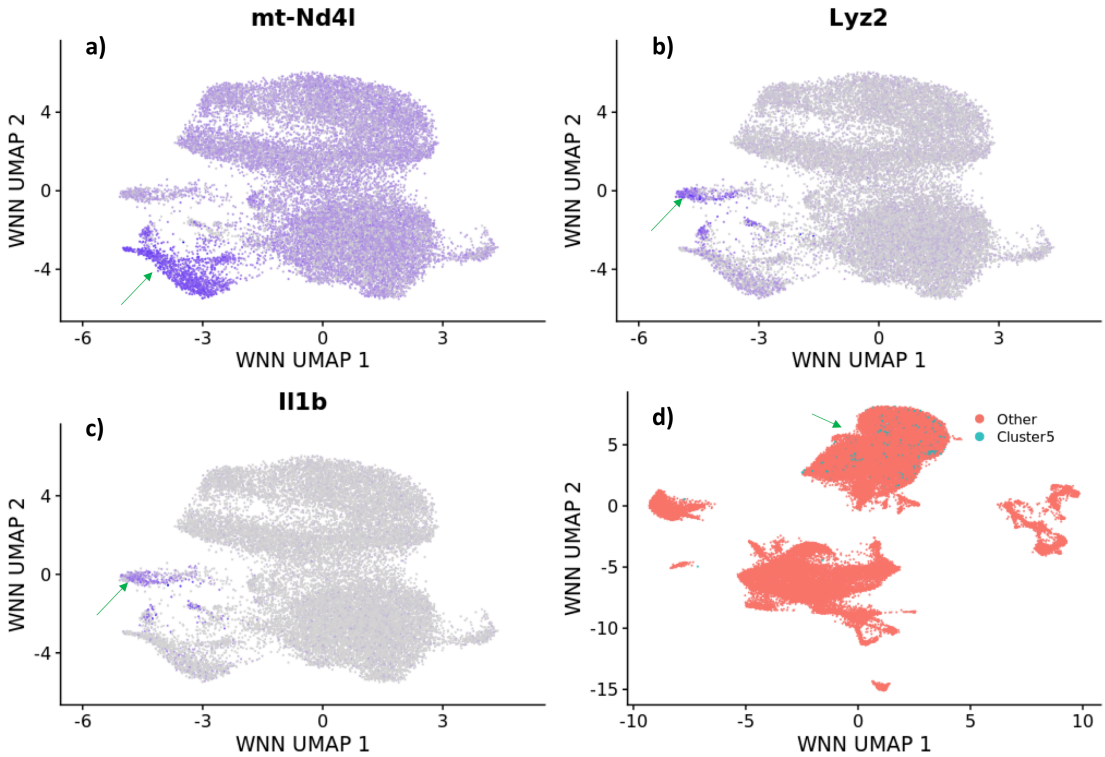

Figure 73. Poor quality clusters 10 mice with 3LL tumours were treated with control (5 mice) or MRTX1257 (5 mice). Tumour cells were extracted and subclustered as above. UMAPs demonstrating poor quality clusters. a) Cluster expressing high % of mitochondrial genes (example shown for mt-Nd4l); b & c) Cluster expressing many myeloid-specific genes (two examples shown) d) Cells from the cluster shown in 'b & c)' ('Cluster 5') were projected back onto the original WNN UMAP – cells did not cluster discretely and instead were scattered throughout the tumour cells (green arrow), possibly explaining lack of detection by doublet-detection algorithms

The poor-quality clusters were therefore removed, and the data was re-processed to generate a new integrated representation containing information from both ADT and RNA. Various cluster resolutions were interrogated using this new representation. One example, using a cluster resolution of 0.15, is shown in Figure 74a on a WNN UMAP. The adjacent panel (Figure 74b) instead shows a UMAP representation generated solely from gene expression data (i.e. without using the WNN graph that incorporates ADT information). The clusters in the latter object (generated solely from RNA data) appear to be projected

more distinctly in UMAP space. One explanation for this observation was that our ADT panel was designed primarily to help resolve immune states. Therefore, many of the antibodies would not be useful when defining tumour cell states and, instead, could generate noise. In fact, clustering and UMAP visualisation using ADT information alone (not shown here) appeared to yield little useful information. In order to circumvent the possible problem of noise from unhelpful (immune-specific) ADTs, one could simply discard them and only keep those more relevant to tumour cells (CD44, CD73 and CD274) before re-running the integration pipeline. Alternatively, it is possible just use RNA information alone to integrate the 10 samples and generate clusters. Given the strong transcriptional effect of MRTX1257 on KRAS(G12C)-mutant cells, we chose that latter option and therefore this thesis focuses on the integrated dataset that used gene-expression data alone.

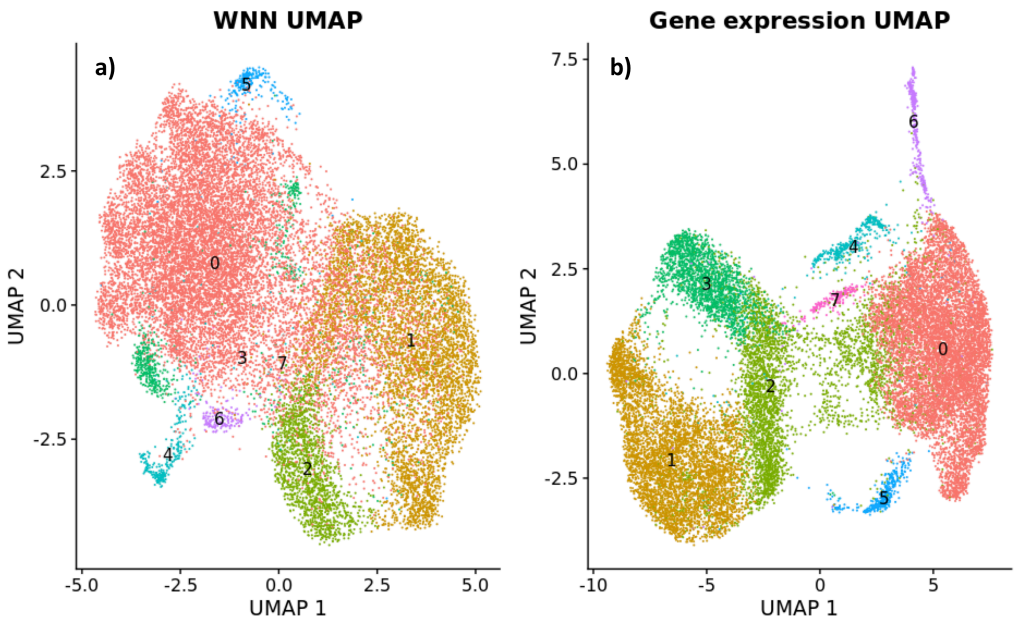

Figure 74. WNN UMAP vs gene expression UMAP 10 mice with 3LL tumours were treated with control (5 mice) or MRTX1257 (5 mice). Tumour cells were extracted and subclustered as above using two different methods: the UMAP in a) was generated using integrated RNA and ADT information. The UMAP in b) was generated using only RNA information.

After deciding to focus on gene expression alone, cluster resolution was determined using the same logic as described for myeloid cells. This included producing a tree of cluster relationships at various resolutions (Figure 75).

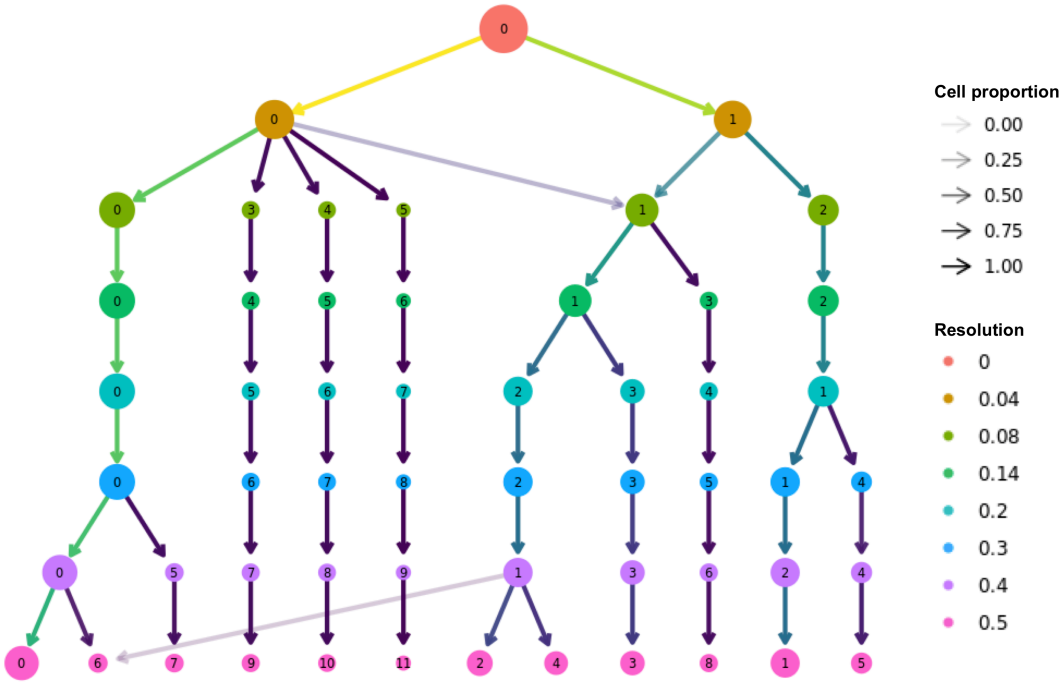

Figure 75. Effect of varying cluster resolution on cluster structure (tumours) 10 mice with 3LL tumours were treated with control (5 mice) or MRTX1257 (5 mice). Tumour cells were extracted and subclustered at various resolutions as above. Each horizontal row of nodes represents the clusters at a given resolution. Arrows indicate how the cells from clusters at one resolution are distributed in clusters at the next.

Given the relatively ‘clean’ tree up until a resolution of 0.4, this resolution was chosen for manual annotation. UMAP visualisation of clusters at different resolutions is shown in Figure 76.

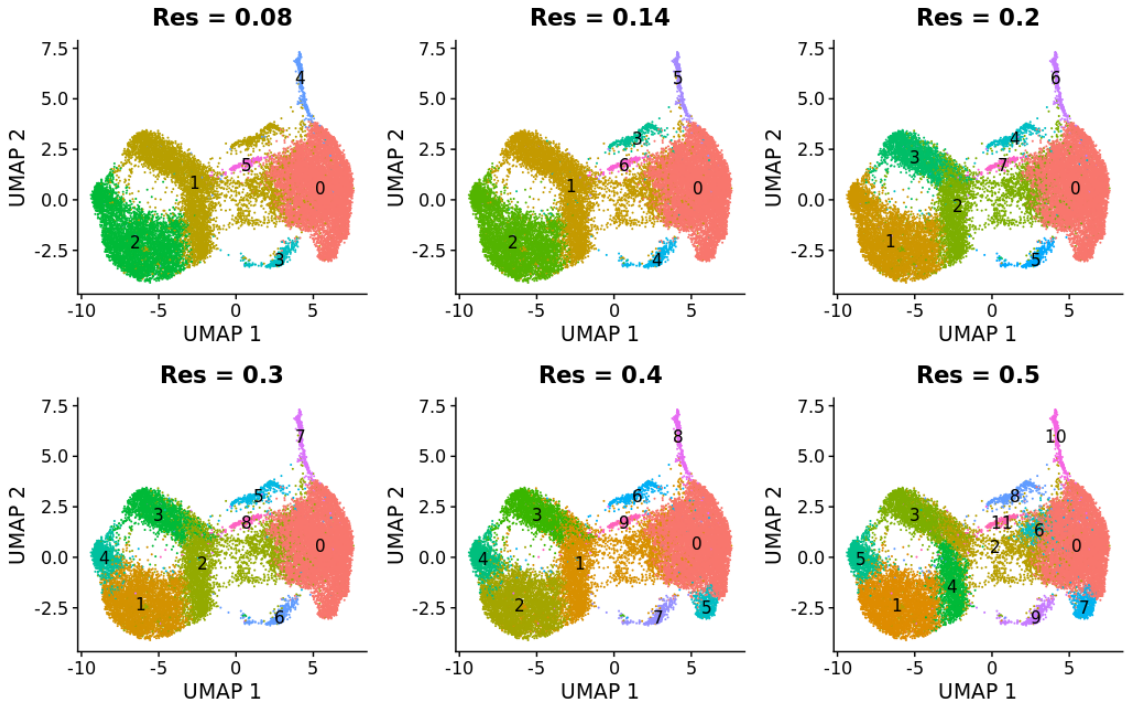

Figure 76. Effect of varying cluster resolution visualised using UMAP

10 mice with 3LL tumours were treated with control (5 mice) or MRTX1257 (5 mice). Tumour cells were extracted and subclustered at various resolutions as above.

5.3.1 Tumour cluster annotation

Following this decision, clusters were manually annotated by performing DE between each cluster and all other clusters combined. Where two or more clusters were closely related, DE was performed between the clusters in question. In addition, cell cycle phase was predicted using Seurat, and the results of this were used to help annotate clusters. As shown (Figure 77) there were clear cell-cycle effects in the data, and we used these to contribute to cluster nomenclature. Beyond this, we also used gene-set enrichment analysis (GSEA) to provide further supporting evidence for naming clusters. A brief description of clusters including improvised nomenclature and overexpressed genes is shown in Table 32.

.

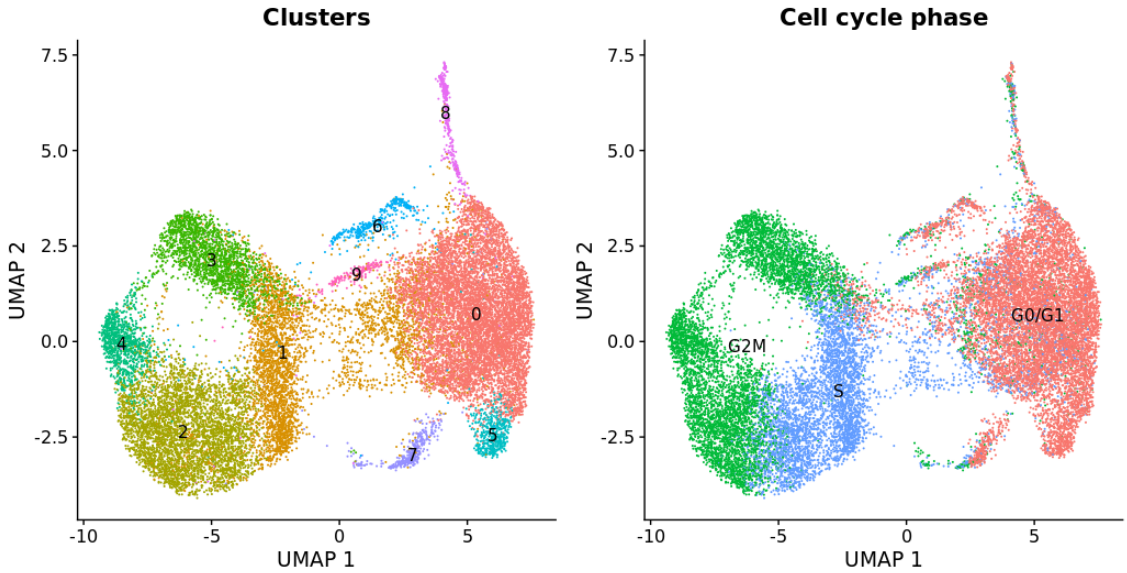

Figure 77. Tumour clusters vs predicted cell cycle phase 10 mice with 3LL tumours were treated with control (5 mice) or MRTX1257 (5 mice). Tumour cells were extracted and subclustered at a resolution of 0.4 using Seurat. Cell cycle phase was also predicted using Seurat, and appeared to segregate closely with clusters

Cluster (name)	Overexpressed genes	Notes
0 (G0)	Dcn, Ramp2, Cited2 & IEGs (Fos, Fosb, Jund)	Lack expression of cell proliferation markers seen in clusters 1-4
1 (Early cycle)	Mcm3/5/6/7, Hells, Cdt1, Ung, Dtl	Lack histone genes expressed in cluster 2
2 (Histone high)	Hist1h1b, Hist1h2ap, Hist1h1e	
3 (Late G2M)	Cdc20, Cenpa, Cenpe, Ccnb2, Cdkn3	Genes not specific (also in cluster 4). Lacks cluster 4 genes
4 (Early G2M)	Ubec2, Prc1, Cenpf, Top2a	Lack histone genes.
5 (Metabolic)	Cyp11a1, G0s2, Idh1, Fdx1, Fdxr	Genes related to (lipid) metabolism

6 (ER-stress)	Trib3, Slc3a2, Myc, Areg, Atf5, Gdf15	Several genes related to ER-stress and the unfolded protein response
7 (ISG High)	Isg15, Ifi203, Ifitm3, Irf6, Irf7, Stat1	High expression of interferon-stimulated genes
8 (Unknown)	Gm26917, Lars2, Tmsb4x, Nfib	Small population, low transcript count, unclear identity
9 (Rp high)	Rps26, Rpl35, Rpl38	Many ribosomal protein genes

Table 32. Manual annotation of tumour cells 10 mice with 3LL tumours were treated with control (5 mice) or MRTX1257 (5 mice). Tumour cells were extracted, subclustered and manually annotated as above. ER = endoplasmic reticulum, IEG = immediate early genes, ISG = interferon-stimulated genes, Rp = ribosomal protein

The largest cluster, 0, was enriched for cells in G0/G1. It lacked expression of the proliferation markers seen in clusters 1-4. Accordingly, when performing GSEA analysis on the genes DE in this cluster versus all others combined, the most strongly downregulated MSigDB hallmark gene sets (Liberzon *et al.*, 2015) were those pertaining to the cell cycle and MYC signalling (Figure 78). While the most upregulated genes included Dcn, Ramp2 and Cited. Despite interrogation of GSEA analysis of various gene sets beyond the hallmark collection, there was no consistent theme(s) that emerged to help functionally group the upregulated genes in this cluster. The five most upregulated hallmark gene sets are shown in (Figure 78).

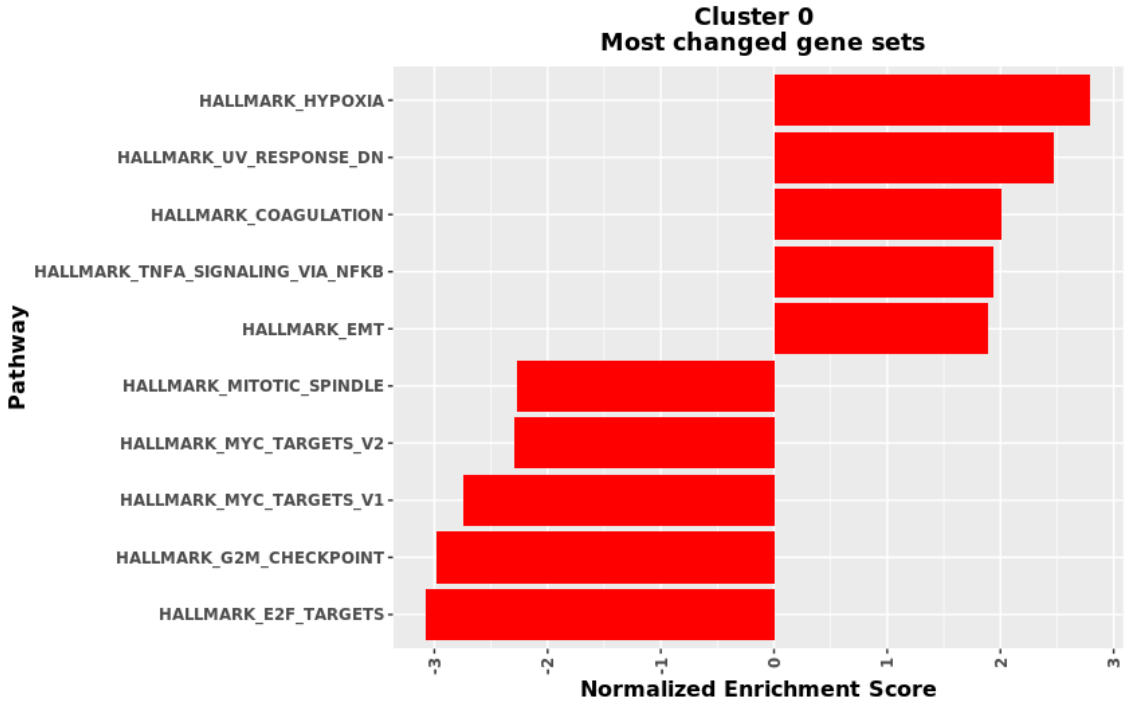

Figure 78. Cluster 0 GSEA 10 mice with 3LL tumours were treated with control (5 mice) or MRTX1257 (5 mice). Tumour cells were extracted and subclustered prior to GSEA analysis per cluster. The five most strongly up or downregulated hallmark gene sets based on DE between cluster 0 and all others combined. Positive normalised enrichment score indicates an upregulated set

In addition, given that these cells were in G0, we looked specifically at gene sets related to KRAS signalling to see if these indicated reduced KRAS signalling in cluster 0. There are two such gene sets in the hallmark collection, 23 such gene sets in the MSigDB v4.0 C6 'oncogenic signature' collection (including the Singh-Settleman signature of KRAS dependency (Singh *et al.*, 2009)) and we also looked at the Sweet-Cordero KRAS signature (Sweet-Cordero *et al.*, 2005). Essentially, while the majority of gene sets within the C6 collection suggested reduced KRAS signalling in cluster 0 compared to all other clusters combined, this was not consistent across all sets. The two hallmark gene sets gave opposing results (one suggested increased while the other decreased KRAS signalling) while the Ras84 signature (East *et al.*, 2021) suggested increased RAS signalling in this cluster (Figure 79). Across these signatures/sets, notable genes upregulated in cluster 0 included Cxcl1, Cxcl2,

Hbegf, Ntrk1 and Ptgs2 as well as immediate early genes (IEGs) such as Dusp1, Dusp4, Junb, Jund and Zfp36. Some of these are shown in Figure 80 where one can see expression restricted to a subset of this cluster. Thus, while cluster 0 represented cells that were not cycling, we were not able to say (using GSEA of various gene sets) that these cells had lower KRAS activity than cells in other clusters.

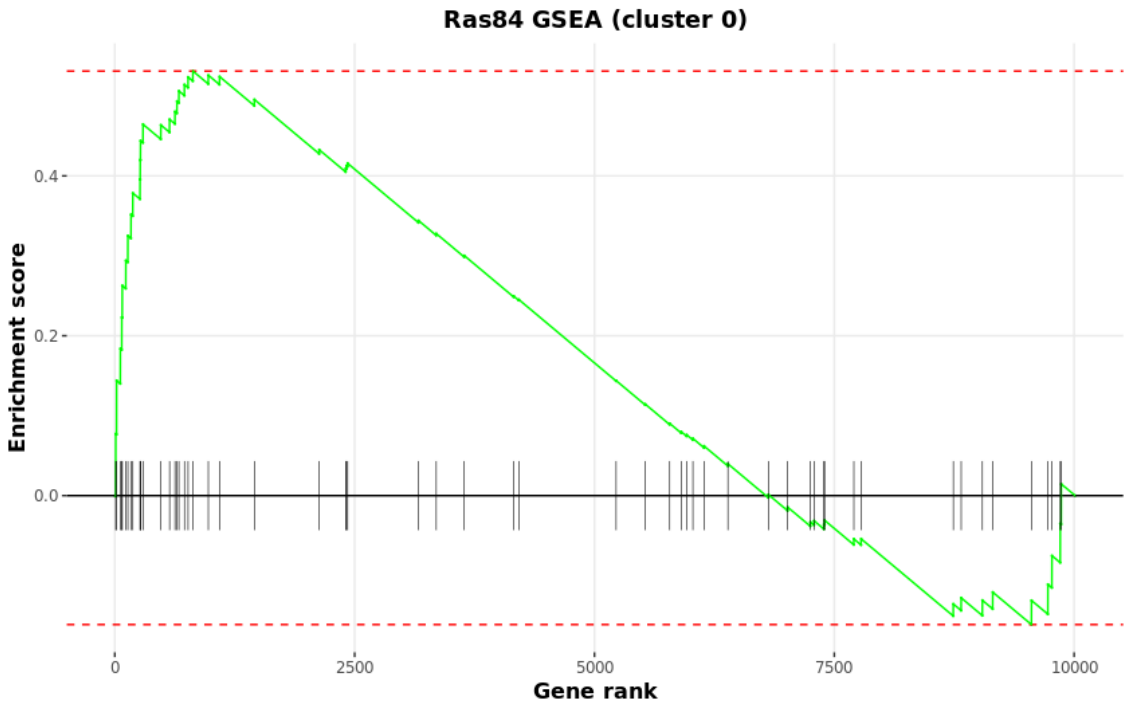

Figure 79. Ras84 GSEA (cluster 0) 10 mice with 3LL tumours were treated with control (5 mice) or MRTX1257 (5 mice). Tumour cells were extracted and subclustered prior to GSEA analysis per cluster. Normalised enrichment score = 1.79 (adj. $p < 0.001$) suggesting these genes are upregulated in this cluster

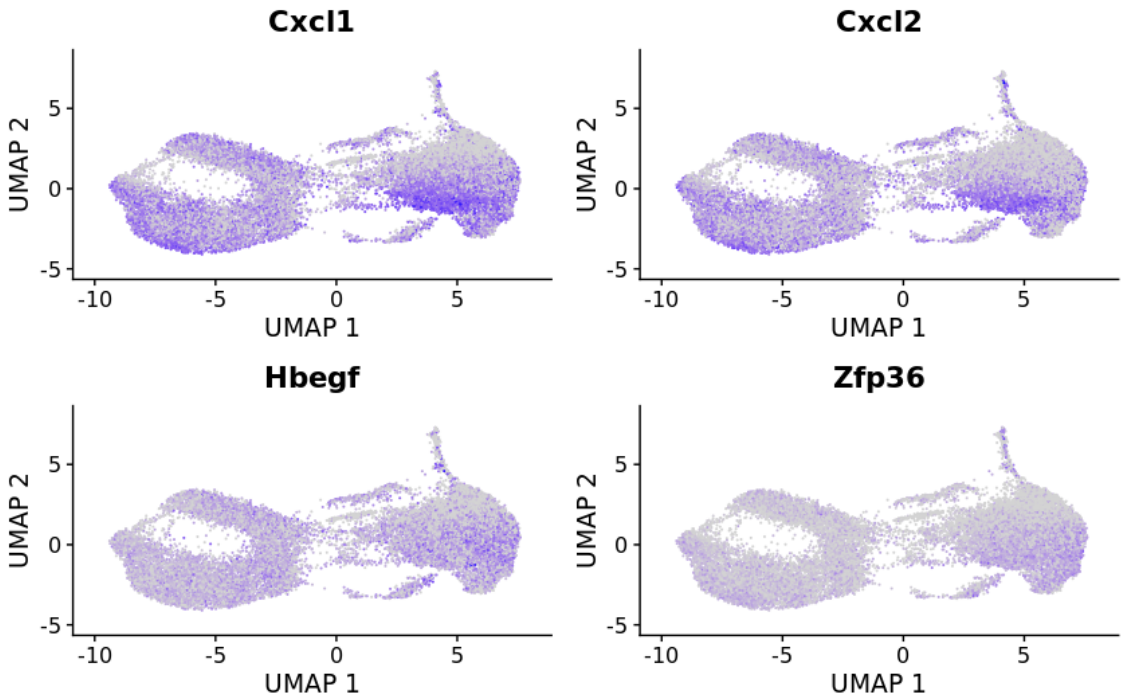

Figure 80. Selected RAS-related gene expression

10 mice with 3LL tumours were treated with control (5 mice) or MRTX1257 (5 mice). Tumour cells were extracted and subclustered. Figure shows selected gene expression in tumour compartment

While cluster 0 lacked expression of cell-cycle genes, clusters 1-4 expressed genes associated with cell cycle processes. These included minichromosome maintenance (Mcm) genes, which were most highly expressed in cluster 1 and replication-dependent histone genes, which were specific to cluster 2. Amongst other genes, clusters 3 and 4 had high expression of centromere-related genes (Cenp genes) and Cdc20 however cluster 4 also expressed Top2a, Prc1 and Cdk1 which cluster 3 did not (Figure 81)

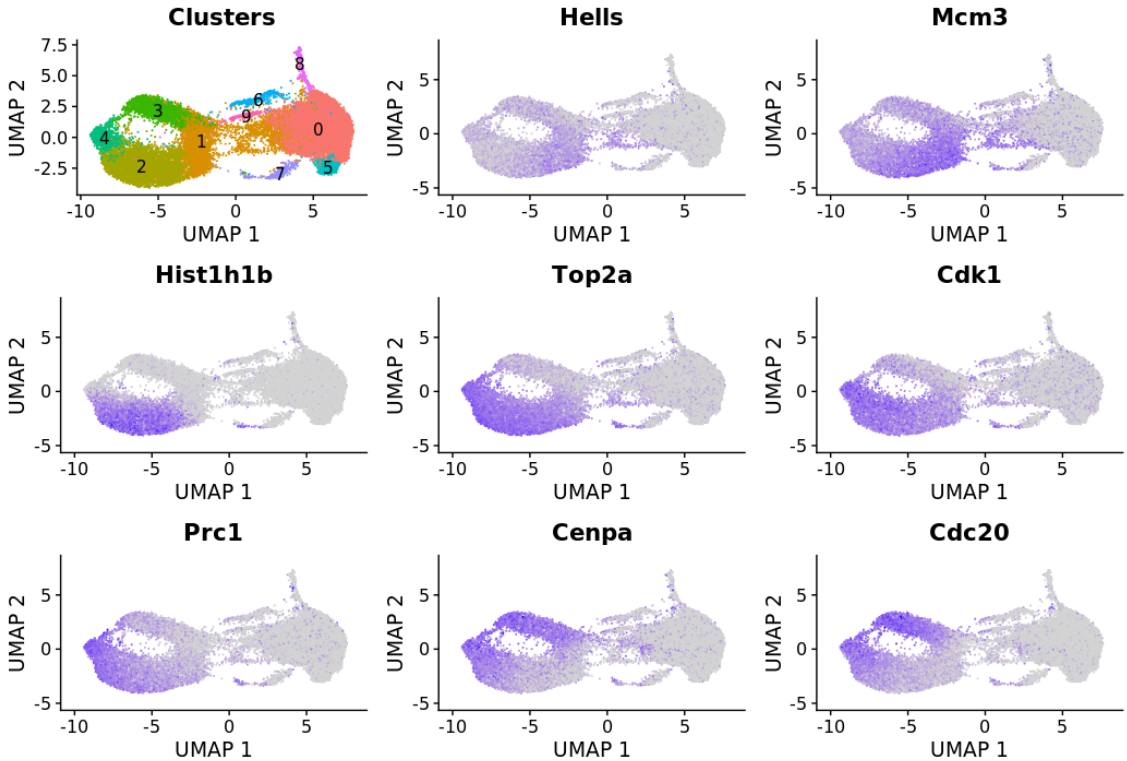

Figure 81. Cell cycle gene expression 10 mice with 3LL tumours were treated with control (5 mice) or MRTX1257 (5 mice). Tumour cells were extracted and subclustered. UMAP visualisation of cell-cycle related genes, illustrating progressive expression from clusters 1 -> 2 -> 4 -> 3.

Cluster 5 represented a small group of cells within the non-cycling compartment. Many of the most strongly overexpressed genes in this cluster code for proteins involved in metabolic processes including Cyp11a1, Idh1, G0s2 and Fdx1/Fdxr. When performing GSEA, hallmark gene sets for adipogenesis (NES = 2.40), bile acid metabolism (NES = 1.87), oxidative phosphorylation (NES = 1.85) and fatty acid metabolism (NES = 1.72) were the most strongly upregulated here, suggesting metabolism may be altered in this cluster (Figure 82).

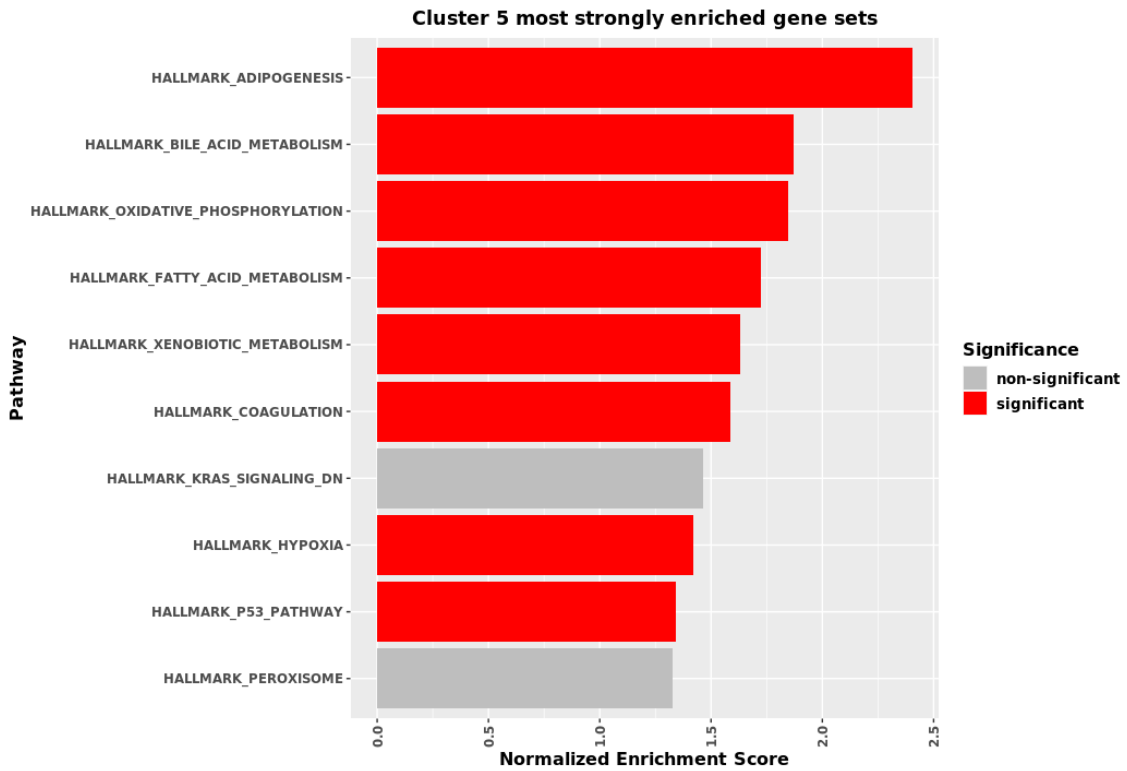

Figure 82. Cluster 5 GSEA - most strongly enriched gene sets 10 mice with 3LL tumours were treated with control (5 mice) or MRTX1257 (5 mice). Tumour cells were extracted and subclustered prior to GSEA analysis per cluster. Significance refers to an adjusted p value of < 0.05

Cluster 6 was another small cluster. Amongst the most strongly overexpressed genes in this cluster were Hspa5, Sdf21l, Manf and Atf5 which are all involved in protein folding in the endoplasmic reticulum (ER). This was reflected in its high NES (FDR < 0.001) for the hallmark unfolded protein response gene set during GSEA testing (Figure 83). Cluster 7 overexpressed many interferon-stimulated genes and also had a high NES (FDR < 0.001) for the corresponding gene sets (Figure 83).

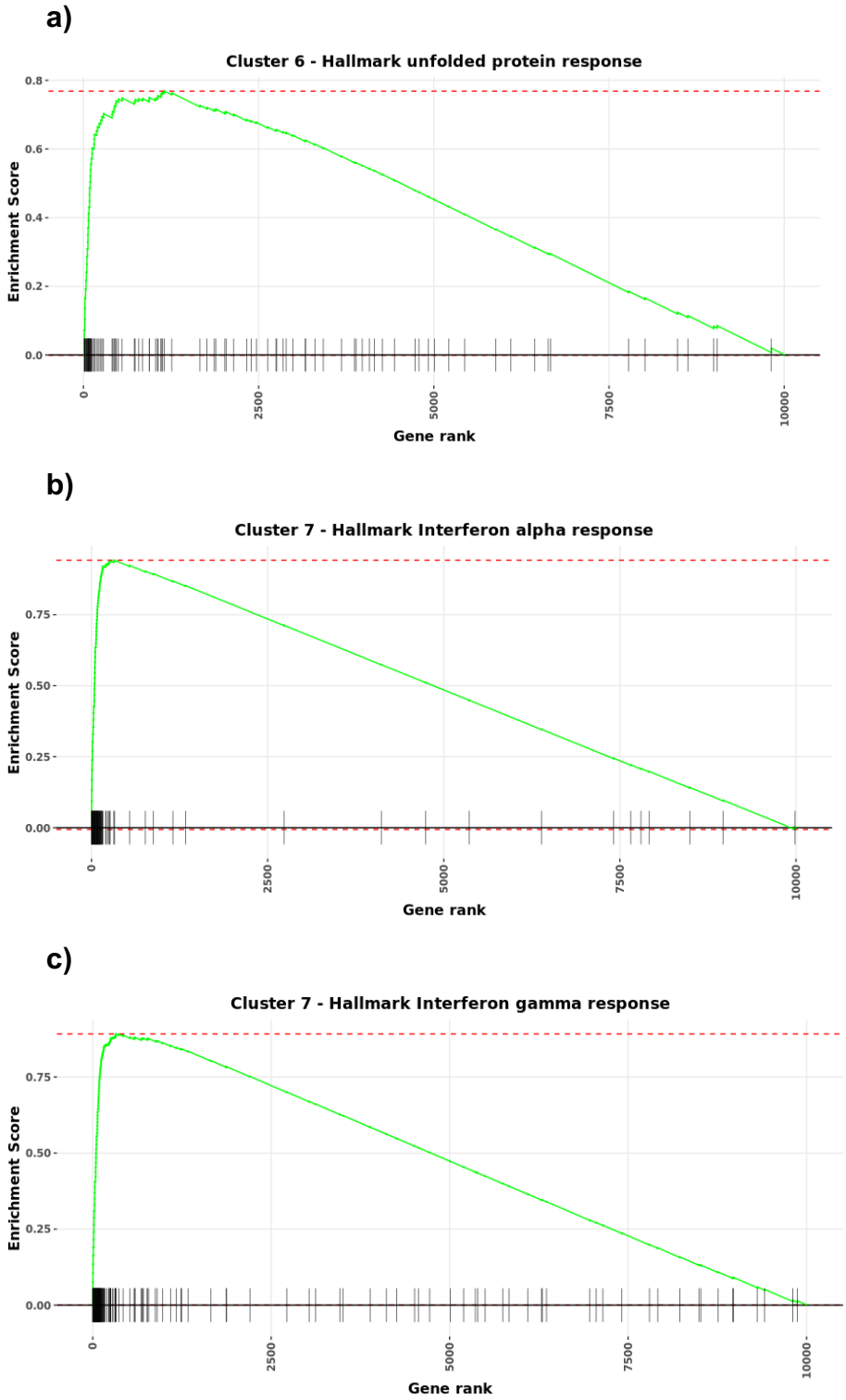

Figure 83. Representative GSEA enrichment plots 10 mice with 3LL tumours were treated with control (5 mice) or MRTX1257 (5 mice). Tumour cells were extracted and subclustered prior to GSEA analysis per cluster. Cluster 6 – Hallmark unfolded protein response, b) Cluster 7 – Hallmark interferon alpha response, c) Hallmark interferon gamma response

We were unable to assign a confident name to cluster 8. The genes most strongly overexpressed in this cluster included the long non-coding RNA (lncRNA) Gm26917, the mitochondrial tRNA leucyl-transferase Lars2 and the pleiotropic Tmsb4x. This cluster was also unique in its expression of H2-K1 which could suggest a non-tumour cell type given the lack of expression of this gene in tumour cells. As is evident in Figure 84, gene expression in this cluster appeared to suggest two distinct patterns of co-expression, one at the tip of the cluster (where cells expressed Tmsb4x, H2-K1, Col1a1, Sparc and Sox4 amongst others) and the other at the opposite end (expressing Lars2 and Gm26917). While this cluster could represent contamination, it is notable that all 10 samples were represented (i.e. it was not rogue cells from a single sample). When looking at other QC metrics, cells from this cluster expressed a lower number of genes (i.e. low transcript diversity) compared to cells from other clusters. We also performed differential expression between cluster 8 and all other clusters using ADTs to see if any immune ADTs were overexpressed. No immune markers were overexpressed here, however there was a significant reduction in CD44, CD73 and CD274 binding in this cluster. We overlaid these antibodies onto the UMAP and saw reduced expression mostly at the tip of the cluster. The significance of the reduced antibody expression in this cluster is uncertain. Incidentally, we noted high expression of CD274 in cluster 7, consistent with its high expression of ISGs. This information about cluster 8 is summarised in Figure 84.

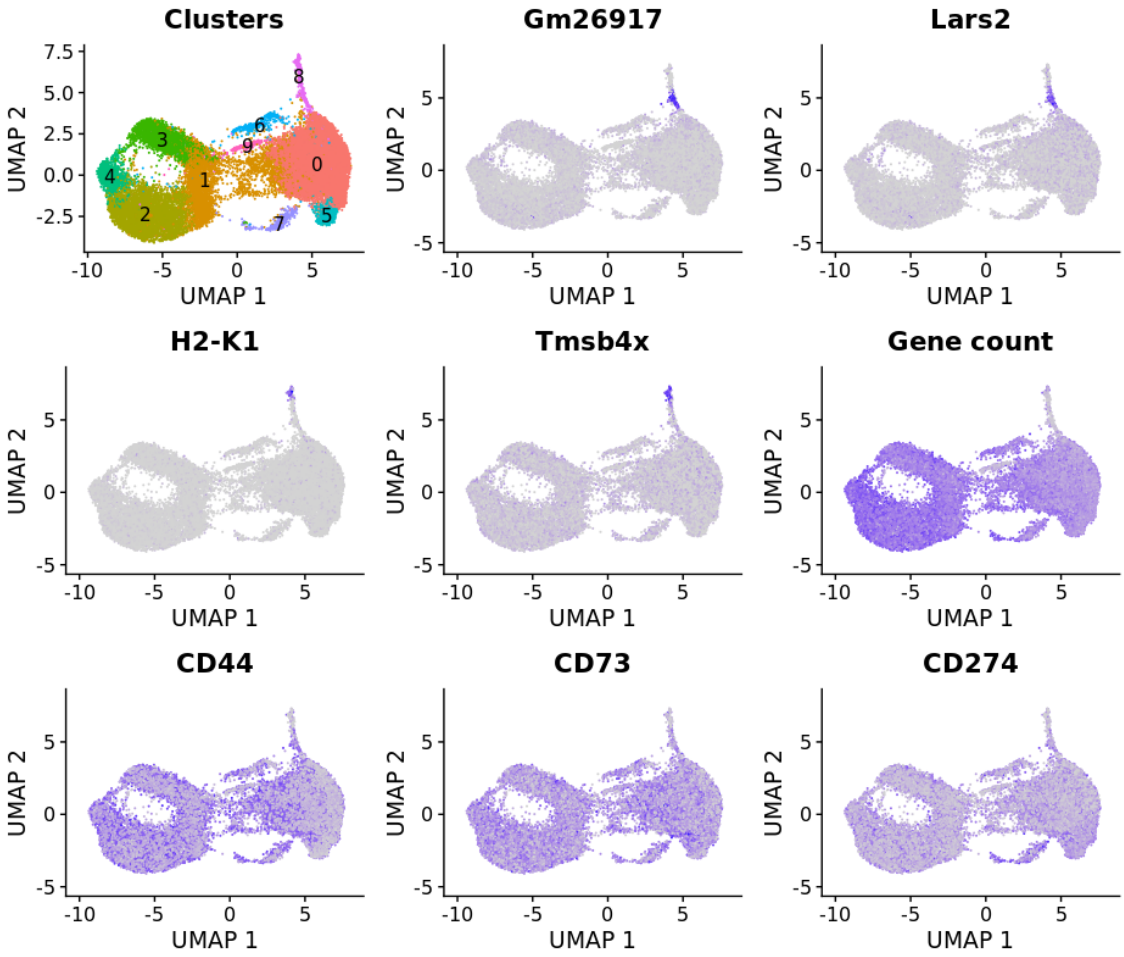

Figure 84. UMAP visualisation of cluster 8 characteristics

10 mice with 3LL tumours were treated with control (5 mice) or MRTX1257 (5 mice). Tumour cells were extracted and subclustered. From top-left, the first panel represents tumour cell clusters. The next four panels show representative mRNA expression. Gene count refers to the number of different genes expressed per cell, with lighter shades representing fewer genes expressed. The bottom three panels represent normalised ADT expression.

Finally, cluster 9 expressed high levels of ribosomal genes in conjunction with low transcript counts, and was therefore deemed to represent poor quality cells.

5.3.2 Tumour cluster composition analysis

Once we had proposed a suggested nomenclature, we began to look at the effect of treatment. We initially looked at the distribution of clusters within each sample and then by condition (Figure 85).

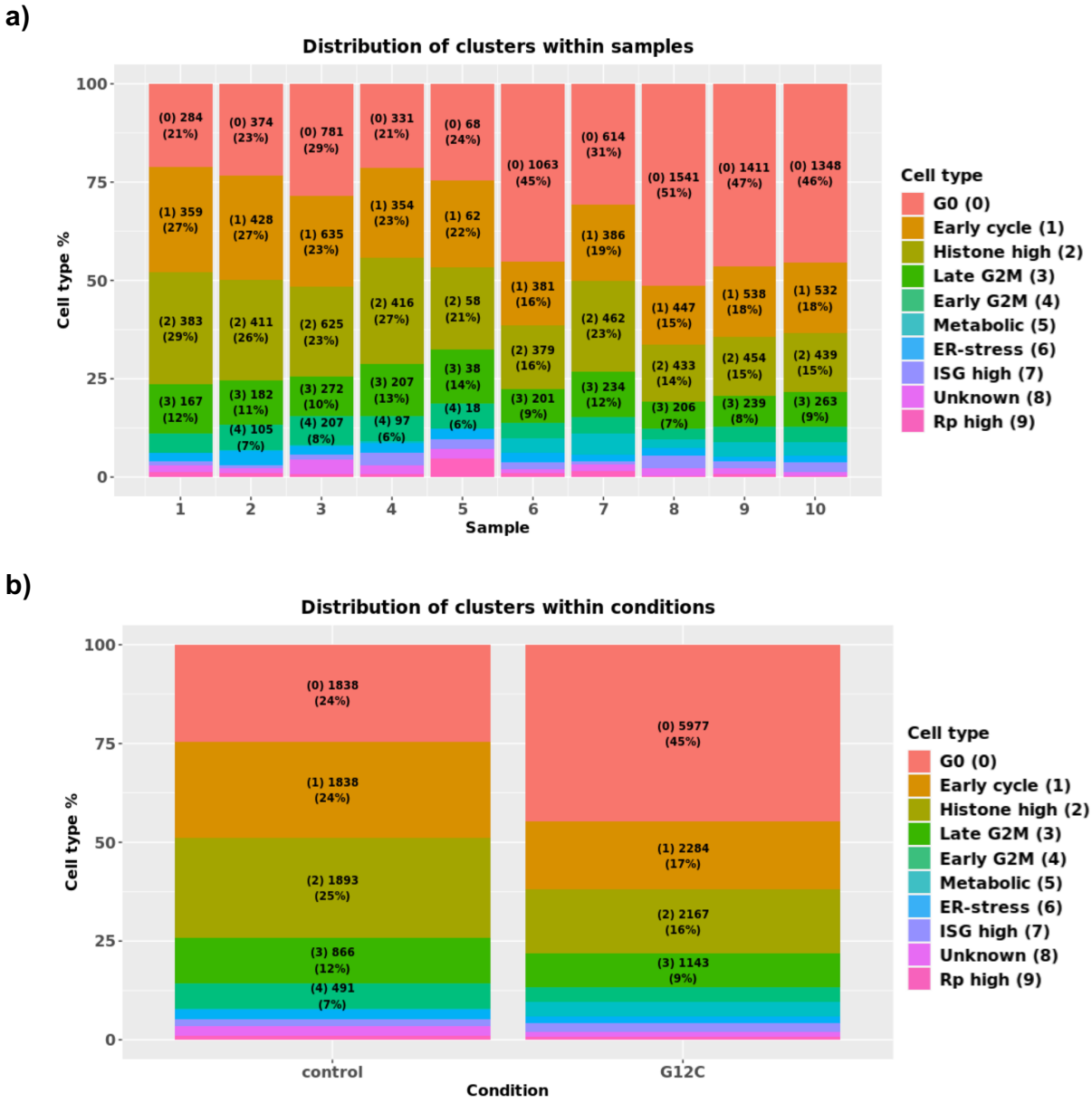

Figure 85. Distribution of tumour clusters per sample & condition 10 mice with 3LL tumours were treated with control (5 mice) or MRTX1257 (5 mice). Tumour cells were extracted and subclustered. Numbers inside the bars = (cluster number) number of cells (% of subset occupied by that cluster). Samples 1-5 are control, 6-10 are MRTX1257-treated.

As evidenced by the figure above, cluster 0 cells made up a higher proportion of treated tumours (31-51%, median 46%) than control tumours (21-29%, median 23%). Conversely, clusters 1-4 made up a smaller proportion of treated tumours than control tumours although the caveat that this is somewhat inevitable, given the high proportion of cluster 0 cells in the treated samples, needs to be borne in mind. Also, strikingly, as shown in Table 33 below, cluster 5 cells (the so-called 'metabolic' cluster) were virtually absent in control tumours but present in treated samples.

	1	**2**	**3**	**4**	**5**	**Control**
G0	284 (21.2)	374 (23.2)	781 (28.5)	331 (21.4)	68 (24.5)	**1838 (24.5)**
Early cycle	359 (26.8)	428 (26.6)	635 (23.2)	354 (22.9)	62 (22.3)	**1838 (24.5)**
Histone high	383 (28.6)	411 (25.5)	625 (22.8)	416 (26.9)	58 (20.9)	**1893 (25.2)**
Late G2M	167 (12.5)	182 (11.3)	272 (9.9)	207 (13.4)	38 (13.7)	**866 (11.5)**
Early G2M	64 (4.8)	105 (6.5)	207 (7.6)	97 (6.3)	18 (6.5)	**491 (6.5)**
Metabolic	2 (0.1)	4 (0.2)	2 (0.1)	7 (0.5)	0 (0)	**15 (0.2)**
ER-stress	29 (2.2)	57 (3.5)	61 (2.2)	38 (2.5)	7 (2.5)	**192 (2.6)**
ISG high	12 (0.9)	14 (0.9)	33 (1.2)	51 (3.3)	7 (2.5)	**117 (1.6)**
Unknown	24 (1.8)	19 (1.2)	102 (3.7)	33 (2.1)	7 (2.5)	**185 (2.5)**
Rp high	17 (1.3)	16 (1)	22 (0.8)	13 (0.8)	13 (4.7)	**81 (1.1)**
	6	**7**	**8**	**9**	**10**	**MRTX1257**
G0	1063 (45.3)	614 (30.7)	1541 (51.4)	1411 (46.5)	1348 (45.5)	**5977 (44.8)**
Early cycle	381 (16.2)	386 (19.3)	447 (14.9)	538 (17.7)	532 (18)	**2284 (17.1)**
Histone high	379 (16.1)	462 (23.1)	433 (14.5)	454 (15)	439 (14.8)	**2167 (16.2)**
Late G2M	201 (8.6)	234 (11.7)	206 (6.9)	239 (7.9)	263 (8.9)	**1143 (8.6)**
Early G2M	92 (3.9)	80 (4)	83 (2.8)	122 (4)	115 (3.9)	**492 (3.7)**
Metabolic	84 (3.6)	108 (5.4)	67 (2.2)	111 (3.7)	104 (3.5)	**474 (3.6)**
ER-stress	59 (2.5)	34 (1.7)	54 (1.8)	36 (1.2)	49 (1.7)	**232 (1.7)**
ISG high	44 (1.9)	19 (1)	95 (3.2)	57 (1.9)	78 (2.6)	**293 (2.2)**
Unknown	22 (0.9)	33 (1.7)	61 (2)	39 (1.3)	26 (0.9)	**181 (1.4)**
Rp high	22 (0.9)	29 (1.5)	9 (0.3)	26 (0.9)	8 (0.3)	**94 (0.7)**

Table 33. Distribution of tumour clusters per sample & condition

10 mice with 3LL tumours were treated with control (5 mice) or MRTX1257 (5 mice). Tumour cells were extracted and subclustered. Values in cells represent number of cells per cluster in given condition (brackets indicate percentage).

As before, to formally analyse composition differences, we performed differential abundance testing. As shown (Table 34) the increases in cluster 0 (the 'G0' cluster) and 5 (the 'metabolic') cluster were both significant. As previously, we performed a sensitivity analysis by removing sample 5 and re-performing compositional analysis; results were consistent with the table below.

Cluster name (no.)	**Log_2 FC**	**p-value**	**Adj. p (FDR)**
Metabolic (5)	4.14	< 0.001	< 0.001
G0 (0)	0.88	< 0.001	< 0.001
Early G2M (4)	-0.77	0.001	0.002
Histone high (2)	-0.60	0.001	0.003
Early cycle (1)	-0.50	0.001	0.003
Late G2M (3)	-0.46	0.015	0.026
ER-stress (6)	-0.53	0.022	0.031
Unknown (8)	-0.76	0.033	0.041
Rp high (9)	-0.69	0.213	0.237
ISG high (7)	0.38	0.259	0.259

Table 34. Differential abundance testing of tumour clusters 10 mice with 3LL tumours were treated with control (5 mice) or MRTX1257 (5 mice). Tumour cells were extracted and subclustered. Log_2 FC represents the differential abundance of the given cluster after treatment with MRTX1257. p-value adjustment performed using the Benjamini Hochberg method.

5.3.3 Tumour per-cluster differential expression (DE)

Once we had carried out formal composition analysis, we performed per-cluster DE between treated and non-treated cells. Given that cluster 9 was poor quality cells and cluster 8 could not be assigned a suitable nomenclature and expressed H2-K1, we focussed our analysis on the remaining clusters.

A summary of the number of DE genes at various different $\log_2$ fold-changes is given in Table 35.

LFC	G0	Early cycle	Histone high	Late G2M	Early G2M
< - 2	285	73	47	20	23
< -1.5	501	158	96	43	44
< -1	925	319	164	91	102
< -0.5	1996	740	341	237	202
< 0	2511	999	408	266	216
> 0	2807	1209	520	381	247
> 0.5	2203	879	401	332	225
> 1	870	282	150	114	80
> 1.5	366	127	73	37	36
> 2	192	62	45	23	20
LFC	**Metabolic**	**ER-stress**	**ISG high**	**Unknown**	**Rp high**
< - 2	32	47	112	6	4
< -1.5	57	121	216	15	5
< -1	85	266	495	85	12
< -0.5	85	559	1161	158	13
< 0	85	564	1194	158	13
> 0	161	606	1200	220	25
> 0.5	161	598	1181	220	25
> 1	161	241	512	151	23
> 1.5	111	68	183	59	8
> 2	74	23	81	27	1

Table 35. Summary of differential expression per cluster 10 mice with 3LL tumours were treated with control (5 mice) or MRTX1257 (5 mice). Tumour cells were extracted and subclustered. Figures refer to numbers of genes exceeding the given $\log_2$ FC at an FDR of < 0.1.

As shown in the table, there were many DE genes across the clusters, including 285 genes with a $\log_2$ FC of <-2 in cluster 0 (the largest cluster) with 192 genes displaying a $\log_2$ FC of > 2. The landscape of gene expression in this cluster is shown in Figure 86. Illustrated on the plot are several KRAS-regulated genes known to play a role in oncogenesis that are downregulated in cluster 0 by a $\log_2$ FC of < -1. These include Ccl2, Ptgs2, Vegfa, Plaur, Myc and the growth factors Areg & Ereg. Conversely, upregulated genes included Dcn, Col3a1, Sparc and Ramp2. As previously mentioned, Ramp2 is thought to have a pro-apoptotic effect in lung cancer while Dcn, Col3a1 and Sparc were all part of a TGF-β signature found to be upregulated upon KRAS knockout in a pancreas cancer model (Ischenko *et al.*, 2021). Thus, some of the effects we saw (in terms of upregulated genes) were consistent with previous single cell data exploring the effect of KRAS inhibition/knockdown. Despite this, the Tgfb1 gene itself was downregulated upon treatment (section 5.3.3.3) and furthermore gene sets relating to TGF-signalling were not enriched when we later performed GSEA (section 5.3.3.1).

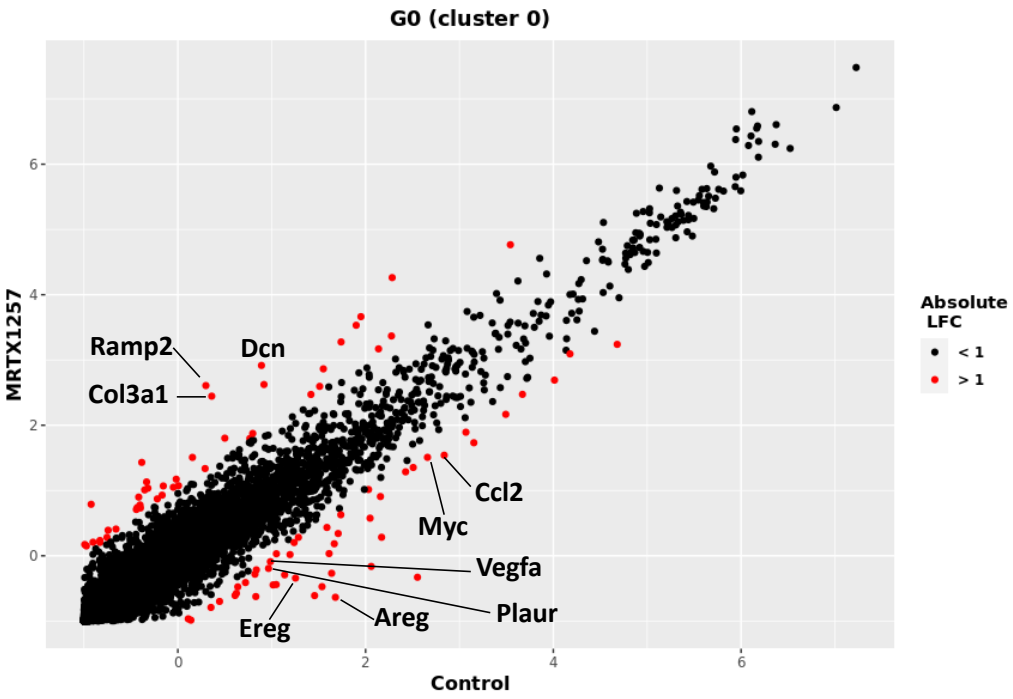

Figure 86. Cluster 0-specific gene expression (MRTX1257 vs. Control) 10 mice with 3LL tumours were treated with control (5 mice) or MRTX1257 (5 mice). Tumour cells were extracted and subclustered. Expression values represent $\log_2$ normalised values (pseudocount 0.5) using library sizes to calculate normalisaton factors. Red dots indicate genes with an absolute $\log_2$ FC of > 1.

Manual comparison of the list of DE genes in cluster 0 with other DE lists of other clusters revealed a generally consistent pattern, with similar genes being up or down-regulated. One exception, was cluster 5 ('metabolic'), where several genes appeared to be specifically regulated in this cluster. Genes upregulated after treatment included Kctd14, Crxos, G0s2, Cyp11a1, Hsd11b1 and Acsbg1 of which all are involved in lipid biogenesis except Kctd14 (unknown function) and Crxos (possible involvement in murine embryonic stem cell self-renewal (Saito *et al.*, 2009)). Four of these genes are visualised in Figure 87. As shown, they are mostly expressed in cluster 5 and increase markedly after treatment.

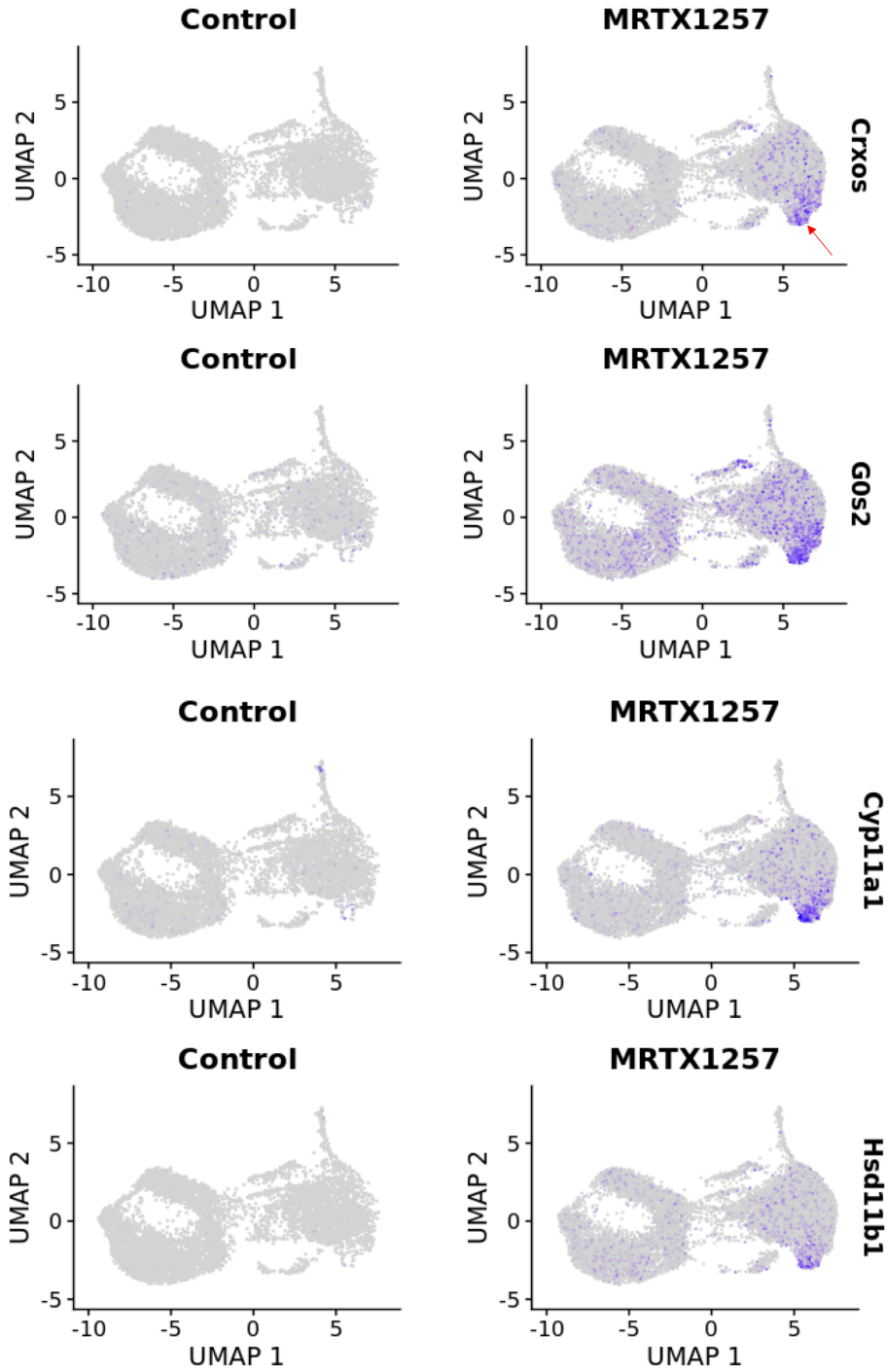

Figure 87. Visualisation of cluster 5-specific gene DE using UMAP10 mice with 3LL tumours were treated with control (5 mice) or MRTX1257 (5 mice). Tumour cells were extracted and subclustered. Red arrow in top panel shows location of cluster 5 cells

After performing DE and manually interrogating the lists, we looked for genes that were specifically DE in one cluster and not others (method in section 2.14.7). Similar to the results that we encountered for the myeloid compartment, the majority of genes that were DE in one cluster tended to be DE in the same direction, and of similar magnitude, in several other clusters. Nonetheless, there were some genes that exhibited a magnitude of DE in one cluster that was significantly different from other clusters. Here, we focus on describing such genes in cluster 0.

In cluster 0, such 'specific' DE genes tended to adopt one of two patterns when visualised using UMAP. One group of genes was expressed equally or more strongly in other clusters, but tended to be DE only (or much more strongly) in cluster 0. For example, Birc5, Mcm2, Mcm3, Dnph1 (a MYC-target gene), Gins2 and Cdt1 were all genes expressed at similar or higher levels in other clusters (mostly in cycling clusters) but exhibited DE at significantly stronger level in cluster 0 (Table 36). This group of genes all have roles in the cell cycle, so it is notable that they were expressed in cluster 0 ('G0' cluster) predominantly in control cells. Of note, some of these genes may have additional functions. For example, Birc5 is thought to play a role in apoptosis inhibition (Nie *et al.*, 2015). It's downregulation after treatment may increase the susceptibility of treated cells to apoptosis. Expression of Birc5 before and after treatment is visualised on a UMAP plot in Figure 88a. Like the other genes mentioned above, it is evident on this plot how treatment appears to modulate expression mainly in cluster 0, with other clusters affected very little.

Gene	LFC (clust 0)	LFC (other)	Mean expr (clust 0)	Mean expr (other)	FDR
Birc5	-2.81	-0.51	0.20	2.65	< 0.01
Cdca7	-1.73	-0.30	0.20	0.50	< 0.01
Cdt1	-1.86	0.05	0.13	0.44	< 0.01
Dnph1	-2.04	-0.16	0.10	0.48	< 0.01
Gins2	-1.56	0.28	0.12	0.50	< 0.01
Mcm2	-2.24	0.06	0.13	0.49	< 0.01
Mcm3	-2.10	0.07	0.42	1.94	< 0.01
Spc24	-2.43	-0.31	0.10	0.92	0.01

Table 36. DE of selected genes in cluster 0 vs other clusters 10 mice with 3LL tumours were treated with control (5 mice) or MRTX1257 (5 mice). Tumour cells were extracted and subclustered. LFC (other) represents the mean $\log_2$ FC of that gene (MRTX1257 vs control) in all other clusters combined. Mean expr represents the normalised mean expression per cell. FDR = false discovery rate (Benjamini-Hochberg procedure) – representing the significance test of the null hypothesis that the cluster 0 LFC lies between zero and the average LFC in all other clusters (e.g. for Birc5, that the LFC is in the interval -0.51 – 0).

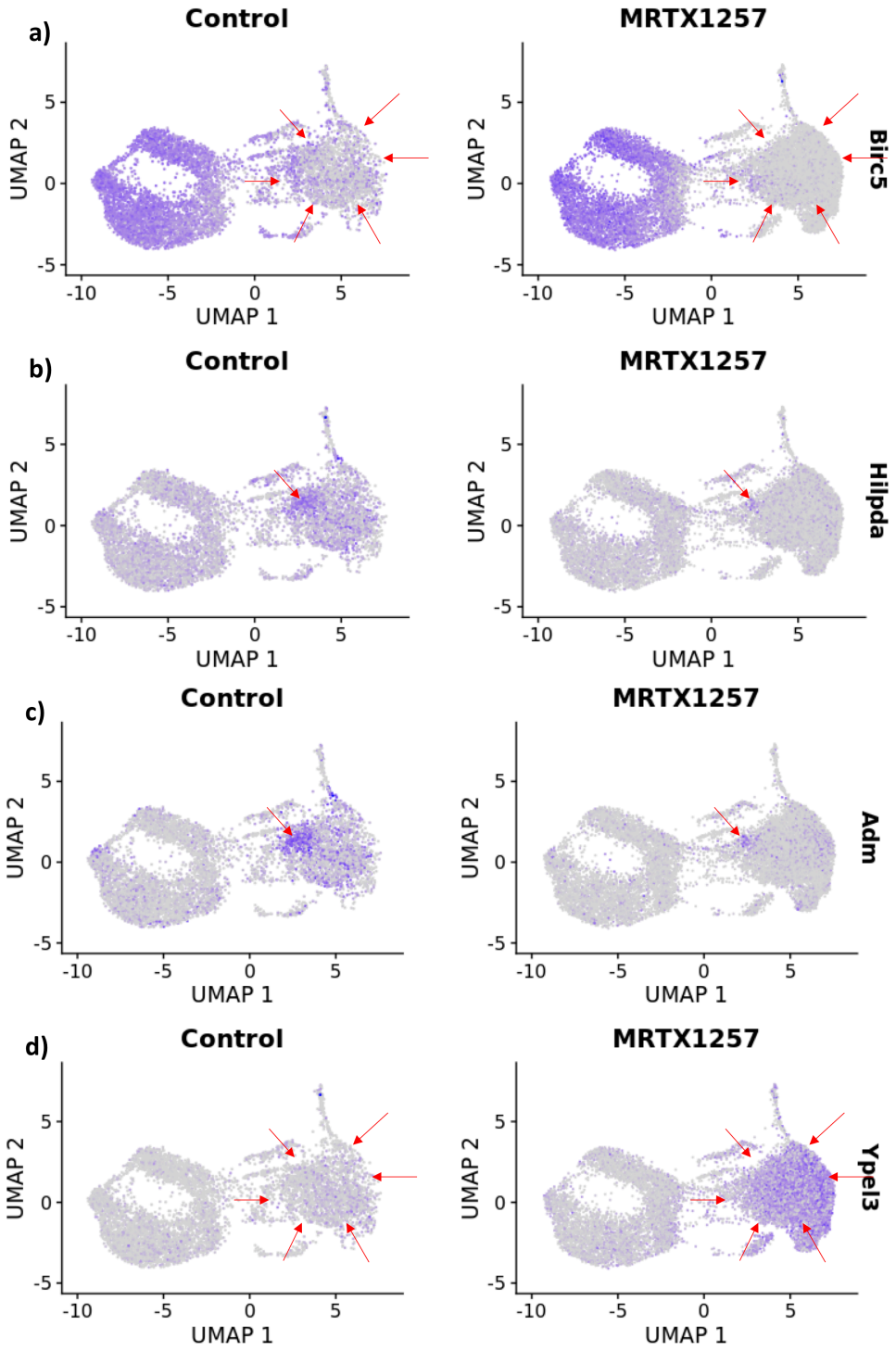

Figure 88. UMAP: DE of selected genes with cluster 0-specific effects

10 mice with 3LL tumours were treated with control (5 mice) or MRTX1257 (5 mice). Tumour cells were extracted and subclustered. Birc5, b) Hilpda, c) Adm, d) Ypel3. Red arrows either indicate cluster 0 (a & d) or highest expressing area of UMAP space (b & c)

The other group of genes whose DE was significantly different in cluster 0 compared to other clusters, were those that were expressed at a higher (or similar) levels in cluster 0 than in other clusters. Within this group of genes, there was one module of genes that were most strongly expressed in a similar area within UMAP space, and which were highly correlated with one another. This group of genes included Hilpda (Hypoxia-inducible lipid droplet-associated), Scl2a1 (codes for GLUT1 transporter) and Ndrg1 (N-myc downstream-regulated gene 1). All of these genes were significantly more strongly downregulated (in treted cells) in cluster 0 than in other clusters. Visualisation on a UMAP plot is shown for Hilpda and Scl2a1 in Figure 88 b&c. This same group of genes was also correlated with other genes known to be modulated by hypoxia including Vegfa and Adm (adrenomedullin) amongst several others. While these latter two genes were more strongly downregulated upon treatment in cluster 0 than other clusters (e.g. for Vegfa, $\log_2$ FC = -1.76 in cluster 0 vs. -1.17 in all other clusters combined), this difference in DE did not reach statistical significance (FDR = 0.18 for Vegfa). Of note, this area of the UMAP contained cells from all samples (plot not shown) demonstrating that this group of cells was not an outlier group from a single sample, but rather reproducible over replicates.

Conversely there were some genes expressed most strongly in cluster 0 which exhibited an increase (rather than decrease) in expression after treatment that was significantly stronger in cluster 0 than other clusters. Some of these genes are shown in Table 37. Of note, both Mgp (Sterzyńska *et al.*, 2018) and Bmp7 (Cortez *et al.*, 2020) have been associated with pro-tumourigenic properties. Conversely, other genes that were most strongly upregulated after treatment in cluster 0 compared to other clusters include Ypel3 (a p53-regulated gene that induces cellular senescence, (Kelley *et al.*, 2010)), Cdkn1b (P27), Gstm2 (Glutathione S-transferase Mu 2), Foxn3 (inhibition of the WNT pathway (Dai *et al.*, 2017)), and Deptor (inhibition of the MTOR pathway (Peterson *et al.*, 2009)). These genes are individually associated with antitumour function and the dramatic increase in Ypel3 is shown in Figure 88d. Also, Cdkn1b, Gstm2 and

Dcn are members of the MsigDB Hallmark apoptosis gene set, possibly suggesting an increased propensity for apoptosis in these cells after treatment. Finally, we also noticed that many immediate early genes including Fos, Fosb, Jun, Zfp36, Dusp1 were also expressed most highly in cluster 0 relative to other clusters, and their expression went up with treatment most strongly in cluster 0 compared to other clusters (e.g. for Fos, $\log_2$ FC = 1.01 in cluster 0 vs. 0.60 in all other clusters combined). However, this difference in DE was not statistically significant (e.g. FDR = 0.30 for Fos).

Gene	LFC (clust 0)	LFC (other)	Mean expr (clust 0)	Mean expr (other)	FDR
Mgp	3.78	1.25	0.23	0.18	0.08
Bmp7	3.83	1.40	0.23	0.08	<0.01
Dhrs3	3.98	1.97	0.51	0.08	0.01
Foxn3	3.65	2.04	0.33	0.09	0.05
Idh1	2.40	0.93	0.99	0.55	<0.01
Rgs10	2.15	0.76	0.67	0.30	0.05
Ghr	1.48	0.15	0.36	0.14	0.03
Atp1b3	1.89	0.67	4.66	1.96	0.01
Apold1	1.64	0.46	0.53	0.24	0.03
Cmbl	2.91	1.76	0.57	0.17	<0.01

Table 37. Selected cluster 0 genes upregulated after treatment 10 mice with 3LL tumours were treated with control (5 mice) or MRTX1257 (5 mice). Tumour cells were extracted and subclustered. LFC (other) represents the mean $\log_2$ FC of that gene (MRTX1257 vs control) in all other clusters combined. Mean expr represents the normalised mean expression per cell. FDR = false discovery rate (Benjamini-Hochberg procedure) – representing the significance test of the null hypothesis that the cluster 0 LFC lies between zero and the average LFC in all other clusters.

While cluster 0 displayed some specific patterns of DE as described above, such specificity was not immediately obvious in other clusters except cluster 5, which has already been discussed above. We therefore next sought to explore the results of our DE analysis using established gene sets and other relevant data from the literature.

5.3.3.1 Gene set enrichment analysis

First, for each cluster, we ranked genes according to their $\log_2$ fold-change (MRTX1257 vs control) and then performed GSEA, initially using the hallmark gene sets (Liberzon *et al.*, 2015). Then, for each cluster, we ranked the normalised enrichment score (NES) of each gene set from lowest (most downregulated) to highest. The results of such ranking are shown for clusters 0-7 in heatmap form, in Figure 89.

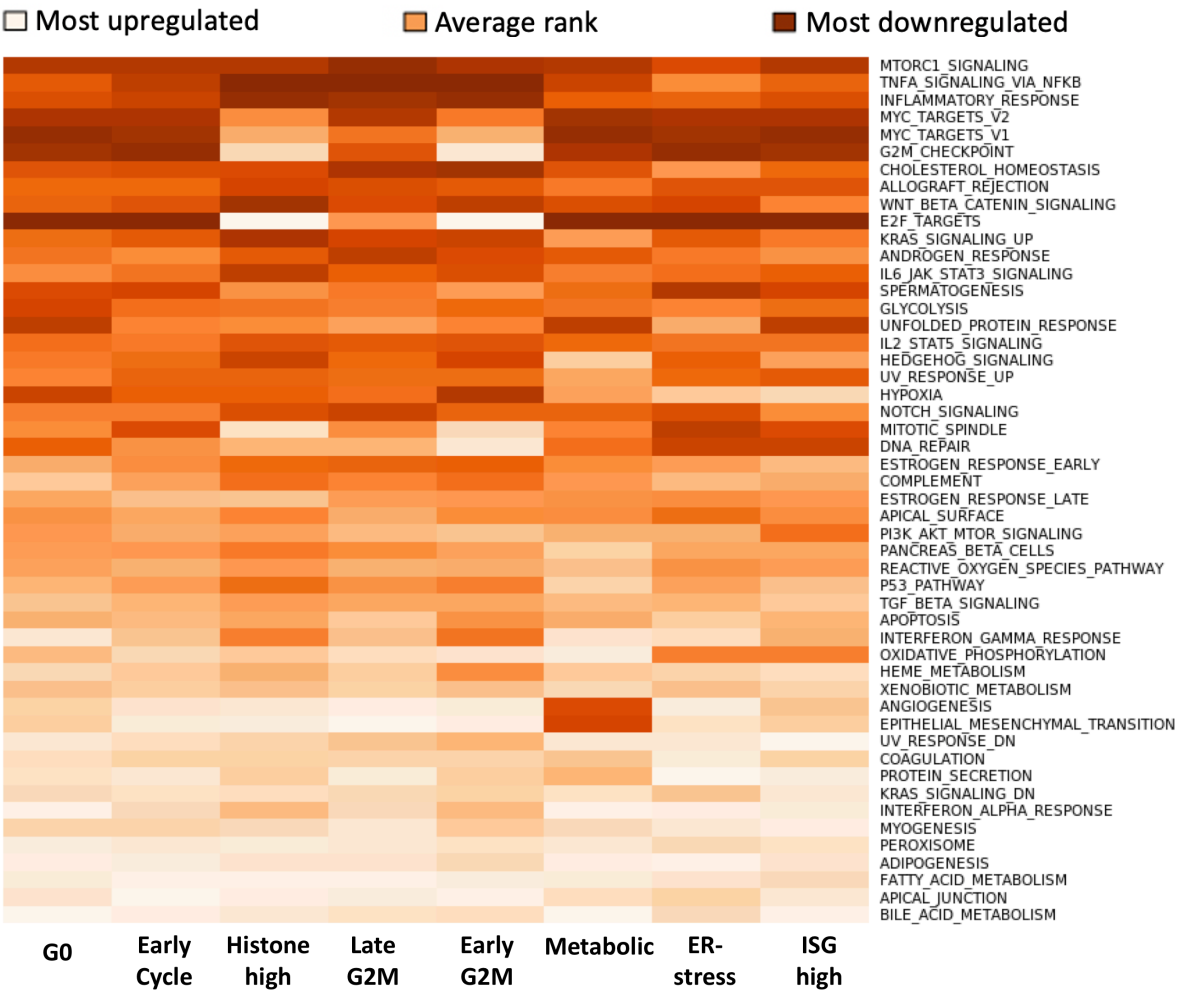

Figure 89. Heatmap of MSigDB hallmark ranks using GSEA10 mice with 3LL tumours were treated with control (5 mice) or MRTX1257 (5 mice). Tumour cells were extracted and subclustered before GSEA analysis. For each cluster, DE analysis (MRTX1257 vs control) was performed, and results used for GSEA on the MSigDB hallmark collection. Resulting normalised enrichment scores were ranked

per-cluster and displayed as above. Gene sets ordered by mean rank across clusters

As shown, several gene sets were consistently downregulated in all clusters, including those for MTORC1 signalling and TNFα signalling (via NFkB). Intriguingly, the E2F-target gene set had the lowest NES in 5 of the 8 clusters tested (0,1,6-8) but paradoxically had the highest NES in clusters 2 and 4 (Histone-high and Early G2M). In those clusters, where the E2F-target NES was negative, genes downregulated after MRTX1257 included Mki67, Ccnb2 and Top2a amongst others. In the clusters where the E2F-target set had the highest NES, upregulated gens included Ung (uracil DNA glyclosylase) and Stmn1 (stathmin – important for microtubule dynamics). Both of these were upregulated in MRTX1257 treated cells in clusters 2 (Histone-high) and 4 (Early G2M) but downregulated in MRTX1257 treated cells in clusters 0 (G0), 5 (Metabolic), 6 (ER-stress) and 7 (ISG). Of note, Myc-related and G2M gene sets showed the same pattern of rank (as the E2F-target set) across the clusters – with low NES scores in most clusters except clusters 2 and 4.

Genes in the leading edge (i.e. those most responsible for) the negative NES scores in the inflammatory and TNFα gene sets included Areg, Ereg, Plaur, Dusp5 Cxcl2 and Myc amongst others. Reassuringly, the 'KRAS_SIGNALLING_UP' gene set (representing genes that increase when KRAS is switched on) had negative NES scores across the cluster while the opposite gene set (those KRAS genes which decrease when KRAS is switched on) had positive NES scores across all clusters.

The other obvious outliers in the heatmap were the cluster 5 ('Metabolic') ranks for the EMT and angiogenesis sets. Most clusters had positive NES scores for these sets while cluster 5 had negative NES scores (-0.57 for the EMT set, FDR = 0.004 and -0.69 for the angiogenesis set, FDR = 0.11). For the EMT set, in clusters where the NES was positive, leading-edge genes included Col3a1, Col1a1, Dcn, Mgp, Sparc and Tgfbi. In cluster 5, the upregulation of many of these genes was much weaker (e.g. $\log_2$ FC for Col3a1 of just 0.5 compared to

a mean of 3.1 in all other clusters and a LFC of 0.23 for Sparc compared to a mean of 1.47 across other clusters). For this reason, underexpressed genes such as Areg, Plaur, Vegfa and Timp1 (which were in fact underexpressed across all clusters) and Spp1 (uniquely downregulated in cluster 5) resulted in a negative NES for the EMT gene set in cluster 5. The difference in the hallmark EMT gene set enrichment plots for clusters 0 and 5 can be seen in Figure 90.

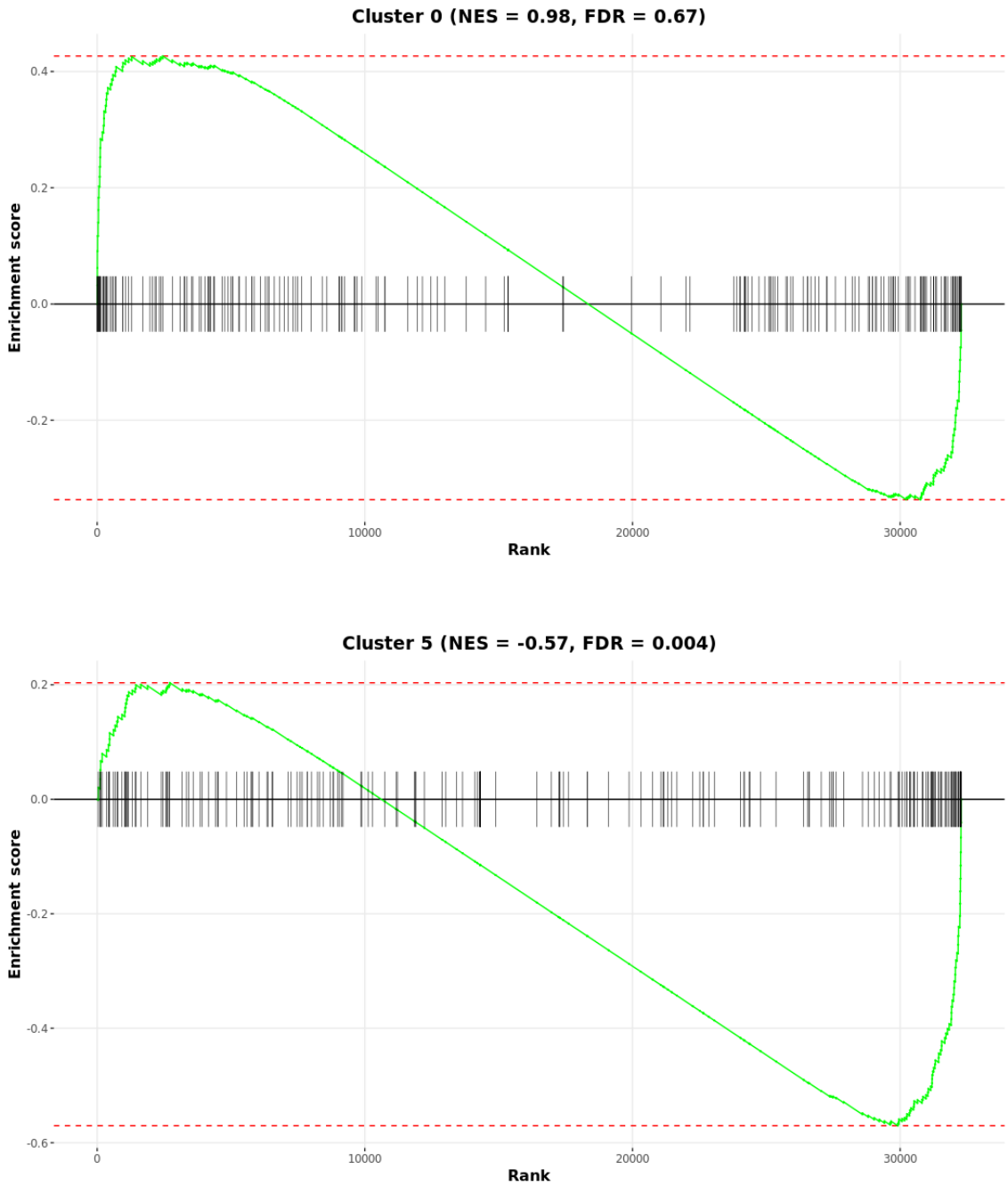

Figure 90. Hallmark EMT enrichment plots for tumour clusters 0 and 5

10 mice with 3LL tumours were treated with control (5 mice) or MRTX1257 (5 mice). Tumour cells were extracted and subclustered before GSEA analysis.

While the gene sets with the most negative NES ranks included those relating to MTORC1, NFkB and MYC signalling, the gene sets with the most positive NES scores across clusters included those pertaining to bile and fatty acid metabolism, genes encoding peroxisome components, genes encoding

components of the apical junction complex and those involved in the interferon alpha response.

Some of the common leading-edge genes for these gene sets are shown in Table 38.

Gene set	Leading edge genes
Bile acid metabolism	Idh1, Fdxr, Abcd1, Abca2, Abca3, Scp2 etc.
Fatty acid metabolism	Pcdb1, Idh1, Acaa2, Acadl, Cpt1a etc.
Apical junction	Vcam1, Tgfbi, Skpa2, Actn2, Jup etc.
Adipogenesis	Ddt, Cmbl, Atp1b3, Idh1, Apoe, Acaa2 etc.
Peroxisome	Dhrs3, Ech1, Lonp2, Acaa1a, Abcd1 etc.
Myogenesis	Col3a1, Fxyd1, Itgb5, Sparc, Actn2 etc.
Interferon alpha	Irf7, Herc6, Samd9l, Casp1, Ifi27 etc.

Table 38. Leading edge genes for sets with the most positive NES scores 10 mice with 3LL tumours were treated with control (5 mice) or MRTX1257 (5 mice). Tumour cells were extracted and subclustered before GSEA analysis per cluster. The leading-edge genes that appeared across the most clusters are listed (maximum of 5 per set are listed in the table above). All genes listed above were in the leading edge for at least 9 (out of the 10) clusters.

Of note, there was some redundancy in the leading-edge genes for some of the gene sets. For example, as shown in the table, Idh1, Actn2 and Acaa (acetyl-CoA acyltransferase) genes appear across multiple sets. Leading edge genes for the interferon alpha set were, however, distinct and included (not shown in the table above) Cd47, Cxcl10 and H2-D1, all of which could have implications for the antitumour immune response.

Next, we focussed on some specific gene sets pertinent to our experimental set up. Firstly, to add credence to our results, we looked at gene sets pertaining to KRAS signalling. There are two such sets in the Hallmark collection and several more in the C2 and C6 collections including the aforementioned Sweet-Cordero

and Singh-Settleman signatures. Full details of the MSigDB gene sets are available online (http://www.gsea-msigdb.org/gsea/msigdb/). We extracted all gene sets pertaining to RAS signalling, and removed any which solely focussed on a non-lung tumour type (e.g. prostate and kidney) before also adding the RAS84 signature (East *et al.*, 2021). For the remainder, per-cluster, we performed GSEA and have displayed the resulting NES scores in heatmap form (Figure 91).

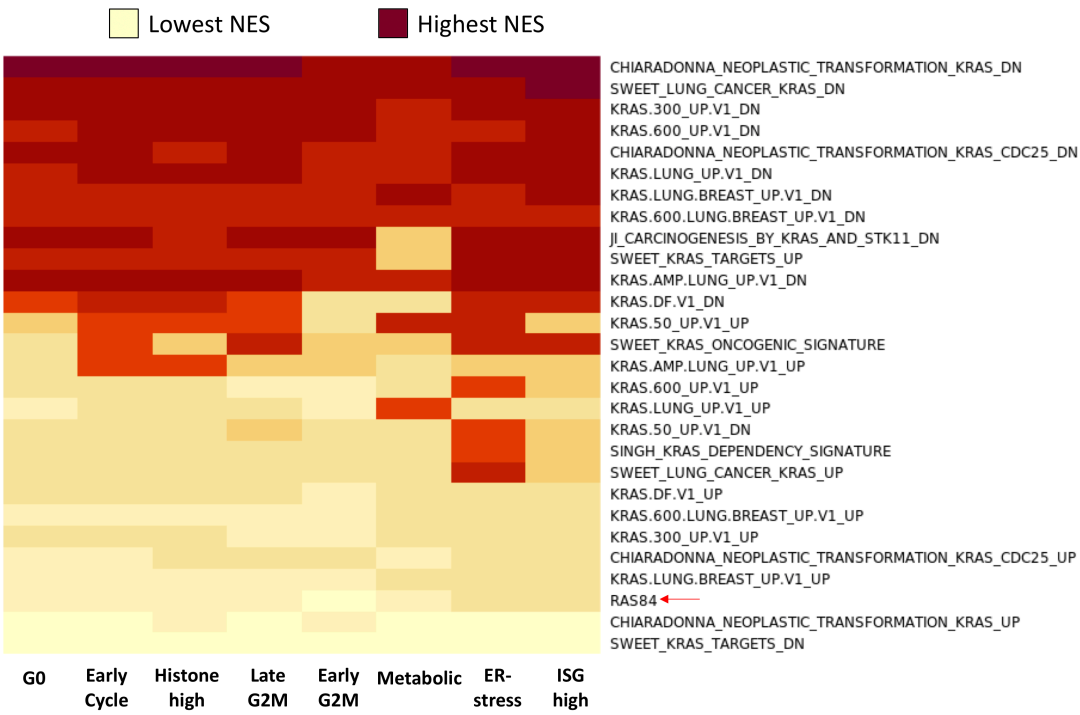

Figure 91. Heatmap of GSEA NES scores per tumour cluster for RAS-related sets 10 mice with 3LL tumours were treated with control (5 mice) or MRTX1257 (5 mice). Tumour cells were extracted and subclustered before GSEA was performed per-cluster using the $\log_2$ fold-changes between MRTX1257 and control treated cells. NES scores displayed as a heatmap. For reference, the lowest NES across the data was – 1.91 and the highest was 1.76. RAS84 signature indicated with red arrow. Gene sets are arranged by mean NES score across the clusters.

Although full details are available online, many of the gene sets represent differentially expressed genes following induction of oncogenic KRAS. The gene-set suffix 'DN' refers to sets containing genes whose expression decreased after such induction and vice-versa for the suffix 'UP'. Therefore, our data is as expected – sets containing genes that increase with KRAS induction

have mostly negative NES scores and vice-versa. Of note, the 'SWEET_KRAS_TARGETS_DN' set, which had the most negative mean NES score across clusters, represents genes that were upregulated in control vs KRAS knockdown cells, and therefore we would expect these genes to decrease (as seen above) with MRTX1257 treatment.

GSEA using the RAS84 signature showed consistently negative NES scores across the clusters. An example enrichment plot for cluster 1 ('Early cycle') is shown below (Figure 92).

Figure 92. Enrichment plot for RAS84 genes in cluster 1

10 mice with 3LL tumours were treated with control (5 mice) or MRTX1257 (5 mice). Tumour cells were extracted and subclustered before GSEA was performed per cluster

Next, we looked at gene sets related to apoptosis. There are several such gene sets across the C2 and C6 spectrum. While NES scores across clusters were generally quite homogenous (for any given gene set) we could not identify a clear pattern where gene sets all showing a similar effect (e.g. gene that go up with apoptosis) had similar NES scores. Of note, the gene sets relating to apoptosis often measured the effects of apoptosis induced by diverse stimuli e.g. serum starvation, TGF-β, CD40, TRAIL etc. and also across different cell

lines. For this reason, it may not be surprising that we did not see consistent effects in our data.

Nonetheless, the two gene sets with the highest mean NES scores (i.e. enriched for upregulated genes) across the data both represented genes that increase with apoptosis. The 'ALCALA_APOPTOSIS' set represents genes able to induce cell death in an expression cDNA library screen (Alcalá *et al.*, 2008) while the 'GRAESMANN_APOPTOSIS_BY_SERUM_DERPRIVATION_UP' represents genes upregulated in a cancer line (ME-A, murine breast) undergoing apoptosis upon serum starvation. Leading edge genes from the Alcalá set included Casp1, Casp4, Cd48 and Temem106c. Leading edge genes from the Graessman GSEA analysis incuded Irf7, Ogn and Gstm2 amongst others.

Furthermore, analysis of gene expression of the Kyoto Encyclopedia of Genes and Genomes (KEGG, (Kanehisa *et al.*, 2021)) apoptosis gene set revealed that of the 86 genes in the pathway, the 5 most upregulated genes after MRTX1257 treatment (mean $\log_2$ FC across the clusters) were Bad, Birc2, Tradd, Bcl2 and Ripk1 in that order. While Bad, Tradd and Ripk1 are pro-apoptotic, Birc2 and Bcl2 are pro-survival. The impact of treatment on expression of Bad and Bcl2 is shown in Figure 93. It is evident that although the expression of both increases, Bad is expressed at a higher level pre and post-treatment. In any case, the fact that both pro-and anti-apoptotic gene expression increased with treatment may make it difficult to infer clear effects with gene expression studies alone.

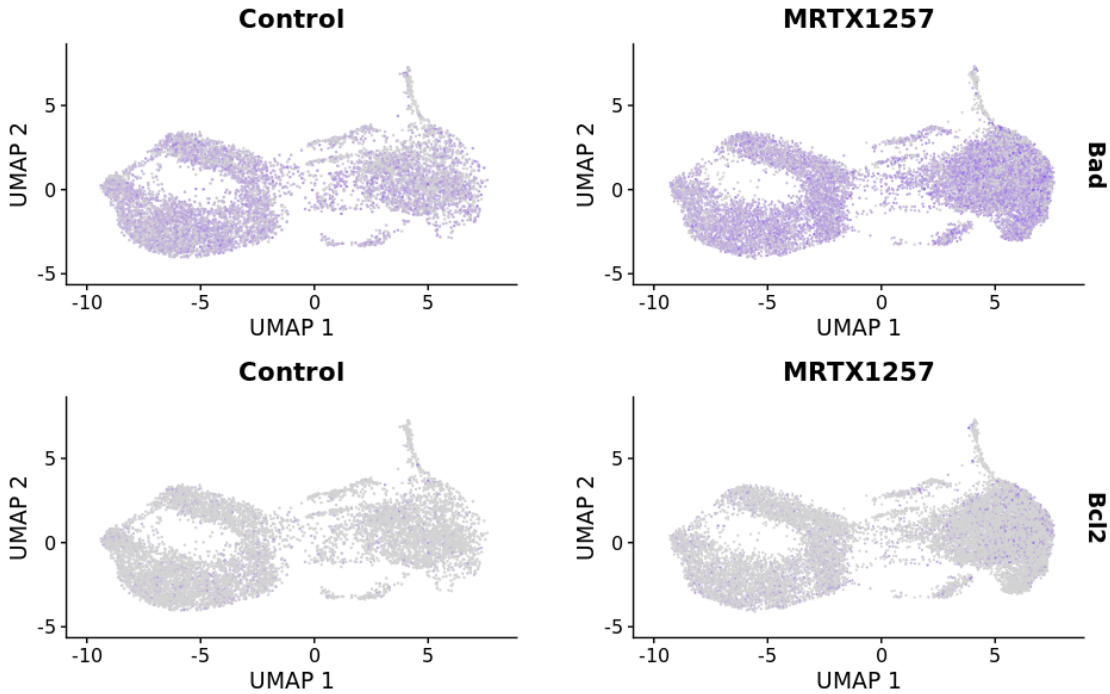

Figure 93. Effect of treatment on Bad and Bcl2 expression

10 mice with 3LL tumours were treated with control (5 mice) or MRTX1257 (5 mice). Tumour cells were extracted and subclustered. Figure shows expression of selected apoptosis genes in tumour compartment between untreated (left) and treated (right) cells.

5.3.3.2 Comparison to published data

Next, we compared our data to some published data in the hope that parallels between the two could help suggest robustness and external validity of our results.

Xue and colleagues (Xue *et al.*, 2020) performed single cell profiling of three KRAS(G12C) human lung cancer lines grown *in vitro* treated with a KRAS(G12C) inhibitor for varying durations. Separately, they used bulk RNA sequencing to devise two signatures. One represented genes induced by KRAS(G12C) (derived from those genes downregulated after KRAS(G12C) inhibition) and the other consisted of genes suppressed by KRAS(G12C) (derived from those genes upregulated after KRAS(G12C) inhibition).

They then applied the signatures to their single cell data. They found that, *in vitro*, single cells treated with KRAS G12C were mostly sequestered in a low output state (characterised by high scores on the 'KRAS suppressed' signature and vice-versa for the 'KRAS induced' score. However, some treated cells had a high output (high 'KRAS induced' score) which they described as heterogeneity of response. We therefore used their signature genes to generate signature scores for each of our treated and untreated cells. As shown in the density plots below (Figure 94), treated cells displayed a bimodal distribution of 'KRAS induced' signature scores, mirroring the data seen in Xue et al. Concomitantly, untreated cells, although also bimodal, were clearly shifted towards the higher end of the induced spectrum indicating that the majority of cells were in the induced rather than suppressed state. A similar conclusion could be reached when we projected the scores (for both the induced and suppressed signatures) onto UMAP plots (Figure 95).

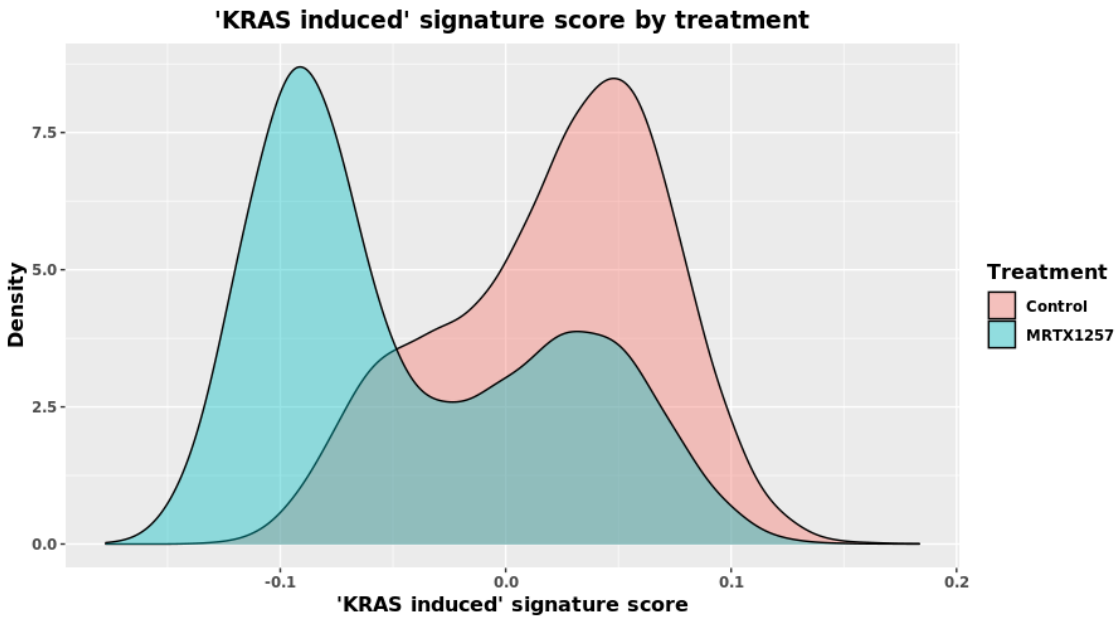

Figure 94. Density plot: 'KRAS induced' module scores 10 mice with 3LL tumours were treated with control (5 mice) or MRTX1257 (5 mice). Tumour cells were extracted and subclustered. Each tumour cell was assigned a module score based on the 'KRAS induced' gene set (Xue *et al.*, 2020)

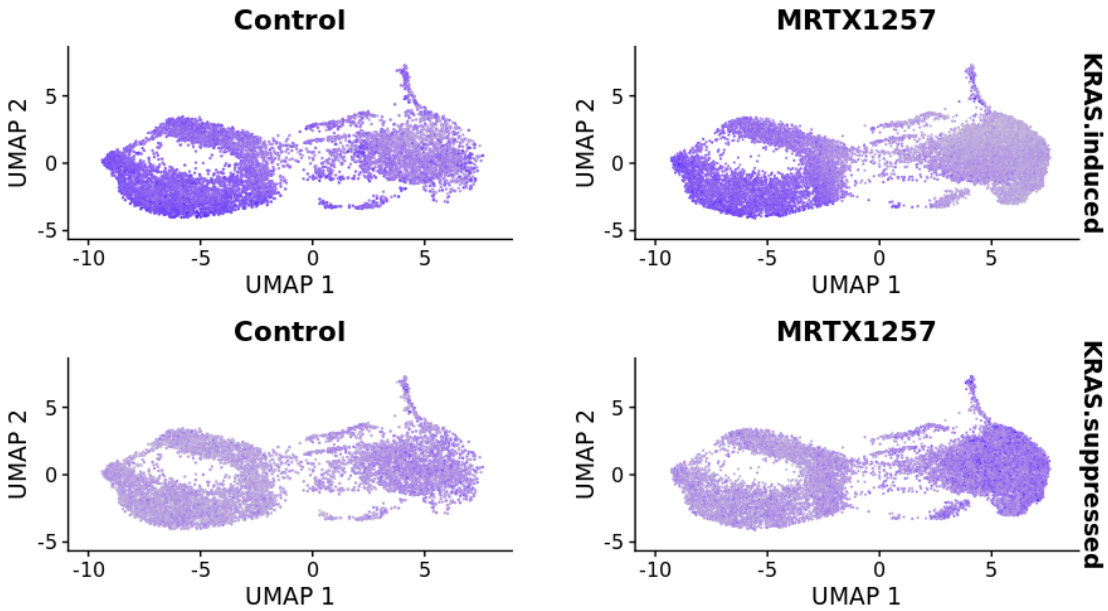

Figure 95. Visualisation of KRAS output module scores in UMAP space 10 mice with 3LL tumours were treated with control (5 mice) or MRTX1257 (5 mice). Tumour cells were extracted and subclustered. Each cell was assigned a module scores for the 'KRAS induced' and then the 'KRAS suppressed' gene sets from Xue et al. (Xue *et al.*, 2020).These scores were overlaid on the UMAP representation

As part of their investigation into the heterogeneity of response to KRAS(G12C) inhibition, they performed *in vitro* experiments where they used a non-cyclin-dependent-kinase binding p27 mutant as a marker of quiescence. This was based on observations that both p21 and p27 were induced (at the protein level) upon G12C inhibition in their models. In our single cells, we found that while Cdkn1b (gene for p27) was upregulated in treated cells, Cdkn1a (the gene for p21) was decreased in treated cells (Figure 96). Of note Xue measured p21 at the protein level, used different (human) KRAS(G12C) models, used ARS1620 for inhibition and operated *in vitro* – all of which could explain the differences seen here and indeed for any comparisons made.

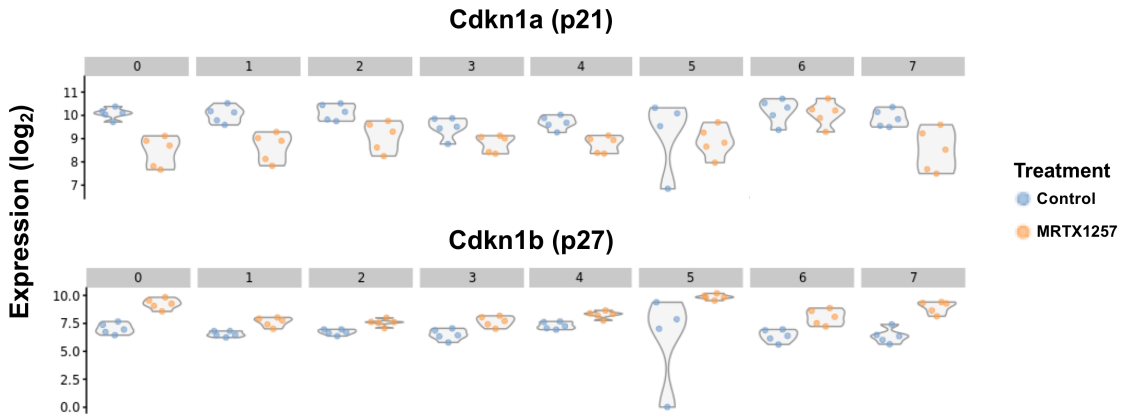

Figure 96. Pseudo-bulk expression of Cdkn1a/b across clusters 10 mice with 3LL tumours were treated with control (5 mice) or MRTX1257 (5 mice). Tumour cells were extracted and subclustered. For each tumour cluster, a pseudo-bulk dataset was created for each sample (control samples in blue). Log_2 normalised expression (normalisation using library size). was plotted for each sample, within each cluster. Numbers in grey bars indicate the cluster number.

Xue et al. also generated trajectories from their single cell data. They suggested that many treated cells fall along an inhibited trajectory while others along an 'adapting' trajectory that may progress toward treatment insensitivity. They compared different clusters along these trajectories and identified DE genes between them. Some of these genes, including Hbegf (heparin binding epidermal growth factor), Aurka (Aurora kinase a) and Kras were also identified in a separate sgRNA screen they had performed to look for modifiers of treatment response. They showed that expression of these genes could be localised to different areas of their low-dimensional representation of single cells. We also looked at expression of these genes in our data to see if we could identify isolated clusters of cells which may draw parallel with their observations.

Figure 97 shows that Hbegf is expressed in all clusters although within cluster 0 specifically, its expression is highest in a locality of UMAP space. This could be consistent with the observations of Xue et al, where Hbegf expression was highest in cells that were 'adapting' to treatment although we cannot say this for certain without also running trajectory inference. In addition to being localised to this area of low-dimensional space, we also noted that Hbegf expression was

moderately increased in treated vs. control cells in non-cycling clusters (clusters 0,5,6,7 e.g. $\log_2$ fold-change = 0.43 in cluster 0). In correlation analysis, Hbegf gene was most highly correlated with several immediate early genes (IEGs) including Fos, Fosb, Klf6 and Dusp1. These genes also showed highest expression in a similar area of UMAP space (
Figure 98) and were upregulated after MRTX1257 although unlike Hbegf they were upregulated in all clusters and not just non-cycling ones. Of note, Dusp1, Fos, Klf6 and Zfp36 (as well as Hbegf) are all part of the RAS84 signature. As shown above, the signature tended to show a negative per-cluster NES when using GSEA on the DE genes between MRTX1257-treated and control cells (suggesting most genes are downregulated by treatment). However our data show that, in this model, this module of genes (containing IEGs) increases with KRAS(G12C) inhibition suggesting they may be co-regulated . Finally, when exploring genes correlated with Hbegf, as well as the IEGs listed we noted that Wee1 also had one of the highest correlations. Its expression also increased with treatment. For example, the $\log_2$ fold-change of Wee1 between MRTX1257 and control treated cells in cluster 0 was 0.79 ($p < 0.001$). Interestingly, an inhibitor of Wee1 is being used to treat KRAS-mutated colorectal carcinoma (Seligmann *et al.*, 2021).

Figure 97 also shows localised expression of Aurka. In Xue et al this gene was most highly expressed at the end of their adapting trajectory, which they showed consisted mostly of cycling cells. In our dataset, expression was highest in clusters 4 (early G2M) and 3 (late G2M) which is not surprising given the role of the protein product of this gene in the cell cycle (Willems *et al.*, 2018). It is also not surprising that, as an important component of the cell cycle, it was identified as being a modifier of the therapeutic response to ARS1620 in the sgRNA screen by Xue.

Finally, Xue et al had identified Kras as being upregulated in the most quiescent cells in their data. We did not detect any gradient of Kras expression in our data. When looking at DE between each cluster and all other clusters, Kras

expression was not increased in any one cluster. However, cluster 5 ('metabolic' cluster) had a lower Kras expression compared to all other clusters ($\log_2$ fold-change = -0.43, $p < 0.001$). In addition, Kras expression was not significantly different in MRTX1257 treated cells vs control cells (in any cluster) and the same was true for the other ras isoforms (data not shown).

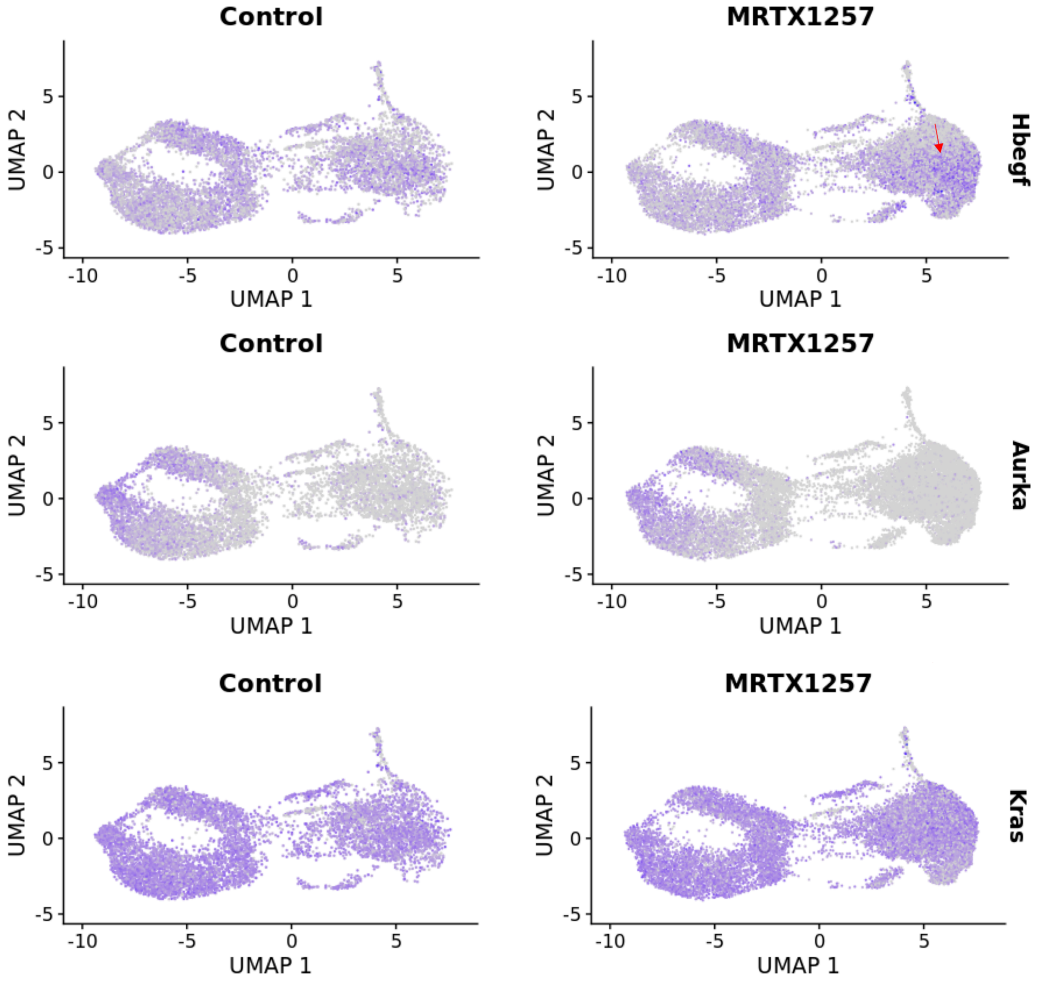

Figure 97. UMAP visualisation of key genes from Xue et al. 10 mice with 3LL tumours were treated with control (5 mice) or MRTX1257 (5 mice). Tumour cells were extracted and subclustered. Red arrow in top panel indicates the area of tumour cluster 0 with highest expression

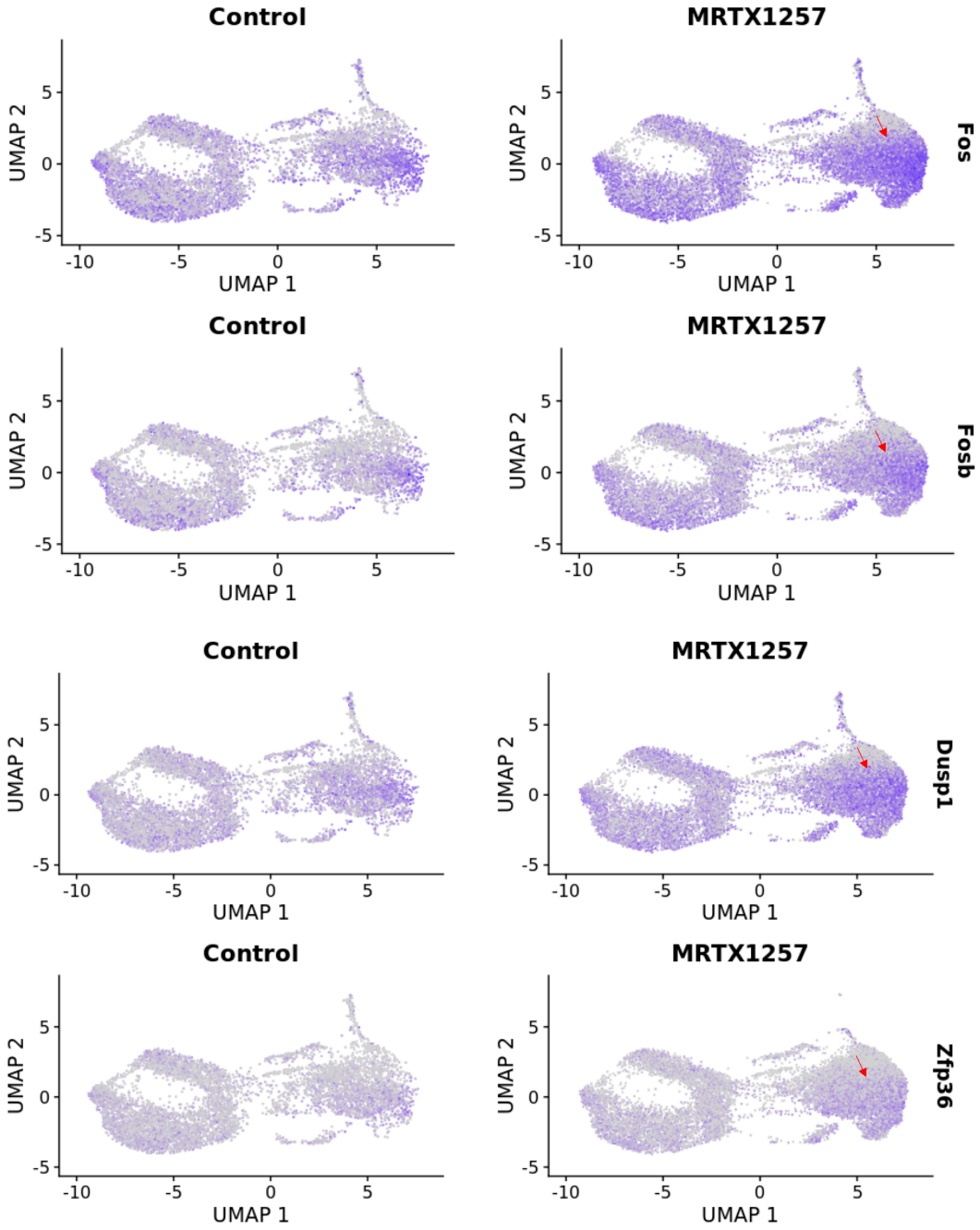

Figure 98. UMAP visualisation of selected IEGs 10 mice with 3LL tumours were treated with control (5 mice) or MRTX1257 (5 mice). Tumour cells were extracted and subclustered. Red arrows indicate area of tumour cluster 0 with highest expression

5.3.3.3 Expression of immune-related genes

The analysis above focussed mainly on unbiased approaches by generating lists of DE genes or using GSEA. In addition, below, we chose to specifically look at genes known to be involved in immune responses.

First we looked at a set of genes that was generated in our lab by Edurne Mugarza who performed RNA sequencing on 3 cell lines grown *in vitro*: H358 and H23 lines (KRAS(G12C)-mutated human lung cancer) treated with control or ARS-1620 and AT2 cells (human type II pneumocyte) that were engineered in our lab to express a tamoxifen-inducible KRAS(G12V) allele (Molina-Arcas *et al.*, 2013). DE analysis was performed to discern which genes were significantly downregulated ($p < 0.05$) when KRAS was inhibited (H358/H23) or not switched on (AT2). Of the 485 genes in common between the 3 lines, 84 were members of one of more immune gene sets from GSEA.

We looked at the per-cluster $\log_2$ fold-change of these 84 genes (Figure 99). As shown in the heatmap, the majority of genes were downregulated across tumour clusters indicating consistency with the *in vitro* data across the three other lines and supporting the hypothesis that some genes are robustly suppressed when inhibiting KRAS across models. Suppressed genes included Lif, Plaur, Vegfa, Pvr and Cxcl2, all with known immunosuppressive function.

Figure 99. Log fold-change of KRAS-regulated immune genes per cluster 10 mice with 3LL tumours were treated with control (5 mice) or MRTX1257 (5 mice). Tumour cells were extracted and subclustered. Pseudo-bulk datasets were created per-cluster and $\log_2$ fold-change calculated between treated and non-treated cells. White spaces indicate inability to calculate $\log_2$ fold-change due to low counts.

After demonstrating that many of the same genes are downregulated by KRAS across models, we next looked at specific groups of genes involved in defined immune functions (Figure 100, Figure 101). The headings used to group these genes have been loosely applied.

As shown, many genes related to interferon signalling were upregulated upon KRAS(G12C) inhibition. The effect was generally consistent across clusters. While the changes did not often reach statistical significance (FDR < 0.1) the consistent change across clusters (and the agreement with other data from the lab (Mugarza *et al.*, 2021)) gives us confidence in the DE is a reflection of true biological effect. Exceptions to the rule included Tap1 (which was generally expressed at low levels in any case) and Stat3, both of which tended to decrease while the other genes related to interferon signalling trended toward increased expression upon KRAS(G12C) inhibition. In addition Myc, which has recently been shown by our lab to contribute to the ability of oncogenic KRAS to suppress intrinsic interferon-related signalling (Mugarza *et al.*, 2021) was robustly and significantly suppressed across clusters (Figure 101, bottom panel) as was Socs1 (suppressor of cytokine signalling 1), a negative mediator of the interferon pathway.

In terms of inflammatory genes, both Il1b and Il6 were suppressed as was Cxcl2, albeit to a lesser degree. Immunosuppressive mediators were generally downregulated too, with Vegfa in particular showing robust and significant suppression.

Finally, given the copious myeloid infiltration in these tumours, we looked at two targets pertinent to myeloid biology in tumours. Secreted gelsolin has recently been shown to be important in tumours' ability to subvert dendritic cell function (Giampazolias *et al.*, 2021) while tumour-expressed CD47 is known to contribute to tumour-avoidance of macrophage phagocytosis (Tseng *et al.*, 2013). We therefore looked at expression of both of these genes. To our surprise, treatment induced an increase in both genes. Cd47, in particular, was

significantly upregulated in 7 of the 8 clusters where DE testing was performed. Given the re-polarisation of the macrophage compartment in MRTX1257-treated samples that we have seen in our dataset, our observation raises the question whether anti-CD47 therapy could help mediate more effective anti-tumour response when given with KRAS(G12C) inhibitor therapy. Clinical trials of CD47-blocking therapy are already underway (Lakhani *et al.*, 2020; Garcia-Manero *et al.*, 2021).

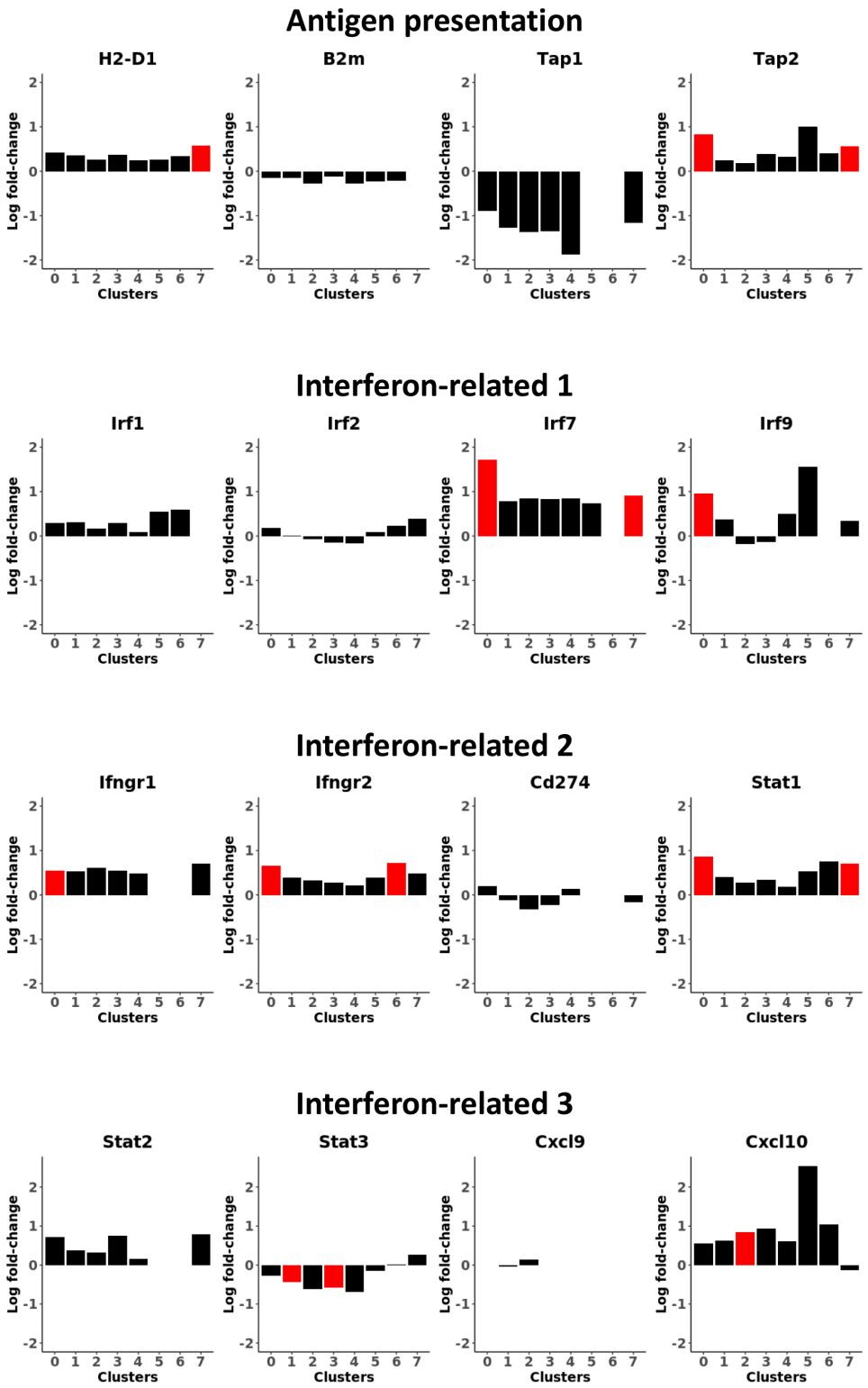

Figure 100. Per-cluster log fold-change of immune mediators (1)10 mice with 3LL tumours were treated with control (5 mice) or MRTX1257 (5 mice). Tumour cells were extracted and subclustered. Pseudo-bulk datasets were created for each tumour cluster and log-fold changes between treated and control cells calculated. Red bars indicate significant DE (FDR < 0.1) using a quasi-likelihood negative binomial model. Missing bars indicate not enough data to compute DE.

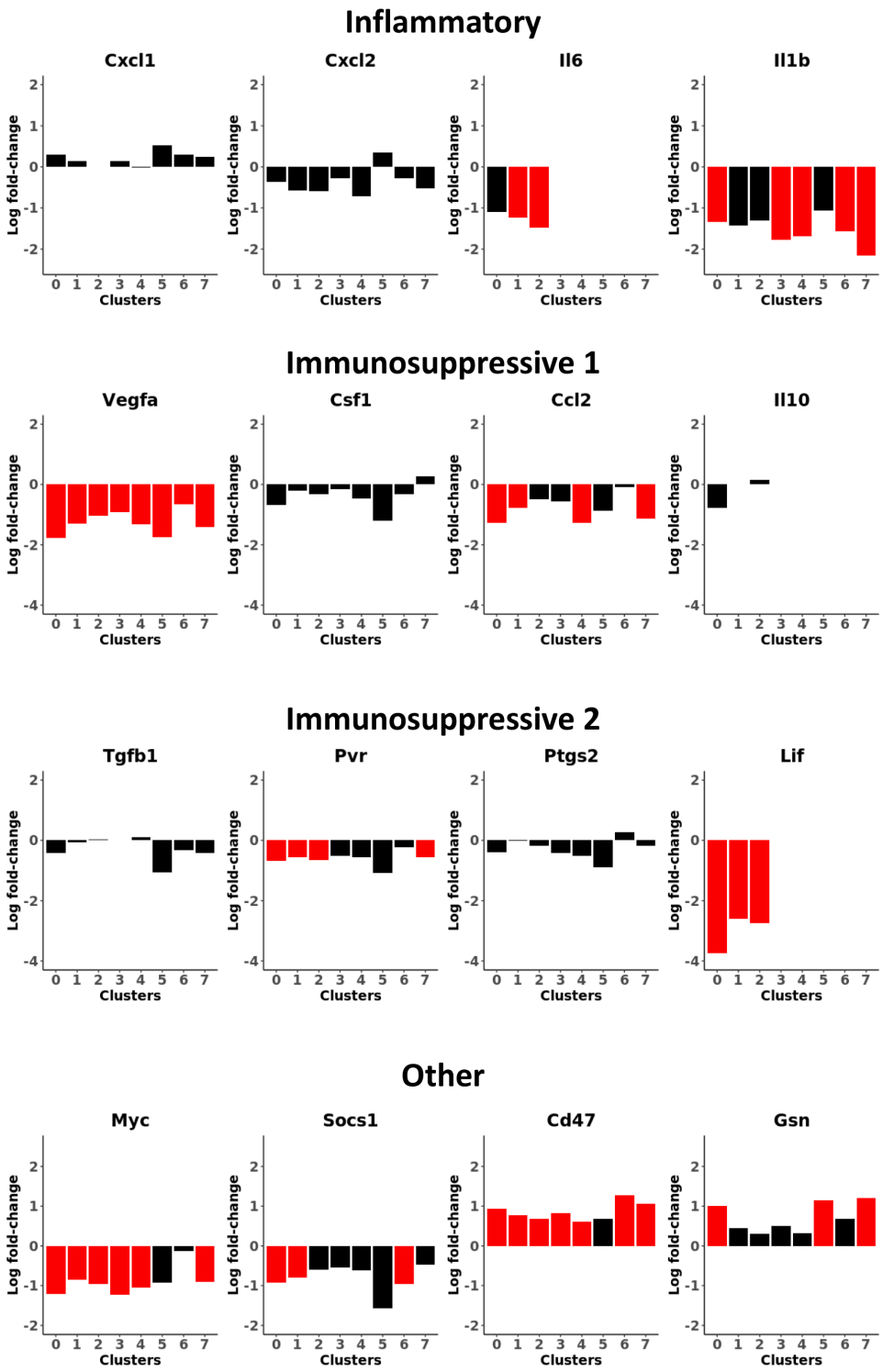

Figure 101. Per-cluster log fold-change of immune mediators (2) 10 mice with 3LL tumours were treated with control (5 mice) or MRTX1257 (5 mice). Tumour cells were extracted and subclustered. Pseudo-bulk datasets were created for each tumour cluster and log-fold changes between treated and control cells calculated.

Red bars indicate significant DE (FDR < 0.1) using a quasi-likelihood negative binomial model. Missing bars indicate not enough data to compute DE.

5.4 Concluding remarks

Treatment of 3LL-ΔNRAS tumours with MRTX1257 resulted in compositional and gene expression changes within the macrophage compartment and, to a lesser extent, gene expression changes within the DC compartment. In general, putative protumourigenic genes such as Arg1, Vegfa and Ptgs2 were downregulated while anti-tumourigenic ones such as class II MHC genes were upregulated. Although we identified several different clusters with unique gene expression patterns, the effect of treatment on gene expression within each cluster was fairly congruent.

We also identified distinct clusters within the tumour compartment, which showed parallels with cell cycle state prediction. Differential expression in the tumour compartment was more marked than in the myeloid compartment, an expected effect given the mutant specific nature of the drugs. MRTX1257 treatment resulted in most treated cells being in the G0/G1 cluster, however a significant proportion of tumour cells remained in the cell cycle. This is consistent with previously published data in this field although our data was *in vivo* in contrast to the *in vitro* data previously published (Xue *et al.*, 2020). Finally we saw that many immunosuppressive transcripts are downregulated in tumour cells after MRTX1257 treatment, with the notable exception of Cd47 and Gsn, raising the possibility of combination treatments targeting these proteins.

Chapter 6. Discussion

6.1 Tristetraprolin, cancer and KRAS

Our interest in TTP stemmed from work done by Matthew Coelho in the Downward lab, who showed that it could destabilise PD-L1 transcripts and that its function was inhibited by signalling downstream of oncogenic RAS. Furthermore, several transcripts that have been suggested to be regulated by TTP are also established RAS-targets (Brooks and Blackshear, 2013b; Cullis, Das and Bar-Sagi, 2018).

TTP has been suggested to be a tumour suppressor (TSG). This assertion is based on two classes of observation (Sanduja, 2011; Guo *et al.*, 2017). Firstly, TTP mRNA expression is suppressed, relative to normal tissue, across many human malignancies. Secondly, TTP has been shown to reduce the mRNA stability of oncogenic transcripts across the spectrum of cancer hallmarks. Despite these observations, studies investigating TTP in the context of malignancy have mainly focussed on just one, or a few, targets in any given model studied. We sought to first investigate the expression of TTP at the mRNA level across several human malignancies, and secondly to investigate the transcriptome-wide effect of TTP in an immunogenic KRAS-mutant tumour model.

Using publicly available data from TCGA, we confirmed that TTP is indeed reliably suppressed across several human malignancies. We extended this observation to show that, across the genome, the magnitude by which TTP is suppressed is amongst the highest of all genes, in several tumour types. As above, these types of observation have contributed to suggestions that TTP is a tumour suppressor. However, in an exploratory observation of bona fide tumour suppressors including tumour protein 53 (p53) and breast cancer type 1 susceptibility protein (BRCA1), across the same tumour types, we noted a paradoxical increase in their expression in several malignancies compared to normal tissue (data not shown). This is consistent with studies suggesting that

both increased p53 or BRCA1 expression actually correlate with worse prognosis and/or more aggressive disease (Huang *et al.*, 2014; Chang *et al.*, 2022). Therefore, TSG expression is not necessarily a reliable guide to function. We also note that TTP is capable of destabilising its own transcripts (Tchen *et al.*, 2004) therefore confounding attempts to correlate its expression with its functional capacity. Furthermore, review of repositories containing data about mutation frequencies within cancers, for example the catalogue of somatic mutations in cancer (COSMIC, cancer.sanger.ac.uk, (Tate *et al.*, 2019)) show low mutation rates without any hotspots at the ZFP36 locus. It has been shown that TTP is completely inactivated by mutations of its zinc finger domain (Lai *et al.*, 2017) however these are not seen in human cancers. While none of this refutes the possibility that TTP is a tumour suppressor, it cautions against using its reduced expression as supportive evidence.

We also noted that ZFP36 expression tended to correlate with its targets, rather than anticorrelate as one might expect. We discovered that across malignancies, there were several genes with very high correlations with ZFP36 and one another. Immediate early genes (IEGs) formed the bulk of this module, an observation not necessarily unexpected given that the discovery of ZFP36 followed investigation of a gene induced by serum and phorbol esters – both stimuli known to induce IEGs (Bahrami and Drabløs, 2016). These same genes are repressed in malignant tissue compared to normal, in a similar manner to ZFP36, suggesting that the reduced ZFP36 expression we see across cancers may be part of a repressed module. Studies in the literature had mostly looked at ZFP36 expression in cancer in isolation without any comment on concomitantly suppressed genes. We believe that in the majority of tumours where ZFP36 is suppressed relative to normal tissue, this occurs as part of a broader gene expression program. We note that EGF has been shown to promote TTP expression via ELK-1 and EGR-1 (Florkowska *et al.*, 2012) and that ELK-1 can promote IEG expression (Sgambato *et al.*, 1998) suggesting that this could be part of the mechanism co-ordinating their expression. Furthermore, as mentioned in the introduction, RAS can activate Elk-1,

therefore linking RAS to this mechanism. Further work would require co-expression network analysis, for example using weighted gene co-expression network analysis (Zhang and Horvath, 2005) to more formally identify the module of genes co-expressed with ZFP36. In addition, transcription factor binding site analysis may suggest shared motifs and possible transcriptional regulators.

One apparent paradox is that while this module of genes appears to be repressed across malignancies, within LUAD samples expression was lowest in KRAS wild-type tumours (and samples with low RAS84 signature scores) and highest in RAS-mutant cancers. This is compounded by the fact that traditionally, the protein products of IEGs promote proliferation (Healy, Khan and Davie, 2013) and indeed work from another lab at the Francis Crick Institute showed that dysregulated FOS expression (via a mutant transcript lacking AU-rich and other 3' UTR regulatory sequences) is a ubiquitous hallmark of osteoblastoma (Fittall *et al.*, 2018). Nonetheless, it is also known that IEG expression is tightly regulated, temporally such that although they may rise acutely after mitogenic stimuli, this rise is short-lived. Furthermore there is some evidence that deregulated expression of FOS can lead to chromosomal instability and replicative failure suggesting that repression of IEG expression in cancers may be a protective mechanism (Guo *et al.*, 2021).

Following exploration of ZFP36 expression across human malignancies we looked at the effects of overexpressing Zfp36 in CT26 cells, an immunogenic murine colorectal carcinoma model. Initially we assayed individual transcripts using qPCR and showed that Ptgs2 was robustly suppressed by ZFP36 overexpression, but Myc (another literature-defined TTP target (Marderosian *et al.*, 2006)) was not, underscoring the model-dependent nature of TTP specificity. After demonstrating that ZFP36 overexpression affected target transcript stability, we performed RNA-sequencing to interrogate the transcripome-wide effect of TTP overexpression. While Ptgs2 was robustly

suppressed, to our surprise amphiregulin (gene Areg) was also robustly suppressed by TTP overexpression using both Tet-On TTP(wt) and Tet-On TTP (aamt) lines. At the time of conducting the experiments, Areg was not a known TTP target although it has since been described by a single group looking at TTP expression in keratinocytes (Assabban *et al.*, 2021).

Using gene set enrichment analysis, we showed that several of the most downregulated gene sets were those important in oncogenic processes, including MYC targets, TNFα signalling-related genes, inflammatory response genes, those involved in MTORC1 or PI3K/ATK/mTOR signalling and cell cycle-related gene sets including E2F targets and G2M checkpoint genes. All of these gene sets had a negative NES and were significantly enriched for downregulated transcripts in the CT26 Tet-On TTP(aamt) line and were downregulated (but not all reached significance) in the CT26 Tet-On TTP(wt) line. Conversely, the gene set pertaining to EMT was significantly enriched for downregulated transcripts in the CT26 Tet-On TTP(wt) line and was enriched for downregulated transcripts (but not significantly) in the CT26 Tet-On TTP(aamt) cell line.

The breadth of gene sets related to oncogenic processes that were enriched for downregulated transcripts upon TTP overexpression would add credence to the suggestion that TTP functions as a tumour suppressor. In addition to the sets mentioned above, the unfolded protein response (UPR) set was significantly enriched for downregulated transcripts in both cell lines. The UPR can help tumour cells adapt to nutrient and oxygen deprivation, and thus promote cell survival (Madden *et al.*, 2019). Conversely, overactivity of this pathway can promote apoptosis (Huang *et al.*, 2021). It is therefore difficult to predict the functional consequences of TTP's effect on this pathway. Perhaps less ambiguous, is the potential consequence of TTP's effect on tumour intrinsic interferon-signalling. The interferon alpha and gamma sets were both enriched for downregulated transcripts in the Tet-On TTP(aamt) line, but not in the Tet-On TTP(wt) line. We cannot therefore be sure about the robustness of this

effect. Tumour-intrinsic interferon signalling can increase expression of antigen presentation components and T cell chemoattractants such as CXCL9 and CXCL10 (Mugarza *et al.*, 2021) and therefore suppression of such signalling may have pro-tumourigenic consequences. However, the effect is likely more nuanced, depending on the concentration and chronogenicity of signalling as evidenced by two studies which suggest that sustained type I or II interferon signalling can mediate resistance to immune therapy (Benci *et al.*, 2016; Jacquelot *et al.*, 2019).

The effect of TTP overexpression on gene sets that are both potentially pro and anti-tumour suggests that the overall effect may be determined net balance of the two processes. This was alluded to in the introduction by reference to a study where TTP destabilised LATS2 (a TSG) yet also E2F1 and cIAP2 (Lee *et al.*, 2018) with consequential suppression of proliferation, invasion and metastasis in that model. Our data support the idea that TTP does not purely affect classical oncogenic transcripts but instead has a broad, non-specific effect which may favour destabilisation of oncogenic transcripts, but not exclusively. The other point of note here, is that we did not see any obvious difference in the magnitude of downregulation of key oncogenic transcripts (e.g. Ptgs2 ,Areg, Lif) between the Tet-On TTP(aamt) and Tet-ON TTP(wt) lines. While the aamt-TTP should be less sensitive to inactivation by p38-mediated signalling, we note that evidence in the literature suggests that serine 316 can also be phosphorylated by MK2 (Ronkina *et al.*, 2019) while our aamt-TTP was only mutated at serines 52 and 178. Furthermore, the forced overexpression of TTP in our system may overwhelm the capacity of the relevant kinases to inactivate it.

After exploring the transcriptome-wide effects of TTP overexpression using GSEA, we sought to create a ‘signature’ of genes downregulated by TTP overexpression and test whether this could predict survival in TCGA data. In a previous section, we were unable to show any effect of expression of TTP and its correlated genes on survival (Figure 11) and so we reasoned that a better

predictor may be to look at the functional effects of TTP, by using expression of the genes that it regulates in our system. We found that this did in fact predict survival in both LUAD and COAD cohorts from TCGA. We therefore feel that any attempts to use TTP for prognostication should focus on the expression of its downstream targets rather than of TTP and/or its co-regulated genes themselves. We appreciate that these targets are regulated by other mediators too, and therefore we could never attribute the survival effect seen with our signature directly to TTP. We have therefore shown that lower expression of genes regulated by TTP in our system is associated with improved survival in the LUAD and COAD TCGA cohorts.

Finally, we sought to look at the overlap between genes regulated by TTP and those by KRAS. As well as Areg and Ptgs2, two other known KRAS targets (polo-like kinase 3 (Plk3) and leukaemia inhibitory factor (Lif)) were also in the top 10 most strongly downregulated targets across both inducible-TTP cell lines. Beyond these most strongly downregulated genes, many other genes known to be regulated by KRAS were also significantly downregulated upon TTP overexpression, including plasminogen activator urokinase receptor (Plaur), Vegfa, immediate early response 3 (Ier3), cardiotrophin-like cytokine factor 1 (Clcf1), Ereg and Bmp2 amongst others. While Clcf1 has previously been identified as a TTP target in a single study (Ross *et al.*, 2015), to our knowledge Ereg and Bmp2 have not. Nonetheless, one study identified that the 3'-UTR of Bmp2 is highly conserved across mammalian species, and the same group identified a protein that bound to the 3'-UTR of the Bmp2 transcript, with a molecular weight similar to TTP, without explicitly identifying said protein (Fritz *et al.*, 2006). While Ereg has not been shown to be regulated by TTP, it does contain TTP consensus motifs in its 3'-UTR (Qiu *et al.*, 2015). Both Bmp2 and Ereg have pro-metastatic/tumourigenic properties and so their identification as potential TTP targets is relevant to the link between TTP and tumorigenesis (Sunaga *et al.*, 2013; Huang *et al.*, 2017).

Given the circumstantial overlap between TTP and KRAS targets, and the biological plausibility that the effect of KRAS on many of these genes is driven, at least in part, by TTP we sought to perturb both in the same model to identify whether one could modify the effect of the other. Using siRNA we achieved between 70-80% knockdown of Zfp36 and observed for effects on the ability of KRAS(G12C) inhibition to downregulate its targets. Despite good knockdown of Zfp36, there was only a modest rise in Ptgs2 expression (the most strongly-regulated TTP target in this system) and no significant difference in Ptgs2 suppression upon addition of KRAS(G12C) inhibitor. Other genes (Lif, Areg) behaved similarly. There are several reasons for the failure to see an obvious effect of Zfp36 knockdown on gene expression changes following KRAS(G12C) inhibition. Firstly, in this system, the effect of KRAS(G12C) inhibition on Ptgs2 expression was small (around a 40% reduction in expression) meaning that a subtle effect of TTP knockdown may be hard to see. Secondly, the Zfp36 knockdown itself was incomplete. While we attempted western blots to confirm decreased protein expression, these were technically challenging with the available antibodies and ultimately we could not draw firm conclusions. We also attempted to knock out the endogenous Zfp36 locus using CRISPR/Cas9 but did not achieve this, again due to technical reasons. Beyond these technical challenges, we also note that KRAS signalling networks are broad, complex and redundant such that any effect of Zfp36 knockdown may be compensated for through bypass signalling. Finally, ZFP36 is part of a family of three RNA-binding proteins (the other being ZFP36L1 and ZFP36L2) and there is incomplete understanding of their binding specificity. As an example, while our lab showed that TTP can destabilise Cd274 transcripts (Coelho *et al.*, 2017), it has also been shown that deletion of Zfp36l2 and Zfp36l2 loci results in increased PD-L1 mRNA suggesting some redundancy in certain systems.

In conclusion, TTP expression is robustly suppressed across several malignancies, likely as part of a module of immediate early genes. It destabilises several targets with oncogenic properties, but more evidence is needed to confirm whether it is truly a relevant TSG in human malignancies. In

an immunogenic colorectal carcinoma model, its overexpression results in downregulation of several gene sets related to tumourigenic hallmarks and also slows tumour growth *in vivo*. Targets in said model include established TTP targets (Ptgs2, Areg, Lif and Plaur amongst others) and the putative novel targets Bmp2 and Ereg. Its targets significantly overlap with those of KRAS, and this effect is seen across model systems. To determine whether TTP directly contributes to the ability of KRAS(G12C) inhibitors to downregulate certain shared targets, TTP would need to be robustly suppressed at the protein level and suitable targets will need to be assayed to establish a relationship.

6.2 CITE-seq analysis

We sought to use CITE-seq to understand the single cell effect of KRAS(G12C) inhibition in an orthotopic murine lung cancer model. This was the first time this technique had been used in our lab. Through our attempts to optimise antibody concentration using flow cytometry, we discovered that our in-house dissociation protocol resulted in preservation of fewer immune cells than the commercial dissociation method that we used. Our in-house method uses a variably prolonged mechanical dissociation step. It has been shown that such techniques can cause disproportionate cell death due to differential sensitivity of individual cell types (Leelatian *et al.*, 2017). For this reason, we took forward the commercial dissociation protocol for the CITE-seq experiment proper.

When planning our experiment, we discussed whether or not to sort our dissociated cells using a live/dead marker. This was based on the trade-off between the prolonged ‘scalpel-to-sequencer’ time required to incorporate a sorting step (we estimated roughly 60-120 minutes extra time required for sorting) versus potentially sequencing dissociated cells with a high proportion of dead/dying cells if we did not sort. We elected to incorporate a sorting step based on variable viability after tumour dissociation during our antibody-concentration optimisation exercise, and the high percentage of dying cells debris that we saw during flow cytometry. Nonetheless we have also performed

a separate experiment where we have bulk-sequenced tumours and cells in suspension at various steps of our single-cell protocol, so that we can better understand the effect that our dissociation procedure has on the transcriptome. This is based on evidence that certain genes, including IEGs, may be sensitive to the dissociation procedure (Denisenko *et al.*, 2019). This is borne in mind during analysis of our CITE-seq data. Of note, both treated and untreated cells were dissociated using the same procedure, but it is impossible to rule out treatment-specific vulnerabilities to the dissociation procedure. This is an inherent caveat of single cell procedures that require tissue dissociation.

Once we had decided on the dissociation protocol, we performed a pilot experiment. By showing consistency between our pilot data and bulk sequencing data previously acquired by our lab (Edurne Mugarza and Miriam Molina-Arcas) we felt more confident in inferences made downstream. Nonetheless, the correlation between the datasets was not perfect. Some of this is expected from random batch effects while other discrepancies will be systematic (bias) from the different techniques (bulk vs single cell). As above, we are investigating this, and data has been submitted to the bioinformatics core at the Francis Crick Institute. Our pilot data also demonstrated the ability of CITE-seq to help resolve distinct populations otherwise similarly clustered in RNA-space. We used the example of $CD4^+$ and $CD8^+$ T cells but the principle is best applied to separate states whose biology was previously unknown (Stoeckius *et al.*, 2017) . Although, downstream, we did not obtain myeloid clusters from RNA-data alone and compare with those clusters we discerned from the WNN data, it is probable that these clusters would have differed (given our antibody panel containing several myeloid-relevant markers). Therefore, using CITE-seq, we are likely to have identified clusters which are more appropriately resolved from one another.

After performing basic processing of the pilot data, we acquired the post-pilot data. During QC, the data from most cells appeared to be of good quality, consistent with our decision to sort cells prior to sequencing. During

composition analysis we noted one sample was an outlier, with a much higher proportion of neutrophils relative to other samples. We decided to keep this sample but ensure that we performed sensitivity analyses by excluding this sample where relevant. Given that we were integrating all 10 samples anyway, we reasoned that if cells from this sample were truly different from other samples, they would have integrated separately. In downstream analysis we did not notice any clusters enriched for cells from this sample. Of note, we have not analysed the neutrophil compartment. Future analyses of this compartment will need to bear in mind that the majority of cells will be from this 'outlier' sample.

In terms of composition analysis of all cells, we noted a decrease in neutrophil proportion and an increase in endothelial cell proportion with treatment, both of which were statistically significant and robust to removal of sample 5. These observations are consistent with other work from our lab using either flow cytometry or imaging mass cytometry (Mugarza *et al.*, 2021; van Maldegem *et al.*, 2021). We also noted the unexpected finding that the proportion of tumour cells in the sample increased with treatment. This is likely explained by our study protocol, rather than being a reflection of truly increased tumour cell proportion or a reflection of a treatment-induced reduction in immune infiltrate.

6.2.1 The myeloid compartment

Myeloid cells made up the majority of the TME. In this thesis we chose to focus on the macrophage and DC compartments given their well-established role in anti-tumour immunity. Nonetheless, the neutrophil compartment was also sizeable, and significantly reduced after treatment. Analysis of this subset will therefore form a part of future work with this data.

Once the myeloid cells had been subsetted, we had to decide on a suitable clustering algorithm and suitable parameters for said algorithm. Many algorithms for clustering single cell data exist, with advantages and disadvantages of each (Kiselev, Andrews and Hemberg, 2019). We chose to

use Seurat's graph-based clustering method given that it has performed well in benchmarking reviews (Duò, Robinson and Soneson, 2020). Furthermore, imaging mass cytometry data on orthotopic 3LL-ΔNRAS tumours from our lab (van Maldegem *et al.*, 2021) was clustered using PhenoGraph (Levine *et al.*, 2015), a graph-based clustering method. The similar methods used for clustering across the two data types may be useful for any attempts to integrate or make hypotheses across the two datasets in the future. Our choice of cluster resolution was justified in the results section. We are however aware that a different clustering algorithm with different parameters may have produced alternate cell-state definitions to the ones that we described. This is an inherent problem of high-dimensional data, with multiple ways of reducing dimensionality and partitioning the data. Validation of our subsets would come from reproducibility in other model systems or from human data. To this end, we have also collected and single cell-sequenced data from several human non-small cell lung carcinomas. Although the analysis of that data was not part of this thesis, it may form part of any future work with the single cell data discussed here.

Once clusters had been formed and annotated, we undertook composition analysis. We found that the population of Arg1 high macrophages significantly decreased after treatment and that its significance was robust to removal of data from sample 5 (a control sample), an outlier in terms of its composition. The reduction in proportion of the Arg1-high macrophages was notable given the established negative effect of increased macrophage Arg1 expression on T cell function (Bronte et al., 2003; Viola et al., 2019). In one study, Arg1 expression was increased in a KRAS(G12C) genetically engineered mouse model (GEMM), relative to normal tissue, and treatment with an arginase 1/2 inhibitor resulted in tumour regression with increased T-cell infiltration (Miret et al., 2019). Also consistent with our findings, a recent pre-print exploring a model of pancreatic cancer with inducible and reversible oncogenic KRAS expression found that KRAS inactivation resulted in a reduction in the proportion of Arg1^{+} macrophages (Velez-Delgado *et al.*, 2021). Given that we have demonstrated a

reduction in the proportion of Arg1-high macrophages upon treatment with KRAS(G12C), it is possible that this effect underlies some of the therapeutic effect of clinical KRAS(G12C) inhibitors. Nonetheless, the clinical efficacy of Arg1 inhibitors is yet to be proven, although trials are ongoing (NCT02903914, NCT03314935).

These Arg1-high macrophages also expressed a number of other potentially tumour-suppressive genes more strongly than other clusters. Amongst these, Cxcl3 was the most strongly upregulated in this cluster compared to others. Its receptor is Cxcr2 which, in our dataset was expressed in the neutrophil compartment (data not shown). Of note, we saw a reduction of neutrophil composition in treated tumours compared to control tumours raising the question whether this mechanism is secondary to the reduction in Cxcl3-high macrophages upon treatment. Indeed, neutrophil recruitment to the lung has been shown to be influenced by CXCL3 (Sokulsky *et al.*, 2020). Beyond Cxcl3, other genes overexpressed in this cluster included Ccl24, Mmp12, Vegfa, Nos2, Il6 and Spp1. Nos2 and Il6 are interesting as they are often considered to be ‘classically activated’ macrophage genes (Orecchioni *et al.*, 2019). However, data also shows that Il6 can polarise to an alternatively activated phenotype (Fernando *et al.*, 2014) and that tumours often simultaneously induce Nos2 and Arg1 in macrophages, to their advantage (Viola *et al.*, 2019).

The specific expression of Spp1 in this cluster was intriguing as it has recently been identified as a marker of a subset of macrophages in single cell analyses of colon cancer (Zhang *et al.*, 2020). In this same study, VEGFA expression was restricted to this SPP1-high population, while C1QC and other complement genes and antigen presenting genes were not expressed, mirroring what we saw. While there are some differences (their SPP1-high macrophages expressed the marker MARCO, while ours did not), future work on our data could aim to investigate the link between our macrophages and the macrophages in that study, particularly as they showed that anti-CSF1R therapy was minimally effective in targeting the SPP1-high population while we

have shown that MRTX1257 therapy resulted in robust reduction of these cells. This suggests that, for example, combinations of MRTX1257 and CSF1R-targeting therapy may provide a broader depletion of the tumour macrophage compartment than either therapy alone.

As well as the Arg1 (and Spp1)-high macrophages, we also saw a reduction in Saa3-high macrophages that was significant after removal of sample 5 (the outlier in terms of composition). Although this cluster is small, it is intriguing given its distinct projection in UMAP space and the fact that it is conserved across models – an analogous subtype was seen in a KP (Kras-Lox-STOP-Lox-G12D p53 flox/flox) murine lung cancer model (Zilionis *et al.*, 2019). Very little literature exists about this subtype, however three genes only or predominantly expressed in this subtype of macrophage – Alox15, Ltc4s and Ptgs1 - are involved in leukotriene or prostaglandin synthesis. Like many soluble mediators in lung cancer, the role of leukotrienes is complex and pleiotropic (Tian *et al.*, 2020) but it is conceivable that these cells, which are more prevalent in untreated tumours, could contribute to the inflammatory milieu by production of leukotrienes.

Following composition analysis we performed DE, looking at the effect of treatment within clusters. Although there was a similar pattern of DE across the macrophage clusters, it was striking that the most downregulated genes, including Arg1, Vegfa and Mmp9 have putative protumour genic functions while those genes consistently upregulated across clusters, including class II MHC genes are those which should aid immune rejection of tumours.

There were of course some exceptions. The Apoe gene, which codes for apoplipiprotein E, was upregulated after treatment and has been shown to promote immune suppression in pancreatic tumour models (Kemp *et al.*, 2021). Nonetheless, ApoE in this study acted through production of CXCL1, which is unlikely to be relevant here as we saw a decrease in CXCL1 upon treatment. Other notable exceptions were Ccl8 and Gpnmb (glycoprotein nonmetastatic

B). The former is a monocyte chemoattractant (Farmaki *et al.*, 2020) and may contribute to the high myeloid infiltration in these tumours. Of note while Ccl2 was robustly suppressed across clusters, Ccl7 (another monocyte chemoattractant) showed variable effect, being downregulated in some clusters and upregulated in others. Gpnmb has been shown to induce tumour stemness in a fibrosarcoma model, via action on CD44 (Liguori *et al.*, 2021) and there are many other reports linking it to tumourigenic processes. Finally, we also noted that transmembrane proteins 176a and 176b (Tmem176a and Tmem176b) were strongly upregulated with treatment. A large study which included the use of 3LL and CT26 models showed that knockdown of Tmem176a/b could augment the efficacy of checkpoint inhibitor therapy.

As well as macrophages, we interrogated the DC compartment. There were far fewer DCs than macrophages, and this may partly explain why there were far fewer DE genes in this compartment. Of the DE genes that we did see, the upregulation of Il12b in Ccr7-high (activated) DCs was intriguing given its fundamental role in Th1 immunity and antitumour immune responses (Garris *et al.*, 2018).

To conclude, we saw both compositional and gene expression effects in the macrophage compartment following MRTX1257 treatment. In general, the gene expression changes were robust across clusters and indicative of polarisation toward a more favourable tumour immune environment. Nonetheless, some entities with reported pro-tumourigenic properties increased with treatment, as described above. Knowledge of these sorts of changes is important as they can help suggest combinations to augment the efficacy of KRAS(G12C) inhibition. In order to build evidence, future work could include looking across other model systems and at human data to observe which of these effects are robust and which are model-specific. Furthermore, given the few changes we saw in the DC compartment, we would like to cluster and analyse these cells separately to see whether other effects of MRTX1257 become apparent. Finally, given the changes in secreted factors such as Vegfa and Cxcl3 seen here, it would be

prudent to apply cell-cell communication analysis where one looks at the expression of their cognate receptors amongst all cells within the tumour ecosystem, and how this changes with treatment. This would enable hypotheses about the possible functional effects of the changes that we see.

6.2.2 The tumour compartment

Pre-processing of data for analysis of the tumour compartment was similar to the pre-processing used to analyse myeloid cells. One difference, was that clustering the tumour cells alone appeared to yield a distinct population enriched for myeloid transcripts. This was consistent with doublets. These cells had not been identified by the doublet-detection algorithms that were previously used when all cells (immune/stromal and tumour) were clustered together. Doublet detection is a difficult problem in single-cell analysis with variability between the available methods (Xi and Li, 2021). Our data suggests that in heterogenous samples with a transcriptionally dominant subtype (tumour cells were more transcriptionally active than myeloid cells), doublet detection may be difficult when applied to the whole dataset. When sub-clustering the transcriptionally dominant type, doublets may become apparent.

We chose not to regress out cell-cycle effects, something that is commonly done in single cell analysis. This is because we expected effects on the cell-cycle to be biologically relevant. Nonetheless, future analyses will also look at the data after regressing out cell-cycle effects as there may be additional information to be gained.

By not regressing out cell-cycle effects, we found that our clusters closely aligned with cell-cycle phase prediction. For example, cluster 0 cells were almost all predicted to be in G0/G1. Nonetheless, the most strongly upregulated genes in this cluster tended to have anti-tumourigenic effects unrelated to the cell cycle. For example, Dcn (decorin) is a putative TSG (Järvinen and Prince, 2015), Ramp2 is involved in calcitonin signalling but also suggested to have a

pro-apoptotic effect in lung cancer (Yue *et al.*, 2007) and Cited2 although less clear, has the ability to decrease tumour invasiveness (Bai and Merchant, 2007).

Given that cluster 0 cells were in G0, we wondered whether they may have a lower 'KRAS activity' than other clusters. We assayed this by performing GSEA using several gene sets in the MSigDB collection pertaining to KRAS modulation. The results were inconsistent. Of note, many genes associated with oncogenic KRAS signalling (including Dusp1 and Dusp4) were actually increased in this cluster relative to others. Later in the analysis, we used another metric of KRAS activity that was based on a gene set that was derived from bulk sequencing of cells growth *in vitro* treated with a KRAS(G12C) inhibitor (Xue *et al.*, 2020). When we overlaid this score onto UMAP plots, cells in cluster 0 clearly had lower KRAS activity scores than other clusters (). It is possible that this signature seemed to reflect our data better because it was derived from cells specifically treated with a KRAS(G12C) inhibitor while other signatures used heterogenous means to perturb KRAS along with heterogeneity in other aspects of these signatures e.g. whether they were derived from *in vitro* or *in vivo* data (where immune cells may have confounded effects).

One intriguing outcome of our clustering procedure was the formation of a cluster predominantly composed of treated cells (cluster 5). We termed this the 'metabolic' cluster as cells showed upregulation of several genes whose protein products are involved in adipogenesis and oxidative phosphorylation. Oncogenic KRAS is known to promote a shift from oxidative phosphorylation to aerobic glycolysis (Pylayeva-Gupta, Grabocka and Bar-Sagi, 2011b) and therefore and increase in gene expression related to oxidative phosphorylation may not be surprising. Nonetheless, the magnitude of change in this cluster was markedly different from other treated cells, marking them as a separate state. The significance of this is not clear however it was also notable that they had reduced expression of several genes relative to cluster 0 (which contained

the bulk of the treated cells) including Ccnd1 and Areg suggesting perhaps that they were in more 'quiescent' state. In addition, treatment induced an upregulation of the gene Crxos, purported to be involved in embryonic stem cell renewal (Saito *et al.*, 2009), specifically in this cluster.

Analysis of composition demonstrated, as expected, that the proportion of treated cells in cluster 0 (non-cycling, 44% of treated cells) was higher than the proportion of untreated cells in this cluster (24% of untreated cells). Conversely, it may be surprising that a cumulative 45.6% of treated cells were in clusters 2-5, which we deemed to be clusters in the cell cycle. The 3LL-ΔNRAS model does not regress with MRTX1257 treatment and our data suggest that perhaps the bulk of cells are outside the cell cycle (where perhaps they are subject to immune attack or susceptible to apoptosis) but also that many cells are still able to enter the cycle.

Differential expression analysis of the clusters revealed many expected changes. This included downregulation of bona fide KRAS-related genes including Areg, Ereg, Myc, Vegfa and Plaur. Beyond this however, other interesting observations were noted. One, was a consistent upregulation of genes related to TGF-β signalling including Col3a1, Sparc and Dcn. Although, during GSEA, TGF-β gene sets did not consistently have negative NES scores, this triplicate of genes were the three most strongly upregulated genes when KRAS was knocked out in a KPC pancreas cancer model (Ischenko *et al.*, 2021). This observation is even more pertinent in the light of recent data showing that upregulation of TGF-β signalling can contribute to resistance to KRAS(G12C) inhibitors (Tsai *et al.*, 2022).

When looking at DE specific to the clusters, there were a few interesting observations. One module of genes downregulated after treatment were genes related to hypoxia, which were specifically reduced in cluster 0. This could

suggest that treated tumours (perhaps because of their size, or because of their vessel integrity) are more susceptible to hypoxia, and that KRAS inhibition normalises this process. Of note, Spp1 (which was specifically high in the Arg1-high macrophage population) is known to be induced by hypoxia in tumours (Wei *et al.*, 2021). Perhaps the cluster 3 (Arg1-high) macrophages and the hypoxia-gene-high group of untreated cells in cluster 0 ('G0') of the tumour compartment may have shared a hypoxic niche in their respective tumours. Of note, these cells did not just come from one sample, suggesting that whatever the underlying process, it is reproducible across biological replicates. Another interesting observation was the very strong, and cluster specific, induction of Ypel3 after treatment. This is a p53-responsive gene that has been shown to induce tumour senescence (Kelley *et al.*, 2010) and was only upregulated in non-cycling clusters (including cluster 0 and the treatment-specific cluster 5).

The final part of our analysis involved looking at immune-related transcripts. We first noted consistency with data previously generated in the lab *in vitro* using different models. Most genes that were suppressed in those models were also suppressed in our data. A notable exception was Plau, the pro-tumourigenic gene for urokinase-type plasminogen activator. Nonetheless, its receptor (gene Plaur) was suppressed, and this could mean that any negative functional effects of Plau induction are, to some extent, mitigated by the reduced expression of its receptor. In general the gene expression changes induced by MRTX1257 are those thought to be favourable in the sense of generating a successful antitumour response. However, possibly the most surprising and relevant discovery from this analysis, was the robust increase in Cd47 across all tumour clusters upon treatment. Given the generally anti-tumourigenic effects on the myeloid compartment that we discussed above, the increased expression of Cd47 could be relevant. Tumour expression of CD47 has been shown to help protect against phagocytosis (Jaiswal *et al.*, 2009). If indeed, the increased expression of Cd47 is part of an adaptive mechanism to the repolarised TME, combination MRTX1257/anti-CD47 therapy could provide additive or even synergistic efficacy.

To conclude, we have shown that KRAS(G12C) inhibition in the 3LL-ΔNRAS model repolarises the myeloid compartment and has profound effect on tumour intrinsic signalling. In general, these effects are those which are believed to be antitumorigenic, most profoundly the reduction of Arg1 and upregulation of class II MHC in macrophages and the reduction in tumour-intrinsic expression of various KRAS-targets including growth factors and genes involved in angiogenesis and tumour immune evasion. Nonetheless, given the breadth of effect, some gene expression changes have the potential to be protumourigenic. An understanding of how generalisable these effects are, across models and in patients, will enable the design of rational combinations with the potential to be additive or even synergistic.

Reference List

Adachi, Y. *et al.* (2020) 'Epithelial-to-Mesenchymal Transition is a Cause of Both Intrinsic and Acquired Resistance to KRAS G12C Inhibitor in KRAS G12C–Mutant Non–Small Cell Lung Cancer', *Clinical Cancer Research*, 26(22), pp. 5962 LP – 5973. doi: 10.1158/1078-0432.CCR-20-2077.

Adams, S. *et al.* (2012) 'Topical TLR7 agonist imiquimod can induce immune-mediated rejection of skin metastases in patients with breast cancer', *Clinical Cancer Research*, 18(24), pp. 6748–6757. doi: 10.1158/1078-0432.CCR-12-1149.

Alcalá, S. *et al.* (2008) 'A high-throughput screening for mammalian cell death effectors identifies the mitochondrial phosphate carrier as a regulator of cytochrome c release', *Oncogene*, 27(1), pp. 44–54. doi: 10.1038/sj.onc.1210600.

Amodio, V. *et al.* (2020) 'Egfr blockade reverts resistance to krasg12c inhibition in colorectal cancer', *Cancer Discovery*, 10(8), pp. 1129–1139. doi: 10.1158/2159-8290.CD-20-0187.

Amouzegar, A. *et al.* (2021) 'Sting agonists as cancer therapeutics', *Cancers*, 13(11). doi: 10.3390/cancers13112695.

Ancrile, B., Lim, K. H. and Counter, C. M. (2007) 'Oncogenic Ras-induced secretion of IL6 is required for tumorigenesis', *Genes and Development*, 21(14), pp. 1714–1719. doi: 10.1101/gad.1549407.

Arwert, E. N. *et al.* (2021) *Europe PMC Funders Group Europe PMC Funders Author Manuscripts STING and IRF3 function in stromal fibroblasts enables sensing of genomic stress in cancer cells thereby undermining oncolytic viral therapy*. doi: 10.1038/s41556-020-0527-7.STING.

Assabban, A. *et al.* (2021) 'Tristetraprolin expression by keratinocytes protects against skin carcinogenesis', *JCI Insight*, 6(5). doi: 10.1172/jci.insight.140669.

Atefi, M. *et al.* (2014) 'Effects of MAPK and PI3K pathways on PD-L1 expression in melanoma', *Clinical Cancer Research*, 20(13), pp. 3446–3457. doi: 10.1158/1078-0432.CCR-13-2797.

Atsaves, V. *et al.* (2019) 'AP-1 transcription factors as regulators of immune

responses in cancer', *Cancers*, 11(7). doi: 10.3390/cancers11071037.
Awad, M., Liu, S. and Arbour, K. (2021) 'Mechanisms of acquired resistance to KRAS G12C inhibition in cancer.', in *American Association for Cancer Research Annual Meeting*, p. Abstract LB002.
Bahrami, S. and Drabløs, F. (2016) 'Gene regulation in the immediate-early response process', *Advances in Biological Regulation*. Elsevier Ltd, 62(7491), pp. 37–49. doi: 10.1016/j.jbior.2016.05.001.
Bai, L. and Merchant, J. L. (2007) 'A role for CITED2, a CBP/p300 interacting protein, in colon cancer cell invasion', *FEBS Letters*, 581(30), pp. 5904–5910. doi: 10.1016/j.febslet.2007.11.072.
Bakheet, T. *et al.* (2001) 'ARED: Human AU-rich element-containing mRNA database reveals an unexpectedly diverse functional repertoire of encoded proteins', *Nucleic Acids Research*, 29(1), pp. 246–254. doi: 10.1093/nar/29.1.246.
Bakheet, T., Hitti, E. and Khabar, K. S. A. (2018) 'ARED-Plus: An updated and expanded database of AU-rich element-containing mRNAs and pre-mRNAs', *Nucleic Acids Research*. Oxford University Press, 46(D1), pp. D218–D220. doi: 10.1093/nar/gkx975.
Barlic, J., Zhu, W. and Murphy, P. M. (2009) 'Atherogenic Lipids Induce High-Density Lipoprotein Uptake and Cholesterol Efflux in Human Macrophages by Up-Regulating Transmembrane Chemokine CXCL16 without Engaging CXCL16-Dependent Cell Adhesion', *The Journal of Immunology*, 182(12), pp. 7928–7936. doi: 10.4049/jimmunol.0804112.
Barreau, C., Paillard, L. and Osborne, H. B. (2005) 'AU-rich elements and associated factors: Are there unifying principles?', *Nucleic Acids Research*, 33(22), pp. 7138–7150. doi: 10.1093/nar/gki1012.
Bayne, L. J. *et al.* (2012) 'Tumor-Derived Granulocyte-Macrophage Colony-Stimulating Factor Regulates Myeloid Inflammation and T Cell Immunity in Pancreatic Cancer', *Cancer Cell*. Elsevier Inc., 21(6), pp. 822–835. doi: 10.1016/j.ccr.2012.04.025.
Beatty, G. L. *et al.* (2015) 'Exclusion of T Cells From Pancreatic Carcinomas in Mice Is Regulated by Ly6Clow F4/80+ Extratumoral Macrophages',

Gastroenterology. Elsevier, Inc, 149(1), pp. 201–210. doi: 10.1053/j.gastro.2015.04.010.

Benci, J. L. *et al.* (2016) 'Tumor Interferon Signaling Regulates a Multigenic Resistance Program to Immune Checkpoint Blockade', *Cell*. Elsevier, 167(6), pp. 1540-1554.e12. doi: 10.1016/j.cell.2016.11.022.

Binnewies, M. *et al.* (2018) 'Understanding the tumor immune microenvironment (TIME) for effective therapy', *Nature Medicine*. Springer US, 24(5), pp. 541–550. doi: 10.1038/s41591-018-0014-x.

Blagih, J. *et al.* (2020) 'Cancer-Specific Loss of p53 Leads to a Modulation of Article Cancer-Specific Loss of p53 Leads to a Modulation of Myeloid and T Cell Responses', *CellReports*. ElsevierCompany., 30(2), pp. 481-496.e6. doi: 10.1016/j.celrep.2019.12.028.

Blagih, J., Buck, M. D. and Vousden, K. H. (2020) 'p53 , cancer and the immune response'. doi: 10.1242/jcs.237453.

Blum, R. *et al.* (2005) 'Ras inhibition in glioblastoma down-regulates hypoxia-inducible factor-1α, causing glycolysis shutdown and cell death', *Cancer Research*, 65(3), pp. 999–1006.

Boni, A. *et al.* (2010) 'Selective BRAFV600E inhibition enhances T-cell recognition of melanoma without affecting lymphocyte function', *Cancer Research*, 70(13), pp. 5213–5219. doi: 10.1158/0008-5472.CAN-10-0118.

Böttcher, J. P. *et al.* (2018) 'NK Cells Stimulate Recruitment of cDC1 into the Tumor Microenvironment Promoting Cancer Immune Control', *Cell*, 172(5), pp. 1022-1037.e14. doi: 10.1016/j.cell.2018.01.004.

Brazil, J. C. *et al.* (2019) 'Innate immune cell–epithelial crosstalk during wound repair', *Journal of Clinical Investigation*, 129(8), pp. 2983–2993. doi: 10.1172/JCI124618.

Briere, D. M. *et al.* (2019) 'Abstract LB-C09: The KRASG12 inhibitor MRTX849 reconditions the tumor immune microenvironment and leads to durable complete responses in combination with anti-PD-1 therapy in a syngeneic mouse model', *Molecular Cancer Therapeutics*, 18(12 Supplement), p. LB-C09 LP-LB-C09. doi: 10.1158/1535-7163.TARG-19-LB-C09.

Bronte, V. *et al.* (2003) 'IL-4-induced arginase 1 suppresses alloreactive T cells

in tumor-bearing mice.', *Journal of immunology (Baltimore, Md. : 1950)*. United States, 170(1), pp. 270–278. doi: 10.4049/jimmunol.170.1.270.

Brooks, S. A. and Blackshear, P. J. (2013a) 'Tristetraprolin (TTP): Interactions with mRNA and proteins, and current thoughts on mechanisms of action', *Biochimica et Biophysica Acta - Gene Regulatory Mechanisms*. Elsevier B.V., 1829(6–7), pp. 666–679. doi: 10.1016/j.bbagrm.2013.02.003.

Brooks, S. A. and Blackshear, P. J. (2013b) 'Tristetraprolin (TTP): Interactions with mRNA and proteins, and current thoughts on mechanisms of action', *Biochimica et Biophysica Acta - Gene Regulatory Mechanisms*. Elsevier B.V., 1829(6–7), pp. 666–679. doi: 10.1016/j.bbagrm.2013.02.003.

Brown, C. C. *et al.* (2019) 'Transcriptional Basis of Mouse and Human Dendritic Cell Heterogeneity', *Cell*, 179(4), pp. 846-863.e24. doi: 10.1016/j.cell.2019.09.035.

Buus, T. B. *et al.* (2020) 'Improving oligo-conjugated antibody signal in multimodal single-cell analysis', *bioRxiv*, p. 2020.06.15.153080. doi: 10.1101/2020.06.15.153080.

Cabrita, R. *et al.* (2020) 'Tertiary lymphoid structures improve immunotherapy and survival in melanoma', *Nature*, 577(7791), pp. 561–565. doi: 10.1038/s41586-019-1914-8.

Caetano, M. S. *et al.* (2016) 'IL6 blockade reprograms the lung tumor microenvironment to limit the development and progression of K-ras-mutant lung cancer', *Cancer Research*, 76(11), pp. 3189–3199. doi: 10.1158/0008-5472.CAN-15-2840.

Canli, Ö. *et al.* (2017) 'Myeloid Cell-Derived Reactive Oxygen Species Induce Epithelial Mutagenesis', *Cancer Cell*, 32(6), pp. 869-883.e5. doi: 10.1016/j.ccell.2017.11.004.

Canon, J. *et al.* (2019) 'The clinical KRAS(G12C) inhibitor AMG 510 drives anti-tumour immunity', *Nature*. Springer US, 575(7781), pp. 217–223. doi: 10.1038/s41586-019-1694-1.

Carballo, E., Gilkeson, G. S. and Blackshear, P. J. (1997) 'Bone marrow transplantation reproduces the tristetraprolin-deficiency syndrome in recombination activating gene-2 (-/-) mice. Evidence that

monocyte/macrophage progenitors may be responsible for TNFα overproduction', *Journal of Clinical Investigation*, 100(5), pp. 986–995. doi: 10.1172/JCI119649.

de Carné Trécesson, S. *et al.* (2020) 'APOBEC3B expression generates an immunogenic model of Kras mutant lung cancer', *bioRxiv*, p. 2020.12.22.423126. doi: 10.1101/2020.12.22.423126.

Carvalho, P. D. *et al.* (2018) 'KRAS oncogenic signaling extends beyond cancer cells to orchestrate the microenvironment', *Cancer Research*, 78(1), pp. 7–14. doi: 10.1158/0008-5472.CAN-17-2084.

Casanova-Acebes, M. *et al.* (2021) 'Tissue-resident macrophages provide a pro-tumorigenic niche to early NSCLC cells', *Nature*, 595(7868), pp. 578–584. doi: 10.1038/s41586-021-03651-8.

Cassetta, L. and Pollard, J. W. (2018) 'Targeting macrophages: Therapeutic approaches in cancer', *Nature Reviews Drug Discovery*. Nature Publishing Group, 17(12), pp. 887–904. doi: 10.1038/nrd.2018.169.

Cendrowicz, E. *et al.* (2021) 'The role of macrophages in cancer development and therapy', *Cancers*, 13(8). doi: 10.3390/cancers13081946.

Chang, H. J. *et al.* (2022) 'High BRCA1 gene expression increases the risk of early distant metastasis in ER+ breast cancers', *Scientific Reports*. Nature Publishing Group UK, 12(1), pp. 1–13. doi: 10.1038/s41598-021-03471-w.

Chen, D. S. and Mellman, I. (2013) 'Oncology meets immunology: The cancer-immunity cycle', *Immunity*, 39(1), pp. 1–10. doi: 10.1016/j.immuni.2013.07.012.

Chen, N. *et al.* (2017) 'KRAS mutation-induced upregulation of PD-L1 mediates immune escape in human lung adenocarcinoma', *Cancer Immunology, Immunotherapy*. Springer Berlin Heidelberg, 66(9), pp. 1175–1187. doi: 10.1007/s00262-017-2005-z.

Chiba, S. *et al.* (2012) 'Tumor-infiltrating DCs suppress nucleic acid-mediated innate immune responses through interactions between the receptor TIM-3 and the alarmin HMGB1', *Nature Immunology*, 13(9), pp. 832–842. doi: 10.1038/ni.2376.

Christian U. Blank, John B. Haanen, A. R. and T. N. S. (2106) 'The "cancer immunogram"', *Science*, 352(6286), pp. 658–60. doi: 10.1126/science.aaf2834.

Ciais, D., Cherradi, N. and Feige, J. J. (2013) 'Multiple functions of tristetraprolin/TIS11 RNA-binding proteins in the regulation of mRNA biogenesis and degradation', *Cellular and Molecular Life Sciences*, 70(12), pp. 2031–2044. doi: 10.1007/s00018-012-1150-y.

Clark, A. R. and Dean, J. L. E. (2016) 'The control of inflammation via the phosphorylation and dephosphorylation of tristetraprolin: A tale of two phosphatases', *Biochemical Society Transactions*, 44(5), pp. 1321–1337. doi: 10.1042/BST20160166.

Clement, S. L. *et al.* (2011) 'Phosphorylation of Tristetraprolin by MK2 Impairs AU-Rich Element mRNA Decay by Preventing Deadenylase Recruitment', *Molecular and Cellular Biology*, 31(2), pp. 256–266. doi: 10.1128/mcb.00717-10.

Coelho, M. *et al.* (2017) 'Oncogenic RAS Signaling Promotes Tumor Immunoresistance by Stabilizing PD-L1 mRNA', *Immunity*, 47(6), pp. 1083-1099.e6. doi: 10.1016/j.immuni.2017.11.016.

Cortez-Retamozo, V. *et al.* (2012) 'Origins of tumor-associated macrophages and neutrophils', *Proceedings of the National Academy of Sciences of the United States of America*, 109(7), pp. 2491–2496. doi: 10.1073/pnas.1113744109.

Cortez, M. A. *et al.* (2020) 'Bone morphogenetic protein 7 promotes resistance to immunotherapy', *Nature Communications*. Springer US, 11(1). doi: 10.1038/s41467-020-18617-z.

Coulie, P. G. *et al.* (2014) 'Tumour antigens recognized by T lymphocytes: At the core of cancer immunotherapy', *Nature Reviews Cancer*. Nature Publishing Group, 14(2), pp. 135–146. doi: 10.1038/nrc3670.

Cózar, B. *et al.* (2021) 'Tumor-infiltrating natural killer cells', *Cancer Discovery*, 11(1), pp. 34–44. doi: 10.1158/2159-8290.CD-20-0655.

Creelan, B. C. *et al.* (2021) 'Tumor-infiltrating lymphocyte treatment for anti-PD-1-resistant metastatic lung cancer: a phase 1 trial', *Nature Medicine*. Springer US, 27(8), pp. 1410–1418. doi: 10.1038/s41591-021-01462-y.

Crusz, S. M. and Balkwill, F. R. (2015) 'Inflammation and cancer: Advances and new agents', *Nature Reviews Clinical Oncology*. Nature Publishing Group,

12(10), pp. 584–596. doi: 10.1038/nrclinonc.2015.105.
Cullis, J., Das, S. and Bar-Sagi, D. (2018) 'Kras and tumor immunity: Friend or foe?', *Cold Spring Harbor Perspectives in Medicine*, 8(9). doi: 10.1101/cshperspect.a031849.
Dai, Y. *et al.* (2017) 'Loss of FOXN3 in colon cancer activates beta-catenin/TCF signaling and promotes the growth and migration of cancer cells', *Oncotarget*, 8(6), pp. 9783–9793. doi: 10.18632/oncotarget.14189.
Dalod, M. *et al.* (2014) 'Dendritic cell maturation: Functional specialization through signaling specificity and transcriptional programming', *EMBO Journal*, 33(10), pp. 1104–1116. doi: 10.1002/embj.201488027.
Dalton, D. K. *et al.* (1993) 'Multiple defects of immune cell function in mice with disrupted interferon-γ genes', *Science*, 259(5102), pp. 1739–1742. doi: 10.1126/science.8456300.
Daud, A. I. *et al.* (2016) 'Tumor immune profiling predicts response to anti-PD-1 therapy in human melanoma', *Journal of Clinical Investigation*, 126(9), pp. 3447–3452. doi: 10.1172/JCI87324.
Deleault, K. M., Skinner, S. J. and Brooks, S. A. (2008) 'Tristetraprolin regulates TNF TNF-α mRNA stability via a proteasome dependent mechanism involving the combined action of the ERK and p38 pathways', *Molecular Immunology*, 45(1), pp. 13–24. doi: 10.1016/j.molimm.2007.05.017.
DeNardo, D. G. and Ruffell, B. (2019) 'Macrophages as regulators of tumour immunity and immunotherapy', *Nature Reviews Immunology*. Springer US, 19(6), pp. 369–382. doi: 10.1038/s41577-019-0127-6.
Denisenko, E. *et al.* (2019) 'Systematic assessment of tissue dissociation and storage biases in single-cell and single-nucleus RNA-seq workflows', *bioRxiv*. Genome Biology, pp. 1–25. doi: 10.1101/832444.
Dogan, S. *et al.* (2012) 'Molecular epidemiology of EGFR and KRAS mutations in 3,026 lung adenocarcinomas: Higher susceptibility of women to smoking-related KRAS-mutant cancers', *Clinical Cancer Research*, 18(22), pp. 6169–6177. doi: 10.1158/1078-0432.CCR-11-3265.
Downward, J. (1998) 'Ras signalling and apoptosis', *Current Opinion in Genetics and Development*, 8(1), pp. 49–54. doi: 10.1016/S0959-

437X(98)80061-0.
Downward, J. (2003) 'Targeting RAS signalling pathways in cancer therapy', *Nature Reviews Cancer*, 3(1), pp. 11–22. doi: 10.1038/nrc969.
Duò, A., Robinson, M. D. and Soneson, C. (2020) 'A systematic performance evaluation of clustering methods for single-cell RNA-seq data', *F1000Research*, 7, p. 1141. doi: 10.12688/f1000research.15666.3.
East, P. *et al.* (2021) 'Oncogenic RAS activity predicts response to chemotherapy and outcome in lung adenocarcinoma', *bioRxiv*, p. 2021.04.02.437896. doi: 10.1101/2021.04.02.437896.
Eruslanov, E. B. *et al.* (2014) 'Tumor-associated neutrophils stimulate T cell responses in early-stage human lung cancer', *Journal of Clinical Investigation*, 124(12), pp. 5466–5480. doi: 10.1172/JCI77053.
Fabian, M. R. *et al.* (2013) 'Structural basis for the recruitment of the human CCR4-NOT deadenylase complex by tristetraprolin', *Nature Structural and Molecular Biology*. Nature Publishing Group, 20(6), pp. 735–739. doi: 10.1038/nsmb.2572.
Fallahi, M. *et al.* (2014) 'CREB targets define the gene expression signature of malignancies having reduced levels of the tumor suppressor tristetraprolin', *PLoS ONE*, 9(12), pp. 1–24. doi: 10.1371/journal.pone.0115517.
Farmaki, E. *et al.* (2020) 'CCL8 Promotes Postpartum Breast Cancer by Recruiting M2 Macrophages', *iScience*. Elsevier Inc., 23(6), p. 101217. doi: 10.1016/j.isci.2020.101217.
FDA approves pexidartinib for tenosynovial giant cell tumor (no date). Available at: https://www.fda.gov/drugs/resources-information-approved-drugs/fda-approves-pexidartinib-tenosynovial-giant-cell-tumor.
Fedele, C., Li, S., Teng, K. W., Foster, Connor J R, *et al.* (2021) 'SHP2 inhibition diminishes KRASG12C cycling and promotes tumor microenvironment remodeling.', *The Journal of experimental medicine*, 218(1). doi: 10.1084/jem.20201414.
Fedele, C., Li, S., Teng, K. W., Foster, Connor J.R., *et al.* (2021) 'SHP2 inhibition diminishes KRASG12C cycling and promotes tumor microenvironment remodeling', *The Journal of experimental medicine*, 218(1). doi:

10.1084/jem.20201414.

Feig, C. *et al.* (2013) 'Targeting CXCL12 from FAP-expressing carcinoma-associated fibroblasts synergizes with anti-PD-L1 immunotherapy in pancreatic cancer', *Proceedings of the National Academy of Sciences of the United States of America*, 110(50), pp. 20212–20217. doi: 10.1073/pnas.1320318110.

Fernando, M. R. *et al.* (2014) 'The pro-inflammatory cytokine, interleukin-6, enhances the polarization of alternatively activated macrophages', *PLoS ONE*, 9(4). doi: 10.1371/journal.pone.0094188.

Filmus, J. *et al.* (1994) 'Induction of cyclin D1 overexpression by activated ras.', *Oncogene*. England, 9(12), pp. 3627–3633.

Finco, T. S. *et al.* (1997) 'Oncogenic Ha-Ras-induced signaling activates NF-κB transcriptional activity, which is required for cellular transformation', *Journal of Biological Chemistry*, 272(39), pp. 24113–24116. doi: 10.1074/jbc.272.39.24113.

Fittall, M. W. *et al.* (2018) 'Recurrent rearrangements of FOS and FOSB define osteoblastoma', *Nature Communications*, 9(1), pp. 1–6. doi: 10.1038/s41467-018-04530-z.

Florkowska, M. *et al.* (2012) 'EGF activates TTP expression by activation of ELK-1 and EGR-1 transcription factors', *BMC Molecular Biology*, 13, pp. 1–11. doi: 10.1186/1471-2199-13-8.

Frederick, D. T. *et al.* (2013) 'BRAF inhibition is associated with enhanced melanoma antigen expression and a more favorable tumor microenvironment in patients with metastatic melanoma', *Clinical Cancer Research*, 19(5), pp. 1225–1231. doi: 10.1158/1078-0432.CCR-12-1630.

Freeman, G. J. *et al.* (2000) 'Engagement of the PD-1 immunoinhibitory receptor by a novel B7 family member leads to negative regulation of lymphocyte activation', *Journal of Experimental Medicine*, 192(7), pp. 1027–1034. doi: 10.1084/jem.192.7.1027.

Fritz, D. T. *et al.* (2006) 'A polymorphism in a conserved posttranscriptional regulatory motif alters bone morphogenetic protein 2 (BMP2) RNA:Protein interactions', *Molecular Endocrinology*, 20(7), pp. 1574–1586. doi: 10.1210/me.2005-0469.

Fukuda, A. *et al.* (2011) 'Stat3 and MMP7 Contribute to Pancreatic Ductal Adenocarcinoma Initiation and Progression', *Cancer Cell*. Elsevier Inc., 19(4), pp. 441–455. doi: 10.1016/j.ccr.2011.03.002.

Gabrilovich, D. I. and Nagaraj, S. (2009) 'Myeloid-derived suppressor cells as regulators of the immune system', *Nature Reviews Immunology*, 9(3), pp. 162–174. doi: 10.1038/nri2506.

Garcia-Manero, G. *et al.* (2021) 'Magrolimab + azacitidine versus azacitidine + placebo in untreated higher risk (HR) myelodysplastic syndrome (MDS): The phase 3, randomized, ENHANCE study.', *Journal of Clinical Oncology*. Wolters Kluwer, 39(15_suppl), pp. TPS7055–TPS7055. doi: 10.1200/JCO.2021.39.15_suppl.TPS7055.

Gardner, A., de Mingo Pulido, Á. and Ruffell, B. (2020) 'Dendritic Cells and Their Role in Immunotherapy', *Frontiers in Immunology*, 11(May), pp. 1–14. doi: 10.3389/fimmu.2020.00924.

Garneau, N. L., Wilusz, J. and Wilusz, C. J. (2007) 'The highways and byways of mRNA decay', *Nature Reviews Molecular Cell Biology*, 8(2), pp. 113–126. doi: 10.1038/nrm2104.

Garnett, M. J. *et al.* (2012) 'Systematic identification of genomic markers of drug sensitivity in cancer cells.', *Nature*, 483(7391), pp. 570–575. doi: 10.1038/nature11005.

Garris, C. S. *et al.* (2018) 'Successful Anti-PD-1 Cancer Immunotherapy Requires T Cell-Dendritic Cell Crosstalk Involving the Cytokines IFN-γ and IL-12', *Immunity*, 49(6), pp. 1148-1161.e7. doi: 10.1016/j.immuni.2018.09.024.

Gentles, A. J. *et al.* (2015) 'The prognostic landscape of genes and infiltrating immune cells across human cancers', *Nature Medicine*. Nature Publishing Group, 21(8), pp. 938–945. doi: 10.1038/nm.3909.

Giampazolias, E. *et al.* (2021) 'Secreted gelsolin inhibits DNGR-1-dependent cross-presentation and cancer immunity', *Cell*. Elsevier Inc., 184(15), pp. 4016-4031.e22. doi: 10.1016/j.cell.2021.05.021.

Gibbs, J. B. *et al.* (1984) 'Intrinsic GTPase activity distinguishes normal and oncogenic ras p21 molecules', *Proceedings of the National Academy of Sciences of the United States of America*, 81(18 I), pp. 5704–5708. doi:

10.1073/pnas.81.18.5704.
Gimple, R. C. and Wang, X. (2019) 'RAS: Striking at the Core of the Oncogenic Circuitry', *Frontiers in Oncology*, 9(September), pp. 1–16. doi: 10.3389/fonc.2019.00965.
Ginhoux, F. and Guilliams, M. (2016) 'Tissue-Resident Macrophage Ontogeny and Homeostasis', *Immunity*. Elsevier Inc., 44(3), pp. 439–449. doi: 10.1016/j.immuni.2016.02.024.
Goel, S. *et al.* (2017) 'CDK4/6 inhibition triggers anti-tumour immunity', *Nature*. Nature Publishing Group, 548(7668), pp. 471–475. doi: 10.1038/nature23465.
Gordon, S. R. *et al.* (2017) 'PD-1 expression by tumour-associated macrophages inhibits phagocytosis and tumour immunity', *Nature*. Nature Publishing Group, 545(7655), pp. 495–499. doi: 10.1038/nature22396.
Goveia, J. *et al.* (2020) 'An Integrated Gene Expression Landscape Profiling Approach to Identify Lung Tumor Endothelial Cell Heterogeneity and Angiogenic Candidates', *Cancer Cell*, 37(1), pp. 21-36.e13. doi: 10.1016/j.ccell.2019.12.001.
Guinney, J. *et al.* (2015) 'The consensus molecular subtypes of colorectal cancer', *Nature Medicine*, 21(11), pp. 1350–1356. doi: 10.1038/nm.3967.
Guo, H. *et al.* (2021) 'NR4A1 regulates expression of immediate early genes, suppressing replication stress in cancer', *Molecular Cell*. Elsevier Inc., 81(19), pp. 4041-4058.e15. doi: 10.1016/j.molcel.2021.09.016.
Guo, J. *et al.* (2017) 'The role of RNA-binding protein tristetraprolin in cancer and immunity', *Medical Oncology*. Springer US, 34(12), pp. 1–12. doi: 10.1007/s12032-017-1055-6.
Hafemeister, C. and Satija, R. (2019) 'Normalization and variance stabilization of single-cell RNA-seq data using regularized negative binomial regression', *Genome Biology*. Genome Biology, 20(1), pp. 1–15. doi: 10.1186/s13059-019-1874-1.
Hallin, J. *et al.* (2019) 'The KRASG12C Inhibitor, MRTX849, Provides Insight Toward Therapeutic Susceptibility of KRAS Mutant Cancers in Mouse Models and Patients.', *Cancer discovery*. doi: 10.1158/2159-8290.CD-19-1167.
Hamarsheh, S. *et al.* (2020) 'Immune modulatory effects of oncogenic KRAS in

cancer', *Nature Communications*, 11(1). doi: 10.1038/s41467-020-19288-6.
Hanahan, D. and Weinberg, R. A. (2011) 'Hallmarks of cancer: The next generation', *Cell*. Elsevier Inc., 144(5), pp. 646–674. doi: 10.1016/j.cell.2011.02.013.
Hao, Y. *et al.* (2021) 'Integrated analysis of multimodal single-cell data', *Cell*. Elsevier Inc., 184(13), pp. 3573-3587.e29. doi: 10.1016/j.cell.2021.04.048.
Haque, A. *et al.* (2017) 'A practical guide to single-cell RNA-sequencing for biomedical research and clinical applications', *Genome Medicine*. Genome Medicine, 9(1), pp. 1–12. doi: 10.1186/s13073-017-0467-4.
Hatzivassiliou, G. *et al.* (2010) 'RAF inhibitors prime wild-type RAF to activate the MAPK pathway and enhance growth', *Nature*. Nature Publishing Group, 464(7287), pp. 431–435. doi: 10.1038/nature08833.
Hatzivassiliou, G. *et al.* (2013) 'Mechanism of MEK inhibition determines efficacy in mutant KRAS- versus BRAF-driven cancers', *Nature*. Nature Publishing Group, 501(7466), pp. 232–236. doi: 10.1038/nature12441.
Havel, J. J., Chowell, D. and Chan, T. A. (2019) 'The evolving landscape of biomarkers for checkpoint inhibitor immunotherapy', *Nature Reviews Cancer*. Springer US, 19(3), pp. 133–150. doi: 10.1038/s41568-019-0116-x.
Healy, S., Khan, P. and Davie, J. R. (2013) 'Immediate early response genes and cell transformation', *Pharmacology and Therapeutics*. Elsevier Inc., 137(1), pp. 64–77. doi: 10.1016/j.pharmthera.2012.09.001.
Hegde, P. S., Karanikas, V. and Evers, S. (2016) 'The where, the when, and the how of immune monitoring for cancer immunotherapies in the era of checkpoint inhibition', *Clinical Cancer Research*, 22(8), pp. 1865–1874. doi: 10.1158/1078-0432.CCR-15-1507.
Helmink, B. A. *et al.* (2020) 'B cells and tertiary lymphoid structures promote immunotherapy response', *Nature*. Springer US, 577(7791), pp. 549–555. doi: 10.1038/s41586-019-1922-8.
Heng, T. S. P. *et al.* (2008) 'The Immunological Genome Project : networks of gene expression in immune cells', 9(10), pp. 1091–1094.
Herbst, R. S. *et al.* (2014) 'Predictive correlates of response to the anti-PD-L1 antibody MPDL3280A in cancer patients', *Nature*. Nature Publishing Group,

515(7528), pp. 563–567. doi: 10.1038/nature14011.
Hildner, K. *et al.* (2008) 'Batf3 deficiency reveals a critical role for CD8α+ dendritic cells in cytotoxic T cell immunity', *Science*, 322(5904), pp. 1097–1100. doi: 10.1126/science.1164206.
Hitti, E. *et al.* (2016) 'Systematic analysis of AU-Rich element expression in cancer reveals common functional clusters regulated by key RNA-Binding proteins', *Cancer Research*, 76(14), pp. 4068–4080. doi: 10.1158/0008-5472.CAN-15-3110.
Hobbs, G. A., Der, C. J. and Rossman, K. L. (2016) 'RAS isoforms and mutations in cancer at a glance', *Journal of Cell Science*, 129(7), pp. 1287–1292. doi: 10.1242/jcs.182873.
Hong, D. S. *et al.* (2020) ' KRAS G12C Inhibition with Sotorasib in Advanced Solid Tumors ', *New England Journal of Medicine*, 383(13), pp. 1207–1217. doi: 10.1056/nejmoa1917239.
Hoption Cann, S. A., Van Netten, J. P. and Van Netten, C. (2003) 'Dr William Coley and tumour regression: A place in history or in the future', *Postgraduate Medical Journal*, 79(938), pp. 672–680.
Huang, J. *et al.* (2021) 'Unfolded protein response in colorectal cancer', *Cell and Bioscience*. BioMed Central, 11(1), pp. 1–16. doi: 10.1186/s13578-021-00538-z.
Huang, K. *et al.* (2014) 'Elevated p53 expression levels correlate with tumor progression and poor prognosis in patients exhibiting esophageal squamous cell carcinoma', *Oncology Letters*, 8(4), pp. 1441–1446. doi: 10.3892/ol.2014.2343.
Huang, P. *et al.* (2017) 'BMP-2 induces EMT and breast cancer stemness through Rb and CD44', *Cell Death Discovery*. Nature Publishing Group, 3(1). doi: 10.1038/cddiscovery.2017.39.
Hunter, J. C. *et al.* (2015) 'Biochemical and structural analysis of common cancer-associated KRAS mutations', *Molecular Cancer Research*, 13(9), pp. 1325–1335. doi: 10.1158/1541-7786.MCR-15-0203.
Huynh, T. G. *et al.* (2016) 'Programmed cell death ligand 1 expression in resected lung adenocarcinomas: Association with immune microenvironment',

Journal of Thoracic Oncology. Elsevier Inc, 11(11), pp. 1869–1878. doi: 10.1016/j.jtho.2016.08.134.

Ischenko, I. *et al.* (2021) 'KRAS drives immune evasion in a genetic model of pancreatic cancer', *Nature Communications*. Springer US, 12(1), pp. 1–15. doi: 10.1038/s41467-021-21736-w.

Jacquelot, N. *et al.* (2019) 'Sustained Type I interferon signaling as a mechanism of resistance to PD-1 blockade', *Cell Research*. Springer US, 29(10), pp. 846–861. doi: 10.1038/s41422-019-0224-x.

Jaiswal, S. *et al.* (2009) 'CD47 Is Upregulated on Circulating Hematopoietic Stem Cells and Leukemia Cells to Avoid Phagocytosis', *Cell*. Elsevier Ltd, 138(2), pp. 271–285. doi: 10.1016/j.cell.2009.05.046.

Janes, M. R. *et al.* (2018) 'Targeting KRAS Mutant Cancers with a Covalent G12C-Specific Inhibitor.', *Cell*, 172(3), pp. 578-589.e17. doi: 10.1016/j.cell.2018.01.006.

Järvinen, T. A. H. and Prince, S. (2015) 'Decorin: A Growth Factor Antagonist for Tumor Growth Inhibition', *BioMed Research International*, 2015. doi: 10.1155/2015/654765.

Jerby-Arnon, L. *et al.* (2018) 'A Cancer Cell Program Promotes T Cell Exclusion and Resistance to Checkpoint Blockade', *Cell*, 175(4), pp. 984-997.e24. doi: 10.1016/j.cell.2018.09.006.

Ji, M. *et al.* (2016) 'PD-1/PD-L1 expression in non-small-cell lung cancer and its correlation with EGFR/KRAS mutations', *Cancer Biology and Therapy*. Taylor & Francis, 17(4), pp. 407–413. doi: 10.1080/15384047.2016.1156256.

Johnson, M. L., Ou, S.-H. I. and Barve, M. (2020) *KRYSTAL-1: Activity and Safety of Adagrasib (MRTX849) in Patients With Colorectal Cancer (CRC) and Other Solid Tumors Harboring a KRASG12C Mutation*, *32nd EORTC-NCI-AACR Symposium, October 24-25, 2020*.

Kalbasi, A. and Ribas, A. (2020) 'intrinsic resistance to immune checkpoint blockade', *Nature Reviews Immunology*. Springer US, 20(January), pp. 25–39. doi: 10.1038/s41577-019-0218-4.

Kaneda, M. M. *et al.* (2016) 'PI3Kγ 3 is a molecular switch that controls immune suppression', *Nature*. Nature Publishing Group, 539(7629), pp. 437–442. doi:

10.1038/nature19834.
Kanehisa, M. *et al.* (2021) 'KEGG: integrating viruses and cellular organisms.', *Nucleic acids research*, 49(D1), pp. D545–D551. doi: 10.1093/nar/gkaa970.
Karre, K. *et al.* (1986) 'Selective rejection of H-2-deficient lymphoma variants suggests alternative immune defence strategy', *Nature*, 319, pp. 675–678.
Kawasaki, T. and Kawai, T. (2014) 'Toll-like receptor signaling pathways', *Frontiers in Immunology*, 5(SEP), pp. 1–8. doi: 10.3389/fimmu.2014.00461.
Kelley, K. D. *et al.* (2010) 'YPEL3, a p53-regulated gene that induces cellular senescence', *Cancer Research*, 70(9), pp. 3566–3575. doi: 10.1158/0008-5472.CAN-09-3219.
Kemp, S. B. *et al.* (2021) 'Apolipoprotein E promotes immune suppression in pancreatic cancer through NF-κB-Mediated production of CXCL1', *Cancer Research*, 81(16), pp. 4305–4318. doi: 10.1158/0008-5472.CAN-20-3929.
Kenkel, J. A. *et al.* (2017) 'An immunosuppressive dendritic cell subset accumulates at secondary sites and promotes metastasis in pancreatic cancer', *Cancer Research*, 77(15), pp. 4158–4170. doi: 10.1158/0008-5472.CAN-16-2212.
Kim, B. Y. *et al.* (2002) 'Constitutive activation of NF-kB in Ki-ras-transformed prostate epithelial cells', *Oncogene*, 21(29), pp. 4490–4497. doi: 10.1038/sj.onc.1205547.
Kim, S. *et al.* (2009) 'Carcinoma-produced factors activate myeloid cells through TLR2 to stimulate metastasis', *Nature*. Nature Publishing Group, 457(7225), pp. 102–106. doi: 10.1038/nature07623.
Kiselev, V. Y., Andrews, T. S. and Hemberg, M. (2019) 'Challenges in unsupervised clustering of single-cell RNA-seq data', *Nature Reviews Genetics*. Springer US, 20(5), pp. 273–282. doi: 10.1038/s41576-018-0088-9.
Kitajima, S. *et al.* (2019) 'Suppression of STING associated with lkb1 loss in KRAS-driven lung cancer', *Cancer Discovery*, 9(1), pp. 34–45. doi: 10.1158/2159-8290.CD-18-0689.
Kochan, G. *et al.* (2013) 'Role of non-classical MHC class I molecules in cancer immunosuppression', *OncoImmunology*, 2(11), pp. 1–8. doi: 10.4161/onci.26491.

Kohl, N. E. *et al.* (1995) 'Inhibition of farnesyltransferase induces regression of mammary and salivary carcinomas in ras transgenic mice.', *Nature medicine*. United States, 1(8), pp. 792–797. doi: 10.1038/nm0895-792.

Kortlever, R. M. *et al.* (2017) 'Myc Cooperates with Ras by Programming Inflammation and Immune Suppression', *Cell*. Elsevier, 171(6), pp. 1301-1315.e14. doi: 10.1016/j.cell.2017.11.013.

Kroemer, G. *et al.* (2013) 'Immunogenic cell death in cancer therapy', *Annual Review of Immunology*, 31, pp. 51–72. doi: 10.1146/annurev-immunol-032712-100008.

Kuhn, K. A. *et al.* (2014) 'IL-6 stimulates intestinal epithelial proliferation and repair after injury', *PLoS ONE*, 9(12), pp. 1–18. doi: 10.1371/journal.pone.0114195.

Kura Oncology Receives FDA Breakthrough Therapy Designation for Tipifarnib in Head and Neck Squamous Cell Carcinoma (no date).

Lahmar, Q. *et al.* (2016) 'Tissue-resident versus monocyte-derived macrophages in the tumor microenvironment', *Biochimica et Biophysica Acta - Reviews on Cancer*. Elsevier B.V., 1865(1), pp. 23–34. doi: 10.1016/j.bbcan.2015.06.009.

Lai, W. S. *et al.* (1995) 'Promoter analysis of Zfp-36, the mitogen-inducible gene encoding the zinc finger protein tristetraprolin', *Journal of Biological Chemistry*, 270(42), pp. 25266–25272. doi: 10.1074/jbc.270.42.25266.

Lai, W. S. *et al.* (2017) 'A Knock-In Tristetraprolin (TTP) Zinc Finger Point Mutation in Mice: Comparison with Complete TTP Deficiency', *Molecular and Cellular Biology*, 38(4), pp. 1–21. doi: 10.1128/mcb.00488-17.

Lai, W. S., Stumpos, J. and Blackshear, P. J. (1990) 'Rapid Insulin-stimulated Protein * Accumulation of an mRNA Encoding a', *Jbc*, 265(27), pp. 16556–16563.

Lakhani, N. *et al.* (2020) '295 First-in-human Phase I trial of IBI188, an anti-CD47 targeting monoclonal antibody, in patients with advanced solid tumors and lymphomas', *Journal for ImmunoTherapy of Cancer*, 8(Suppl 3), p. A180 LP-A180. doi: 10.1136/jitc-2020-SITC2020.0295.

Lastwika, K. J. *et al.* (2016) 'Control of PD-L1 expression by oncogenic

activation of the AKT-mTOR pathway in non-small cell lung cancer', *Cancer Research*, 76(2), pp. 227–238. doi: 10.1158/0008-5472.CAN-14-3362.

Lee, H. H., Lee, S. R. and Leem, S. H. (2014) 'Tristetraprolin regulates prostate cancer cell growth through suppression of E2F1', *Journal of Microbiology and Biotechnology*, 24(2), pp. 287–294. doi: 10.4014/jmb.1309.09070.

Lee, J. Y. *et al.* (2013) 'Tumor suppressor p53 plays a key role in induction of both tristetraprolin and let-7 in human cancer cells', *Nucleic Acids Research*, 41(11), pp. 5614–5625. doi: 10.1093/nar/gkt222.

Lee, S. *et al.* (2020) 'A post-transcriptional program of chemoresistance by AU-rich elements and TTP in quiescent leukemic cells', *Genome Biology*. Genome Biology, 21(1), pp. 1–23. doi: 10.1186/s13059-020-1936-4.

Lee, S. R. *et al.* (2018) 'Tristetraprolin activation by resveratrol inhibits the proliferation and metastasis of colorectal cancer cells', *International Journal of Oncology*, 53(3), pp. 1269–1278. doi: 10.3892/ijo.2018.4453.

Leelatian, N. *et al.* (2017) 'Single cell analysis of human tissues and solid tumors with mass cytometry', *Cytometry Part B - Clinical Cytometry*, 92(1), pp. 68–78. doi: 10.1002/cyto.b.21481.

Levine, J. H. *et al.* (2015) 'Data-Driven Phenotypic Dissection of AML Reveals Progenitor-like Cells that Correlate with Prognosis', *Cell*. Elsevier Inc., 162(1), pp. 184–197. doi: 10.1016/j.cell.2015.05.047.

Liberzon, A. *et al.* (2015) 'The Molecular Signatures Database (MSigDB) hallmark gene set collection', *Cell Systems*, 1(6), pp. 417–425. doi: 10.1016/j.cels.2015.12.004.The.

Liguori, M. *et al.* (2021) 'The soluble glycoprotein NMB (GPNMB) produced by macrophages induces cancer stemness and metastasis via CD44 and IL-33', *Cellular and Molecular Immunology*, 18(3), pp. 711–722. doi: 10.1038/s41423-020-0501-0.

Lin, E. Y. *et al.* (2006) 'Macrophages regulate the angiogenic switch in a mouse model of breast cancer', *Cancer Research*, 66(23), pp. 11238–11246. doi: 10.1158/0008-5472.CAN-06-1278.

Liu, J. *et al.* (2018) 'An Integrated TCGA Pan-Cancer Clinical Data Resource to Drive High-Quality Survival Outcome Analytics', *Cell*, 173(2), pp. 400-416.e11.

doi: 10.1016/j.cell.2018.02.052.
Luecken, M. D. and Theis, F. J. (2019) 'Current best practices in single-cell RNA-seq analysis: a tutorial', *Molecular Systems Biology*, 15(6). doi: 10.15252/msb.20188746.
Luke, J. J. *et al.* (2019) 'WNT/β-catenin Pathway Activation Correlates with Immune Exclusion across Human Cancers', *Clinical Cancer Research*, 25(10), pp. 3074 LP – 3083. doi: 10.1158/1078-0432.CCR-18-1942.
Lung cancer patients to get breakthrough drug on NHS (2021). Available at: https://www.england.nhs.uk/2021/09/lung-cancer-patients-to-get-breakthrough-drug-on-nhs/ (Accessed: 11 November 2021).
Madden, E. *et al.* (2019) 'The role of the unfolded protein response in cancer progression: From oncogenesis to chemoresistance', *Biology of the Cell*, 111(1), pp. 1–17. doi: 10.1111/boc.201800050.
van Maldegem, F. *et al.* (2021) 'Characterisation of tumour immune microenvironment remodelling following oncogene inhibition in preclinical studies using an optimised imaging mass cytometry workflow', *bioRxiv*, p. 2021.02.02.429358. doi: 10.1101/2021.02.02.429358.
Malumbres, M. and Barbacid, M. (2003) 'RAS oncogenes: The first 30 years', *Nature Reviews Cancer*, 3(6), pp. 459–465. doi: 10.1038/nrc1097.
Marchese, F. P. *et al.* (2010) 'MAPKAP kinase 2 blocks tristetraprolin-directed mRNA decay by inhibiting CAF1 deadenylase recruitment', *Journal of Biological Chemistry*. Â© 2010 ASBMB. Currently published by Elsevier Inc; originally published by American Society for Biochemistry and Molecular Biology., 285(36), pp. 27590–27600. doi: 10.1074/jbc.M110.136473.
Marderosian, M. *et al.* (2006) 'Tristetraprolin regulates cyclin D1 and c-Myc mRNA stability in response to rapamycin in an Akt-dependent manner via p38 MAPK signaling', *Oncogene*, 25(47), pp. 6277–6290. doi: 10.1038/sj.onc.1209645.
Martinez, F. O. and Gordon, S. (2014) 'The M1 and M2 paradigm of macrophage activation: Time for reassessment', *F1000Prime Reports*, 6(March), pp. 1–13. doi: 10.12703/P6-13.
Mayo, J. G. (1972) 'Biologic characterization of the subcutaneously implanted

Lewis lung tumor.', *Cancer chemotherapy reports. Part 2*. United States, 3(1), pp. 325–330.
Mccormick, F. (2018) 'Targeting KRAS Directly', *Annual Review of Cancer Biology*, 2, pp. 81–90. doi: 10.1146/annurev-cancerbio-050216-122010.
Michaud, D. *et al.* (2021) 'Regulatory B cells in cancer', *Immunological Reviews*, 299(1), pp. 74–92. doi: 10.1111/imr.12939.
Miller, J. S. and Lanier, L. L. (2019) 'Natural killer cells in cancer immunotherapy', *Annual Review of Cancer Biology*, 3(1), pp. 77–103. doi: 10.1146/annurev-cancerbio-030518-055653.
Miltenyi Biotec (2016) *Epitope preservation list*. Available at: https://www.miltenyibiotec.com/_Resources/Persistent/32afd208d0b3e4c7c21aab28e58afc3c3058115c/Epitope preservation list TDK%2C mouse.pdf (Accessed: 27 December 2021).
Mirati Therapeutics' Adagrasib Receives Breakthrough Therapy Designation from U.S. Food and Drug Administration for Patients with Advanced Non-Small Cell Lung Cancer Harboring the KRASG12C Mutation (2021). Available at: https://ir.mirati.com/press-releases/press-release-details/2021/Mirati-Therapeutics-Adagrasib-Receives-Breakthrough-Therapy-Designation-from-U.S.-Food-and-Drug-Administration-for-Patients-with-Advanced-Non-Small-Cell-Lung-Cancer-Harboring-the-KRAS-G12C-Mu (Accessed: 11 November 2021).
Miret, J. J. *et al.* (2019) 'Suppression of Myeloid Cell Arginase Activity leads to Therapeutic Response in a NSCLC Mouse Model by Activating Anti-Tumor Immunity', *Journal for ImmunoTherapy of Cancer*. Journal for ImmunoTherapy of Cancer, 7(1), pp. 1–12. doi: 10.1186/s40425-019-0504-5.
Misale, S. *et al.* (2019) 'KRAS G12C NSCLC models are sensitive to direct targeting of KRAS in combination with PI3K inhibition', *Clinical Cancer Research*, 25(2), pp. 796–807. doi: 10.1158/1078-0432.CCR-18-0368.
Molina-Arcas, M. *et al.* (2013) 'Coordinate direct input of both KRAS and IGF1 receptor to activation of PI3 kinase in KRAS -mutant lung cancer', *Cancer Discovery*, 3(5), pp. 548–563. doi: 10.1158/2159-8290.CD-12-0446.
Molina-Arcas, M. *et al.* (2019) 'Development of combination therapies to

maximize the impact of KRAS-G12C inhibitors in lung cancer', *Science Translational Medicine*, 11(510). doi: 10.1126/scitranslmed.aaw7999.
Montorsi, L. *et al.* (2016) 'Loss of zfp36 expression in colorectal cancer correlates to wnt/β-catenin activity and enhances epithelial-to-mesenchymal transition through upregulation of zeb1, sox9 and macc1', *Oncotarget*, 7(37), pp. 59144–59157. doi: 10.18632/oncotarget.10828.
Moore, A. R. *et al.* (2020) 'RAS-targeted therapies: is the undruggable drugged?', *Nature Reviews Drug Discovery*. Springer US, 19(8), pp. 533–552. doi: 10.1038/s41573-020-0068-6.
Mugarza, E. *et al.* (2021) 'Therapeutic KRASG12C inhibition drives effective interferon-mediated anti-tumour immunity in immunogenic lung cancers', *bioRxiv*, p. 2021.10.18.464819. Available at: https://www.biorxiv.org/content/10.1101/2021.10.18.464819v1%0Ahttps://www.biorxiv.org/content/10.1101/2021.10.18.464819v1.abstract.
Muhl, L. *et al.* (2020) 'Single-cell analysis uncovers fibroblast heterogeneity and criteria for fibroblast and mural cell identification and discrimination', *Nature Communications*. Springer US, 11(1), pp. 1–18. doi: 10.1038/s41467-020-17740-1.
Mukaida, N., Sasaki, S. I. and Baba, T. (2020) 'Two-faced roles of tumor-associated neutrophils in cancer development and progression', *International Journal of Molecular Sciences*, 21(10). doi: 10.3390/ijms21103457.
Mukherjee, N. *et al.* (2014) 'Global target mRNA specification and regulation by the RNA-binding protein ZFP36', *Genome Biology*, 15(1), pp. 1–16. doi: 10.1186/gb-2014-15-1-r12.
Muthalagu, N. *et al.* (2020) 'Repression of the Type I Interferon Pathway Underlies MYC- and KRAS-Dependent Evasion of NK and B Cells in Pancreatic Ductal Adenocarcinoma', *Cancer Discovery*, 10(6), pp. 872 LP – 887. doi: 10.1158/2159-8290.CD-19-0620.
Muzumdar, M. D. *et al.* (2017) 'Survival of pancreatic cancer cells lacking KRAS function', *Nature Communications*. Springer US, 8(1), pp. 1–18. doi: 10.1038/s41467-017-00942-5.
Nguyen, K. B. and Spranger, S. (2020) 'Modulation of the immune

microenvironment by tumor-intrinsic oncogenic signaling', *Journal of Cell Biology*, 219(1), pp. 1–13. doi: 10.1083/jcb.201908224.

Nichols, R. J. *et al.* (2018) 'RAS nucleotide cycling underlies the SHP2 phosphatase dependence of mutant BRAF-, NF1- and RAS-driven cancers', *Nature Cell Biology*. Springer US, 20(9), pp. 1064–1073. doi: 10.1038/s41556-018-0169-1.

Nie, P. *et al.* (2015) 'Synergistic induction of erlotinib-mediated apoptosis by resveratrol in human non-small-cell lung cancer cells by down-regulating survivin and up-regulating PUMA', *Cellular Physiology and Biochemistry*, 35(6), pp. 2255–2271. doi: 10.1159/000374030.

Noy, R. and Pollard, J. W. (2014) 'Tumor-Associated Macrophages: From Mechanisms to Therapy', *Immunity*. Elsevier Inc., 41(1), pp. 49–61. doi: 10.1016/j.immuni.2014.06.010.

O'Hayer, K. M., Brady, D. C. and Counter, C. M. (2009) 'ELR+ CXC chemokines and oncogenic Ras-mediated tumorigenesis', *Carcinogenesis*, 30(11), pp. 1841–1847. doi: 10.1093/carcin/bgp198.

Ogawa, K. *et al.* (2003) 'Transcriptional regulation of tristetraprolin by transforming growth factor-β in human T cells', *Journal of Biological Chemistry*. Â© 2003 ASBMB. Currently published by Elsevier Inc; originally published by American Society for Biochemistry and Molecular Biology., 278(32), pp. 30373–30381. doi: 10.1074/jbc.M304856200.

Orecchioni, M. *et al.* (2019) 'Macrophage polarization: Different gene signatures in M1(Lps+) vs. Classically and M2(LPS-) vs. Alternatively activated macrophages', *Frontiers in Immunology*, 10(MAY), pp. 1–14. doi: 10.3389/fimmu.2019.01084.

Oronsky, B. *et al.* (2019) 'REPLATINUM Phase III randomized study: RRx-001 + platinum doublet versus platinum doublet in third-line small cell lung cancer.', *Future oncology (London, England)*. England, 15(30), pp. 3427–3433. doi: 10.2217/fon-2019-0317.

Oronsky, B. *et al.* (2021) 'Discovery of RRx-001, a Myc and CD47 Downregulating Small Molecule with Tumor Targeted Cytotoxicity and Healthy Tissue Cytoprotective Properties in Clinical Development', *Journal of Medicinal*

Chemistry, 64(11), pp. 7261–7271. doi: 10.1021/acs.jmedchem.1c00599.
Ostrem, J. M. *et al.* (2013) 'K-Ras(G12C) inhibitors allosterically control GTP affinity and effector interactions', *Nature*. Nature Publishing Group, 503(7477), pp. 548–551. doi: 10.1038/nature12796.
De Palma, M. *et al.* (2005) 'Tie2 identifies a hematopoietic lineage of proangiogenic monocytes required for tumor vessel formation and a mesenchymal population of pericyte progenitors', *Cancer Cell*, 8(3), pp. 211–226. doi: 10.1016/j.ccr.2005.08.002.
Patricelli, M. P. *et al.* (2016) 'Selective inhibition of oncogenic KRAS output with small molecules targeting the inactive state', *Cancer Discovery*, 6(3), pp. 316–329. doi: 10.1158/2159-8290.CD-15-1105.
Peng, W. *et al.* (2016) 'Loss of PTEN promotes resistance to T cell–mediated immunotherapy', *Cancer Discovery*, 6(2), pp. 202–216. doi: 10.1158/2159-8290.CD-15-0283.
Pennycuick, A. *et al.* (2020) 'Immune surveillance in clinical regression of preinvasive squamous cell lung cancer', *Cancer Discovery*, 10(10), pp. 1489–1499. doi: 10.1158/2159-8290.CD-19-1366.
Peterson, T. R. *et al.* (2009) 'DEPTOR Is an mTOR Inhibitor Frequently Overexpressed in Multiple Myeloma Cells and Required for Their Survival', *Cell*, 137(5), pp. 873–886. doi: 10.1016/j.cell.2009.03.046.
Philip, M. *et al.* (2017) 'Chromatin states define tumour-specific T cell dysfunction and reprogramming', *Nature*. Nature Publishing Group, 545(7655), pp. 452–456. doi: 10.1038/nature22367.
Philip, M. and Schietinger, A. (2021) 'CD8+ T cell differentiation and dysfunction in cancer', *Nature Reviews Immunology*. Springer US, 0123456789. doi: 10.1038/s41577-021-00574-3.
Pickup, M., Novitskiy, S. and Moses, H. L. (2013) 'The roles of TGFβ in the tumour microenvironment', *Nature Reviews Cancer*. Nature Publishing Group, 13(11), pp. 788–799. doi: 10.1038/nrc3603.
Plotnikov, A. *et al.* (2011) 'The MAPK cascades: Signaling components, nuclear roles and mechanisms of nuclear translocation', *Biochimica et Biophysica Acta - Molecular Cell Research*. Elsevier B.V., 1813(9), pp. 1619–1633. doi:

10.1016/j.bbamcr.2010.12.012.

Pollock, C. B. *et al.* (2005) 'Oncogenic K-RAS is required to maintain changes in cytoskeletal organization, adhesion, and motility in colon cancer cells', *Cancer Research*, 65(4), pp. 1244–1250. doi: 10.1158/0008-5472.CAN-04-1911.

Prior, I. A., Hood, F. E. and Hartley, J. L. (2020) 'The frequency of ras mutations in cancer', *Cancer Research*, 80(14), pp. 2669–2974. doi: 10.1158/0008-5472.CAN-19-3682.

Prior IA; Lewis, P. M. C. (2012) 'A comprehensive survey of Ras mutations in cancer Ian', 72(10), pp. 1–24. doi: 10.1158/0008-5472.CAN-11-2612.A.

Pylayeva-Gupta, Y. *et al.* (2012) 'Oncogenic Kras-Induced GM-CSF Production Promotes the Development of Pancreatic Neoplasia', *Cancer Cell*. Elsevier Inc., 21(6), pp. 836–847. doi: 10.1016/j.ccr.2012.04.024.

Pylayeva-Gupta, Y., Grabocka, E. and Bar-Sagi, D. (2011a) 'RAS oncogenes: Weaving a tumorigenic web', *Nature Reviews Cancer*. Nature Publishing Group, 11(11), pp. 761–774. doi: 10.1038/nrc3106.

Pylayeva-Gupta, Y., Grabocka, E. and Bar-Sagi, D. (2011b) 'RAS oncogenes: Weaving a tumorigenic web', *Nature Reviews Cancer*. Nature Publishing Group, 11(11), pp. 761–774. doi: 10.1038/nrc3106.

Qian, B. *et al.* (2011) 'CCL2 recruits inflammatory monocytes to facilitate breast tumor metastasis', *Nature*, 475(7355), pp. 222–225. doi: 10.1038/nature10138.CCL2.

Qiu, L.-Q. *et al.* (2015) 'Tristetraprolin (TTP) coordinately regulates primary and secondary cellular responses to proinflammatory stimuli', *Journal of leukocyte biology*. 2015/02/05. Society for Leukocyte Biology, 97(4), pp. 723–736. doi: 10.1189/jlb.3A0214-106R.

Qiu, L.-Q., Stumpo, D. J. and Blackshear, P. J. (2012) 'Myeloid-Specific Tristetraprolin Deficiency in Mice Results in Extreme Lipopolysaccharide Sensitivity in an Otherwise Minimal Phenotype', *The Journal of Immunology*, 188(10), pp. 5150–5159. doi: 10.4049/jimmunol.1103700.

Qu, Z. *et al.* (2015) 'Interleukin-6 prevents the initiation but enhances the progression of lung cancer', *Cancer Research*, 75(16), pp. 3209–3215. doi:

10.1158/0008-5472.CAN-14-3042.
Raskov, H. *et al.* (2021) 'Cytotoxic CD8+ T cells in cancer and cancer immunotherapy', *British Journal of Cancer*. Springer US, 124(2), pp. 359–367. doi: 10.1038/s41416-020-01048-4.
Rezcallah, M. C., Al-mazi, T. and Ammit, A. J. (2021) 'Cataloguing the phosphorylation sites of tristetraprolin (TTP): Functional implications for inflammatory diseases', *Cellular Signalling*. Elsevier Inc., 78(October 2020), p. 109868. doi: 10.1016/j.cellsig.2020.109868.
Ribas, A. *et al.* (2019) 'Combined BRAF and MEK inhibition with PD-1 blockade immunotherapy in BRAF-mutant melanoma', *Nature Medicine*. Springer US, 25(6), pp. 936–940. doi: 10.1038/s41591-019-0476-5.
Ribas, A. *et al.* (2020) 'PD-L1 blockade in combination with inhibition of MAPK oncogenic signaling in patients with advanced melanoma', *Nature Communications*. Springer US, 11(1). doi: 10.1038/s41467-020-19810-w.
Ridker, P. M. *et al.* (2017) 'Effect of interleukin-1β inhibition with canakinumab on incident lung cancer in patients with atherosclerosis: exploratory results from a randomised, double-blind, placebo-controlled trial', *The Lancet*, 390(10105), pp. 1833–1842. doi: 10.1016/S0140-6736(17)32247-X.
Riely, G. J. *et al.* (2021) '99O_PR KRYSTAL-1: Activity and preliminary pharmacodynamic (PD) analysis of adagrasib (MRTX849) in patients (Pts) with advanced non–small cell lung cancer (NSCLC) harboring KRASG12C mutation', *Journal of Thoracic Oncology*, 16(4, Supplement), pp. S751–S752. doi: https://doi.org/10.1016/S1556-0864(21)01941-9.
Robert, C. (2020) 'A decade of immune-checkpoint inhibitors in cancer therapy', *Nature Communications*. Springer US, 11(1), pp. 10–12. doi: 10.1038/s41467-020-17670-y.
Rodig, S. J. *et al.* (2018) 'MHC proteins confer differential sensitivity to CTLA-4 and PD-1 blockade in untreated metastatic melanoma', *Science Translational Medicine*, 10(450), pp. 1–14. doi: 10.1126/scitranslmed.aar3342.
Rodriguez, P. C. *et al.* (2004) 'Arginase I production in the tumor microenvironment by mature myeloid cells inhibits T-cell receptor expression and antigen-specific T-cell responses', *Cancer Research*, 64(16), pp. 5839–

5849. doi: 10.1158/0008-5472.CAN-04-0465.
Ronkina, N. *et al.* (2019) 'The Role of TTP Phosphorylation in the Regulation of Inflammatory Cytokine Production by MK2/3', *The Journal of Immunology*, 203(8), pp. 2291–2300. doi: 10.4049/jimmunol.1801221.
Rosenthal, R. *et al.* (2019) 'Neoantigen-directed immune escape in lung cancer evolution', *Nature*, 567(7749), pp. 479–485. doi: 10.1038/s41586-019-1032-7.
Ross, E. A. *et al.* (2015) 'Dominant Suppression of Inflammation via Targeted Mutation of the mRNA Destabilizing Protein Tristetraprolin', *The Journal of Immunology*, 195(1), pp. 265–276. doi: 10.4049/jimmunol.1402826.
Rounbehler, R. J. *et al.* (2012) 'Tristetraprolin impairs Myc-induced lymphoma and abolishes the malignant state', *Cell*, 150(3), pp. 563–574. doi: 10.1016/j.cell.2012.06.033.
Ryan, M. B. *et al.* (2020) 'Vertical pathway inhibition overcomes adaptive feedback resistance to KrasG12C inhibition', *Clinical Cancer Research*, 26(7), pp. 1617–1643. doi: 10.1158/1078-0432.CCR-19-3523.
Ryu, J. *et al.* (2015) 'Resveratrol induces glioma cell apoptosis through activation of tristetraprolin', *Molecules and Cells*, 38(11), pp. 991–997. doi: 10.14348/molcells.2015.0197.
Saeland, E. *et al.* (2007) 'The C-type lectin MGL expressed by dendritic cells detects glycan changes on MUC1 in colon carcinoma', *Cancer Immunology, Immunotherapy*, 56(8), pp. 1225–1236. doi: 10.1007/s00262-006-0274-z.
Saini, Y., Chen, J. and Patial, S. (2020) 'The tristetraprolin family of RNA-binding proteins in cancer: Progress and future prospects', *Cancers*, 12(6), pp. 1–21. doi: 10.3390/cancers12061539.
Saito, R. *et al.* (2009) 'CrxOS maintains the self-renewal capacity of murine embryonic stem cells', *Biochemical and Biophysical Research Communications*. Elsevier Inc., 390(4), pp. 1129–1135. doi: 10.1016/j.bbrc.2009.09.118.
Sanduja, S. (2011) 'The role of tristetraprolin in cancer and inflammation', *Frontiers in Bioscience*, 17(1), p. 174. doi: 10.2741/3920.
Sautès-Fridman, C. *et al.* (2019) 'Tertiary lymphoid structures in the era of cancer immunotherapy', *Nature Reviews Cancer*. Springer US, 19(6), pp. 307–325. doi: 10.1038/s41568-019-0144-6.

Sawanobori, Y. *et al.* (2008) 'Chemokine-mediated rapid turnover of myeloid-derived suppressor cells in tumor-bearing mice', *Blood*, 111(12), pp. 5457–5466. doi: 10.1182/blood-2008-01-136895.

Scharping, N. E. *et al.* (2021) 'Mitochondrial stress induced by continuous stimulation under hypoxia rapidly drives T cell exhaustion', *Nature Immunology*. Springer US, 22(2), pp. 205–215. doi: 10.1038/s41590-020-00834-9.

Scheffzek, K. *et al.* (1997) 'The Ras-RasGAP complex: Structural basis for GTPase activation and its loss in oncogenic ras mutants', *Science*, 277(5324), pp. 333–338. doi: 10.1126/science.277.5324.333.

Schmidt, C. R. *et al.* (2005) 'E-cadherin is regulated by the transcriptional repressor SLUG during Ras-mediated transformation of intestinal epithelial cells', *Surgery*, 138(2), pp. 306–312. doi: 10.1016/j.surg.2005.06.007.

Schreiber, R. D., Old, L. J. and Smyth, M. J. (2011) 'Cancer immunoediting: Integrating immunity's roles in cancer suppression and promotion', *Science*, 331(6024), pp. 1565–1570. doi: 10.1126/science.1203486.

Sedlyarov, V. *et al.* (2016) 'Tristetraprolin binding site atlas in the macrophage transcriptome reveals a switch for inflammation resolution', *Molecular Systems Biology*, 12(5), p. 868. doi: 10.15252/msb.20156628.

Seligmann, J. F. *et al.* (2021) 'Inhibition of WEE1 Is Effective in TP53- and RAS-Mutant Metastatic Colorectal Cancer: A Randomized Trial (FOCUS4-C) Comparing Adavosertib (AZD1775) With Active Monitoring.', *Journal of clinical oncology : official journal of the American Society of Clinical Oncology*, 39(33), pp. 3705–3715. doi: 10.1200/JCO.21.01435.

Selmi, T. *et al.* (2012) 'ZFP36 expression impairs glioblastoma cell lines viability and invasiveness by targeting multiple signal transduction pathways', *Cell Cycle*, 11(10), pp. 1977–1987. doi: 10.4161/cc.20309.

Sgambato, V. *et al.* (1998) 'In vivo expression and regulation of Elk-1, a target of the extracellular-regulated kinase signaling pathway, in the adult rat brain.', *The Journal of neuroscience : the official journal of the Society for Neuroscience*, 18(1), pp. 214–226. doi: 10.1523/JNEUROSCI.18-01-00214.1998.

Sharma, P., Hu-Lieskovan, S., Wargo, Jennifer A, *et al.* (2017) 'Primary,

Adaptive, and Acquired Resistance to Cancer Immunotherapy.', *Cell*. Elsevier Inc., 168(4), pp. 707–723. doi: 10.1016/j.cell.2017.01.017.

Sharma, P., Hu-Lieskovan, S., Wargo, Jennifer A., *et al.* (2017) 'Primary, Adaptive, and Acquired Resistance to Cancer Immunotherapy', *Cell*. Elsevier Inc., 168(4), pp. 707–723. doi: 10.1016/j.cell.2017.01.017.

Shaul, M. E. and Fridlender, Z. G. (2019) 'Tumour-associated neutrophils in patients with cancer', *Nature Reviews Clinical Oncology*. Springer US, 16(10), pp. 601–620. doi: 10.1038/s41571-019-0222-4.

Singh, A. *et al.* (2009) 'A gene expression signature associated with "K-Ras addiction" reveals regulators of EMT and tumor cell survival.', *Cancer cell*, 15(6), pp. 489–500. doi: 10.1016/j.ccr.2009.03.022.

Singhal, S. *et al.* (2016) 'Origin and Role of a Subset of Tumor-Associated Neutrophils with Antigen-Presenting Cell Features in Early-Stage Human Lung Cancer', *Cancer Cell*. Elsevier Inc., 30(1), pp. 120–135. doi: 10.1016/j.ccell.2016.06.001.

Skoulidis, F. *et al.* (2015) 'Co-occurring genomic alterations define major subsets of KRAS-mutant lung adenocarcinoma with distinct biology, immune profiles, and therapeutic vulnerabilities', *Cancer Discovery*, 5(8), pp. 861–878. doi: 10.1158/2159-8290.CD-14-1236.

Skoulidis, F. *et al.* (2018) 'STK11/LKB1 Mutations and PD-1 Inhibitor Resistance in KRAS-Mutant Lung Adenocarcinoma.', *Cancer discovery*, 8(7), pp. 822–835. doi: 10.1158/2159-8290.CD-18-0099.

Skoulidis, F. *et al.* (2021) ' Sotorasib for Lung Cancers with KRAS p.G12C Mutation ', *New England Journal of Medicine*, 384(25), pp. 2371–2381. doi: 10.1056/nejmoa2103695.

Śledzińska, A. *et al.* (2020) 'Regulatory T Cells Restrain Interleukin-2- and Blimp-1-Dependent Acquisition of Cytotoxic Function by CD4+ T Cells', *Immunity*, 52(1), pp. 151-166.e6. doi: 10.1016/j.immuni.2019.12.007.

Sohn, B. H. *et al.* (2010) 'Functional Switching of TGF-β1 Signaling in Liver Cancer via Epigenetic Modulation of a Single CpG Site in TTP Promoter', *Gastroenterology*. Elsevier Inc., 138(5), pp. 1898-1908.e12. doi: 10.1053/j.gastro.2009.12.044.

Sokulsky, L. A. *et al.* (2020) 'A Critical Role for the CXCL3/CXCL5/CXCR2 Neutrophilic Chemotactic Axis in the Regulation of Type 2 Responses in a Model of Rhinoviral-Induced Asthma Exacerbation', *The Journal of Immunology*, 205(9), pp. 2468–2478. doi: 10.4049/jimmunol.1901350.

Solanki, H. S. *et al.* (2021) 'Cell Type–specific Adaptive Signaling Responses to KRAS^{G12C} Inhibition', *Clinical Cancer Research*. doi: 10.1158/1078-0432.CCR-20-3872.

Sparmann, A. and Bar-Sagi, D. (2004) 'Ras-induced interleukin-8 expression plays a critical role in tumor growth and angiogenesis', *Cancer Cell*, 6(5), pp. 447–458. doi: 10.1016/j.ccr.2004.09.028.

Spranger, S. (2016) 'Mechanisms of tumor escape in the context of the T-cell-inflamed and the non-T-cell-inflamed tumor microenvironment', *International Immunology*, 28(8), pp. 383–391. doi: 10.1093/intimm/dxw014.

Spranger, S. *et al.* (2017) 'Tumor-Residing Batf3 Dendritic Cells Are Required for Effector T Cell Trafficking and Adoptive T Cell Therapy', *Cancer Cell*. Elsevier Inc., 31(5), pp. 711-723.e4. doi: 10.1016/j.ccell.2017.04.003.

Spranger, S., Bao, R. and Gajewski, T. F. (2015) 'Melanoma-intrinsic β-catenin signalling prevents anti-tumour immunity', *Nature*, 523(7559), pp. 231–235. doi: 10.1038/nature14404.

Stein, M. *et al.* (1992) 'Interleukin 4 potently enhances murine macrophage mannose receptor activity: A marker of alternative immunologic macrophage activation', *Journal of Experimental Medicine*, 176(1), pp. 287–292. doi: 10.1084/jem.176.1.287.

Sterzyńska, K. *et al.* (2018) 'The role of matrix gla protein (MGP) expression in paclitaxel and topotecan resistant ovarian cancer cell lines', *International Journal of Molecular Sciences*, 19(10). doi: 10.3390/ijms19102901.

Stoeckius, M. *et al.* (2017) 'Simultaneous epitope and transcriptome measurement in single cells', *Nature Methods*, 14(9), pp. 865–868. doi: 10.1038/nmeth.4380.

Stoeckius, M. *et al.* (2018) 'Cell Hashing with barcoded antibodies enables multiplexing and doublet detection for single cell genomics', *Genome Biology*. Genome Biology, 19(1), pp. 1–12. doi: 10.1186/s13059-018-1603-1.

Stuart, T. *et al.* (2019) 'Comprehensive Integration of Single-Cell Data', *Cell*. Elsevier Inc., 177(7), pp. 1888-1902.e21. doi: 10.1016/j.cell.2019.05.031.
Sumimoto, H. *et al.* (2006) 'The BRAF-MAPK signaling pathway is essential for cancer-immune evasion in human melanoma cells', *Journal of Experimental Medicine*, 203(7), pp. 1651–1656. doi: 10.1084/jem.20051848.
Sumimoto, H. *et al.* (2016) 'RAS-mitogen-activated protein kinase signal is required for enhanced PD-L1 expression in human lung cancers', *PLoS ONE*, 11(11), pp. 1–18. doi: 10.1371/journal.pone.0166626.
Sun, X. J. *et al.* (2015) 'MicroRNA-29a Promotes Pancreatic Cancer Growth by Inhibiting Tristetraprolin', *Cellular Physiology and Biochemistry*, 37(2), pp. 707–718. doi: 10.1159/000430389.
Sunaga, N. *et al.* (2013) 'Oncogenic KRAS-induced epiregulin overexpression contributes to aggressive phenotype and is a promising therapeutic target in non-small-cell lung cancer', *Oncogene*. Nature Publishing Group, 32(34), pp. 4034–4042. doi: 10.1038/onc.2012.402.
Sweet-Cordero, A. *et al.* (2005) 'An oncogenic KRAS2 expression signature identified by cross-species gene-expression analysis.', *Nature genetics*. United States, 37(1), pp. 48–55. doi: 10.1038/ng1490.
Tanaka, N. *et al.* (2021) ' Clinical Acquired Resistance to KRAS G12C Inhibition through a Novel KRAS Switch-II Pocket Mutation and Polyclonal Alterations Converging on RAS–MAPK Reactivation ', *Cancer Discovery*, (August), pp. 1913–1923. doi: 10.1158/2159-8290.cd-21-0365.
Tap, W. D. *et al.* (2015) 'Structure-Guided Blockade of CSF1R Kinase in Tenosynovial Giant-Cell Tumor', *New England Journal of Medicine*, 373(5), pp. 428–437. doi: 10.1056/nejmoa1411366.
Tate, J. G. *et al.* (2019) 'COSMIC: the Catalogue Of Somatic Mutations In Cancer', *Nucleic Acids Research*, 47(D1), pp. D941–D947. doi: 10.1093/nar/gky1015.
Taylor, G. A. *et al.* (1996) 'A pathogenetic role for TNFα in the syndrome of cachexia, arthritis, and autoimmunity resulting from tristetraprolin (TTP) deficiency', *Immunity*, 4(5), pp. 445–454. doi: 10.1016/S1074-7613(00)80411-2.
Tchen, C. R. *et al.* (2004) 'The stability of tristetraprolin mRNA is regulated by

mitogen-activated protein kinase p38 and by tristetraprolin itself', *Journal of Biological Chemistry*, 279(31), pp. 32393–32400. doi: 10.1074/jbc.M402059200.

Tian, W. *et al.* (2020) 'Leukotrienes in Tumor-Associated Inflammation', *Frontiers in Pharmacology*, 11(August), pp. 1–11. doi: 10.3389/fphar.2020.01289.

Tiedje, C. *et al.* (2016) 'The RNA-binding protein TTP is a global post-transcriptional regulator of feedback control in inflammation', *Nucleic Acids Research*, 44(15), pp. 7418–7440. doi: 10.1093/nar/gkw474.

Timar, J. and Kashofer, K. (2020) 'Molecular epidemiology and diagnostics of KRAS mutations in human cancer', *Cancer and Metastasis Reviews*, 39(4), pp. 1029–1038. doi: 10.1007/s10555-020-09915-5.

Togashi, Y., Shitara, K. and Nishikawa, H. (2019) 'Regulatory T cells in cancer immunosuppression — implications for anticancer therapy', *Nature Reviews Clinical Oncology*. Springer US, 16(6), pp. 356–371. doi: 10.1038/s41571-019-0175-7.

Tran, E. *et al.* (2014) 'Cancer immunotherapy based on mutation-specific CD4+ T cells in a patient with epithelial cancer', *Science*, 344(6184), pp. 641–645. doi: 10.1126/science.1251102.

Tsai, Y. S. *et al.* (2022) 'Rapid idiosyncratic mechanisms of clinical resistance to KRAS G12C inhibition', *Journal of Clinical Investigation*, 132(4), pp. 1–9. doi: 10.1172/jci155523.

Tseng, D. *et al.* (2013) 'Anti-CD47 antibody-mediated phagocytosis of cancer by macrophages primes an effective antitumor T-cell response', *Proceedings of the National Academy of Sciences of the United States of America*, 110(27), pp. 11103–11108. doi: 10.1073/pnas.1305569110.

Tumeh, P. C. *et al.* (2014) 'PD-1 blockade induces responses by inhibiting adaptive immune resistance', *Nature*, 515(7528), pp. 568–571. doi: 10.1038/nature13954.

Velez-Delgado, A. *et al.* (2021) 'Extrinsic KRAS signaling shapes the pancreatic microenvironment through fibroblast reprogramming', *bioRxiv*, p. 2021.08.26.457660. doi: 10.1101/2021.08.26.457660.

Vignali, D. A. A., Collison, L. W. and Workman, C. J. (2008) 'How regulatory T cells work', *Nature Reviews Immunology*, 8(7), pp. 523–532. doi: 10.1038/nri2343.

Viola, A. *et al.* (2019) 'The metabolic signature of macrophage responses', *Frontiers in Immunology*, 10(JULY), pp. 1–16. doi: 10.3389/fimmu.2019.01462.

Waldman, A. D., Fritz, J. M. and Lenardo, M. J. (2020) 'A guide to cancer immunotherapy: from T cell basic science to clinical practice', *Nature Reviews Immunology*. Springer US, 20(11), pp. 651–668. doi: 10.1038/s41577-020-0306-5.

Wang, T. *et al.* (2004) 'Regulation of the innate and adaptive immune responses by Stat-3 signaling in tumor cells.', *Nature medicine*. United States, 10(1), pp. 48–54. doi: 10.1038/nm976.

Wculek, S. K. *et al.* (2020) 'Dendritic cells in cancer immunology and immunotherapy', *Nature Reviews Immunology*. Springer US, 20(1), pp. 7–24. doi: 10.1038/s41577-019-0210-z.

Wei, J. *et al.* (2021) 'Characterizing Intercellular Communication of Pan-Cancer Reveals SPP1+ Tumor-Associated Macrophage Expanded in Hypoxia and Promoting Cancer Malignancy Through Single-Cell RNA-Seq Data', *Frontiers in Cell and Developmental Biology*, 9(October), pp. 1–16. doi: 10.3389/fcell.2021.749210.

Wei, S. C., Duffy, C. R. and Allison, J. P. (2018) 'Fundamental mechanisms of immune checkpoint blockade therapy', *Cancer Discovery*, 8(9), pp. 1069–1086. doi: 10.1158/2159-8290.CD-18-0367.

Weiss, J. *et al.* (2021) 'KRYSTAL-1: Adagrasib (MRTX849) as monotherapy or combined with cetuximab (Cetux) in patients (Pts) with colorectal cancer (CRC) harboring a KRASG12C mutation', *Annals of Oncology*, 32(Suppl_5), pp. S1283–S1346.

Willems, E. *et al.* (2018) 'The functional diversity of Aurora kinases: A comprehensive review', *Cell Division*. BioMed Central, 13(1), pp. 1–17. doi: 10.1186/s13008-018-0040-6.

Wing, K. *et al.* (2008) 'CTLA-4 control over Foxp3+ regulatory T cell function', *Science*, 322(5899), pp. 271–275. doi: 10.1126/science.1160062.

Wislez, M. *et al.* (2006) 'High expression of ligands for chemokine receptor CXCR2 in alveolar epithelial neoplasia induced by oncogenic Kras', *Cancer Research*, 66(8), pp. 4198–4207. doi: 10.1158/0008-5472.CAN-05-3842.

Wong, P. P. *et al.* (2020) 'Cancer Burden Is Controlled by Mural Cell-β3-Integrin Regulated Crosstalk with Tumor Cells', *Cell*, 181(6), pp. 1346-1363.e21. doi: 10.1016/j.cell.2020.02.003.

Woo, S. R. *et al.* (2014) 'STING-dependent cytosolic DNA sensing mediates innate immune recognition of immunogenic tumors', *Immunity*. Elsevier Inc., 41(5), pp. 830–842. doi: 10.1016/j.immuni.2014.10.017.

Xi, N. M. and Li, J. J. (2021) 'Benchmarking Computational Doublet-Detection Methods for Single-Cell RNA Sequencing Data', *Cell Systems*. Elsevier Inc., 12(2), pp. 176-194.e6. doi: 10.1016/j.cels.2020.11.008.

Xu, L. *et al.* (2015) 'Tristetraprolin induces cell cycle arrest in breast tumor cells through targeting AP-1/c-Jun and NF-κB pathway', *Oncotarget*, 6(39), pp. 41679–41691. doi: 10.18632/oncotarget.6149.

Xue, J. Y. *et al.* (2020) 'Rapid non-uniform adaptation to conformation-specific KRAS(G12C) inhibition', *Nature*. Springer US, 577(7790), pp. 421–425. doi: 10.1038/s41586-019-1884-x.

Yang, E. *et al.* (2003) 'Decay rates of human mRNAs: Correlation with functional characteristics and sequence attributes', *Genome Research*, 13(8), pp. 1863–1872. doi: 10.1101/gr.1272403.

Yeo, E. J. *et al.* (2014) 'Myeloid wnt7b mediates the angiogenic switch and metastasis in breast cancer', *Cancer Research*, 74(11), pp. 2962–2973. doi: 10.1158/0008-5472.CAN-13-2421.

Yi, Y. S. *et al.* (2014) 'Functional roles of p38 in macrophage-mediated inflammatory responses', *Mediators of Inflammation*, 2014. doi: 10.1155/2014/270302.

Yoon, N. A. *et al.* (2016) 'Tristetraprolin suppresses the EMT through the down-regulation of Twist1 and Snail1 in cancer cells', *Oncotarget*, 7(8), pp. 8931–8943. doi: 10.18632/oncotarget.7094.

Yue, W. *et al.* (2007) 'Frequent inactivation of RAMP2, EFEMP1 and Dutt1 in lung cancer by promoter hypermethylation', *Clinical Cancer Research*, 13(15),

pp. 4336–4344. doi: 10.1158/1078-0432.CCR-07-0015.

Zhang, B. and Horvath, S. (2005) ‘A general framework for weighted gene co-expression network analysis.’, *Statistical applications in genetics and molecular biology*. Germany, 4, p. Article17. doi: 10.2202/1544-6115.1128.

Zhang, L. *et al.* (2020) ‘Single-Cell Analyses Inform Mechanisms of Myeloid-Targeted Therapies in Colon Cancer’, *Cell*. Elsevier, 181(2), pp. 442-459.e29. doi: 10.1016/j.cell.2020.03.048.

Zhao, F. *et al.* (2018) ‘Paracrine Wnt5a-β-Catenin Signaling Triggers a Metabolic Program that Drives Dendritic Cell Tolerization’, *Immunity*. Elsevier Inc., 48(1), pp. 147-160.e7. doi: 10.1016/j.immuni.2017.12.004.

Zhao, Y. *et al.* (2021) ‘Diverse alterations associated with resistance to KRAS(G12C) inhibition.’, *Nature*. Springer US, (March). doi: 10.1038/s41586-021-04065-2.

Zhu, A., Ibrahim, J. G. and Love, M. I. (2019) ‘Heavy-tailed prior distributions for sequence count data: removing the noise and preserving large differences’, *Bioinformatics*, 35(12), pp. 2084–2092. doi: 10.1093/bioinformatics/bty895.

Zilionis, R. *et al.* (2019) ‘Single-Cell Transcriptomics of Human and Mouse Lung Cancers Reveals Conserved Myeloid Populations across Individuals and Species’, *Immunity*. Elsevier Inc., 50(5), pp. 1317-1334.e10. doi: 10.1016/j.immuni.2019.03.009.